ERCB/AGS Open File Report 2012-13

Overview of Airborne-Electromagnetic and -Magnetic Geophysical Data Collection and Interpretation in the Edmonton–Calgary Corridor, Alberta

Energy Resources Conservation Board

Alberta Geological Survey

ERCB/AGS Open File Report 2012-13

Overview of Airborne-Electromagnetic and -Magnetic Geophysical Data Collection and Interpretation in the Edmonton–Calgary Corridor, Alberta

S.R. Slattery[1] and L.D. Andriashek[2]

[1] Formerly of Alberta Geological Survey (see page ii for current address)
[2] Energy Resources Conservation Board
Alberta Geological Survey

June 2012

ISBN 978-0-7785-8666-1

If you use information from this publication in other publications or presentations, please acknowledge the ERCB/AGS. We recommend the following reference format:

Slattery, S.R. and Andriashek, L.D. (2012): Overview of airborne-electromagnetic and -magnetic geophysical data collection and interpretation in the Edmonton–Calgary Corridor, Alberta; Energy Resources Conservation Board, ERCB/AGS Open File Report 2012-13, 218 p.

Author address:
Shawn Slattery
Syncrude Canada Ltd.
P.O. Bag 4009, M.D. A 250
Fort McMurray, AB T9H 3L1
Canada
Tel: 780.715.9579
E-mail: slattery.shawn@syncrude.com

Published June 2012 by:
Energy Resources Conservation Board
Alberta Geological Survey
4th Floor, Twin Atria Building
4999 – 98th Avenue
Edmonton, AB T6B 2X3
Canada

Tel: 780.422.1927
Fax: 780.422.1918
E-mail: AGS-Info@ercb.ca
Website: www.ags.gov.ab.ca

Contents

Table

Figures

Acknowledgements

Comments from T.G. Lemay and N. Atkinson of the Alberta Geological Survey improved an earlier version of this report. We also thank J. Dawson for editing the report.

Abstract

This report is one in a series of eight Alberta Geological Survey (AGS) Open File reports that provide an overview of airborne-electromagnetic and -magnetic geophysical surveys completed over the Edmonton–Calgary Corridor (ECC) by Fugro Airborne Surveys. These surveys were completed between November 2007 to February 2010 as part of a joint AGS and Alberta Environment and Sustainable Resource Development (ESRD) study to determine the usefulness of the RESOLVE®, GEOTEM® and TEMPEST® geophysical survey techniques in mapping the distribution and physical attributes of sediment- and bedrock-aquifer complexes over areas of formerly glaciated terrain.

The ECC was selected as the first test area to support the AGS-ESRD groundwater mapping program as it represents the region with the highest rates of industrial and urban growth in the province. Since this growth will exert increasing demands on water resources in the ECC, it is necessary to reassess the spatial distribution of previously mapped, as well as unmapped, aquifer complexes in the region. By doing so, Alberta may better predict and manage current and/or future stresses on existing aquifer systems caused by industrial, agricultural and urban development. Airborne geophysical survey methods were selected as one of the tools in completing this assessment.

The ECC is an ideal area to evaluate the usefulness of airborne-electromagnetic and -magnetic geophysical survey techniques due to the wealth of existing surficial and subsurface geological datasets (i.e., geological mapping, lithologs, petrophysical data, field observations, etc.). These datasets provide users with a means to calibrate and verify airborne geophysical data, analyses and interpretations within the ECC.

This report describes data collection methods using the Fugro Airborne Surveys' TEMPEST®, RESOLVE® and GEOTEM® survey techniques and data processing. Geophysical interpretations of these data, completed for the ECC by Fugro Airborne Surveys and TerraNotes Ltd., are included as appendices in this report.

1 Introduction

In recognition of increasing rates of urbanization and industrialization in Alberta, and the foreseeable pressures that this will have on existing water supplies, the Alberta Geological Survey (AGS) in partnership with Alberta Environment and Sustainable Resource Development (ESRD) has initiated a multi-year project to characterize nonsaline aquifer complexes within the province. The Edmonton–Calgary Corridor (ECC), the region with the most industrial and urban development in Alberta, was selected as the first study area by the AGS and ESRD (Figure 1).

It is inevitable that future groundwater use in the ECC will place additional stress on existing aquifer systems. Therefore, reassessing previously mapped aquifers, potentially locating unmapped aquifers and implementing management strategies that ensure groundwater resources exist for future use are essential. As management strategies and decision-making tools will require more accurate geological and hydrogeological models, innovative approaches to data collection will be required. In complicated geological terrains, such as the ECC, where hydraulic pathways within glacial sediments and between glacial sediments and underlying bedrock formations are poorly understood, continuous high-resolution geological mapping of both glacial sediments and bedrock formations is necessary to better understand and illustrate the architecture of geological strata. A better understanding of the geological architecture within the ECC will allow for improved geological modelling, which in turn will allow for a better hydrogeological model of the ECC. It is anticipated that this model will form the cornerstone for numerous applications, such as groundwater exploration programs, aquifer protection studies and significant recharge area identification. More importantly, this model will form the framework for groundwater-flow modelling exercises and future water-budget calculations leading to improved water management decisions.

Recognizing the need for high-quality regional geological data, AGS and ESRD have collaborated to obtain airborne-geophysical survey data for near-continuous coverage of the ECC. A similar approach has been taken in other areas of formerly glaciated terrain by geological surveys in the United States, Europe and the United Kingdom (cf., Smith et al., 2003, 2006, 2007; Lahti et al., 2005; Wiederhold et al., 2009). Despite the success of these surveys in mapping the distribution of near-surface and subsurface aquifers, one of the main objectives of our investigation is to evaluate and compare the usefulness of these same types of airborne-geophysical survey techniques in mapping the distribution of aquifers in the ECC.

Between November 2007 and February 2010, airborne-electromagnetic (AEM) and airborne-magnetic (AM) surveys were completed by Fugro Airborne Surveys over 11 study blocks in the ECC on behalf of AGS and AENV. The airborne-geophysical surveys were undertaken using one or a combination of the following survey techniques: fixed-wing, GEOTEM® or TEMPEST® time-domain or helicopter-borne, RESOLVE® frequency-domain (Figure 2). This report provides an overview of data collection and processing completed for the ECC by Fugro Airborne Surveys. A geophysical interpretation of these data, completed by Fugro Airborne Surveys and TerraNotes Ltd., are provided in Appendices 1 and 2. Information on geophysical data collection and processing for individual study blocks in the ECC is presented in Slattery and Andriashek (2012a–g).

2 Purpose and Scope

The reasons for completing AEM and AM geophysical surveys in the ECC are multifaceted. First, it is to evaluate the effectiveness of frequency- and time-domain geophysical surveys to determine the spatial distribution of near-surface and subsurface electrical and magnetic properties of sediments and bedrock. It is anticipated that these properties will be related to geological and hydrogeological features in the ECC, which will provide a better understanding of the geological architecture. This, in turn, will allow for more accurate geological and hydrogeological models to support improved water management decisions.

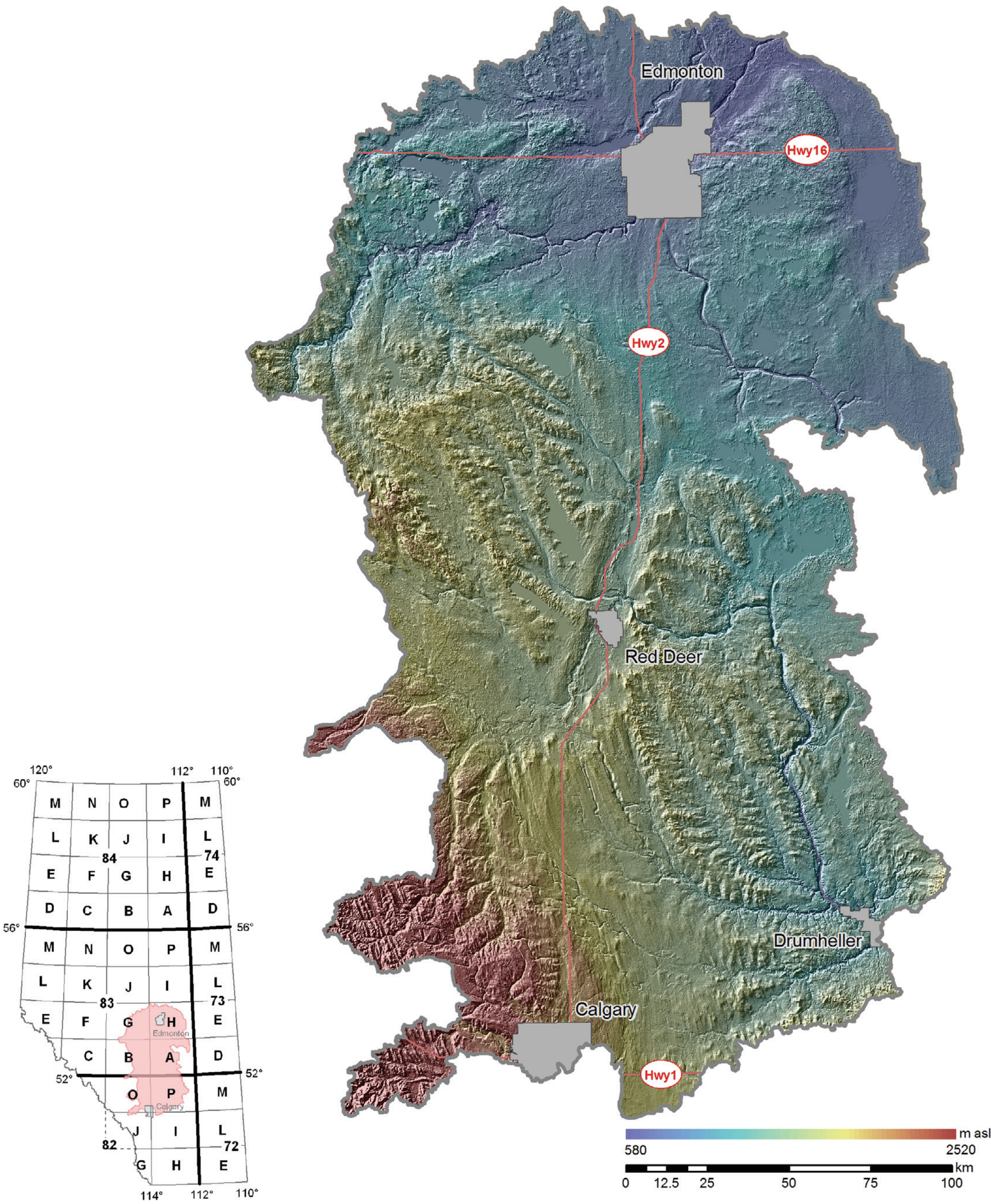

Figure 1. Digital elevation model (DEM) accented by hillshaded relief of surface topography of the Edmonton–Calgary Corridor (ECC), Alberta. Elevation of surface topography in metres above sea level is defined by colour ramp. Vertical exaggeration is 20x. Inset map depicts location of the ECC, Alberta.

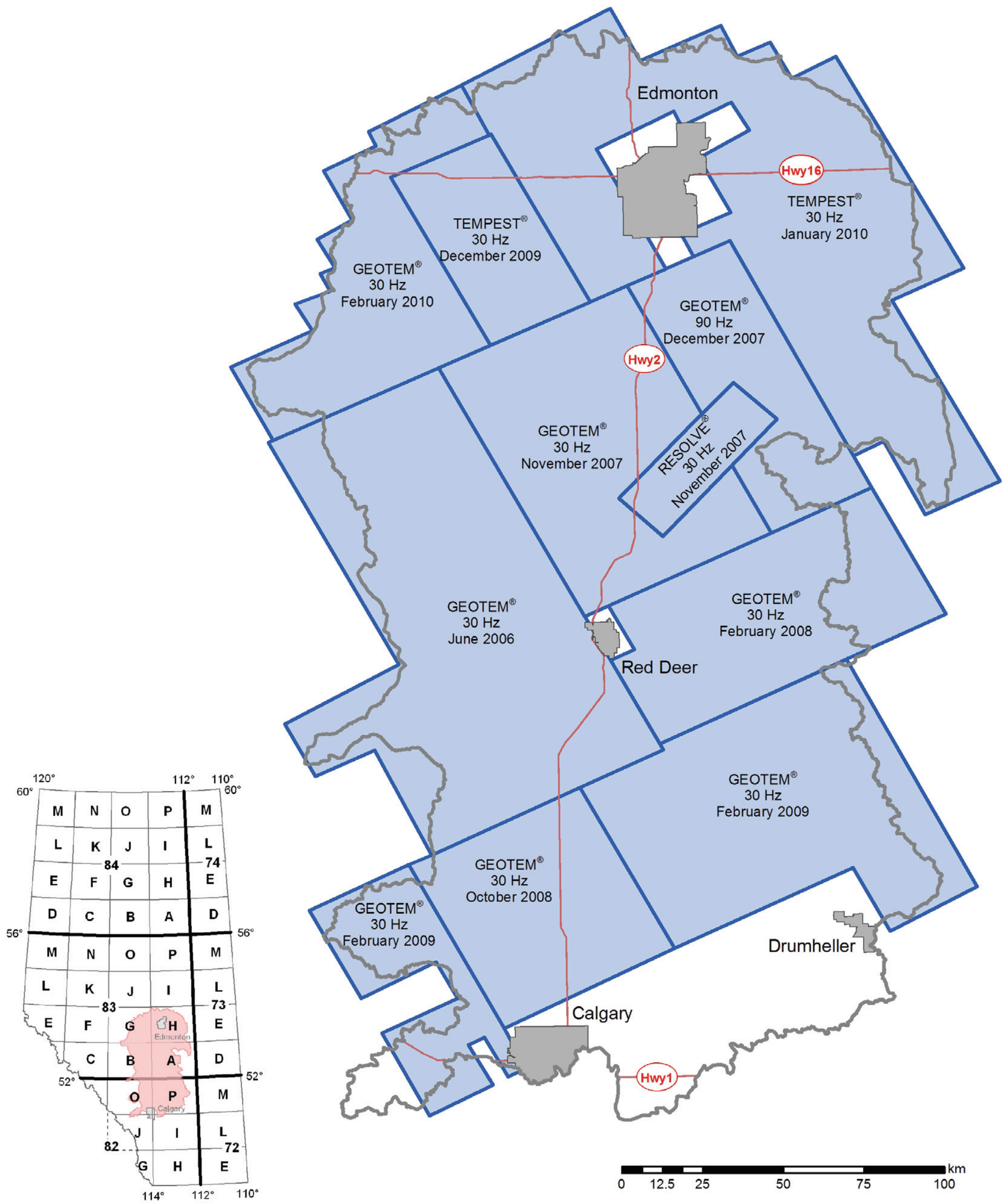

Figure 2. Location of the 11 geophysical study blocks in the Edmonton–Calgary Corridor (ECC). The type of geophysical survey completed and when it was completed are provided on each study block. Inset map depicts location of the ECC, Alberta.

Second, the selection of the ECC for AEM and AM surveying was influenced by the widespread availability of existing surface and subsurface geological and geophysical data in the region (Table 1). These data are needed to validate the results and interpretations of the AEM and AM surveys. If the interpretation of AEM and AM survey data correlates with geological data and ground and downhole geophysical data, then AEM and AM surveying techniques could be used to interpret the geological framework in those areas that have limited subsurface geological and geophysical data. In such areas, AEM and AM surveys may provide a more time- and cost-effective means to acquire continuous, high-quality geological data than traditional drilling methods and geological mapping investigations.

Third, the geological setting of the ECC is such that aquifer complexes can occur at various depths and have a variety of sediment and rock properties. Low-frequency (30 and 90 hertz [Hz]), TEMPEST® and GEOTEM® time-domain surveys were completed to provide greater penetration depths and summary electromagnetic (EM) and magnetic data to improve the delineation of regional-scale geological strata in the ECC. The AGS and ESRD tested the RESOLVE® frequency-domain survey in areas where more detailed resolution of the near-surface geology was required. Simplified cross-sections of the geological settings are depicted in Figure 3.

Table 1. Data sources and types available to validate airborne-electromagnetic (AEM) and airborne-magnetic (AM) geophysical data in the Edmonton–Calgary Corridor, Alberta. Abbreviations: ESRD, Alberta Environment and Sustainable Resource Development; AGS, Alberta Geological Survey; ERCB, Energy Resources Conservation Board.

Data Source	Data Class	Number of Data Points
ESRD digital water-well database	Water-well records and litholog records	234 902
AGS geotechnical database	Geotechnical borehole records	1202
ERCB oil-and-gas–well database	Oil-and-gas–well and petrophysical records	5161
AGS borehole database	Geological borehole and petrophysical records	363
AGS field observations	Field-based geological data	322

3 Location of Study Area and Geophysical Study Blocks

The ECC study area occupies approximately 49 500 km^2 and lies within portions of NTS 82I, J, O and P and 83A, B, G and H. Ten subwatershed boundaries define the irregularly shaped boundary of the ECC study area (Figure 1).

Between November 2007 and February 2010, AEM and AM surveys were completed over 11 study blocks in the ECC (Figure 2). Data collection over the study blocks was completed using one or a combination of the fixed-wing, GEOTEM® or TEMPEST® time-domain or helicopter-borne, RESOLVE® frequency-domain survey techniques (Figure 2).

4 Methodology

4.1 Data Acquisition, Processing and Interpretations

Digital data from the AEM and AM surveys were acquired by the contractor, Fugro Airborne Surveys, using the TEMPEST® and GEOTEM® time-domain and the RESOLVE® frequency-domain survey techniques. These techniques are briefly discussed below. Information pertaining to specific survey techniques, data collection and processing for individual study blocks within the ECC are presented in Slattery and Andriashek (2012a–g). For additional information on geophysical processing techniques, the reader is referred to Fraser (1978), Smith et al. (2003, 2006, 2007), Paine and Minty (2005) and Siemon (2006).

Datasets provided to AGS and ESRD from Fugro Airborne Surveys included both unprocessed and processed tabular datasets, as well as grid-based digital maps illustrating ground resistivity in relation to depth below ground surface. Geophysical interpretations of these datasets, completed by Fugro Airborne Surveys and TerraNotes Ltd., are presented in appendices 1 and 2. AGS and ESRD did not process or interpret any of the geophysical data.

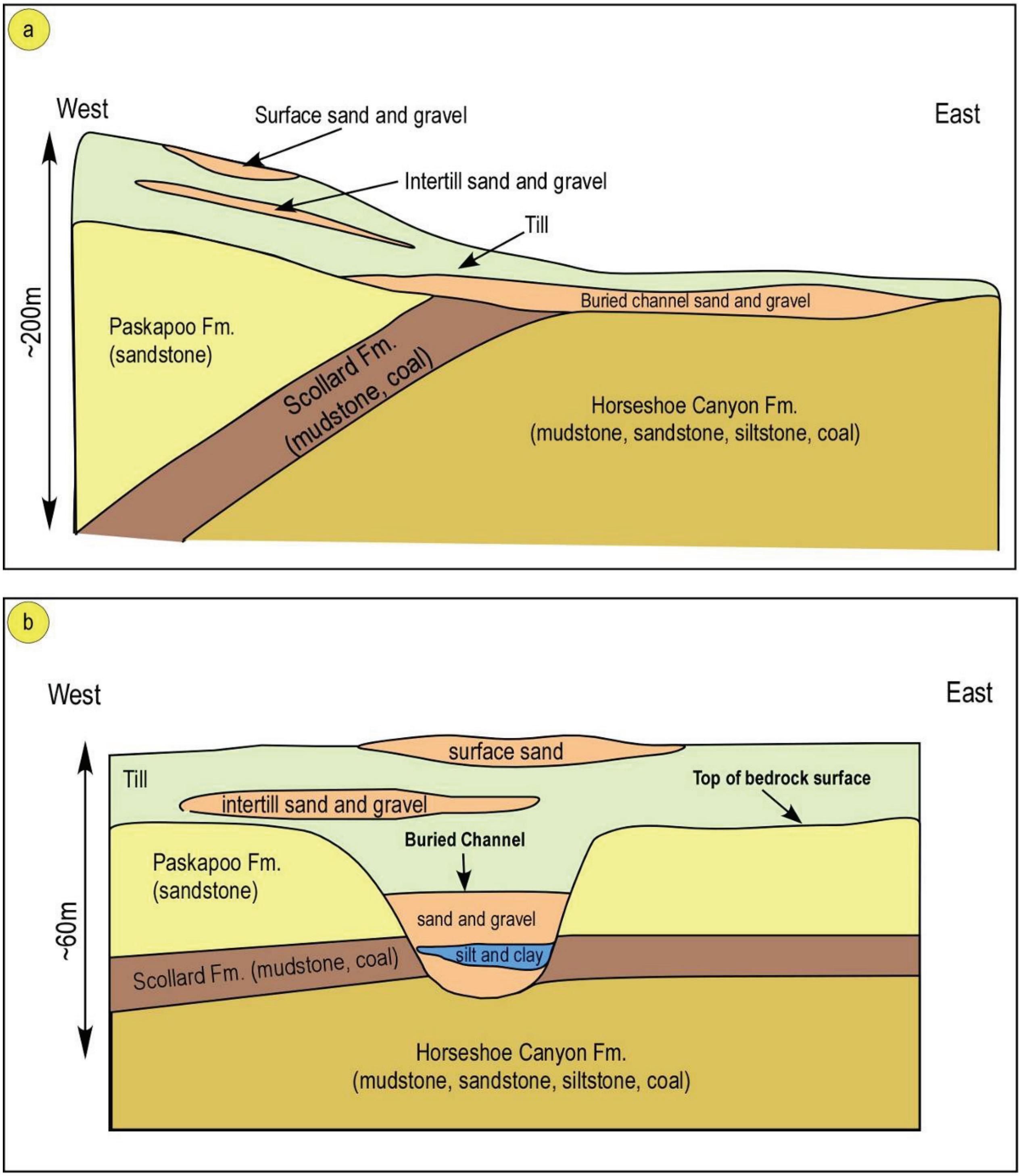

Figure 3. a) Simplified, regional-scale cross-section, oriented west to east, of sediments and bedrock surveyed using the low-frequency, GEOTEM® time-domain survey, central Alberta. b) Simplified, local-scale cross-section, oriented west to east, of sediments and bedrock surveyed with the RESOLVE® frequency-domain survey, central Alberta.

4.2 RESOLVE® Frequency-Domain Geophysical Survey

The RESOLVE® survey is a helicopter-borne, frequency-domain EM survey designed specifically for locating conductive anomalies and mapping earth resistivities. It is completed using a unique six-frequency system, with horizontal coplanar coils measuring the EM response at approximately 400, 1800, 8200, 40 000 and 140 000 Hz, and one coaxial coil at approximately 3300 Hz. Details pertaining to specific frequencies, separation and orientation of the coil pairs used in the survey are discussed in Slattery and Andriashek (2012e).

Ancillary equipment used in this survey consisted of a magnetometer, radar and laser altimeters, a video camera, a digital data recorder and an electronic navigation system. The instrumentation was installed in a modified AS350-B2 helicopter. The helicopter flew with an EM sensor height of approximately 30 m. The main part of the geophysical system is contained within a cylindrical tube, commonly referred to as a receiver, which is towed beneath the helicopter (Figure 4; Slattery and Andriashek, 2012a). All data recorded by the measurement systems in the receiver are transmitted through a cable to a processing and digital recording system located in the helicopter. Measurements of the geophysical data (EM and total field magnetic) are made approximately every 3 m along the flight line.

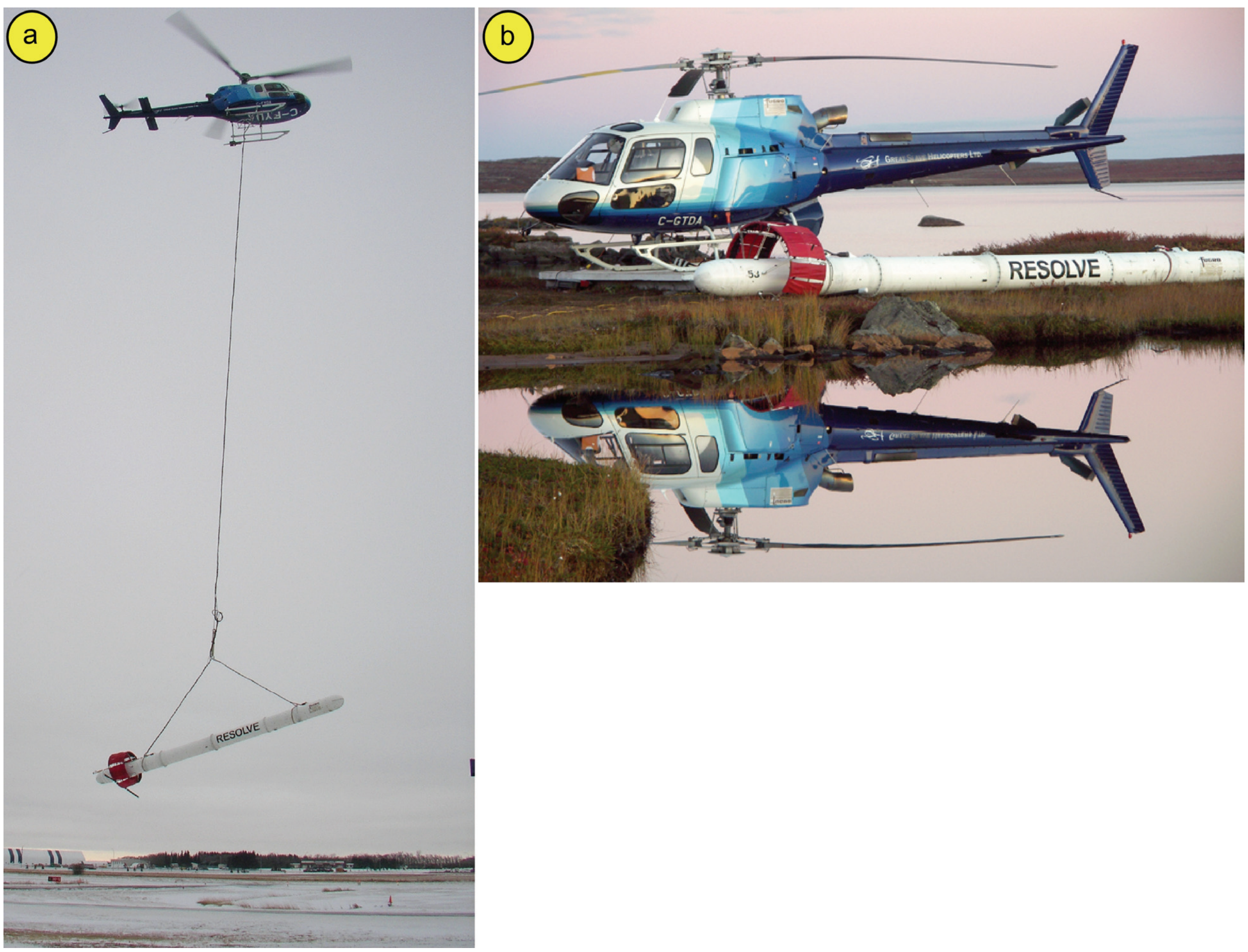

Figure 4. a) RESOLVE® frequency-domain survey in operation. The main part of the geophysical system is contained within a cylindrical tube, commonly referred to as a receiver, which is towed beneath the helicopter. b) The RESOLVE® receiver is approximately 9 m in length.

4.3 TEMPEST® and GEOTEM® Time-Domain Geophysical Surveys

The fixed-wing, TEMPEST® and GEOTEM® time-domain survey techniques consist of a towed-bird EM system. These survey techniques are based on the premise that fluctuations in the primary EM field produced in the transmitting loop will result in eddy currents being generated in any conductors in the ground. The eddy currents then decay to produce a secondary EM field that may be sensed in the receiver coil. Each primary pulse causes decaying eddy currents in the ground to produce a secondary magnetic field. This secondary magnetic field, in turn, induces a voltage in the receiver coils, which is the EM response. Good conductors decay slowly, whereas poor conductors decay more rapidly.

The primary EM pulses are created by a series of discontinuous sinusoidal current pulses fed into a three- or six-turn transmitting loop surrounding the aircraft and fixed to the nose, tail and wing tips. The EM system of the TEMPEST® system is composed of a 30 channel multicoil system, as opposed to the 20 channel multicoil GEOTEM® system. In both these surveys, instrumentation was installed on a modified Casa 212 aircraft (Figure 4). The base frequency rate is selectable: 25, 30, 75, 90, 125, 150, 225 and 270 Hz, and the length of the pulse can be adjusted to suit specific targets. Standard pulse widths available are 0.6, 1.0, 2.0 and 4.0 ms, and the receiver is a three-axis (x, y, z) induction coil that is towed by the aircraft on a 135 m long, nonmagnetic cable (Figure 5). The usual mean terrain clearance for the aircraft is 120 m with the EM receiver normally being situated 50 m below and 130 m behind the aircraft (Figure 5). Additional information on the TEMPEST® and GEOTEM® survey techniques completed in the ECC is provided in Slattery and Andriashek (2012b–g).

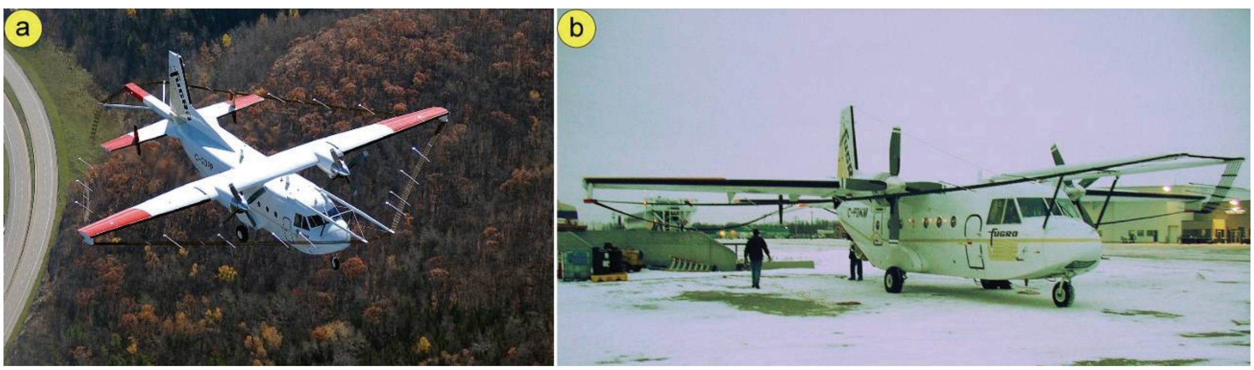

Figure 5. a) The GEOTEM® survey technique in flight. Note the transmitting loop fixed to the aircraft's nose, tail and wing tips. Primary electromagnetic pulses are created by a series of discontinuous sinusoidal current pulses and transmitted into the transmitting loop. b) Modified Casa 212 aircraft used by Fugro Airborne Surveys in this study.

5 References

Fraser, D.C. (1978): Resistivity mapping with an airborne multicoil electromagnetic system; Geophysics, v. 43, p. 144–172.

Lahti, M., Vanhala, H., Mattsson, A., Beamish, D. and Lerssi, J. (2005): Environmental applications of airborne geophysics – groundwater and contaminated soil in Finland, Germany and United Kingdom; Geological Survey of Finland, Special Paper 39, p. 155–175.

Paine, J.G. and Minty, B.R.S. (2005): Airborne hydrogeophysics; *in* Hydrogeophysics, Y. Rubin and S.S. Hubbard (ed.), Water Science and Technology Library, v. 50, p. 333–357.

Siemon, B. (2006): Electromagnetic methods – frequency domain – airborne techniques; *in* Groundwater geophysics – a tool for hydrogeology, R. Kirsch (ed.), Springer-Verlag, p. 155–170.

Slattery, S.R. and Andriashek, L.D. (2012a): Overview of airborne-electromagnetic and -magnetic geophysical data collection using the RESOLVE® and GEOTEM® survey techniques near Red Deer, central Alberta; Energy Resources Conservation Board, ERCB/AGS Open File Report 2012-07, 246 p.

Slattery, S.R. and Andriashek, L.D. (2012b): Overview of airborne-electromagnetic and -magnetic geophysical data collection using the GEOTEM® survey technique in the Sylvan Lake area, central Alberta; Energy Resources Conservation Board, ERCB/AGS Open File Report 2012-08, 175 p.

Slattery, S.R. and Andriashek, L.D. (2012c): Overview of airborne-electromagnetic and -magnetic geophysical data collection using the GEOTEM® survey technique north of Calgary, Alberta; Energy Resources Conservation Board, ERCB/AGS Open File Report 2012-09, 169 p.

Slattery, S.R. and Andriashek, L.D. (2012d): Overview of airborne-electromagnetic and -magnetic geophysical survey data collection using the GEOTEM® survey technique near Three Hills and Cochrane, Alberta; Energy Resources Conservation Board, ERCB/AGS Open File Report 2012-10, 92 p.

Slattery, S.R. and Andriashek, L.D. (2012e): Overview of airborne-electromagnetic and -magnetic geophysical data collection using the TEMPEST® survey technique near Edmonton, Alberta; Energy Resources Conservation Board, ERCB/AGS Open File Report 2012-11, 38 p.

Slattery, S.R. and Andriashek, L.D. (2012f): Overview of airborne-electromagnetic and -magnetic geophysical data collection using the GEOTEM® survey technique near Drayton Valley, central Alberta; Energy Resources Conservation Board, ERCB/AGS Open File Report 2012-12, 92 p.

Slattery, S.R. and Andriashek, L.D. (2012g): Overview of airborne-electromagnetic and -magnetic geophysical data collection using the TEMPEST® survey technique near Wabamun, central Alberta; Energy Resources Conservation Board, ERCB/AGS Open File Report 2012-14, 38 p.

Smith, B.D., Irvine, R., Blome, C.D., Clark, A.K. and Smith, D.V. (2003): Preliminary results, helicopter electromagnetic and magnetic survey of the Seco Creek area, Medina and Uvalde counties, Texas; Proceedings for the Symposium on the Application of Geophysics to Environmental and Engineering Problems, San Antonio, Texas, 15 p.

Smith, B.D., Thamke, J.N., Cain, M.J., Tyrrell, C. and Hill, P.L. (2006): Helicopter electromagnetic and magnetic survey maps and data, East Poplar Oil Field area, Fort Peck Indian Reservation, northeastern Montana, August 2004; United States Geological Survey, Open File Report 2006-1216, 23 p., 1 plate.

Smith, B.D., Grauch, V.J.S., McCafferty, A.E., Smith, D.V., Rodriguez, B.R., Pool, D.R., Deszcz-Pan, M. and Labson, V.F. (2007): Airborne electromagnetic and magnetic surveys for ground-water resources: a decade of study by the U.S. Geological Survey; *in* Proceedings of Exploration 07: Fifth Decennial International Conference on Mineral Exploration, B. Milkereit (ed.), p. 895–899.

Wiederhold, H., Schaumann, G. and Steuer, A. (2009): Airborne geophysical investigations for hydrogeological purposes in northern Germany; Near Surface 2009 – 15th European Meeting of Environmental and Engineering Geophysics, September 7–9, 2009, Dublin, Ireland, 5 p.

Appendix 1 – Interpretation Overview of Airborne Magnetic and Electromagnetic Survey Data for the Edmonton–Calgary Corridor, Alberta

Fugro Airborne Surveys

INTERPRETATION OVERVIEW OF

Airborne Magnetic and Electromagnetic Survey Data

For the

Edmonton – Calgary Corridor, Alberta

Job No. 10401

Alberta Environment

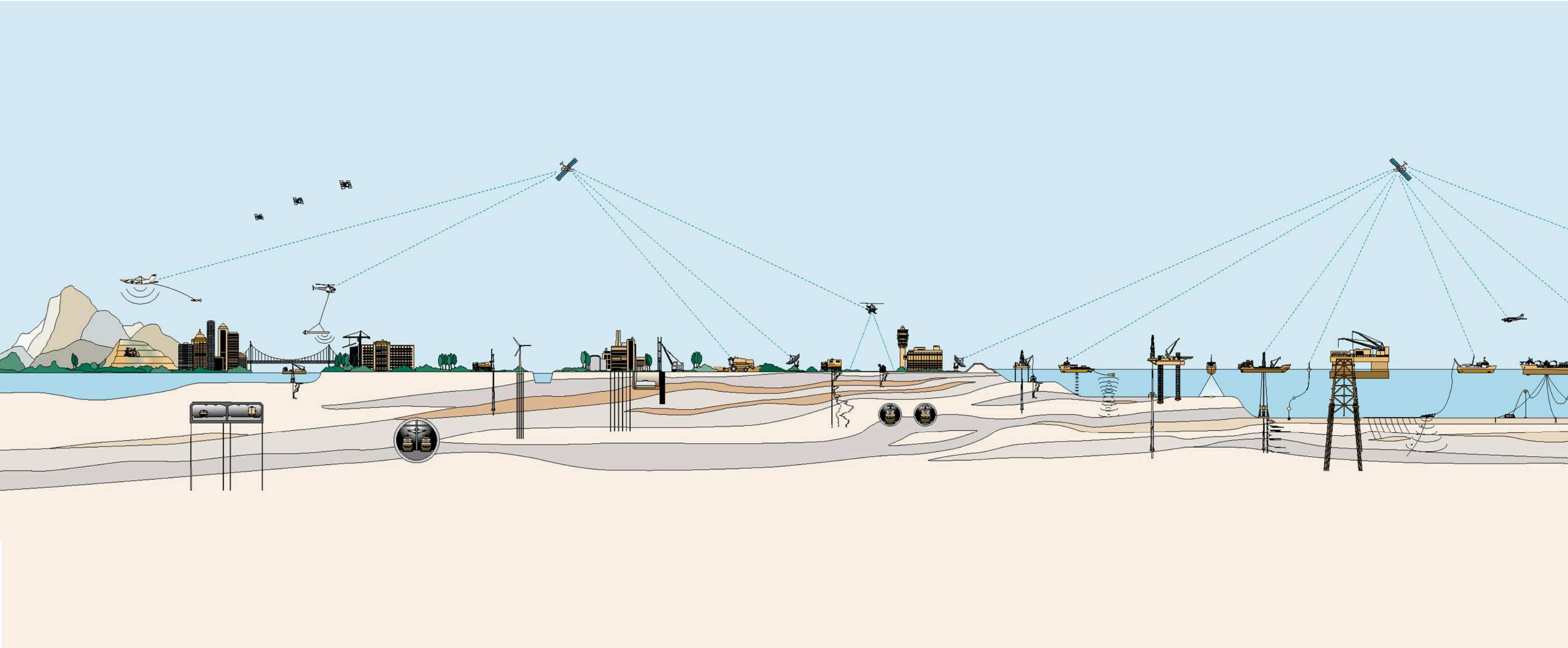

INTERPRETATION OVERVIEW OF
AIRBORNE MAGNETIC AND ELECTROMAGNETIC SURVEY DATA
FOR THE
EDMONTON - CALGARY CORRIDOR, ALBERTA

JOB NO. 10401

Client : Alberta Environment, Water Policy Branch
7th Floor, Oxbridge Place
9820-106 Street
Edmonton, Alberta
T5K 2J6

Date of Report : March, 2010

TABLE OF CONTENTS

I

Introduction

The scope of this interpretation covers Electromagnetic (EM – incorporating both Geotem® and Tempest® data) and Magnetic surveys flown between November 2007 and February 2010 covering the Edmonton - Calgary corridor (ECC) the data was collected using a Casa 212 modified aircraft (Figure 1).

The interpretation is presented in colour on paper and as Geosoft and PDF digital map files. A complete processing report for each has already been presented as separate documents. Refer to the processing report for more details on the survey and system specifications as well as information on the data processing and final products. The following appendices to the processing report are of particular interest to the interpretation:

- Fixed-Wing Airborne Electromagnetic systems.
- Airborne Transient EM Interpretation.
- Multi-component modeling.
- The Usefulness of Multi-component Time-Domain Airborne EM Measurement.

Figure 1: Specially modified Casa 212 aircraft used by Fugro Airborne Surveys.

II

Survey Operations

Location of the Survey Area

Figure 2 below shows the extent of the coverage of this interpretation overview.

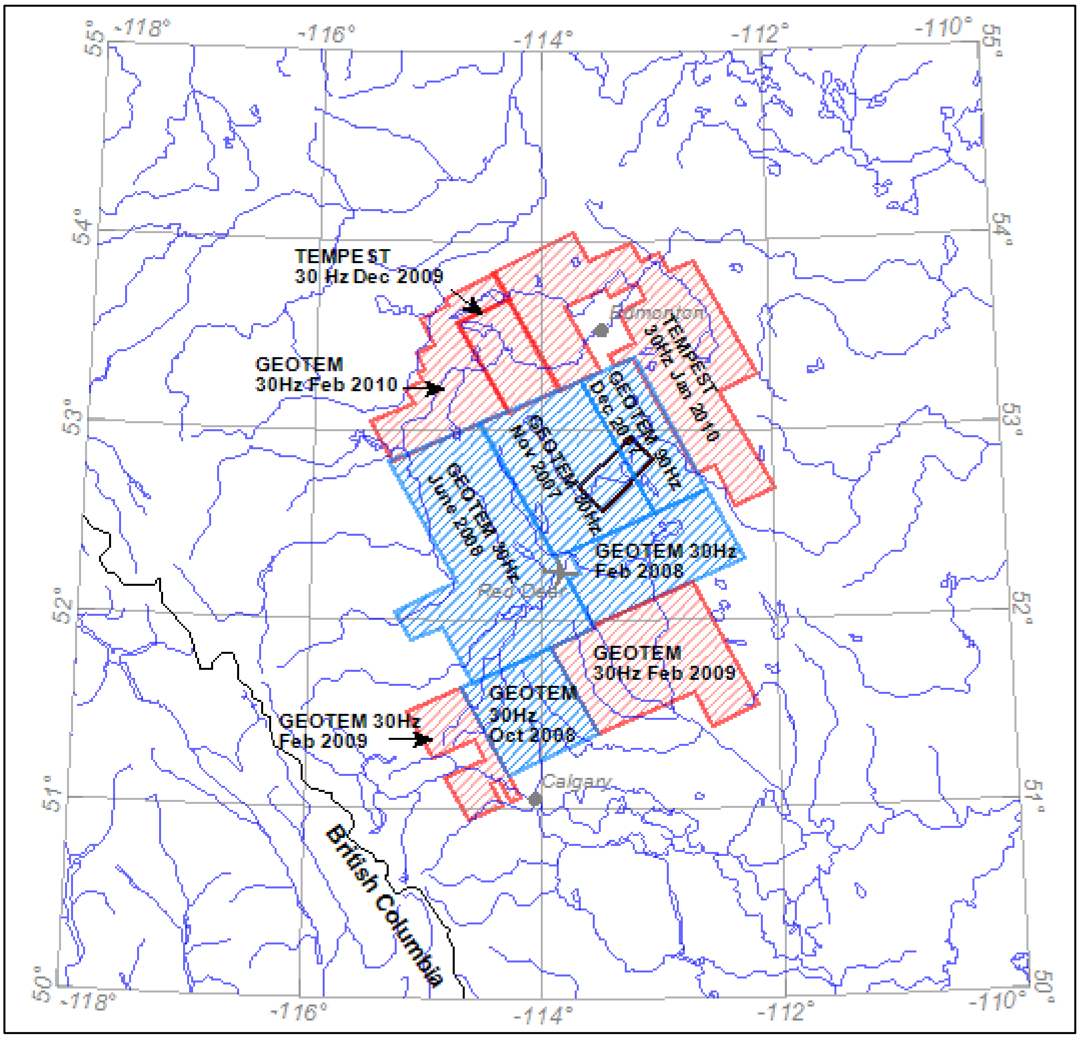

Figure 2: Survey locations. Those surveys outlined in blue indicate areas covered by previous interpretation reports. The small black rectangle outlines the Resolve® system survey, which was also covered by a previous review.

III

INTERPRETATION

Geology

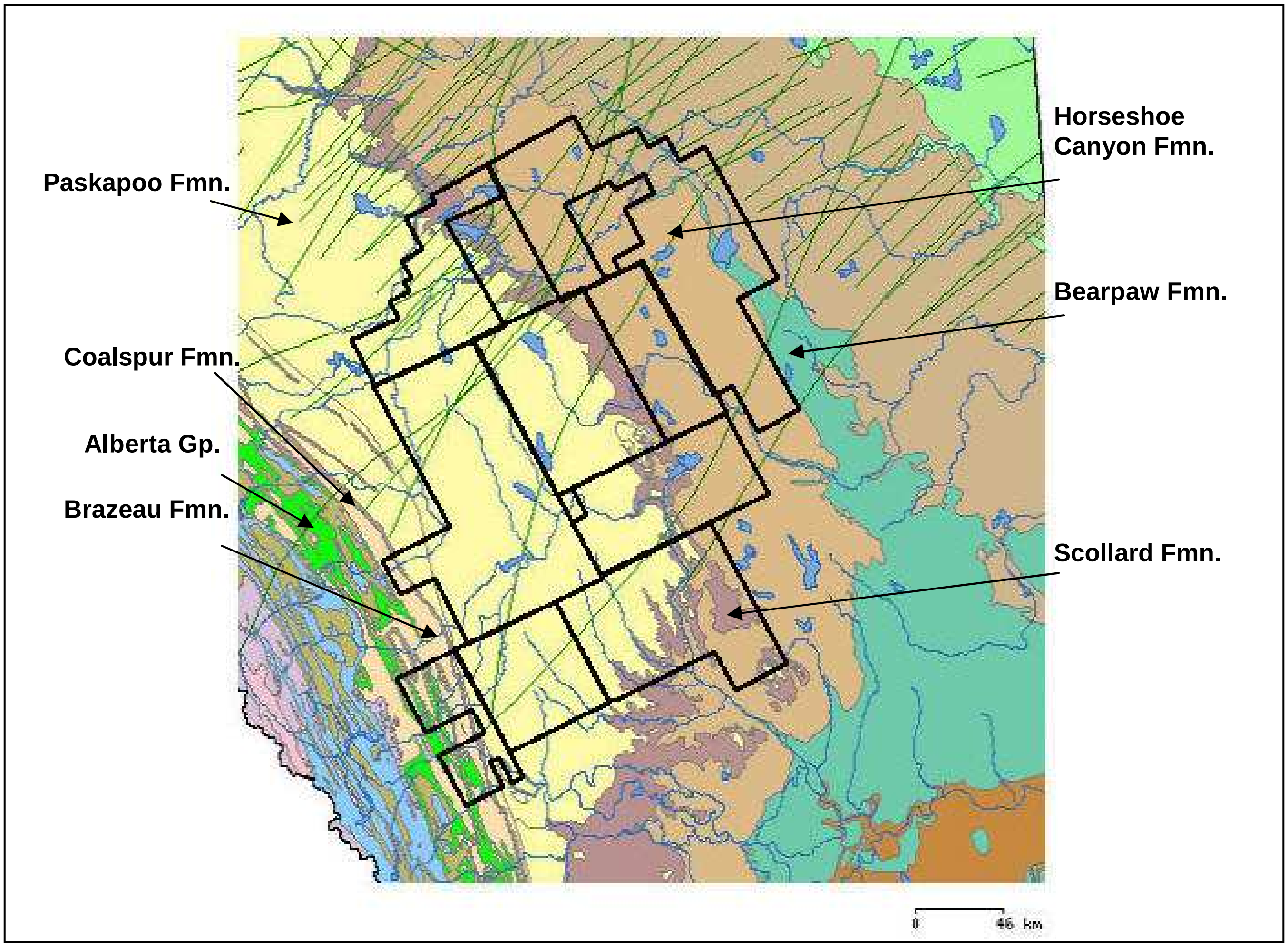

Figure 3: Bedrock geology of the region with the inferred basement lineaments from the (Alberta Geolgogical Survey) AGS website. The image shows the boundaries of the GEOTEM / TEMPEST survey areas.

The Paskapoo Formation of southern Alberta supports more groundwater wells than any other aquifer system in the Canadian Prairies. Located in a region of rapid population growth and straddling watersheds where no new surface water licenses are available, this aquifer system is under increasing pressure to provide water supply. The Paskapoo Formation represents a foreland deposit of a siltstone- and mudstone-dominated fluvial system. The system is highly heterogeneous with broad ranges in physical properties that impact groundwater production. High-porosity coarse-grained channel sandstone can provide productive wells, whereas thin and fractured sands and siltstones are low producers. The basal Haynes Member and western portion of the Paskapoo Formation have higher sandstone volumes than other portions of the system. Fracture density shows a strong inverse relationship to bed thickness, such that fracture flow becomes more important for thinner sandstone beds. There is no regional-scale flow system associated with the Paskapoo Formation; rather it is dominated by local-scale recharge processes.[1]

The surface aquifer thickness changes from approximately 20 m thick in the north, to 50 m in the south, except in the the area of linear bedrock lows, where it can exceed 40 – 60 m. The upper bedrock includes formations that are generally less than 200 m below the bedrock surface, and throughout the survey area these are (besides the Paskapoo formation mentioned above): the Scollard, Battle-Whitemud, Horseshoe Canyon, Bearpaw, and the disturbed belt in the southwest.

Paskapoo/Scollard Formation Boundary

The Paskapoo/Scollard boundary is similar to the Scollard/Battle, inasmuch as it is abrupt and disconformable (Lerbekmo et al., 1990). The contact is defined (at present) as the lowest major sandstone above the Ardley coal zone (Gibson, 1977). In outcrop this contact is normally marked by the thick, buff coloured sandstones of the Paskapoo lying directly on the coal-bearing strata of the Ardley coal zone (Demchuk and Hills, 1991). The sandstone bodies are commonly greater than 30 m thick. In the subsurface the Ardley coal zone is regionally correlatable and can be recognized throughout much of the basin except in the southwest, where climatic conditions hindered the development of peat swamps (Jerzykiewicz and Sweet, 1988). Correlative coals are recognized in the Coalspur and Ravenscrag formations. The Ardley coal zone consists of a lower and upper interval of coal seams separated by about 20 m, resulting in a distinct log response.

The Paskapoo Formation consists of cycles of thick, tabular, buff coloured sandstone beds in excess of 15 m thick and commonly stacked into successions greater than 60 m thick, overlain by interbedded siltstone and mudstone. The formation is normally barren of coal, except for the Obed Marsh coal zone, about 700 m above the formation base. The Paskapoo thickens from east to west and exceeds 800 m in the foothills. Large volumes of clastic sediments were deposited in the basin following the widespread coal development of the upper Scollard, essentially burying the peat swamps and producing extensive deposits of coarse-grained sandstone lying disconformably on the underlying fine-grained sediments (Lerbekmo et al., 1990; Demchuk and Hills, 1991).

[1] Regional characterization of the Paskapoo bedrock aquifer system, Southern Alberta, Stephen E. Grasby et al. Can. J. Earth Sci. 45(12): 1501–1516 (2008)

Scollard/Battle Formation Boundary

The Scollard/Battle Formation boundary appears to be disconformable throughout much of the basin. In outcrop the distinctive mauve shales of the Battle are in sharp contrast to the buff to olive green sediments of the Scollard Formation. In the subsurface, the contact is difficult to place if the distinctive log response of the Battle Formation and the Carbon-Thompson coals are not recognizable. The contact is commonly abrupt, with thick sandstone units (up to 30 m) overlying the fine-grained strata of the Battle Formation. Locally these channel deposits down cut into the Battle Formation and rest disconformably on Whitemud or Horseshoe Canyon Formation strata (Baofang and Dawson, 1988).

Battle-Whitemud/Horseshoe Canyon Formation Boundary[2]

At the top of the Horseshoe Canyon Formation is a laterally persistent coal zone defined as the Carbon-Thompson coal zone. This interval contains up to 10 thin coal seams and is overlain by the Whitemud-Battle formations. The Battle-Whitemud Formations are not shown on the Bedrock geology map image of Figure 3, but lie between the Scollard and Horseshoe Canyon Formations (see the Geologic Column in Tables 2 later in the report). The stratigraphic positions of these strata are distinct in outcrop and are mapped over much of southern Alberta and Saskatchewan (Irish and Havard, 1968). In the subsurface the Battle Formation is easily recognized by its distinctive low-resistivity log response, and by its proximity to the underlying Carbon-Thompson coal zone.

The Horseshoe Canyon Formation forms an eastward-thinning wedge ranging from greater than 750 m in the western foothills to less than 30 m in southern Saskatchewan.

[2] Geology summarized from Chapter 24: Uppermost Cretaceous and Tertiary Strata of the Western Canada Sedimentary Basin. F. M. Dawson et al.

General Magnetic Theory

The Earth's magnetic field, which changes from over 60,000 gammas in a vertical direction at the poles to about 30,000 gammas in a horizontal direction at the equator, induces a secondary magnetic field in rock bodies containing ferromagnetic minerals. It is this property to become magnetized by an external field that is described as the susceptibility of a rock.

Some rocks contain a natural or thermo-remnant magnetization that was acquired when the rock was last heated above the Curie point and subsequently cooled. The direction of this remanent magnetization is parallel to the magnetic field that prevailed during the cooling period. These fields, both the induced and remanent, disturb the otherwise smooth magnetic pattern of the Earth's field, and it is these perturbations that are of prime interest in aeromagnetic interpretation.

The crystalline rocks of igneous or high-grade metamorphic origin, such as granite, basalt, gneiss and schist, usually contain sufficient quantities of ferromagnetic minerals (mainly magnetite) that their influence on the earth's field can be observed even when covered by sedimentary sections thousands of feet thick.

The magnetic pattern over large areas of a single rock type is generally consistent throughout, and whenever the magnetic character changes, it usually implies a change in the rock composition. For example, the contact between a granitic mass and an ultrabasic unit can usually be precisely positioned where the magnetic pattern begins to change from the usual quiet character of granite to the more disturbed pattern of an ultrabasic rock body.

The study of magnetic anomalies does, to some degree, depend upon the latitude; in high latitudes attention is devoted to positive anomalies, while at the equator negative anomalies are of prime interest. This is due to the inclination of the earth's magnetic field, which is near vertical, 90°, at the poles, horizontal, 0°, at the equator, and about 75° North in this survey area. In such a steep magnetic inclination, the strike of a magnetic body has little effect upon the magnitude and symmetry of the anomaly it produces. An E-W dyke will be primarily positive, with a very weak negative on its north side. The same dyke striking magnetic north (azimuth 016 in this area) will be a symmetrical positive, but only about 95% of its E-W amplitude.

Magnetic Interpretation Procedures

Although the previous interpretations of several survey areas (see the caption for Figure 2) provided a full magnetic lineament analysis, the scope within this interpretation will only include magnetic features of interest pertaining to the delineation of potential aquifers, and a general overview of the magnetic boundaries.

Faults are located by offsets, terminations and strike changes in linear anomalies, or level shifts, or simply changes in character. Since the fault symbol is usually used to join isolated points of disruption, its location and direction is much more subjective than the contact symbol.

Overview of the Magnetic Response

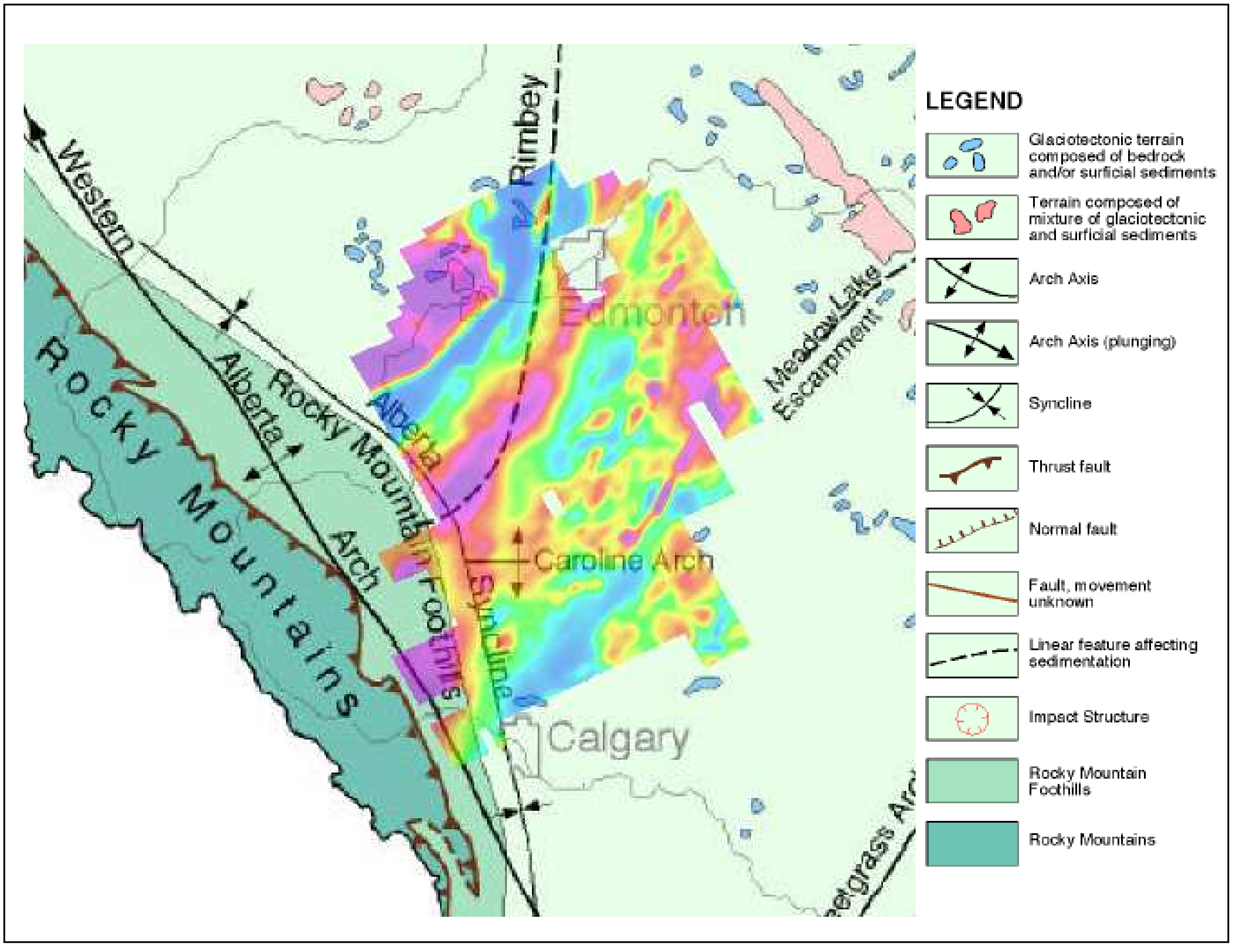

Figure 4: Phanerozoic tectonic features with the Residual Magnetic Intensity (RMI) superimposed.

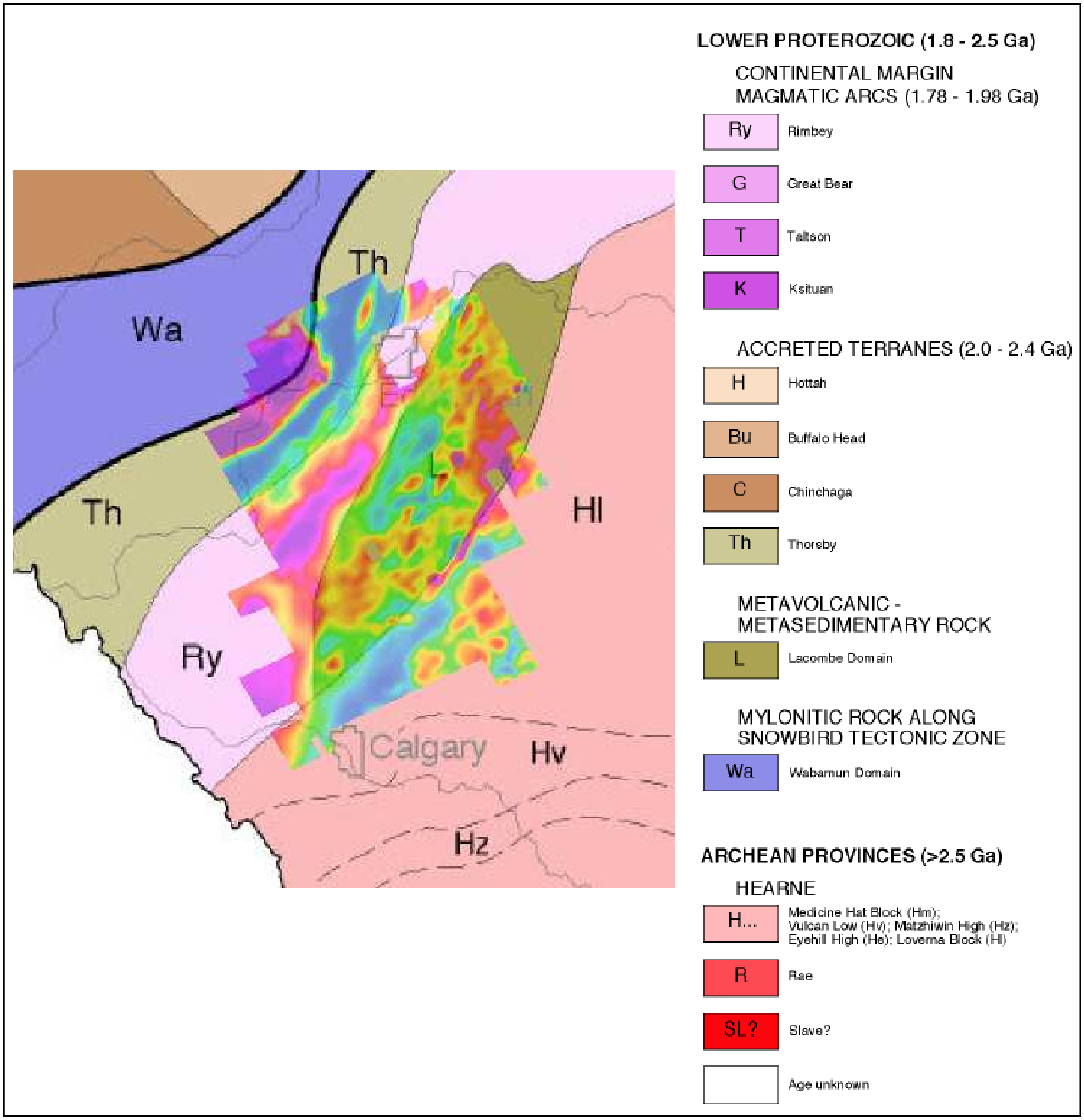

Figure 5: Precambrian basement tectonic features with the RMI superimposed.

From the figures on the previous pages there is a strong correlation between the Precambrian basement tectonic features and the magnetic data. However, there is little correlation between the magnetic data and the Phanerozoic tectonic features.

The predominant major mapped faults direction is NE-SW, as shown in Figure 6 below, but from the analysis of the magnetic data, there is also minor faulting trending E-W and NW-SE (see Figure 7 on the following page).

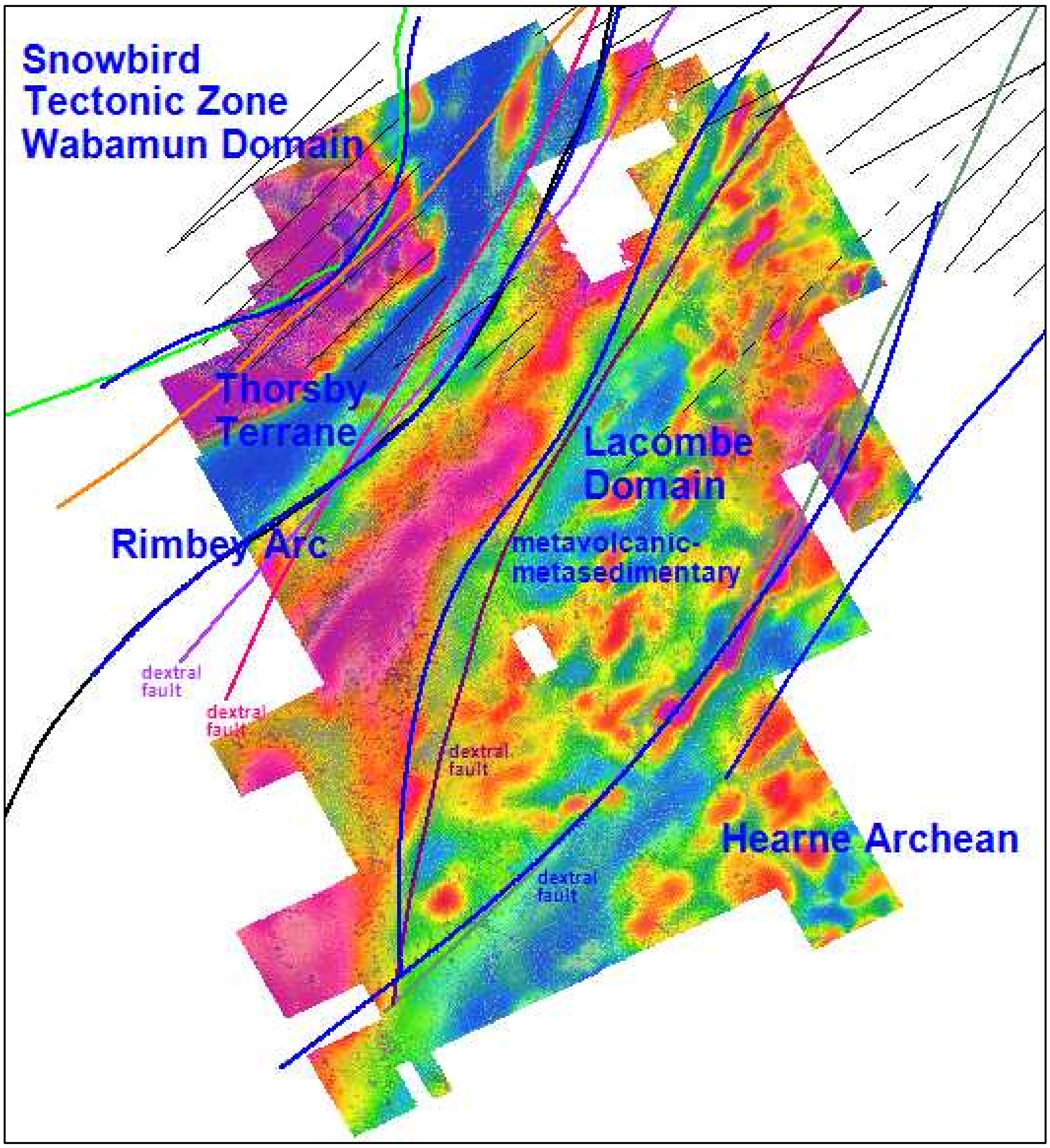

Figure 6: The mapped basement lineaments and major tectonic zones superimposed over the image of the RMI and 1st Vertical Derivative.

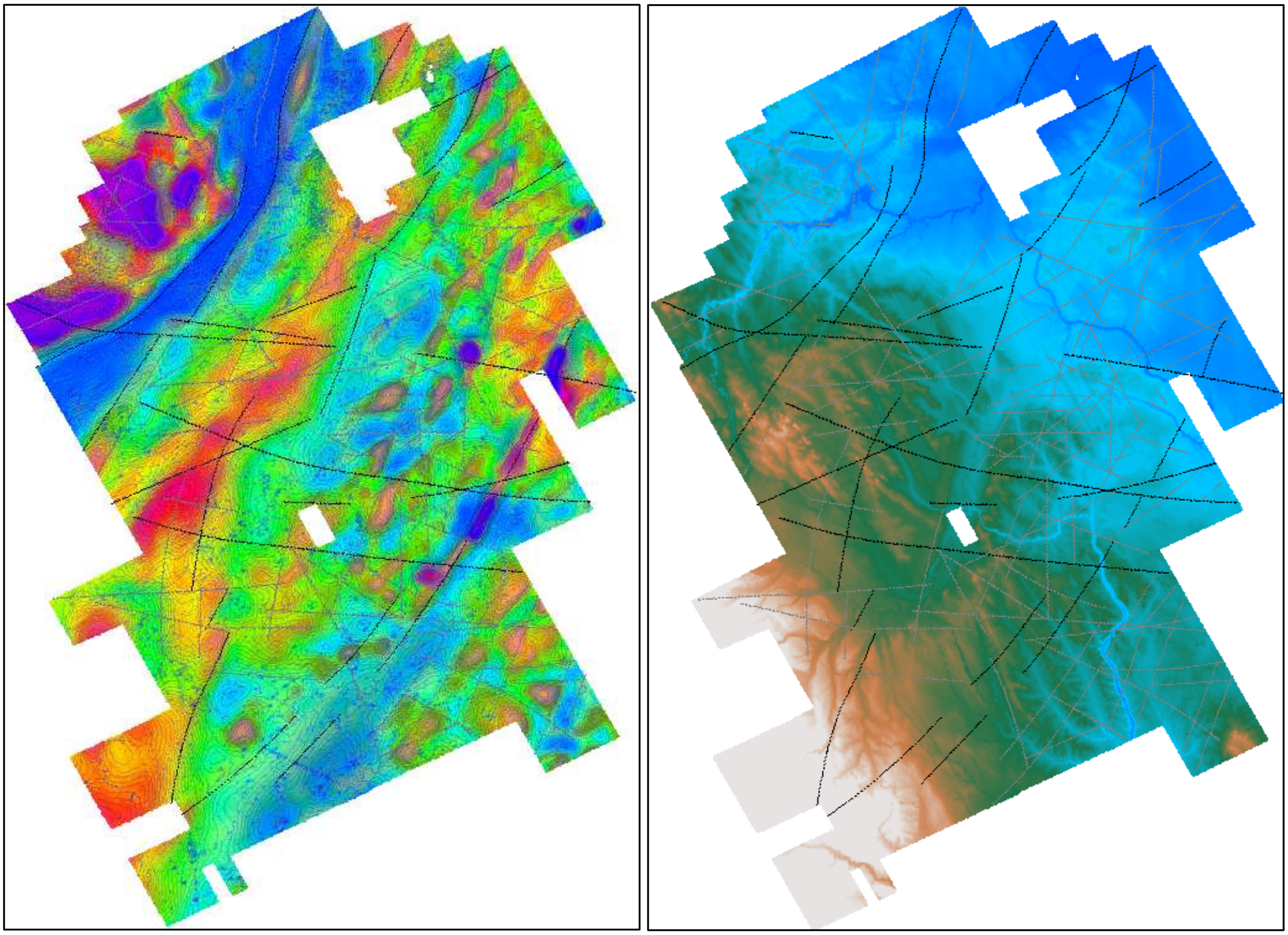

Figure 7: The proposed basement lineaments are superimposed over the image of the RMI and 1st Vertical Derivative (left) and the Digital Terrain Model (right).

There is some limited correlation between the proposed basement lineaments and the current topography which may suggest some reactivation of these proposed faults. The arrows in Figures 8 and 9 indicated areas of some correlation between the magnetic data and the buried bedrock valleys and sand and gravel deposits, and the several dashed lines on these figures indicate trends of the buried bedrock valleys and /or sand and gravel deposits which potentially correlate with large scale magnetic structures/offsets, which due to ambiguity have not be located on the interpretation map. These will also be shown in figures of the EM data later in the report, and discussed in more detail.

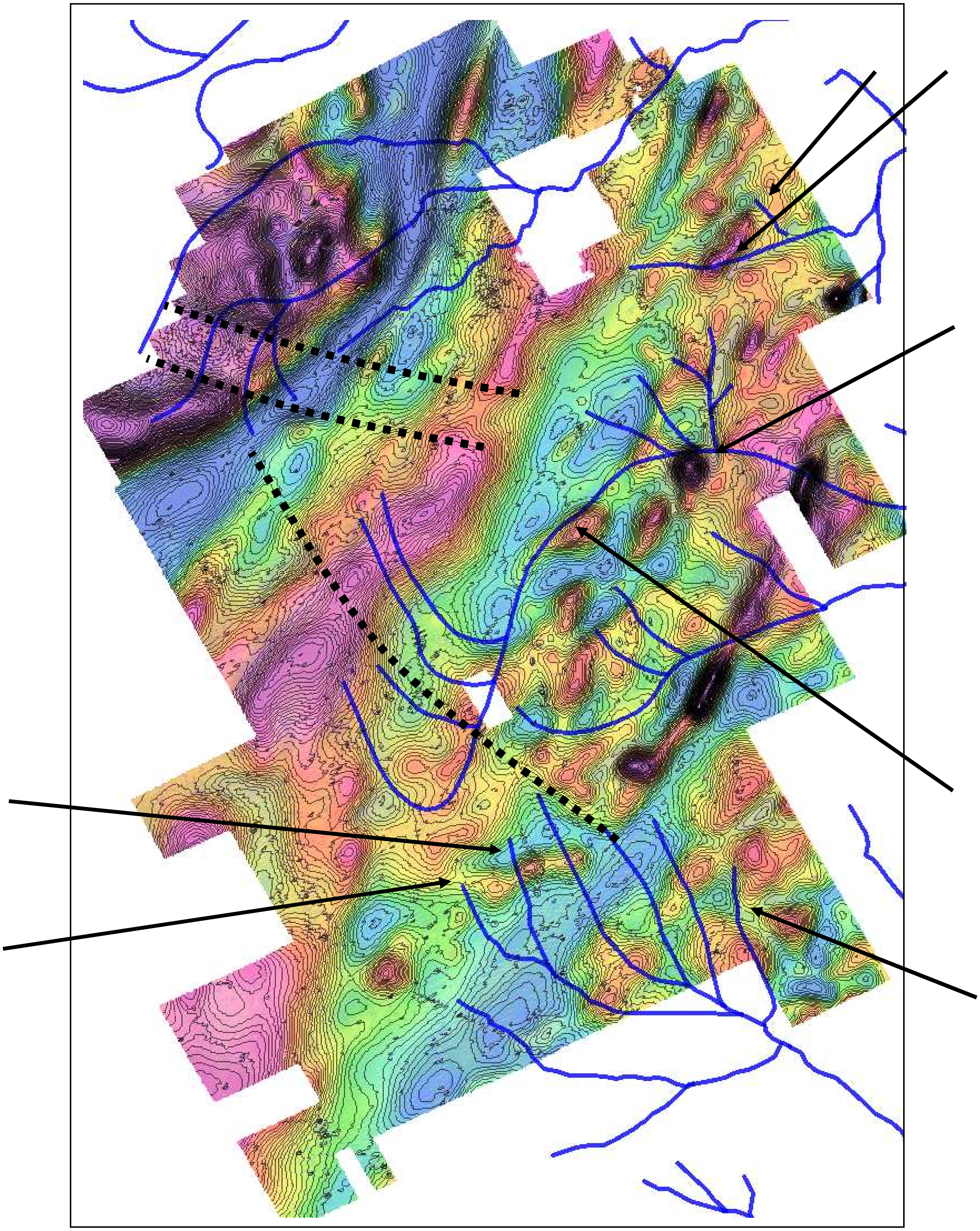

Figure 8: The buried bedrock valleys (thalwegs) are shown over the image of the RMI and 1st Vertical Derivative and magnetic contours.

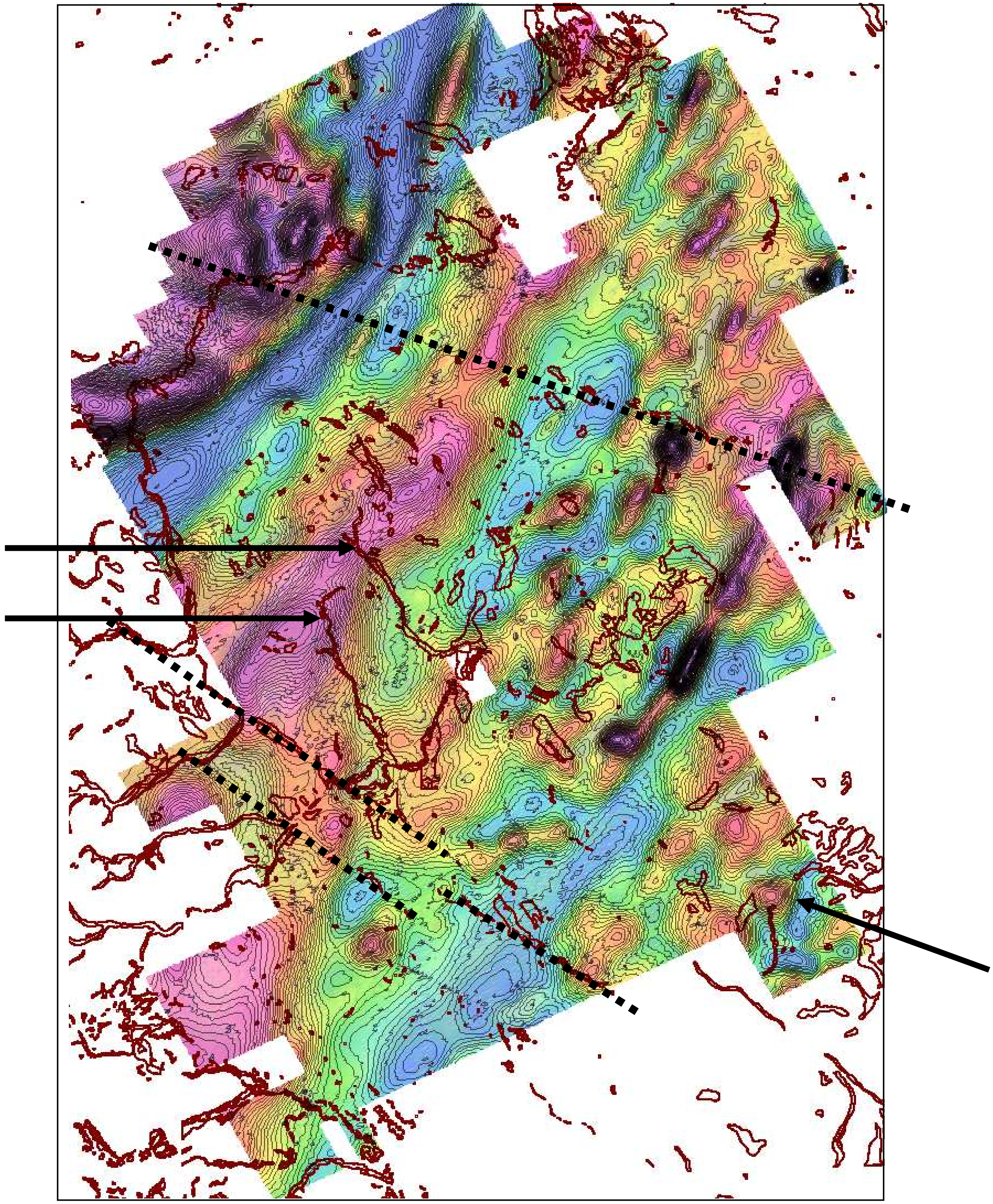

Figure 9: The sand and gravel deposits are shown over the image of the RMI and 1st Vertical Derivative and magnetic contours.

Overview of the Electromagnetic Response

Six optimal EM products were selected and generated from the data, these products are:

- Resistivity Depth slices at – 0, 10, 30, 60, 120 metres
- Apparent resistivity from dB/dt Z

The grids generated from these products were used in the interpretation, along with other grids, which will be shown throughout the report.

The grids were then incorporated into xyz files and a GEOSOFT voxel 3D cube. The grids relative to surface were sampled every 2 m, whereas the terrain corrected grids were sampled every 10 m, in order to maintain a useable file size. For internal use of the interpretation, the 3D cube was also converted to UBC format for use with the University of British Columbia's MeshTools3d application.

Apparent Resistivity

Fugro has developed an algorithm that converts the response in any measurement window (on or off-time) into an apparent resistivity. This is performed using a look-up table that contains the response at a range of half-space conductivities and altimeter heights.

The apparent resistivity for the present dataset was calculated (using dB/dt Z-Coil channels 1 – 20 for the Geotem data, and channels 1 – 30 for the Tempest data) to provide the maximum information on the near-surface resistivity of the ground which, when combined with the magnetic signature, provides good geological mapping.

Resistivity-Depth-Images (RDI)

The Resistivity-Depth-Image (RDI) sections were calculated from the B-Field Z-coil response, using an algorithm that converts the response in any measurement window (on- or off-time) into resistivity. For on-time data, it is not straightforward to identify which depth the apparent resistivity is associated, or identify any variation in resistivity with depth. Hence, the earth is assigned a constant value from surface to depth.

However, for the off-time data, the apparent resistivity can be associated with a depth. This depth, δ, depends on the magnetic permeability μ, the delay time t of the measurement window and the estimated apparent conductivity σ_{app}, i.e.

$$\delta = 0.55\sqrt{\frac{t}{\mu\sigma_{app}}}\ .$$

The electromagnetic method is most sensitive to conductive features so resistive features will be poorly resolved. The process of converting voltage data to resistivity as a function of depth tends to create smoother depth variations than can occur in reality.

The RDI sections were derived from each survey line, relative to surface. An additional set of RDI sections were created that have been corrected for altitude variations such that the top of each section reflects the true terrain topography. The resistivity values were gridded to provide resistivity-depth slices for desired depths.

Electromagnetic Interpretation Discussion

The objectives of this general overview interpretation are two fold:

- If possible determine the thickness of the Paskapoo formation, and;
- locate areas of potential aquifers within the Edmonton-Calgary corridor

The images in Figure 10-14 below and on the following pages indicate that it may be possible to tentatively define the boundary between the Paskapoo and the earlier formations i.e. Scollard, Battle-Whitemud, Horseshoe Canyon etc. It appears that the transition occurs approximately at the 10 ohm-m resistivity. Figure 12 shows depth slices relative to surface, and using this transition value, the images suggest that the Paskapoo formation exceeds a thickness of 260 m, along the western survey boundary.

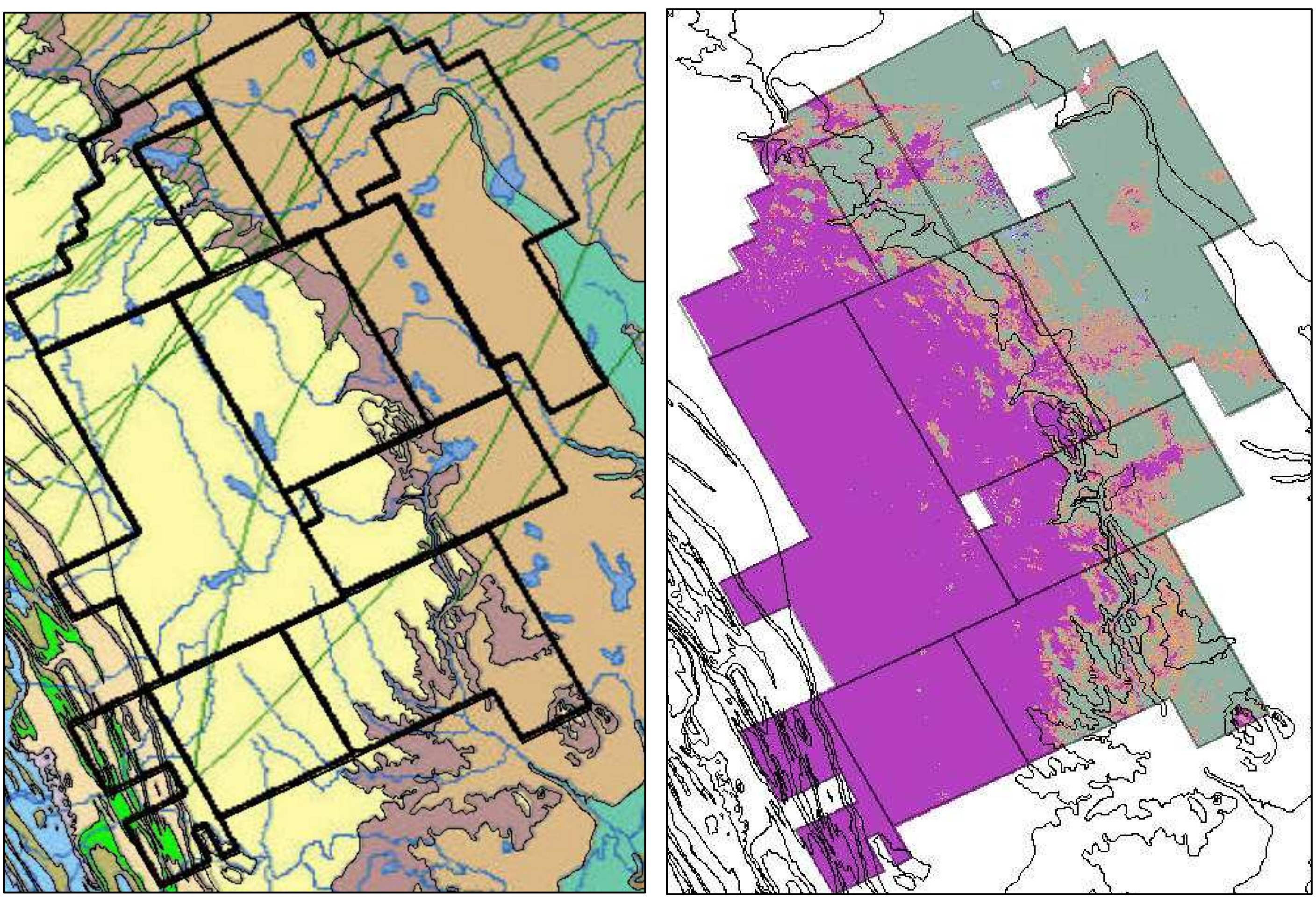

Figure 10: Bedrock geology left (see also Figure 3); depth slice of 40 m superimposed over a depth slice of 70 m relative to surface, truncated at 10 ohm-m (right).

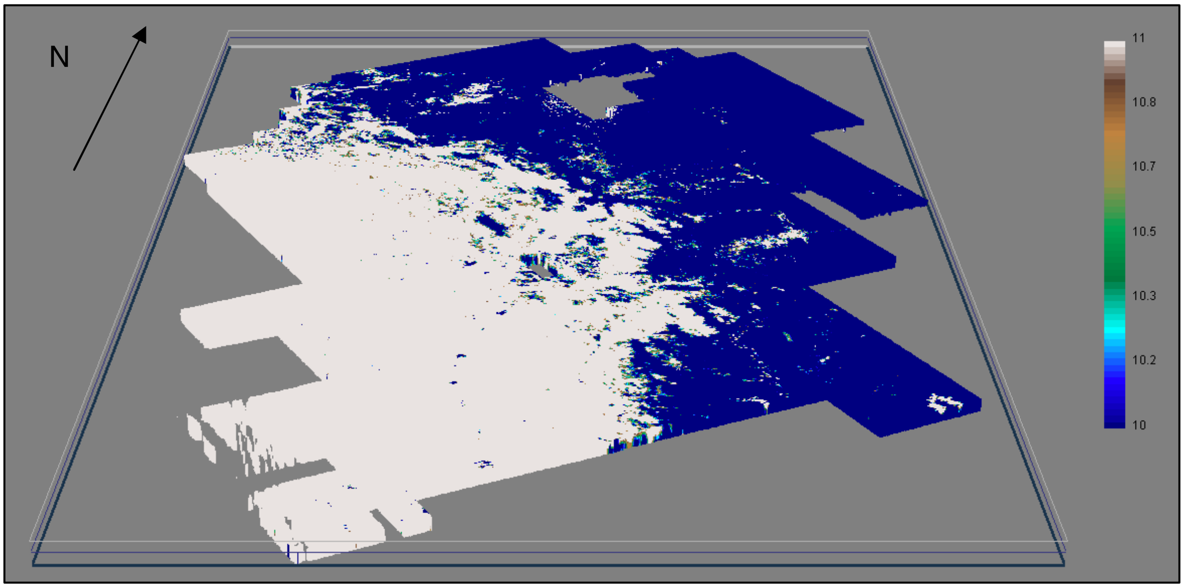

Figure 11: MeshTools3D cube (relative to surface) at a depth of 60 m below surface looking from the south (above). The image shows the entire range of resistivity's limited to a colour range of between 10 and 11 ohm-m. The colour change closely matches the proposed sub-crop boundary between the Paskapoo and Scollard formations. The vertical exaggeration is x50.

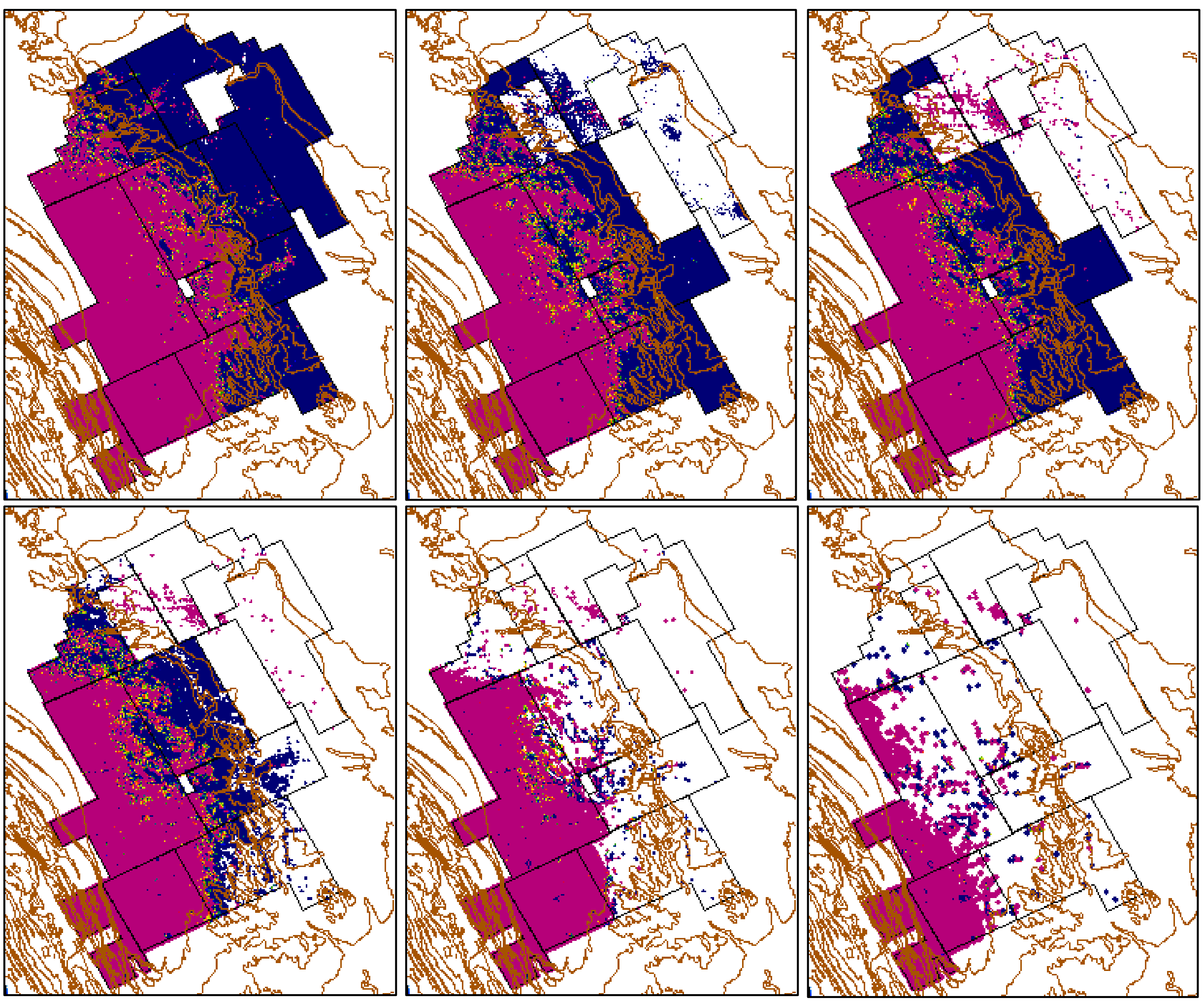

Figure 12: Resistivity depth slices relative to surface. Top row from left to right: 60m, 100m, and 140m depth; Bottom row from left to right: 80m, 220m, and 260m depth

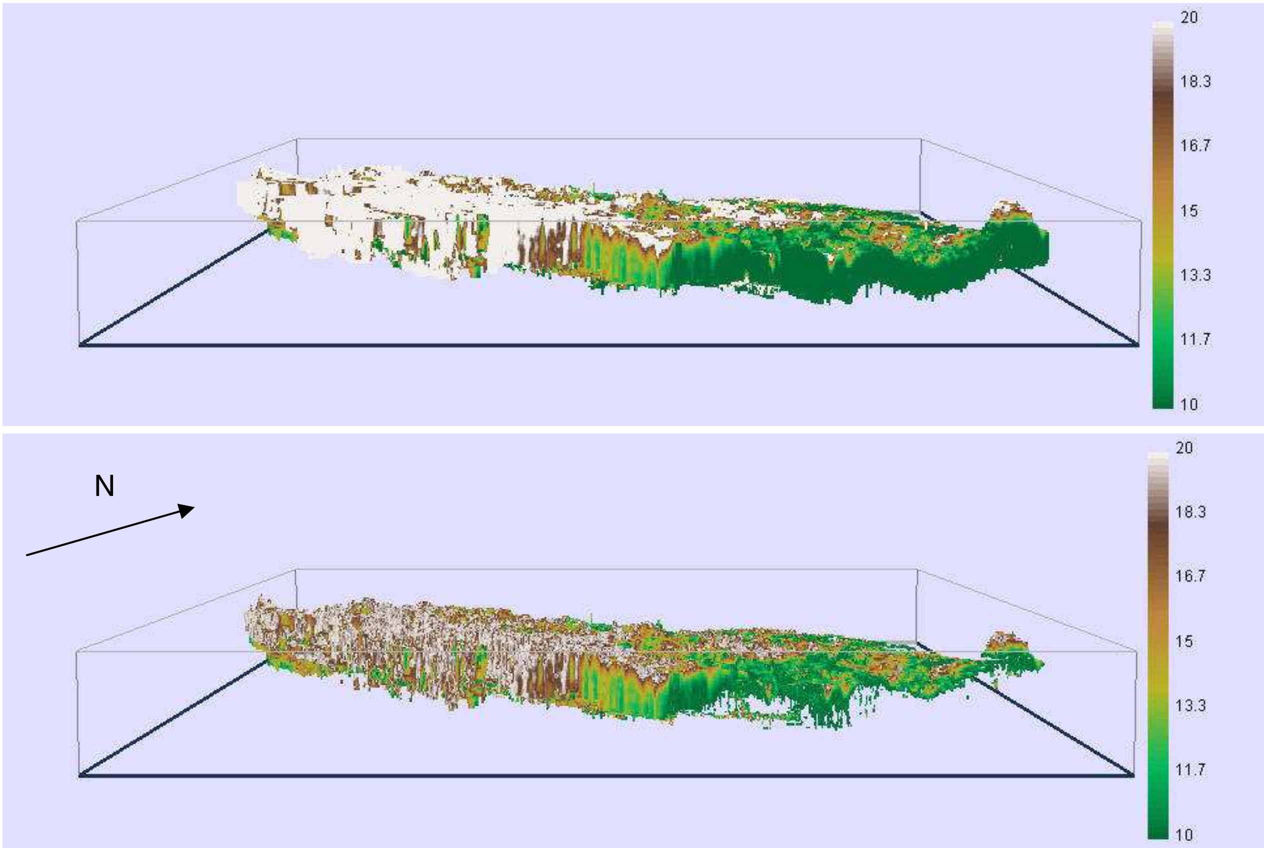

Figure 13: Terrain corrected 3D cubes looking from the south (above) and west (below) from elevations of 550 to 1100 m. The above and below top images show the entire range of resistivities, whereas the above and below lower images show only those resistivities in the 10-20 ohm-m range. The sudden change in resistivity in the centre of the images above may represent the Paskapoo / Scollard boundary. The vertical exaggeration is x50.

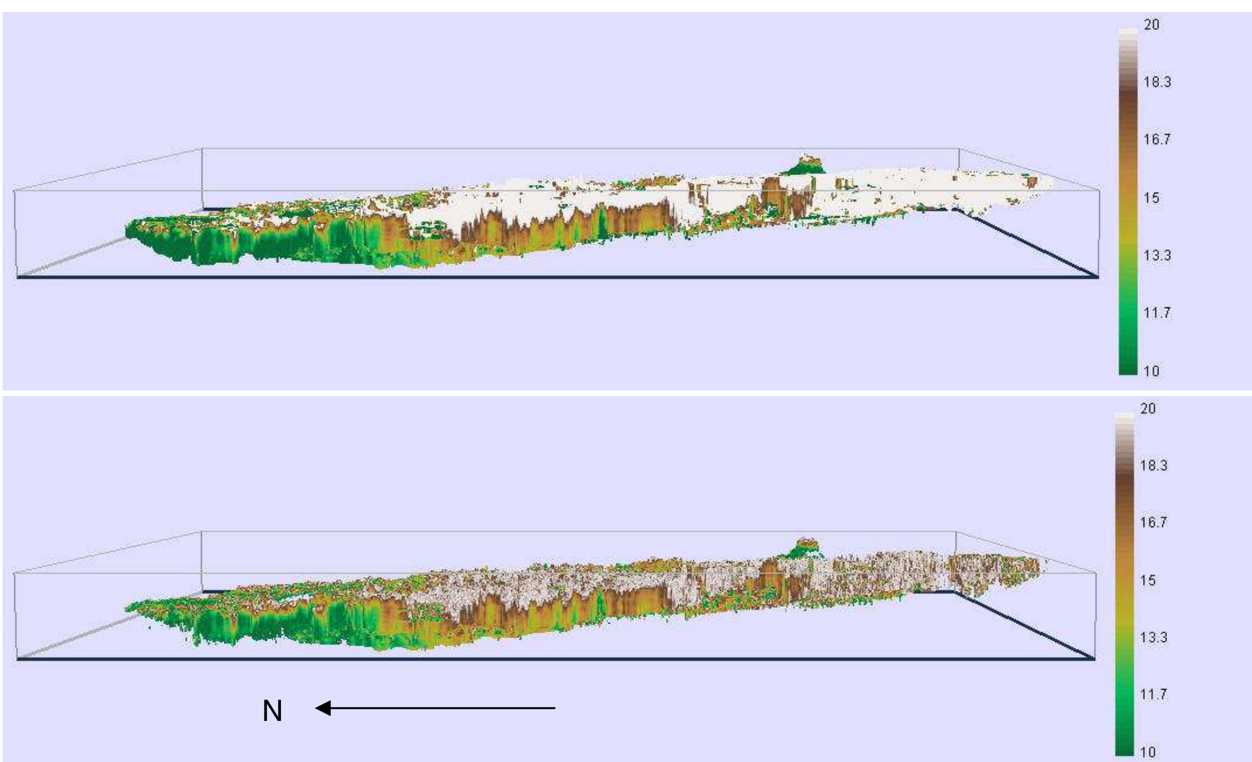

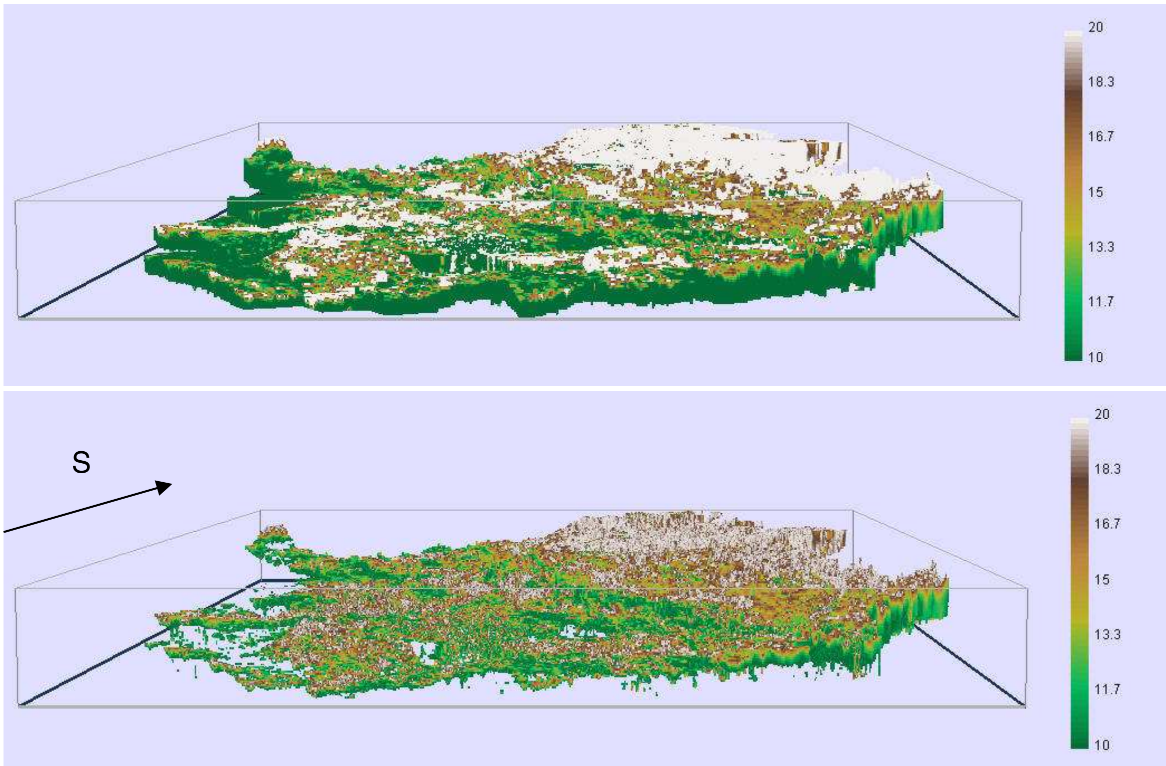

Figure 14: Terrain corrected 3D cubes looking from the north (above) and east (below) from elevations of 550 to 1100 m. The above and below top images show the entire range of resistivities, whereas the above and below bottom images show only those resistivities in the 10-20 ohm-m range. The vertical exaggeration is x50.

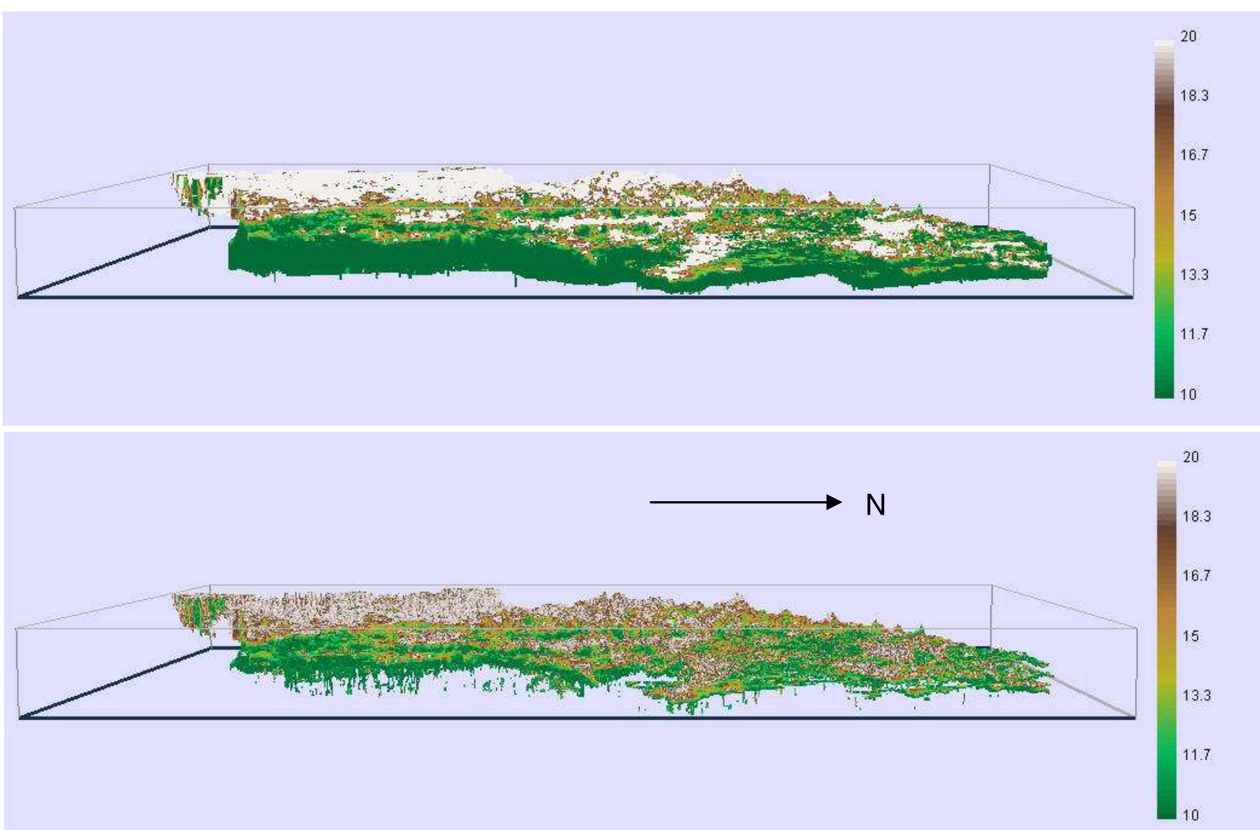

Figure 15: Bedrock geology outlines shown over the 680 m elevation resistivity slice, showing a good correlation between the lower resistivity and the mapped boundaries of the Scollard formation.

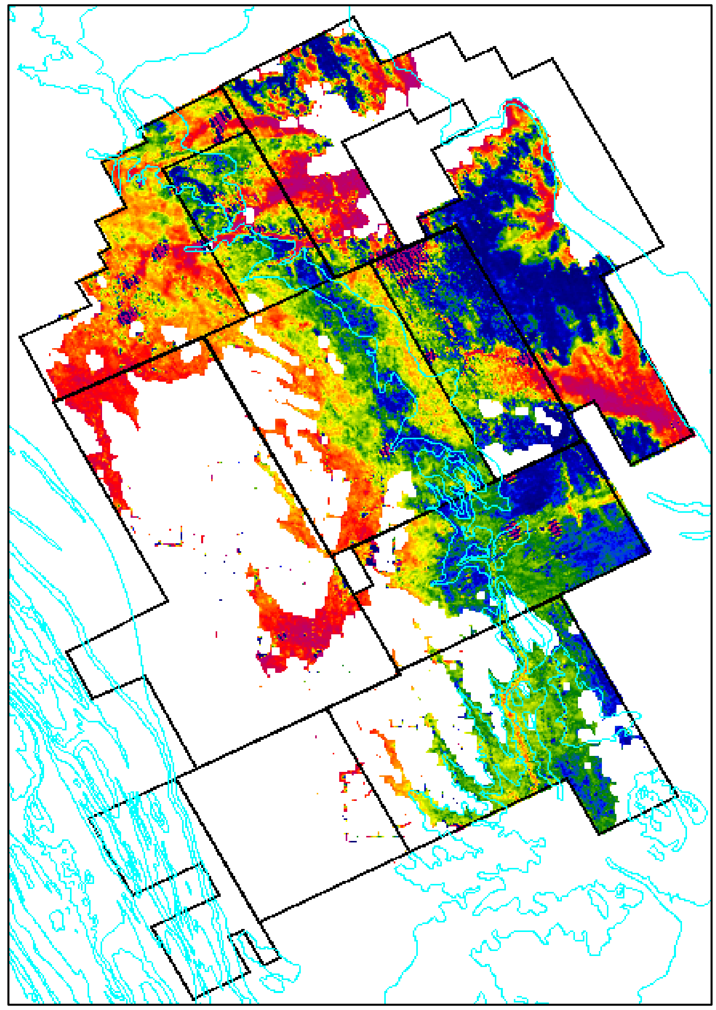

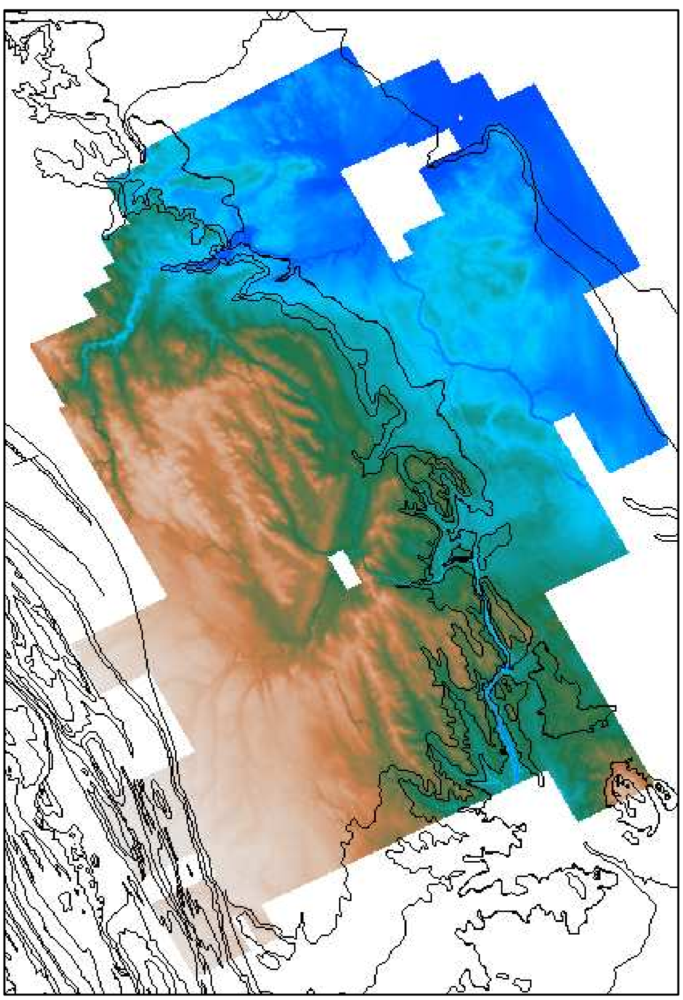

Figure 16: Bedrock geology boundaries shown over the Digital Terrain Model - it is likely that the mapped geology has been derived from the DTM perhaps…..

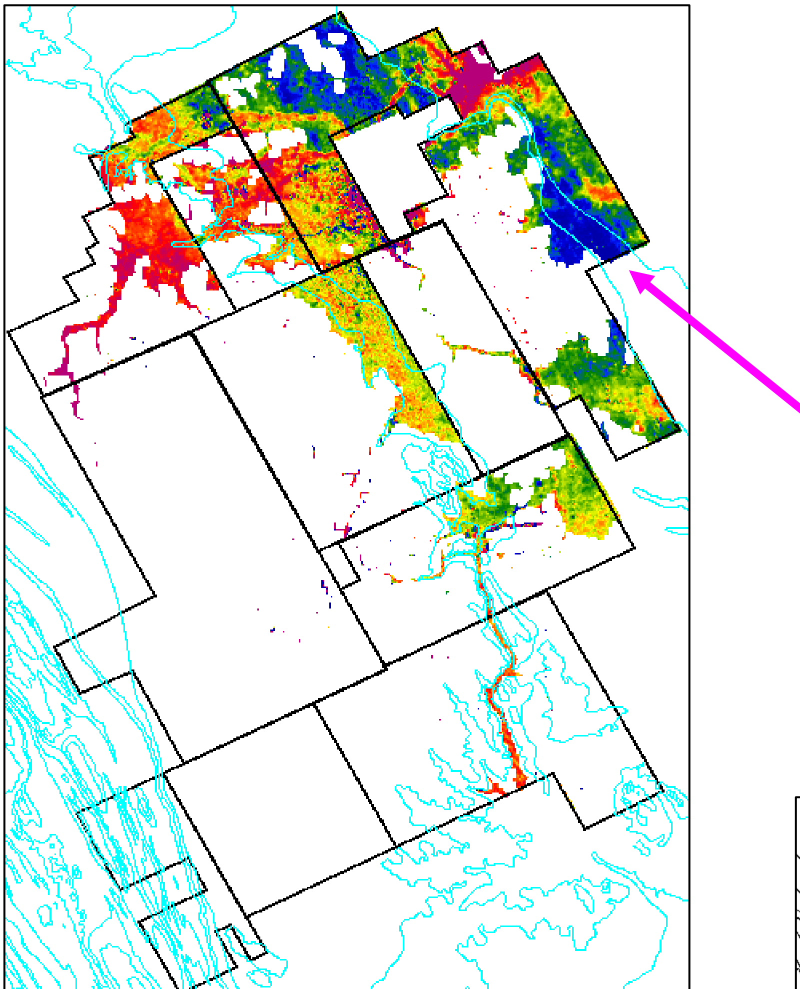

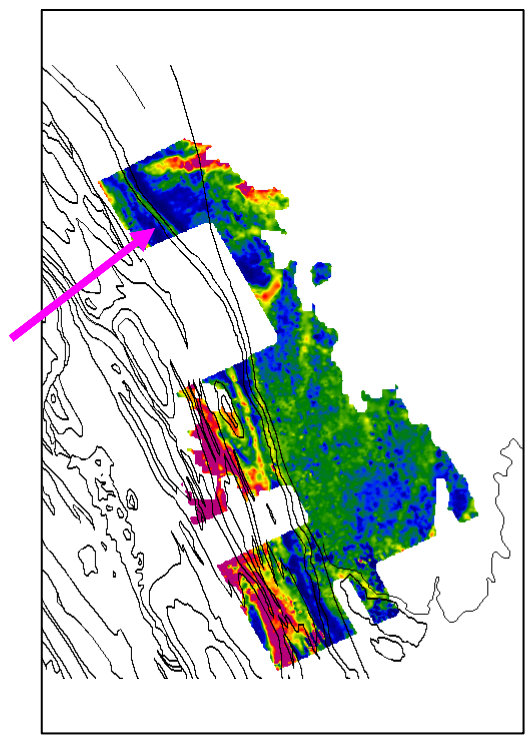

Figure 17: Bedrock geology outlines shown over the 600 m elevation resistivity slice (above) and the 1100 m elevation resistivity slice (right) showing the correlation between the geology and the EM.

Figure 16 shows a close correlation between the DTM and bedrock geology, suggesting perhaps that the mapped geologic boundaries have been determined in part from the current topography. The arrows in Figure 17 point to areas of correlation between the mapped bedrock geology and the EM data.

Figure 18 shows the location of geological cross-sections taken from several Regional Groundwater Assessment Reports, these are as follows:

- Red Deer County, Part of the Red Deer River Basin, tP 034 to 039, R 21 to 28, W4Mand Tp 034 to 039, R 01 to 04, W5M, Regional Groundwater Assessment, May 2006
- Ponoka County, Part of the North Saskatchewan and South Saskatchewan River Basins, Tp 041 to 044, R 22 to 28, W4M & Tp 041 to 045, R 01 to 05, W5M, Regional Groundwater Assessment, September 2003
- County of Stettler No. 6, Part of the Red Deer River and Battle River Basins, Parts of Tp 033 to 042, R 14 to 22, W4M, Regional Groundwater Assessment, November 1999
- M.D. of Rocky View No. 44, Part of the South Saskatchewan River Basin, Tp 021 to 029, R 25 to 29, W4M & Tp 023 to 029, R 01 to 06, W5M, Regional Groundwater Assessment, March 2002

All RDI images in the cross-sections to follow were taken from the terrain corrected Geosoft voxel. Several of the RDI images show a slab rather than a slice, due to the fact that the cross-sections appear at an angle and are not directly north-south or east-west.

Figures 19 to 26 are the cross-sections from the Ponoka County. Figures 22-26 show the change in resistivity between the Paskapoo and the earlier formations. Figures 20 and 21 show the location of features of interest ⑩ which are discussed later in the report.

Figure 27 is the cross-sections from the Stettler County which shows a good correlation between the surface deposits and the higher resistivity in the RDI image.

Figures 28 to 33 are the cross-sections from Red Deer County.

Figures 34 to 36 are the cross-sections from M.D. Rocky View.

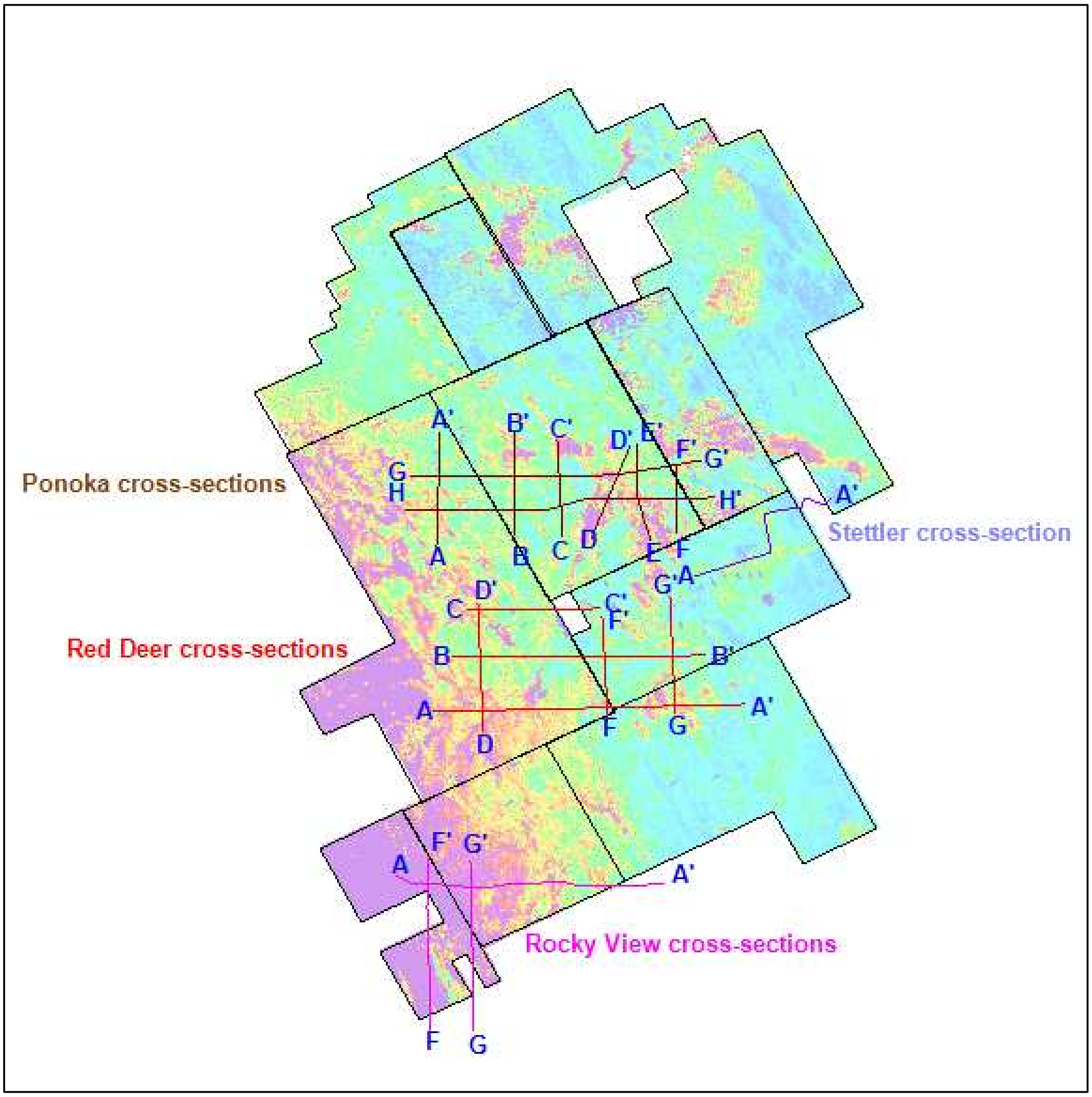

Figure 18: Showing cross-sections within the survey area shown over the resistivity relative to surface

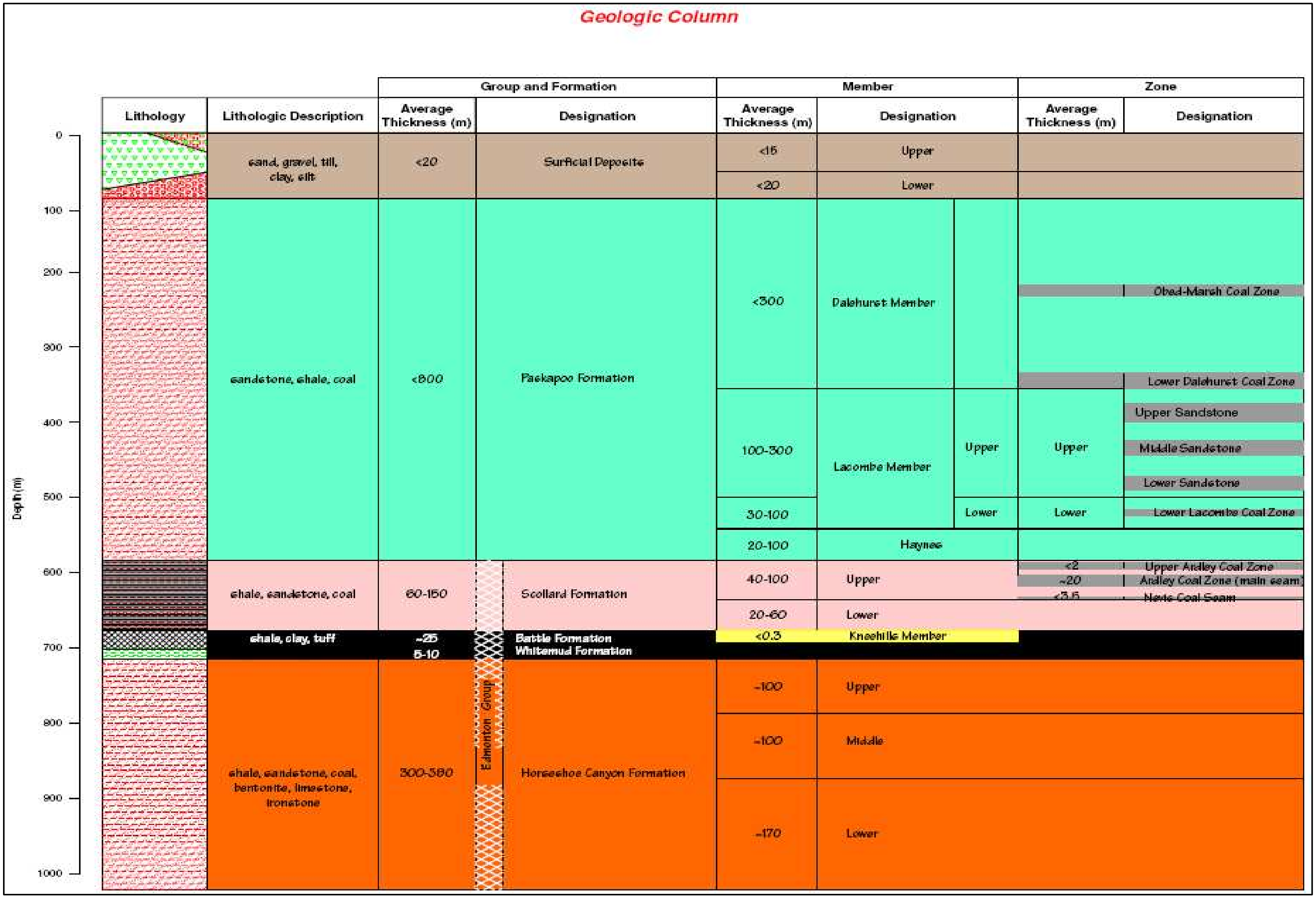

Table 1: Geologic Column. This was taken from the Red Deer Regional Groundwater Assessment Report. It is relevant for all following cross-sections; however the surficial deposit thicknesses will vary from county to county.

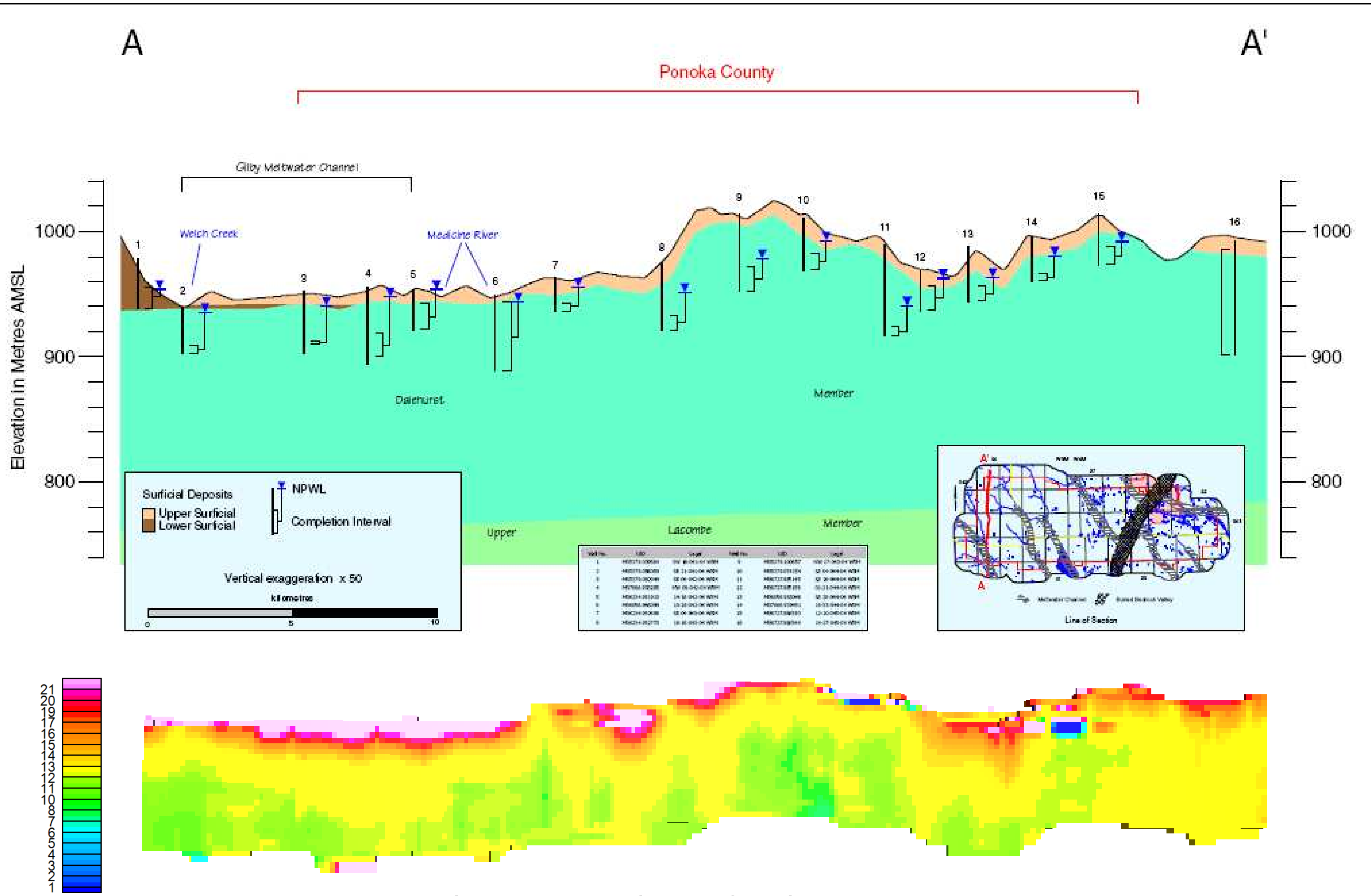

Figure 19: Cross-section A-A' of Ponoka County

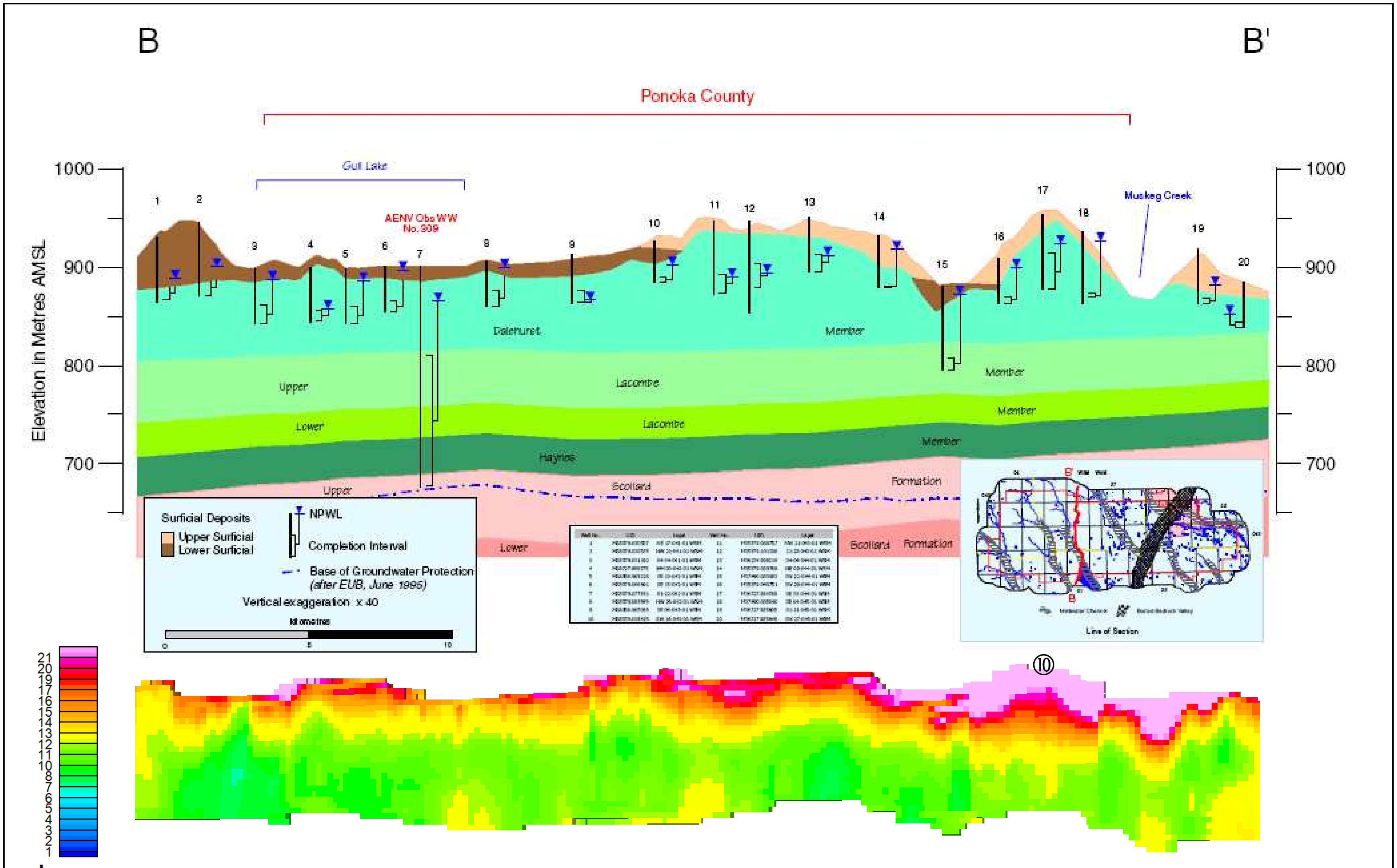

Figure 20: Cross-section B-B' of Ponoka County

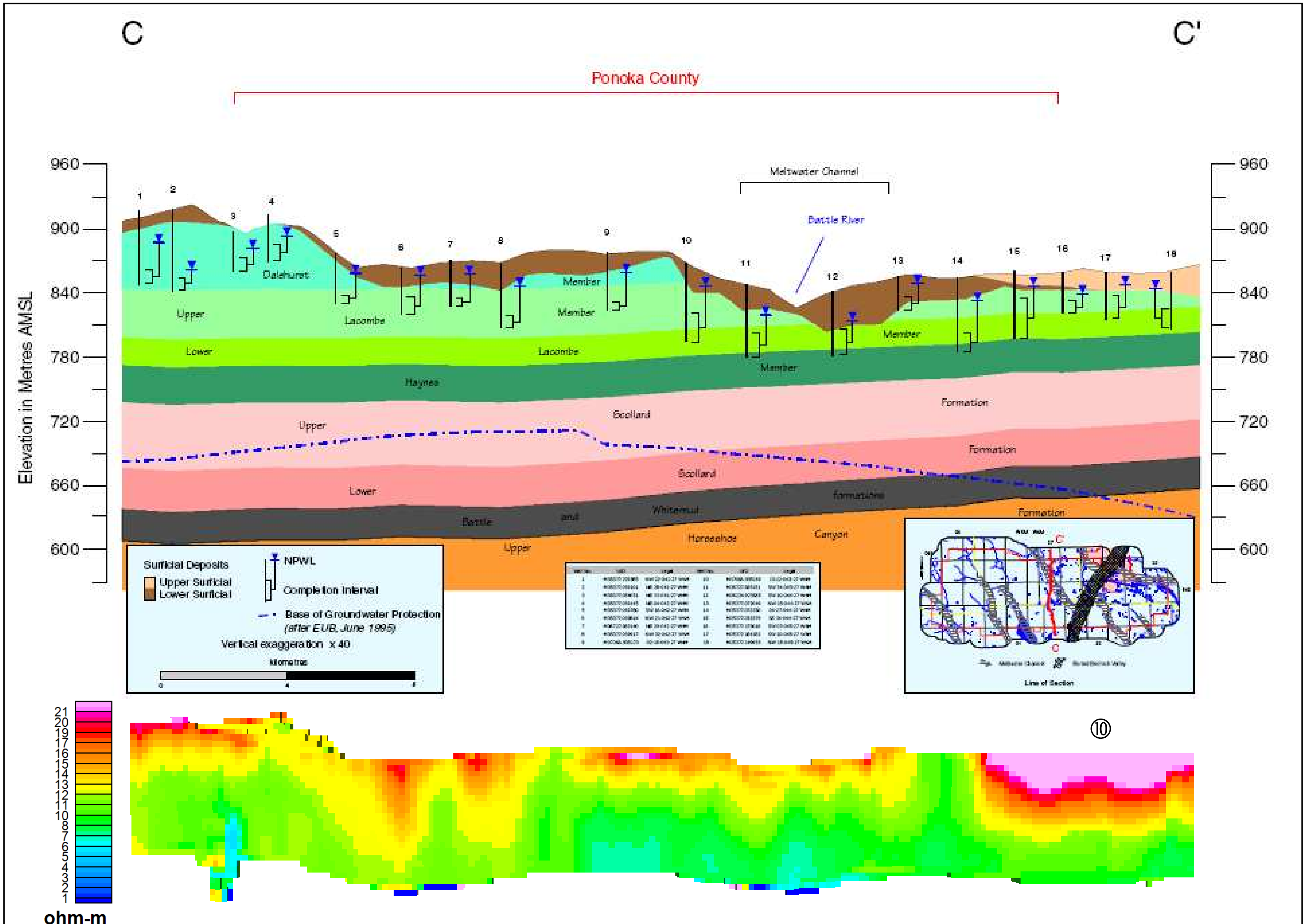

Figure 21: Cross-section C-C' of Ponoka County

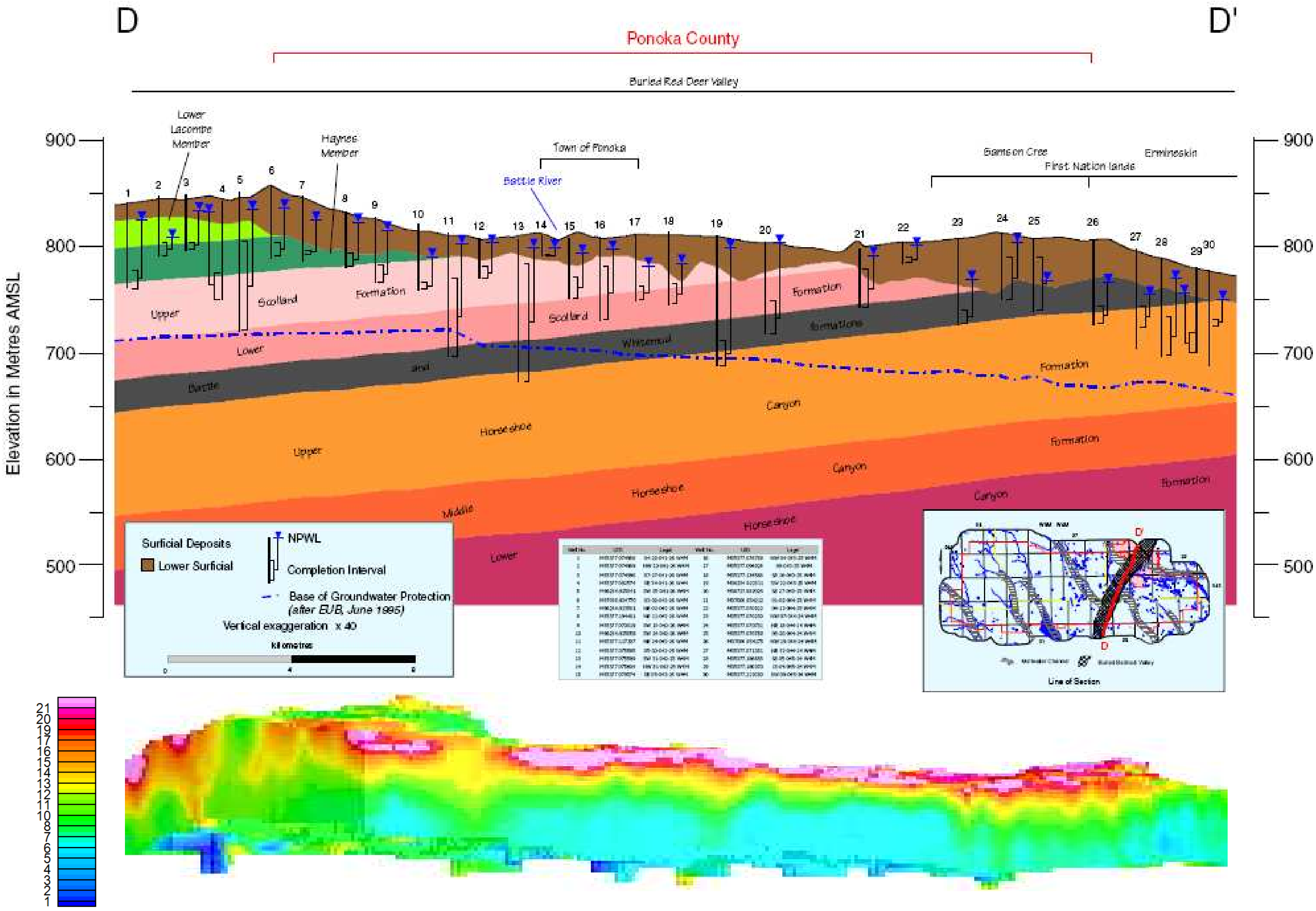

Figure 22: Cross-section D-D' of Ponoka County

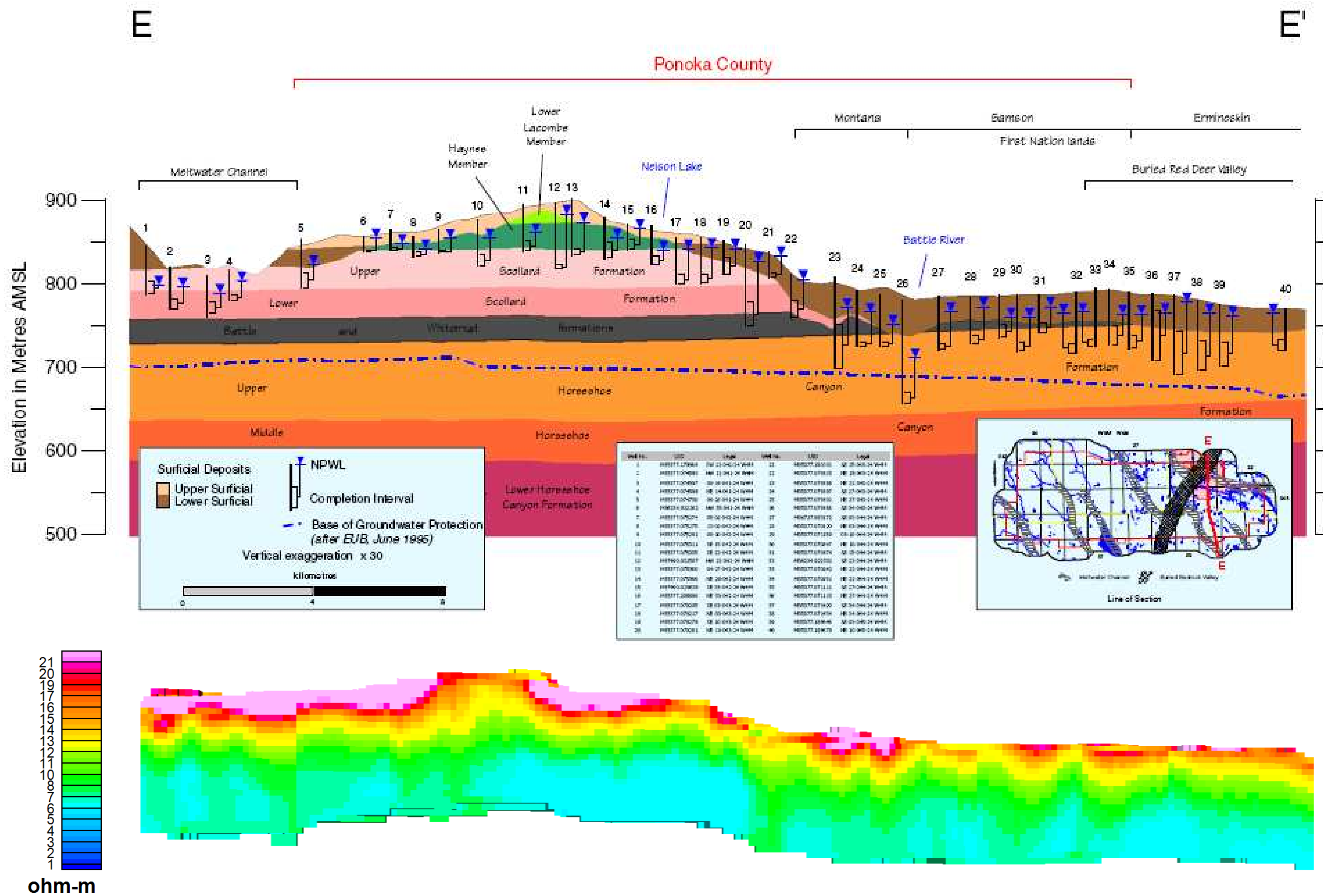

Figure 23: Cross-section E-E' of Ponoka County

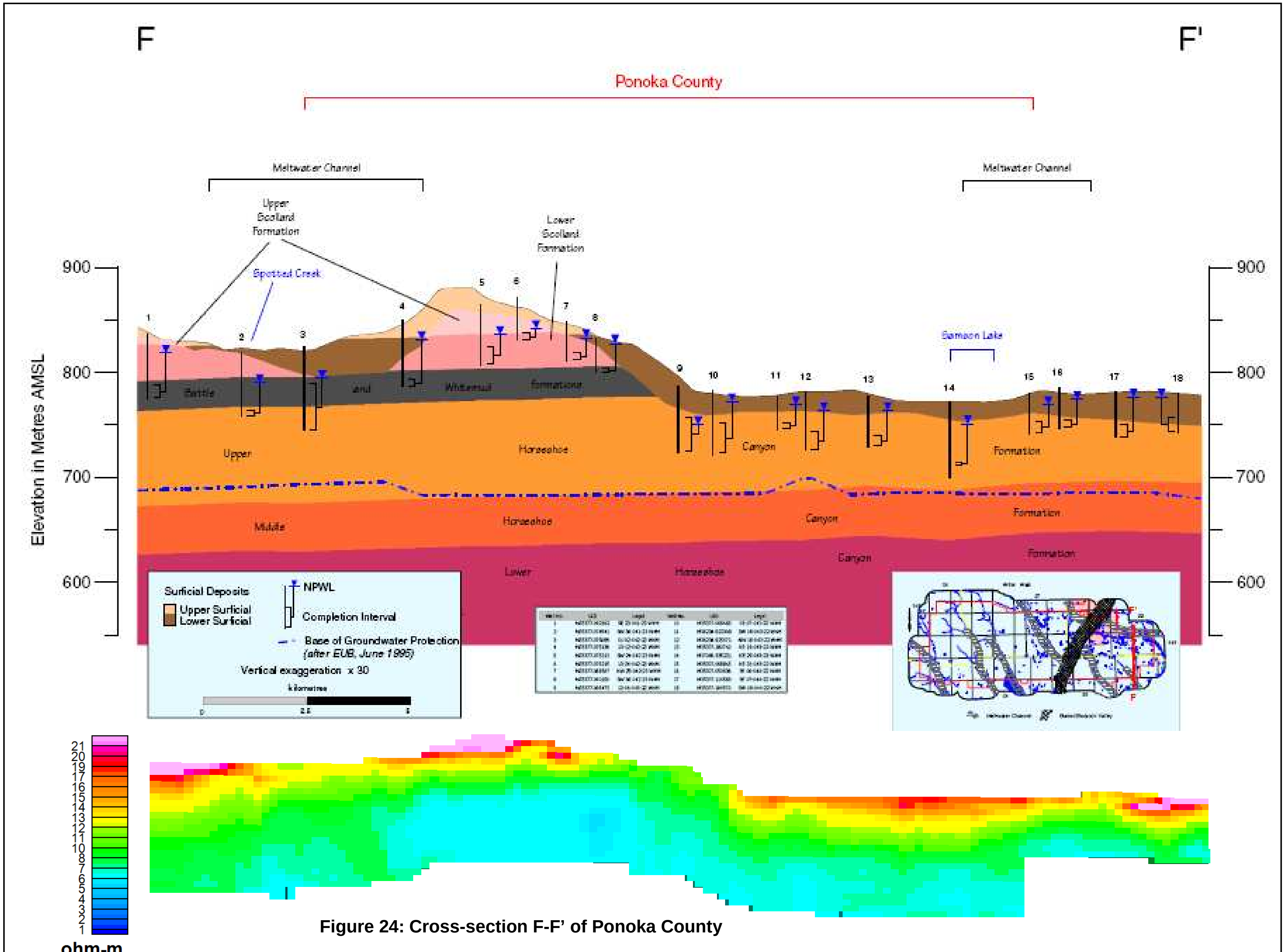

Figure 24: Cross-section F-F' of Ponoka County

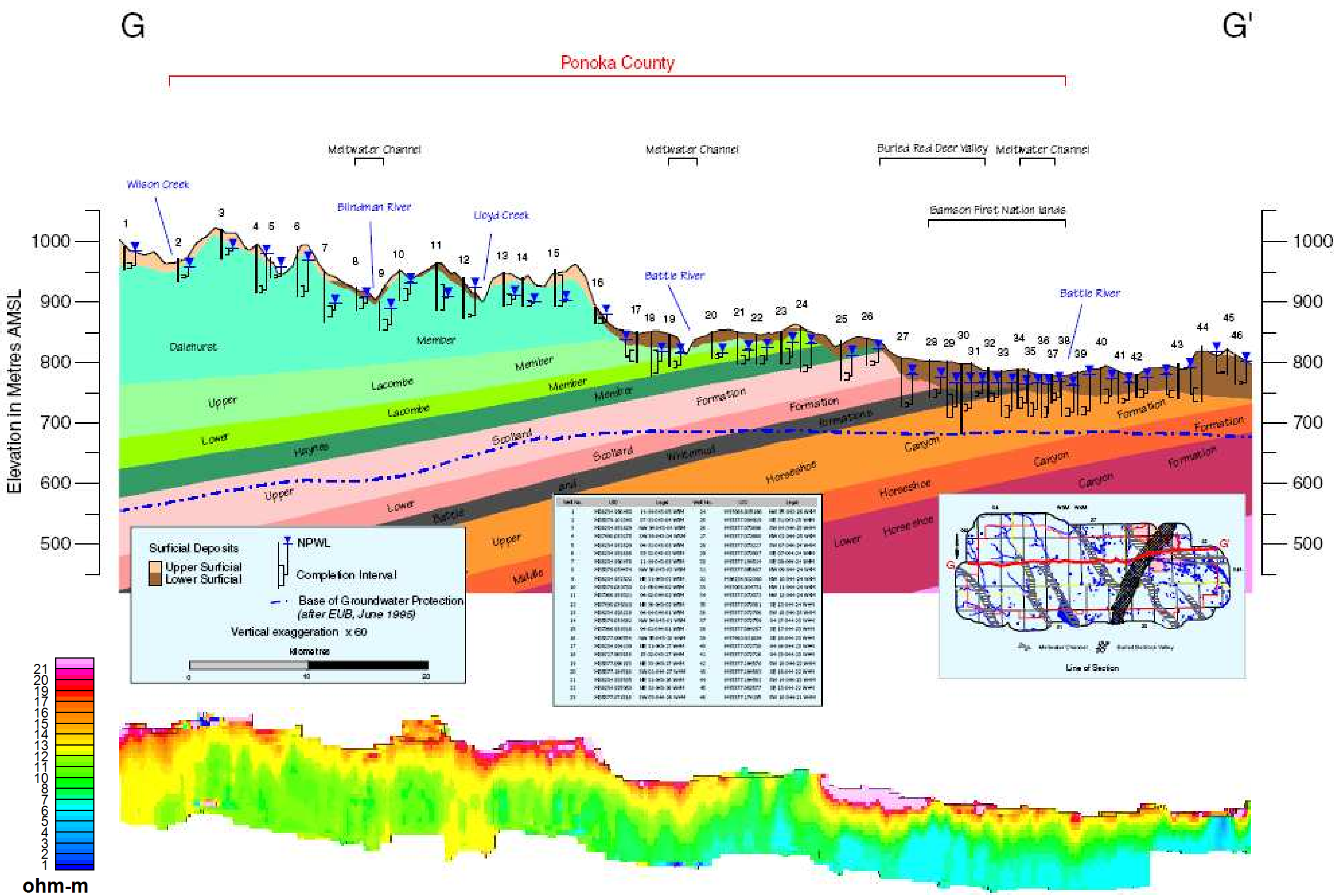

Figure 25: Cross-section G-G' of Ponoka County

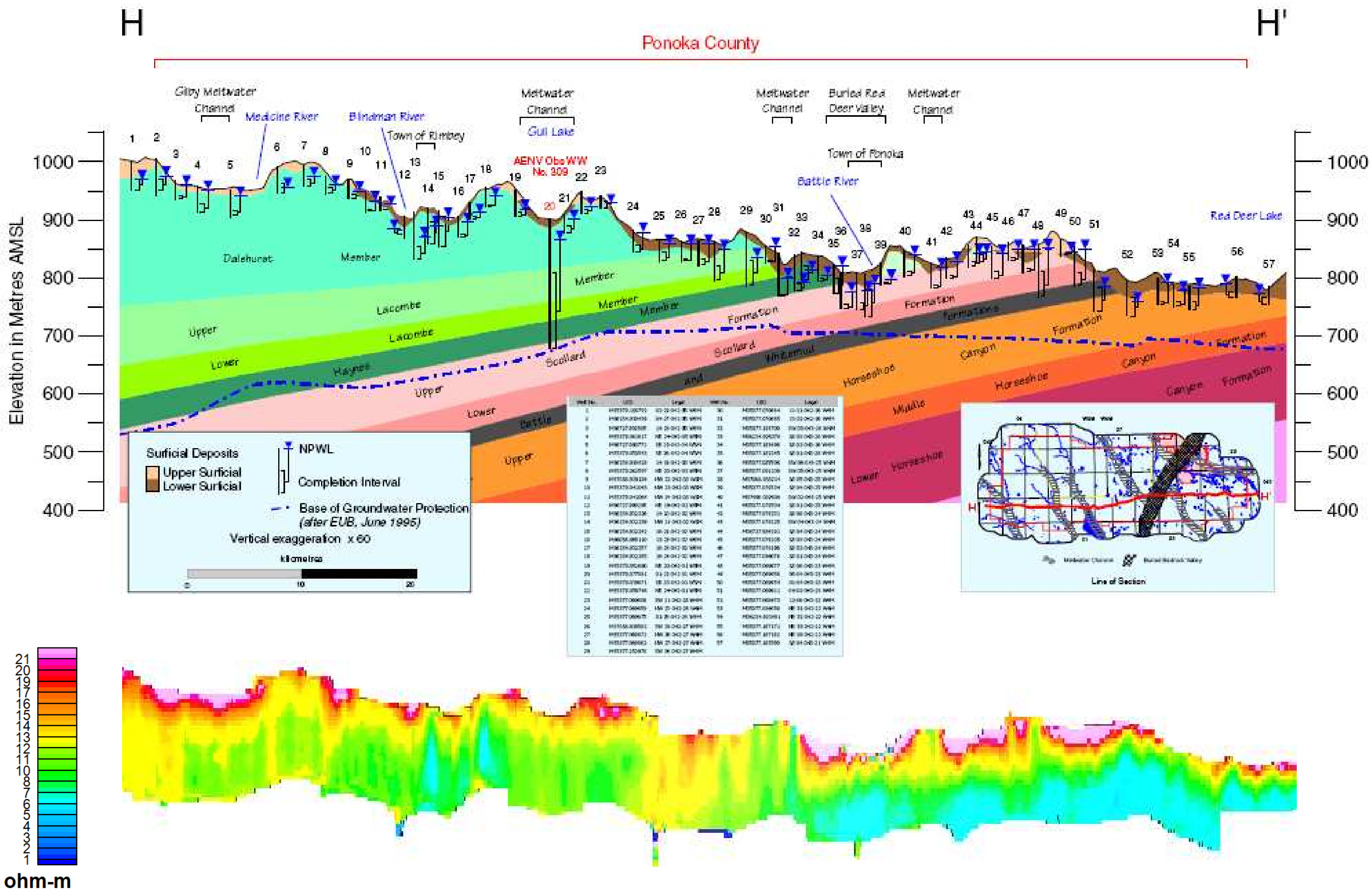

Figure 26: Cross-section H-H' of Ponoka County

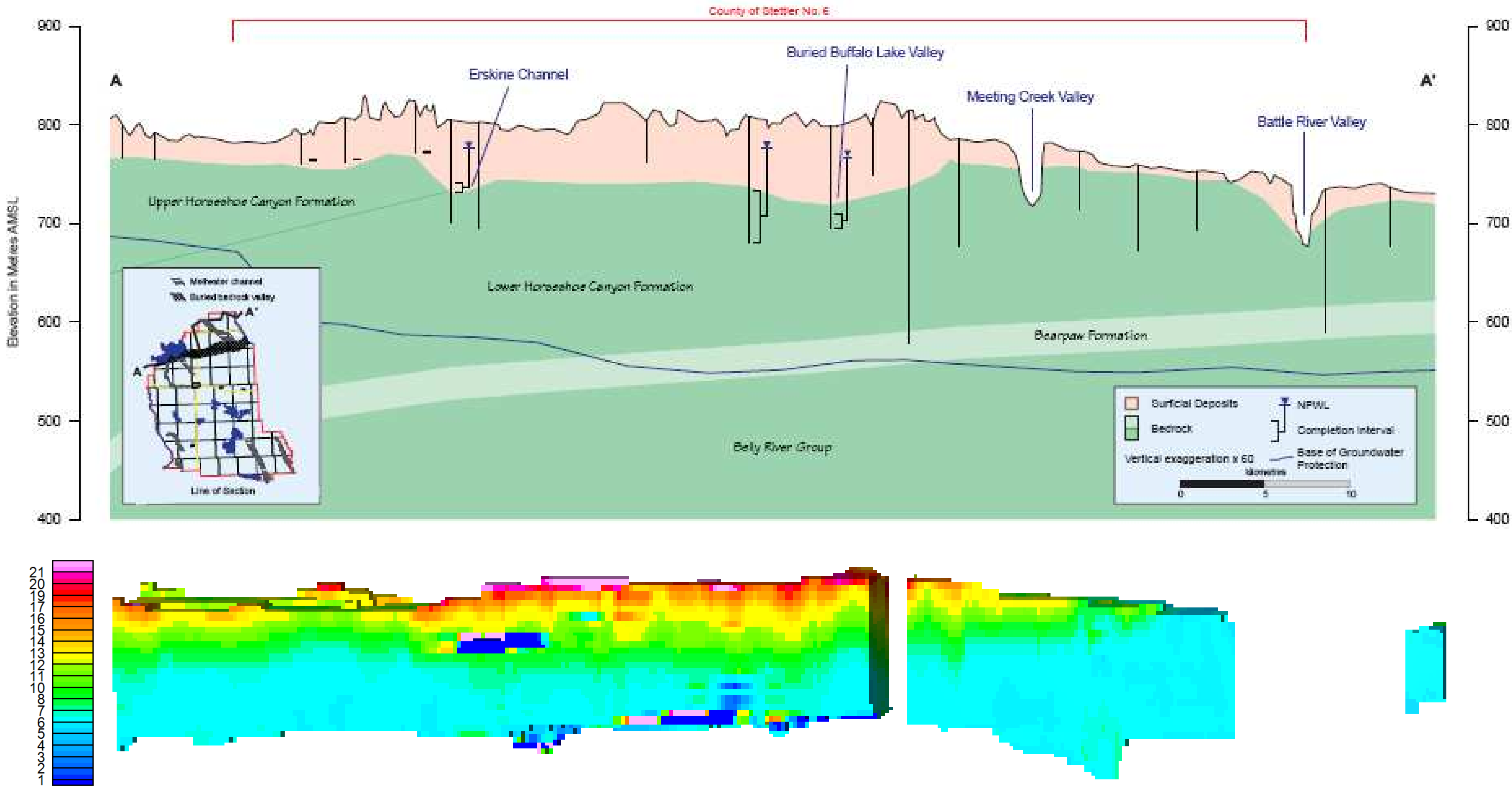

Figure 27: Cross-section A-A' of Stettler County

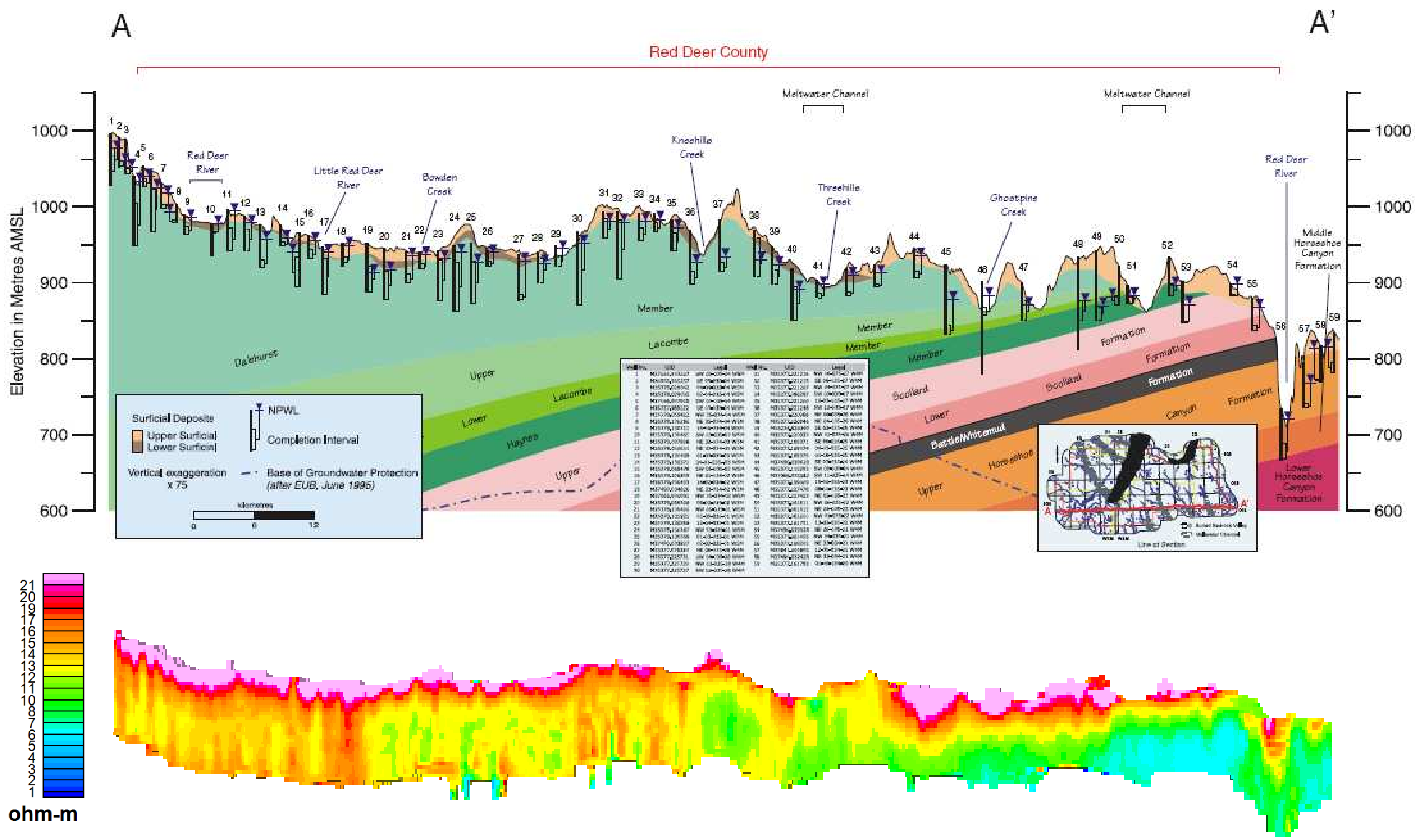

Figure 28: Cross-section A-A' of Red Deer County

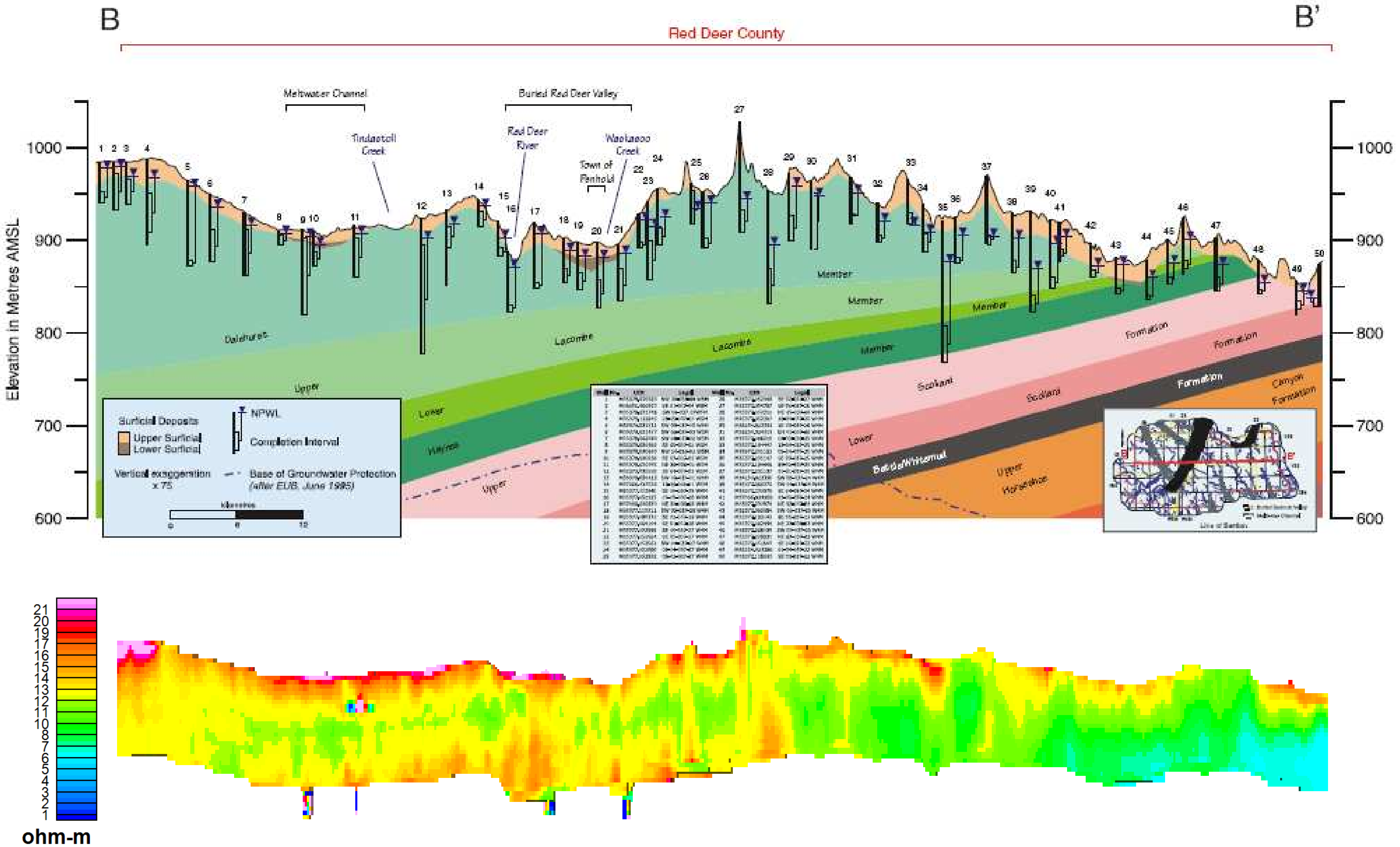

Figure 29: Cross-section B-B' of Red Deer County

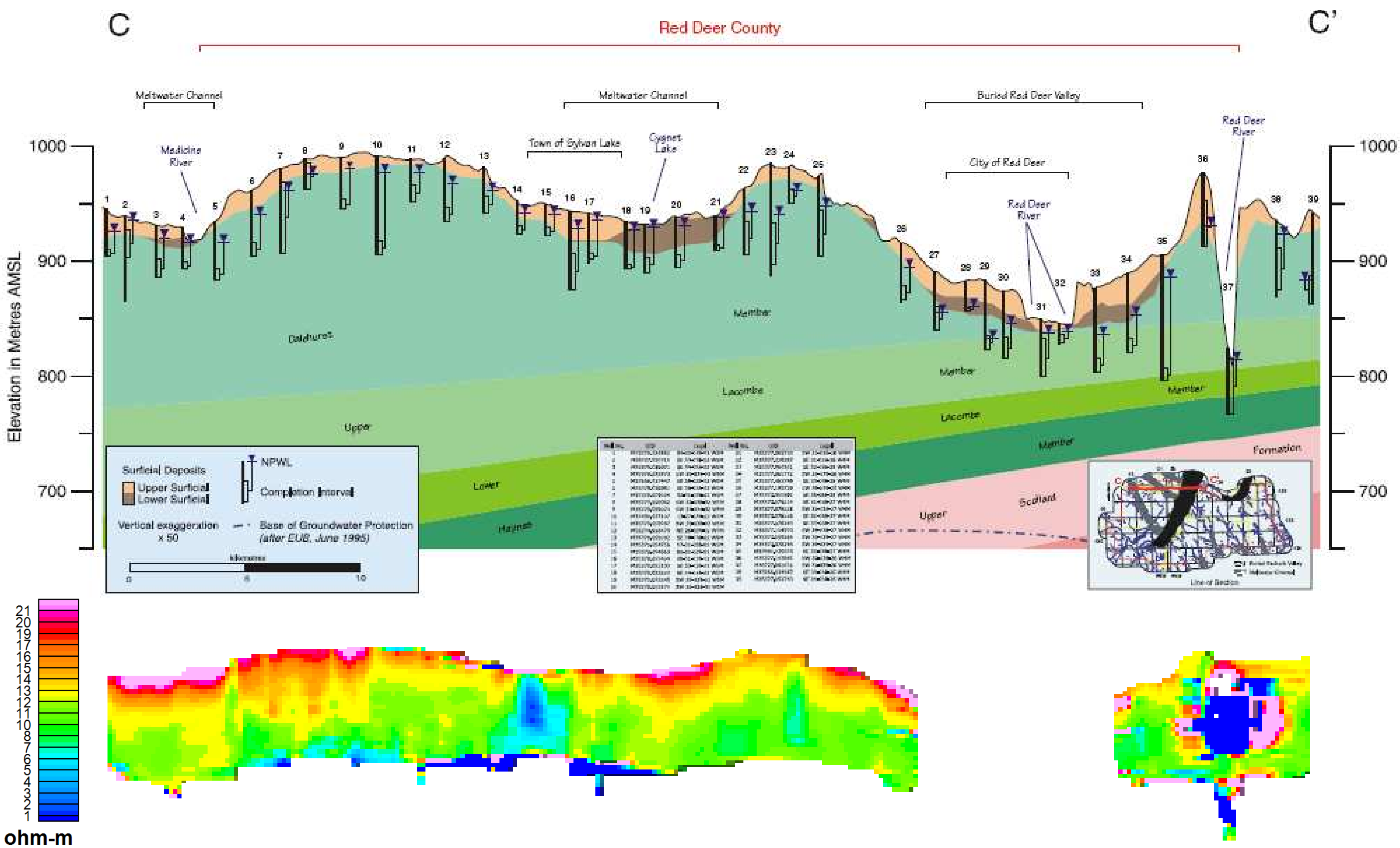

Figure 30: Cross-section C-C' of Red Deer County

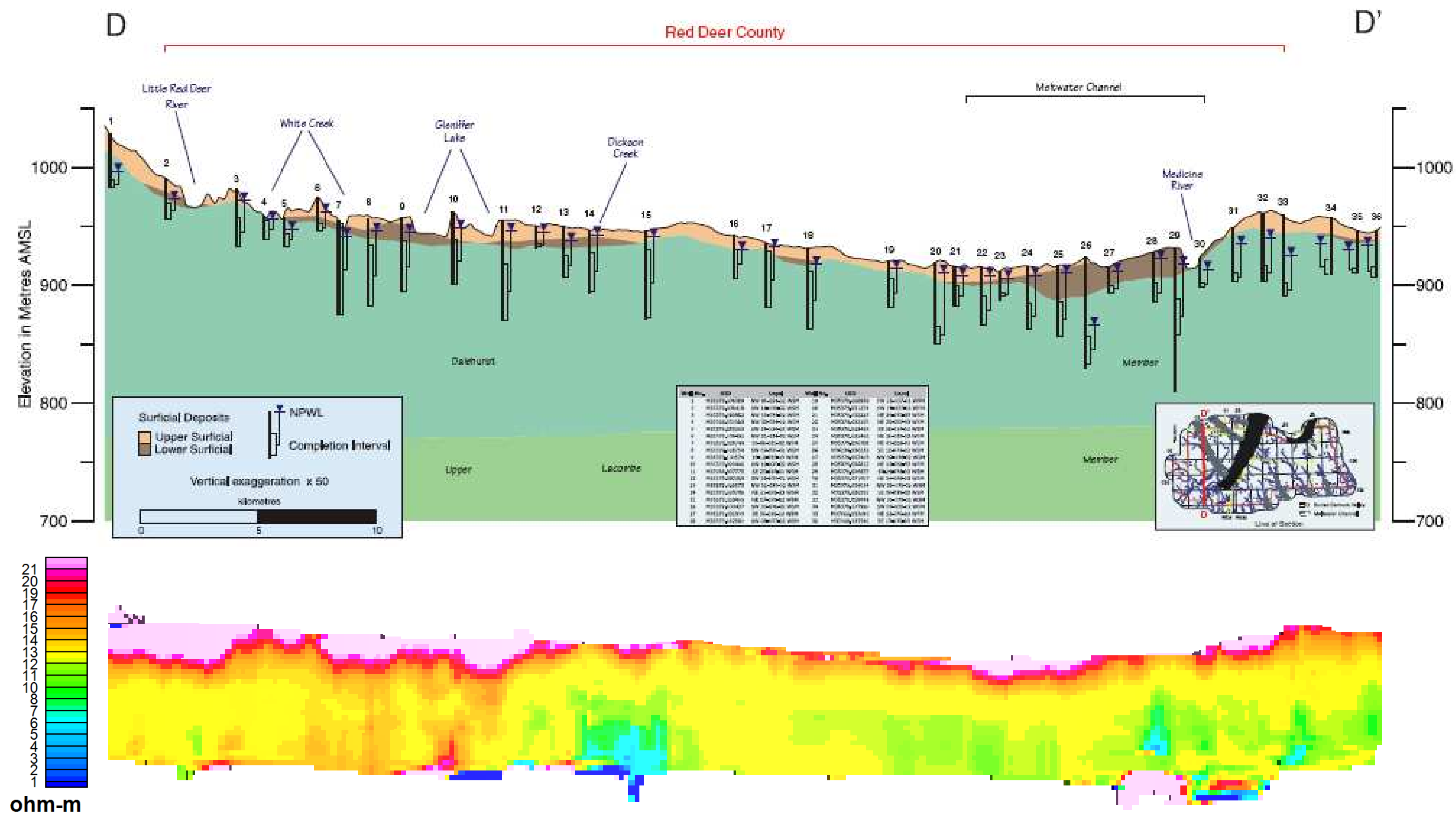

Figure 31: Cross-section D-D' of Red Deer County

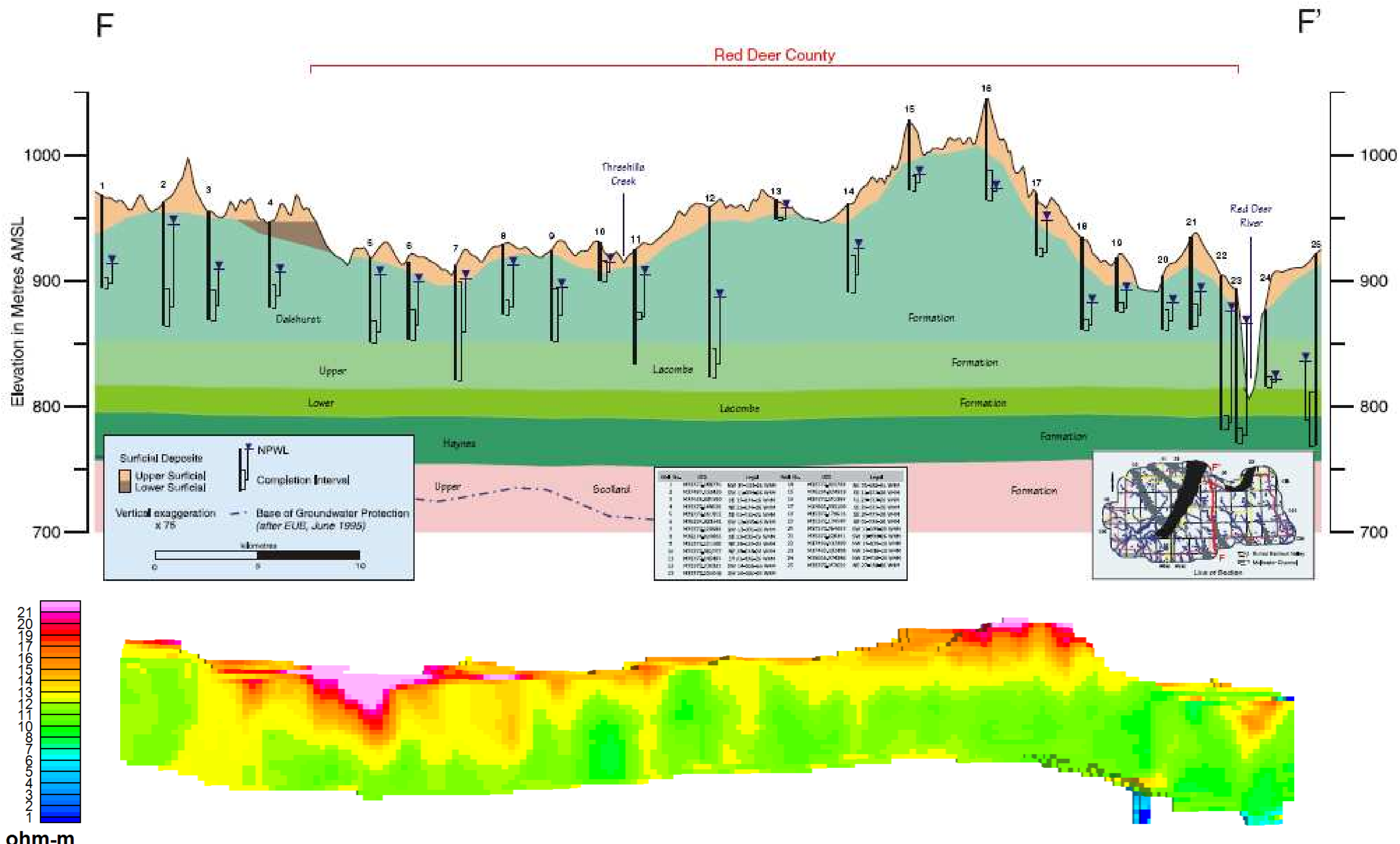

Figure 32: Cross-section F-F' of Red Deer County

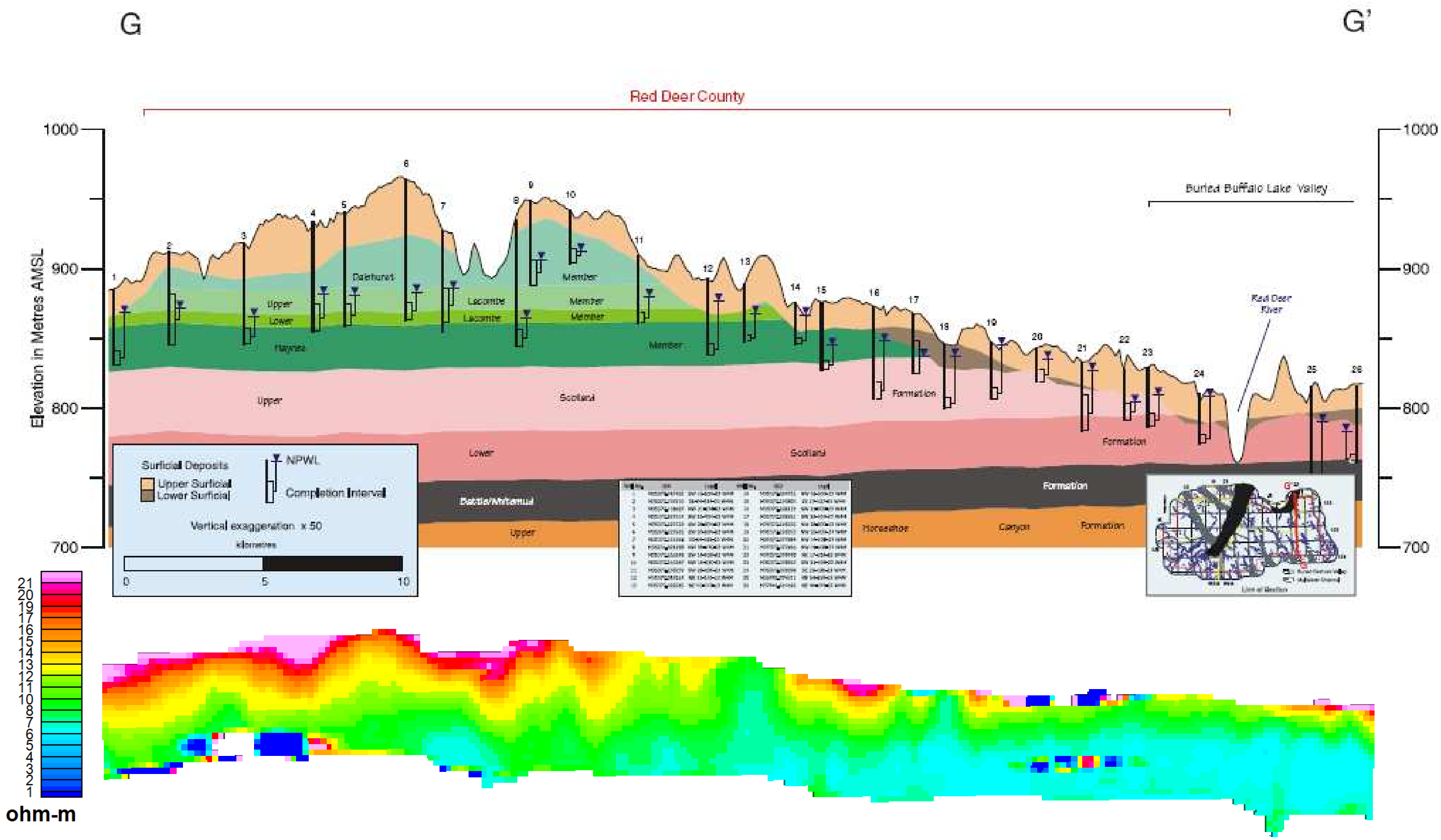

Figure 33: Cross-section G-G' of Red Deer County

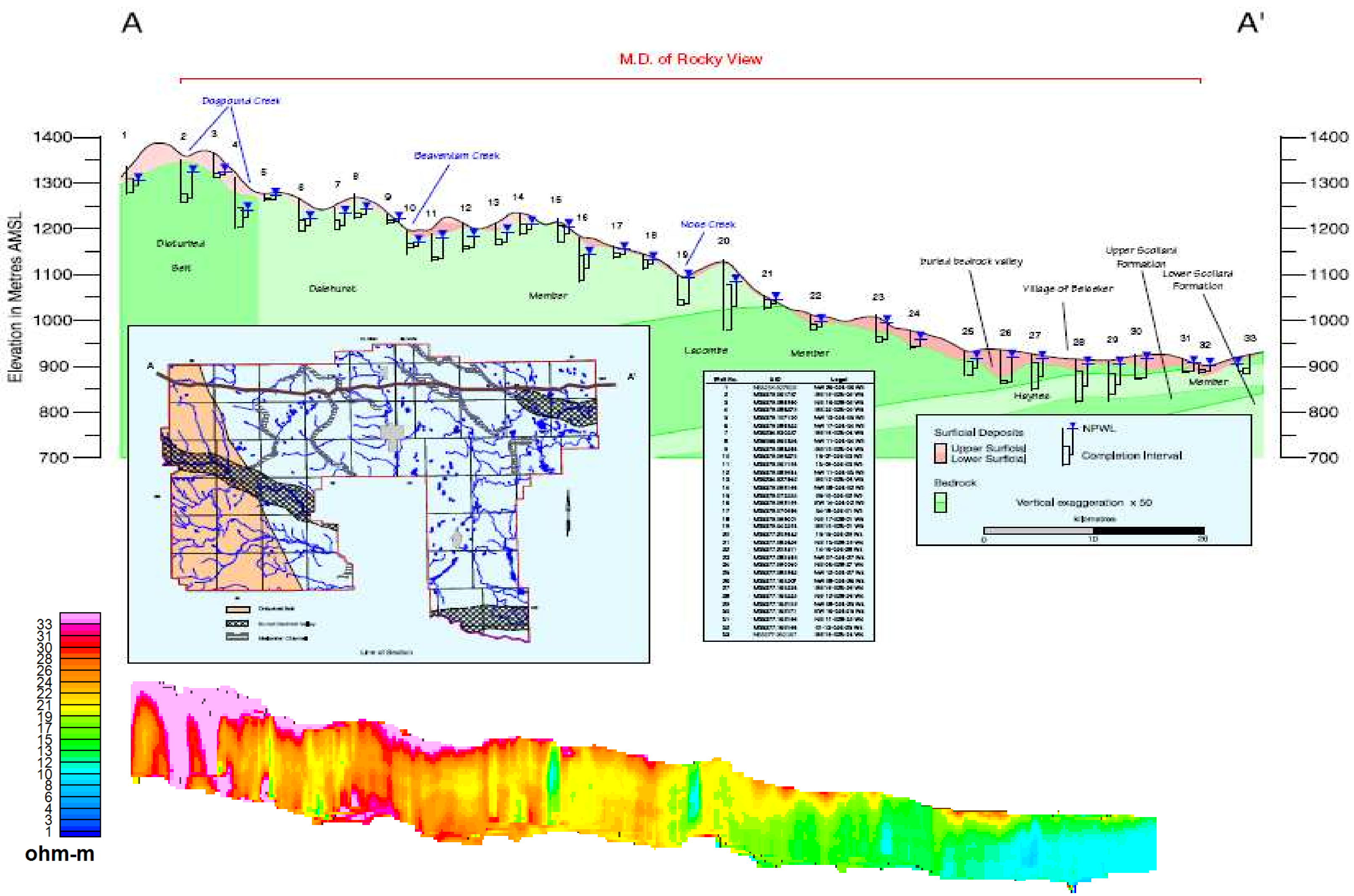

Figure 34: Cross-section A-A' of M.D. Rocky View

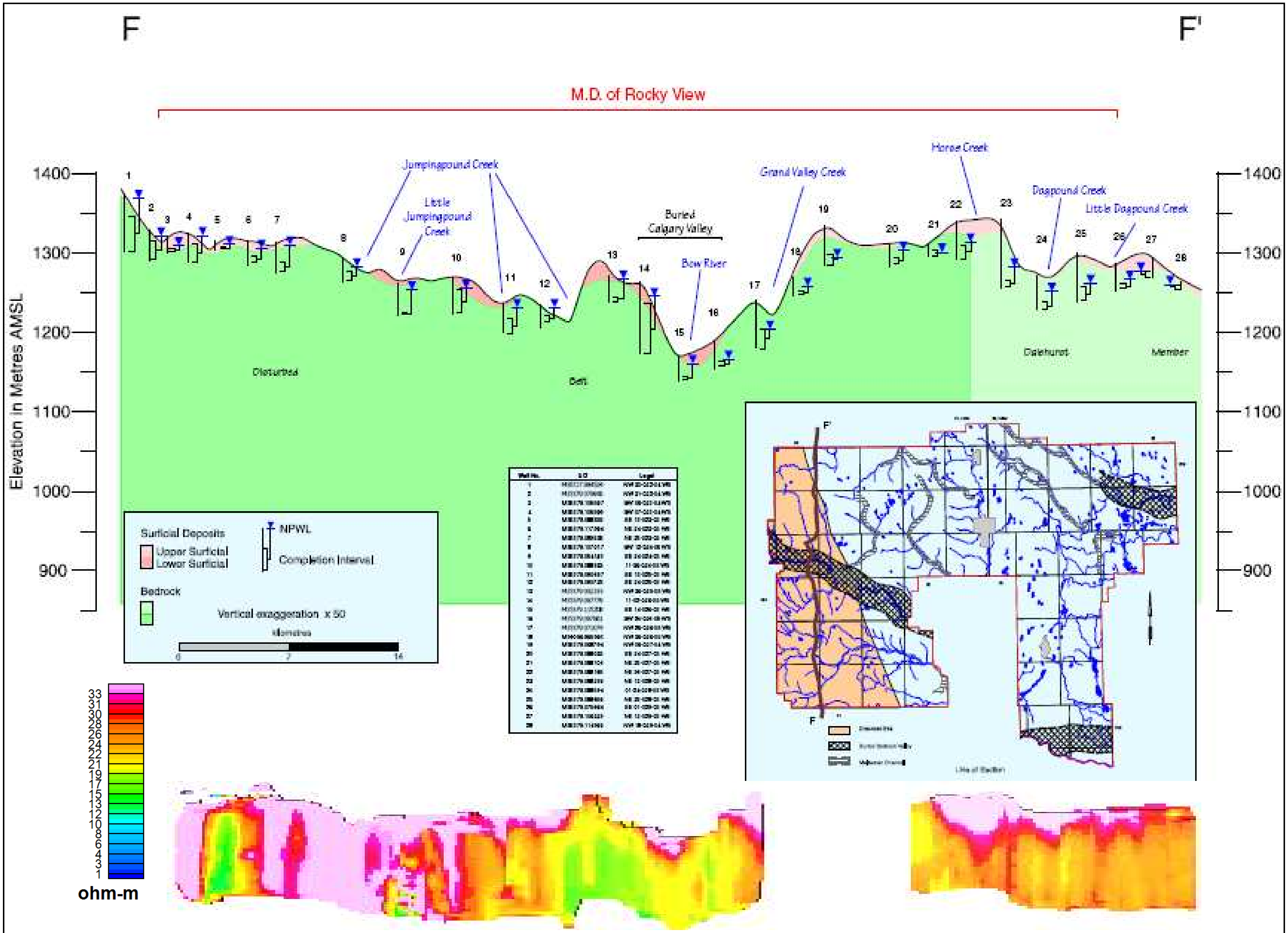

Figure 35: Cross-section F-F' of M.D. Rocky View

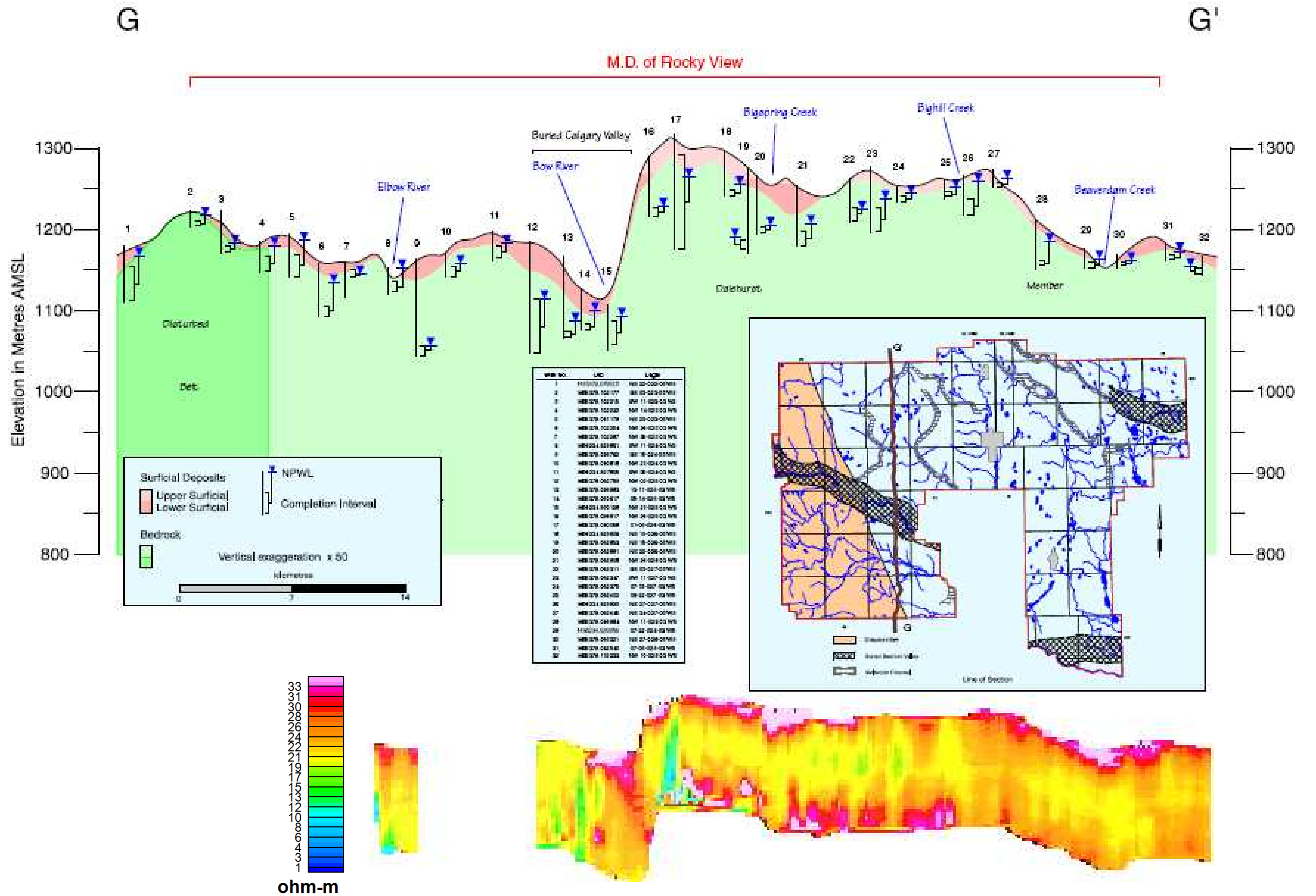

Figure 36: Cross-section G-G' of M.D. Rocky View

A number of tools were used to help define potential aquifers within the Edmonton-Calgary corridor. Firstly, because of the sheer volume of culture in the area, and to prevent mis-interpretation, the culture not defined as road, railway or pipeline, was outlined. Then individual grids relative to surface (a sample of these is shown in Figures 40 and 41) and those corrected for terrain (several are shown in Figures 42 to 51) were examined. Features correlating with culture were either ignored or if still considered of potential interest were, as with other tentative features, marked as dashed (possible) lineaments.

Then, as mentioned previously, the grids were then incorporated into xyz files and a GEOSOFT voxel 3D cube and converted to UBC format for use with the University of British Columbia's MeshTools3d application. This enabled horizontal or vertical slices to be taken through the data to help identify / define areas of interest.

The features of interest for the most part correlate with current low lying areas, rivers valleys etc; or less frequently with possible paleo-channels which cut across current topography. Most of the mapped buried bedrock valleys and meltwater channels are clearly seen throughout the survey. From the EM data, there also appears to be numerous tributaries branching from the buried bedrock valleys and meltwater channels. There is also a general correlation between the surficial EM responses and the mapped gravel and sand deposits, perhaps more so in the large scale trends of the deposits rather than exact positions.

Given that this interpretation is really an examination of the EM data in 3D, it is impossible to display all the features of interest as a single layer, as at different depths, some features appear, others disappear, and some cross-cut other lineaments, therefore, the lineaments and regions of elevated resistivity have, on the interpretation map, been grouped into 50 m elevation intervals, for example at an elevation of 560-600m, 600-650m etc above sea level. The features are all displayed at the absolute lowest/deepest level that they first appear, therefore they may be seen more clearly at higher elevations, but they are shown at their deepest emergence. This explains, why on the map, some features seem to stop and a colour change is seen, even though the feature is obviously continuous.

Most of the lakes in the survey exhibit varying degrees of low resistivity (conductivity) but are often surrounded by areas of elevated resistivity.
A good example of this is Red Deer Lake (right).

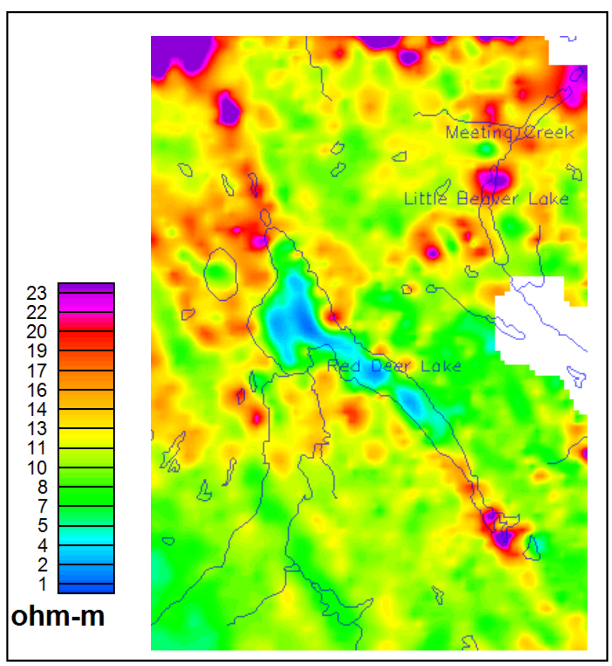

Figure 37: Terrain Corrected grid at 750 m elevation.

Other lakes, Wabamun for example, are slightly more resistive than the surrounding area (see Figure 38).

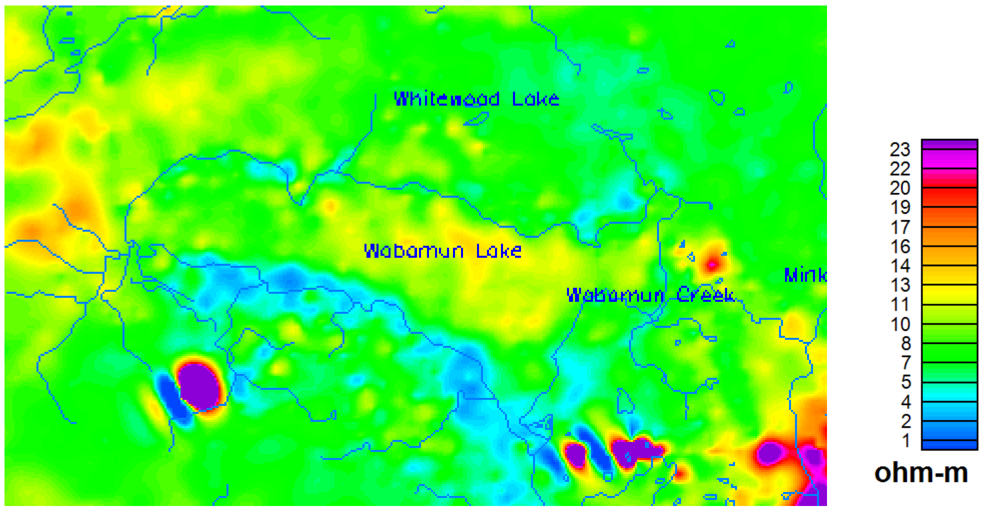

Figure 38: Terrain Corrected grid at 700 m elevation.

And some like Pigeon (already described in an earlier report – Interpretation of the Geotem and Resolve Airborne EM Data, Larch Consulting Ltd, 2008) and Beaverhill, have linear features of slightly more elevated resistivity crossing through them (see Figure 39).

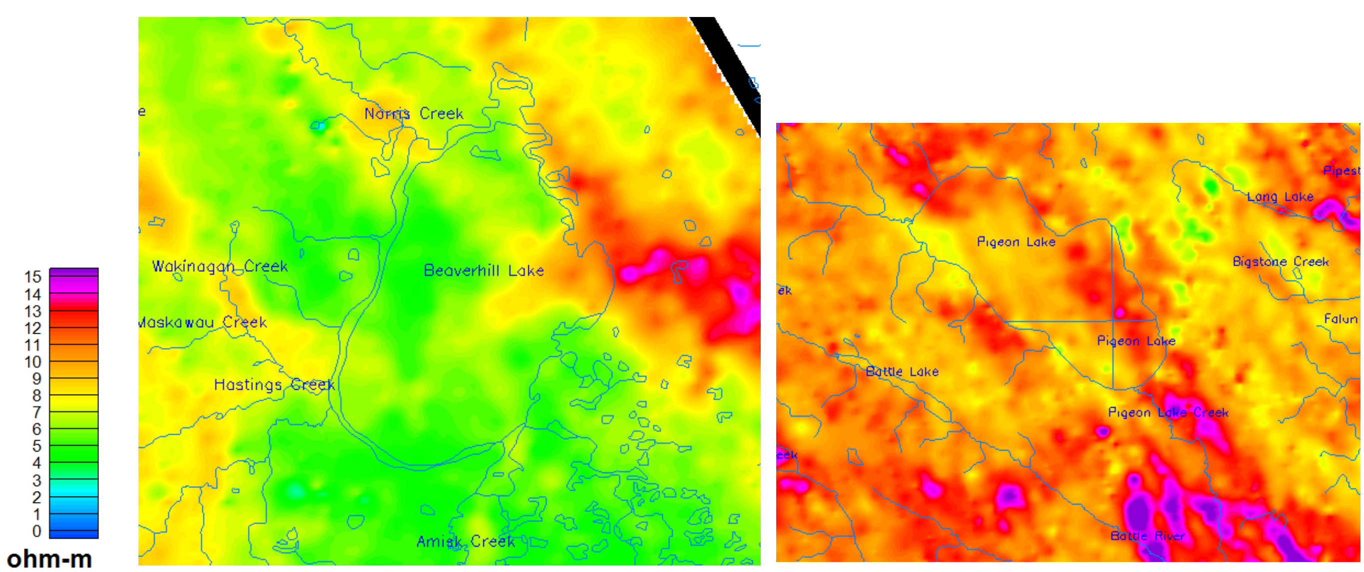

Figure 39: Terrain Corrected grid at 620 m elevation (left) and 750 m elevation (right).

Because of the sheer volume of data in the complete survey area, within the scope of this interpretation which is only a general overview, only a small majority of features can be discussed. However this should not mean that the remaining features shown on the interpretation map should be discounted.

Although certain features of interest will be discussed in some detail further in the report, a general overview of the complete survey areas EM data is shown in Figures 40 to 51.

The images displayed in Figure 40, show resistivity relative to surface for the 0,10,20,30,40,50,60 and 90 m depths. It is obvious from these images that the resistivity increases towards the south west. A number of highly resistive areas maintain elevated responses with depth - ★, whereas others are quickly reduced to background levels - ♦. This may perhaps give some indication to yield levels and/or thicknesses.

Figure 41 is also resistivity relative to surface, for this example at 20 m below surface. Several large scale trends can be seen in the data, which show a direction of approximately WNW-ESE. The trends may well be structural, as they appear to signify a divider between more or less resistive zones, and from the magnetic data several appear to have some correlation with potential basement lineaments. From the image in Figure 41, it is possible that these structures perhaps offset resistive linear features (NE-SW striking), which are also potentially fault controlled. The northern most of the WNW structural trends shown in Figure 41 corresponds in part with one of the magnetic features shown on Figure 9.

Figures 42 to 51 shows the resistivity at different elevations – the EM data shows quite good correlation with the buried bedrock valleys and in places with the sand and gravel deposits. Potential tributaries can be seen branching off from the bedrock valleys / meltwater channels. For the most part these follow current day low-lying areas, creeks and rivers.

Figure 45: 750 m elevation – in the central region of the survey, another of WNW-ESE trends mentioned previously, and which in part is potentially fault controlled, begins to emerge below which the resistivity background is elevated (see the black dashed line), at least close to the western survey boundary.

Near the southern boundary of the survey two thin dotted black lines bound an area of slightly elevated resistivity.

Figure 46: 800 m elevation - At this elevation the WNW structure mentioned in the Figure 45 discussion, and also seen in Figures 40 and 41, becomes a more localized area of elevated resistivity and a second area approximately 40 km to the south of similar expanse now appears. Both these features are identified in the figure, by pale blue dashed lines.

East of the Red Deer buried bedrock valley, shown between two thick grey lines in the figure, is a narrow region, of slightly elevated resistive background, and the strongest responses correspond with mapped sand and gravel deposits, and meltwater channels. These features also appear to maintain elevated resistive values to some depth. The inset indicates an area of slightly elevated resistivity between two dotted lines. These lines align with the lengths of mapped sand and gravel deposits.

Figure 47: 850 m elevation – the two WNW features mentioned previously are joined by a third feature, which also seems to be 40 km south of the second lineament. This lineament is in alignment with the mapped southern extent of the Red Deer buried bedrock valley.

Figures 49 and 50: 1000 m and 1050 elevations respectively – an east-west structure (which is also identified in the magnetic data as a potential fault) signifies a change in resistivity from being more resistive north of the fault to more conductive south of the fault. The fault is shown in the image as a black dotted line in Figure 49.

Figure 51: 1150 m elevation – the EM data shows correlation with the Calgary buried bedrock valley and several of the surrounding meltwater channels. The NNW lithologies of the disturbed belt are also clearly seen (see inset – showing the lithologic boundaries). A pale blue line in the inset, points to a lineament, which may be of some interest, or is simply unmapped Alberta Group.

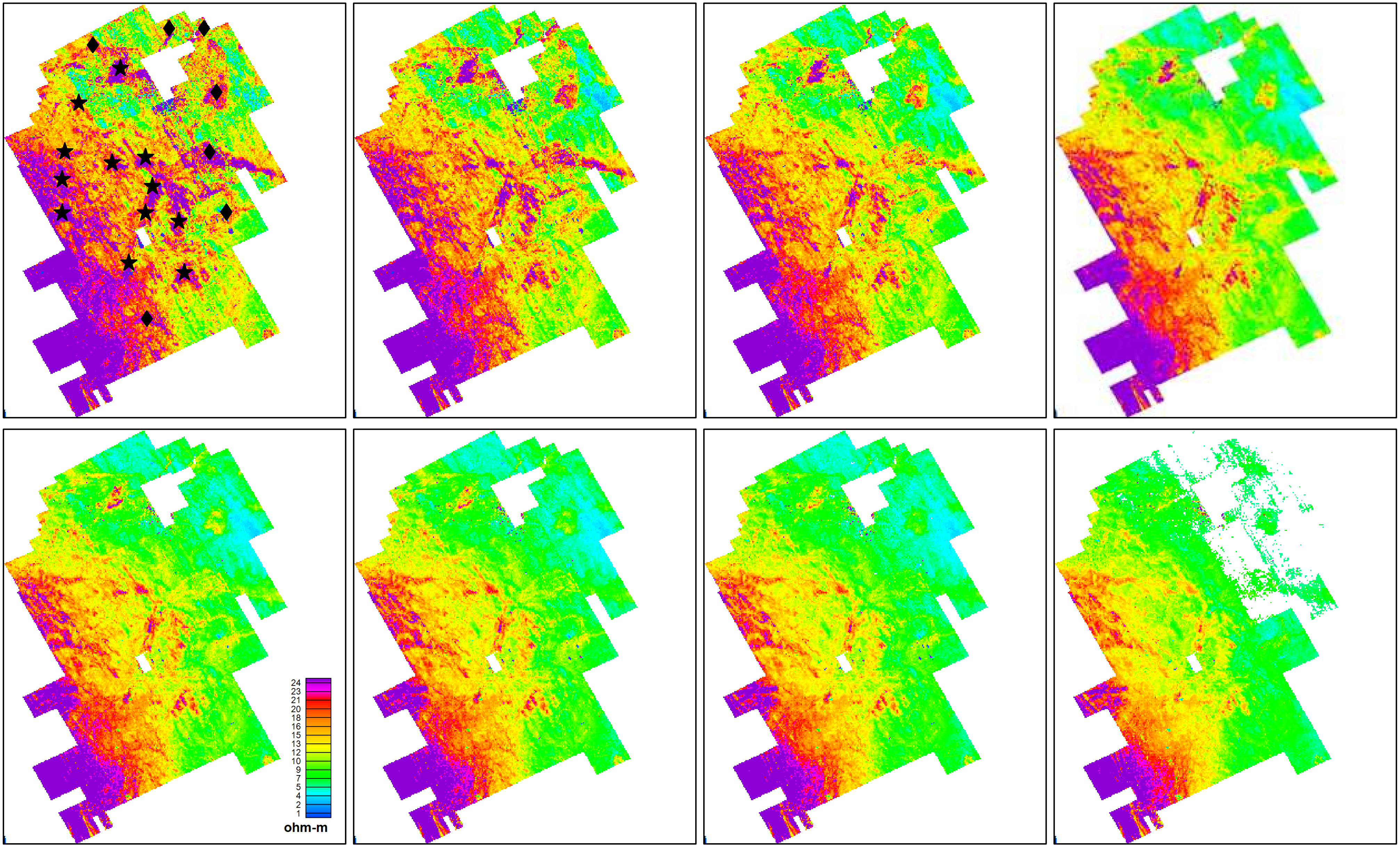

Figure 40: top (left to right); resistivity relative to surface, at 0, 10, 20, and 30 m depth; and bottom (left to right) resistivity relative to surface at 40, 50, 60 and 90 m depth. ★ - Shows regions of high resistivity which continue to depth, ♦ - indicates areas of high resistivity which are reduced to background levels relatively quickly.

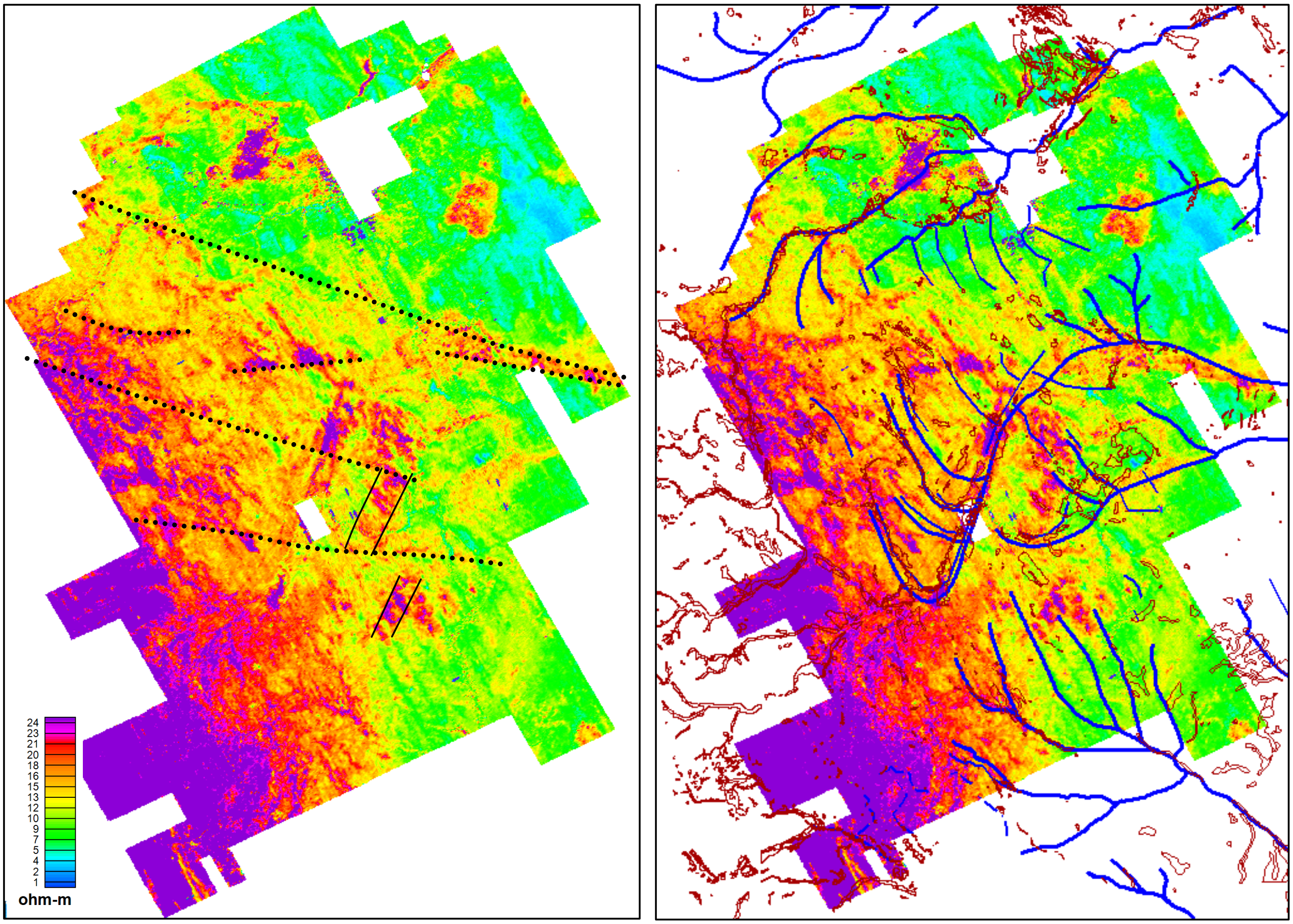

Figure 41: resistivity relative to surface, at 20 m depth with trends (black lines) – left, and with the buried bedrock valleys (heavier blue lines) and meltwater channels (thin blue lines) and the sand and gravel deposits (brown outlines) - right.

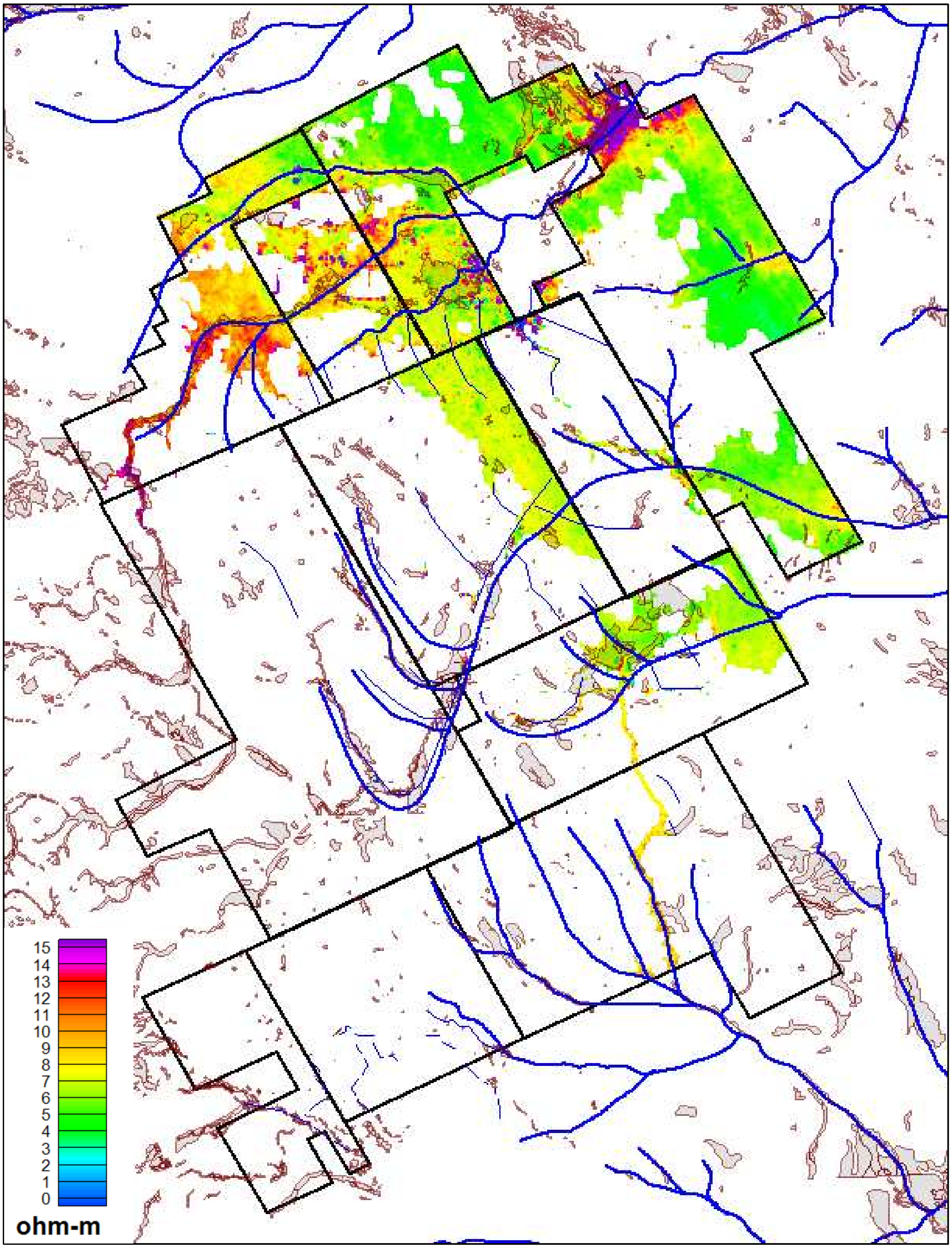

Figure 42: Terrain corrected depth slice at 600 m elevation, showing the locations of the buried bedrock valleys (heavy blue lines), the meltwater channels (thin blue lines), and the sand and gravel deposits (outlined in brown).

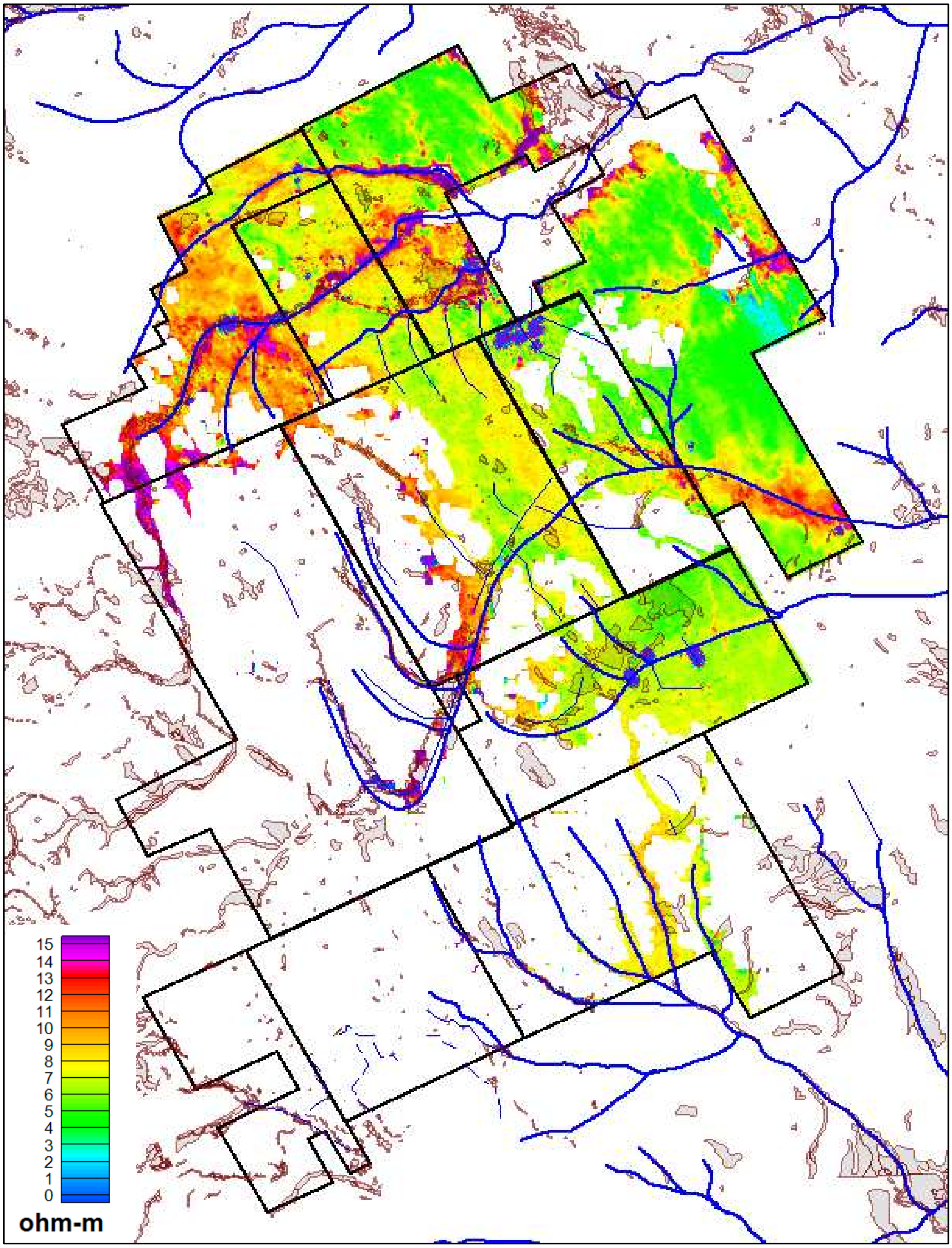

Figure 43: Terrain corrected depth slice at 650 m elevation, showing the locations of the buried bedrock valleys (heavy blue lines), the meltwater channels (thin blue lines), and the sand and gravel deposits (outlined in brown).

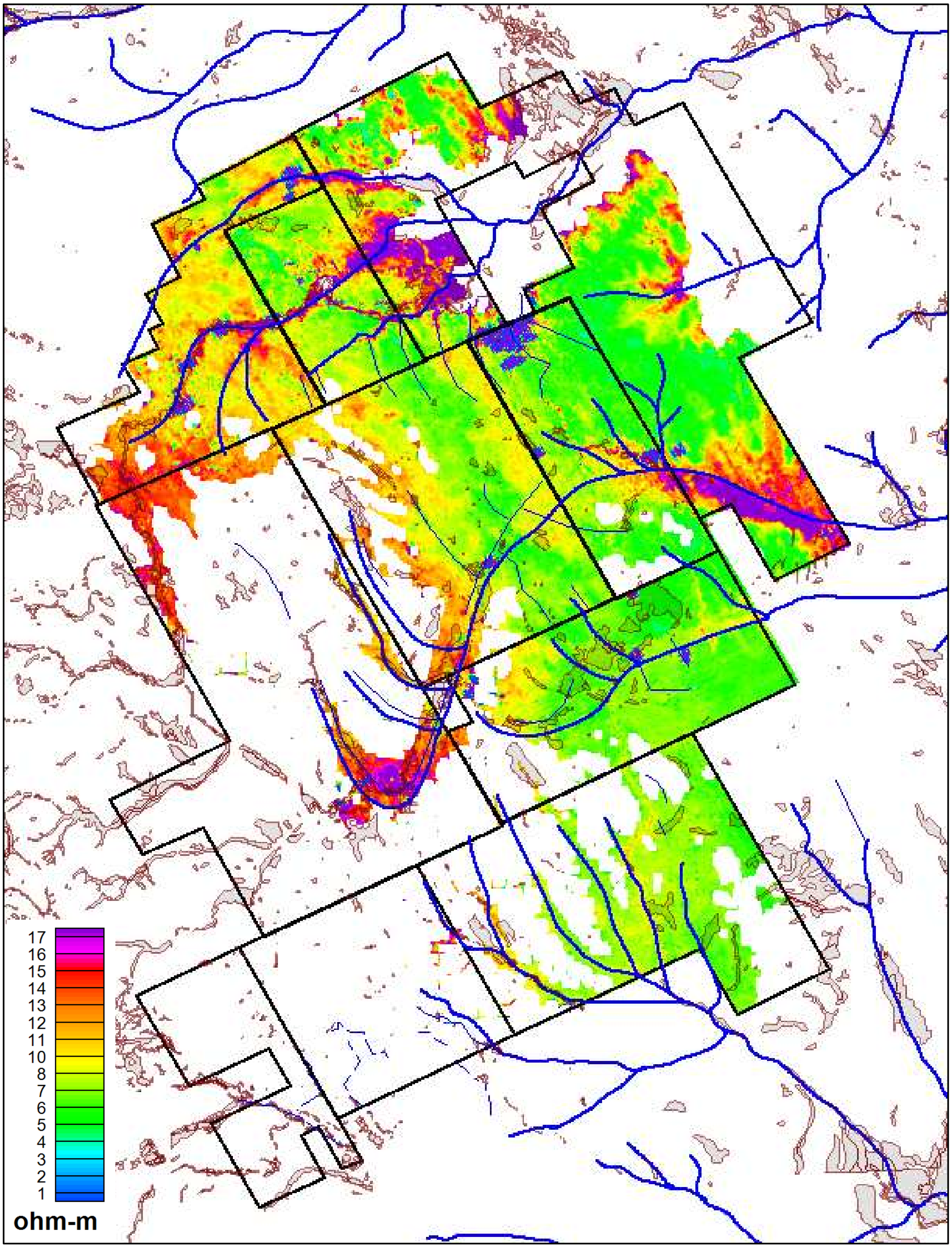

Figure 44: Terrain corrected depth slice at 680 m elevation, showing the locations of the buried bedrock valleys (heavy blue lines), the meltwater channels (thin blue lines), and the sand and gravel deposits (outlined in brown).

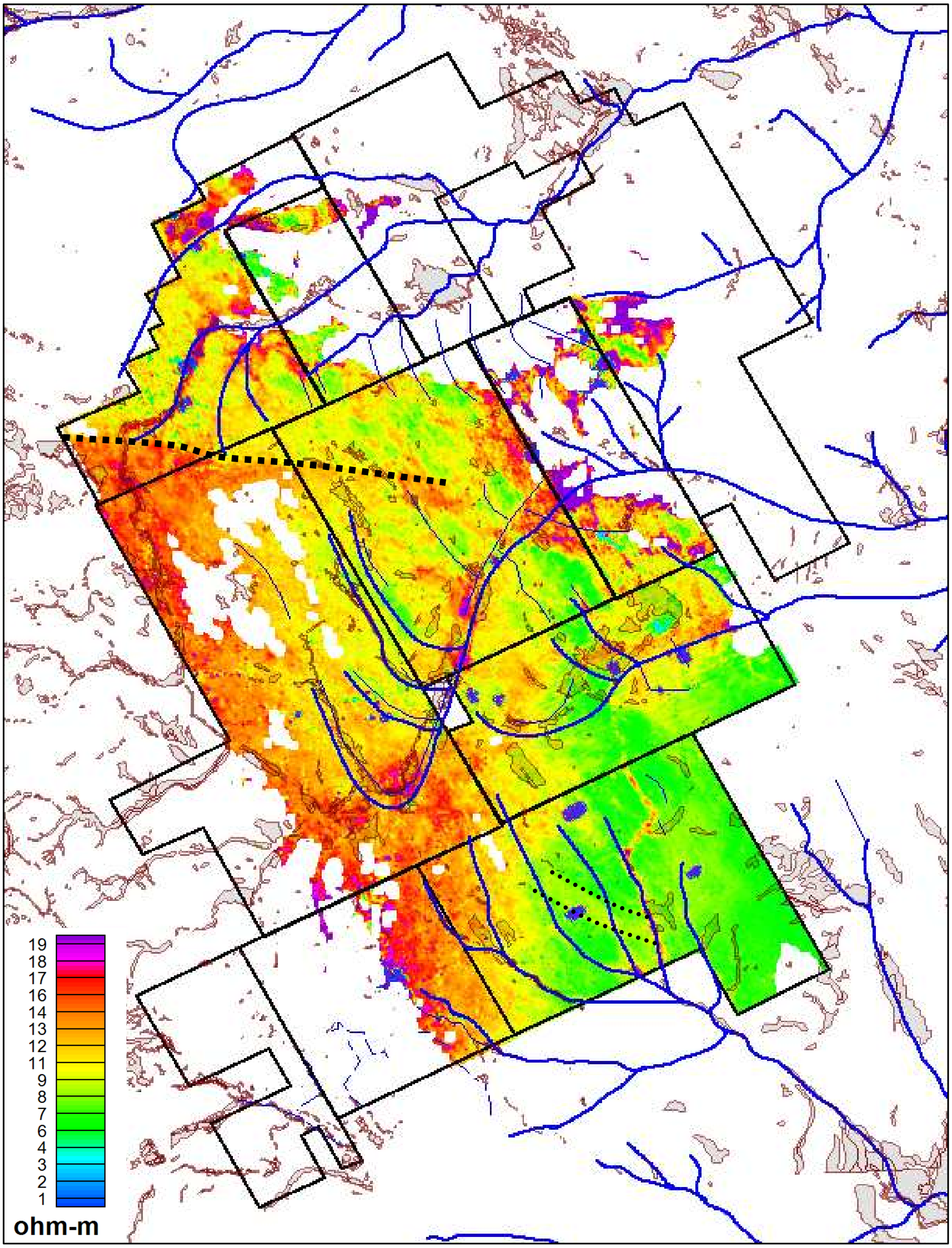

Figure 45: Terrain corrected depth slice at 750 m elevation, showing the locations of the buried bedrock valleys (heavy blue lines), the meltwater channels (thin blue lines), and the sand and gravel deposits (outlined in brown).

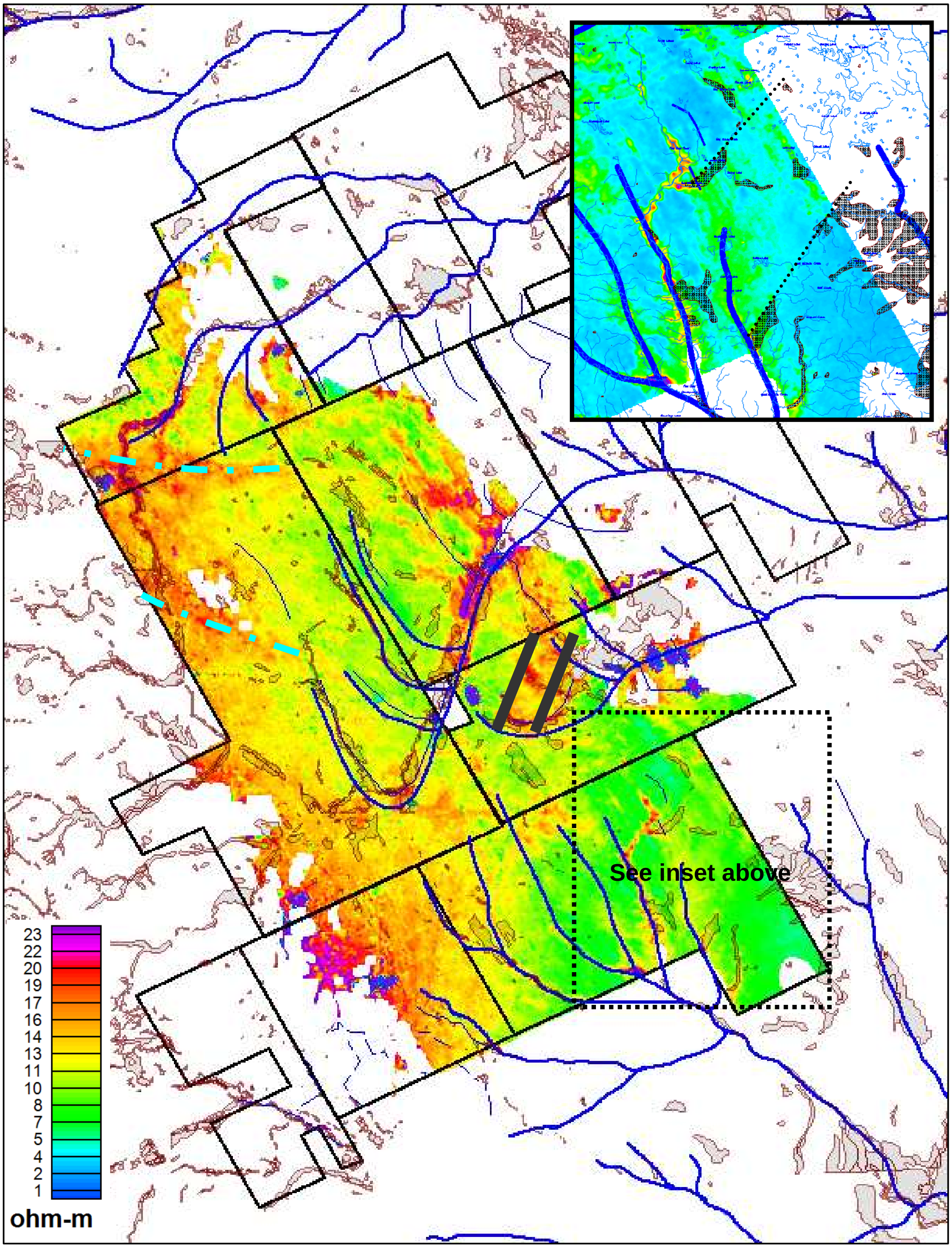

Figure 46: Terrain corrected depth slice at 800 m elevation, showing the locations of the buried bedrock valleys (heavy blue lines), the meltwater channels (thin blue lines), and the sand and gravel deposits (outlined in brown).

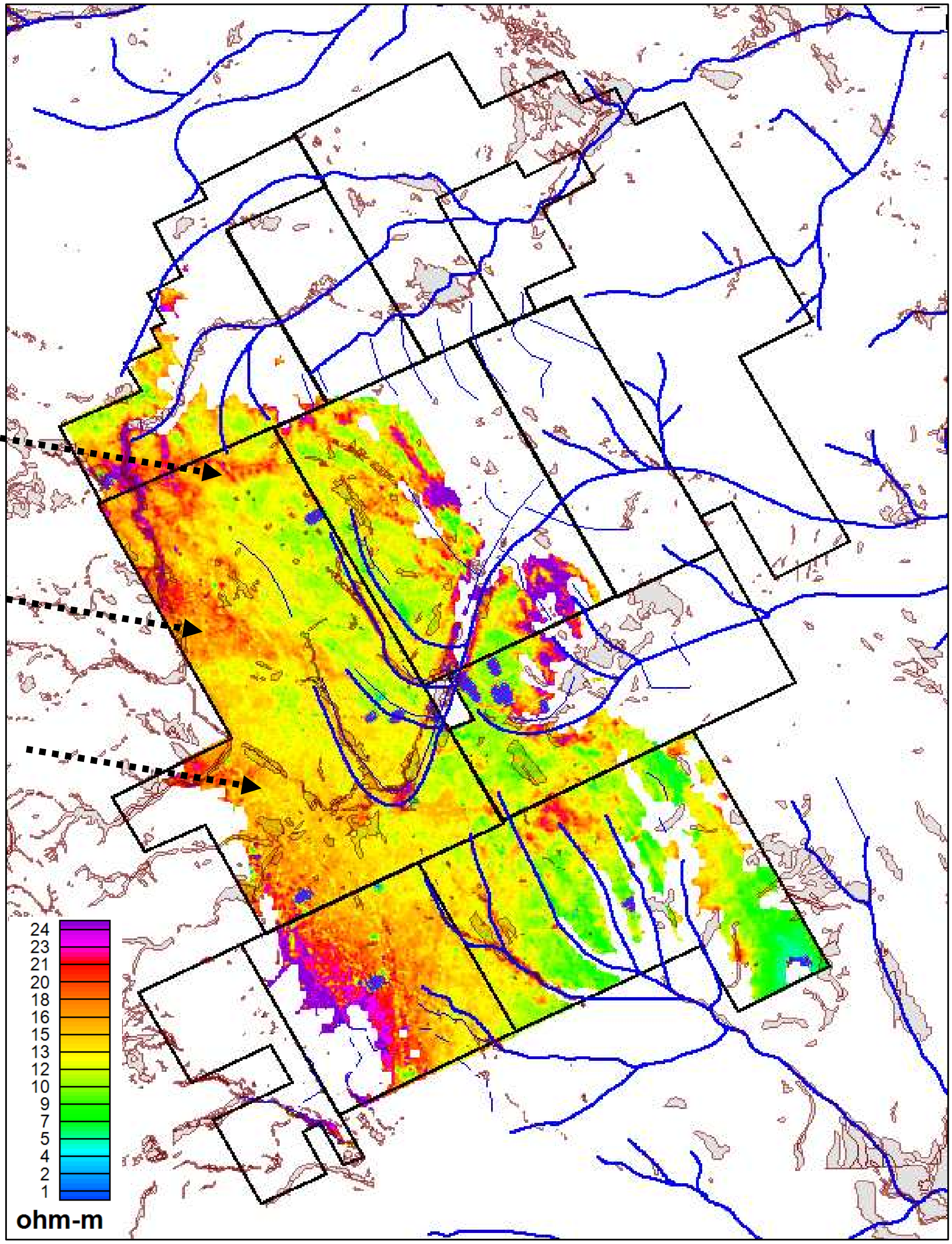

Figure 47: Terrain corrected depth slice at 850 m elevation, showing the locations of the buried bedrock valleys (heavy blue lines), the meltwater channels (thin blue lines), and the sand and gravel deposits (outlined in brown).

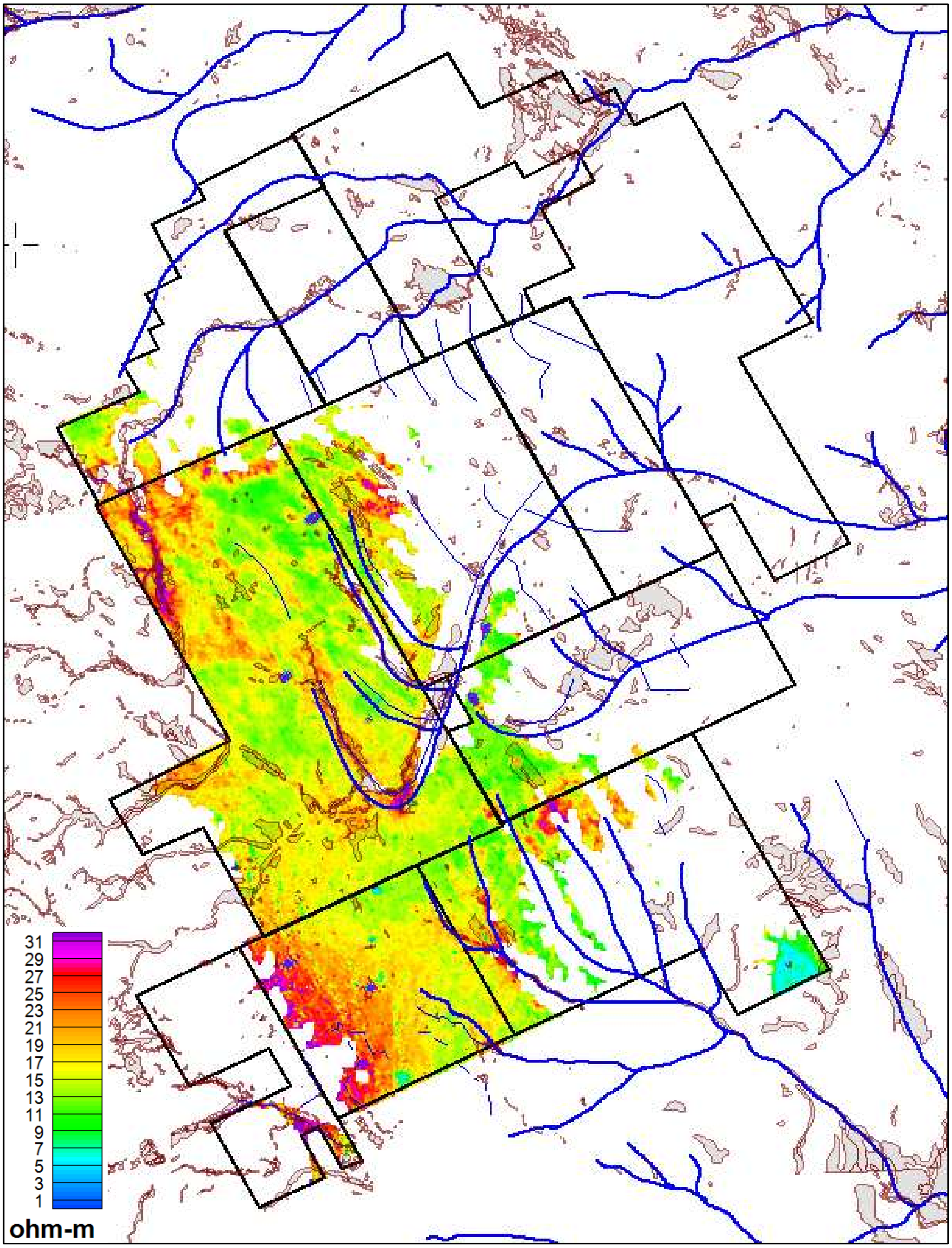

Figure 48: Terrain corrected depth slice at 900 m elevation, showing the locations of the buried bedrock valleys (heavy blue lines), the meltwater channels (thin blue lines), and the sand and gravel deposits (outlined in brown).

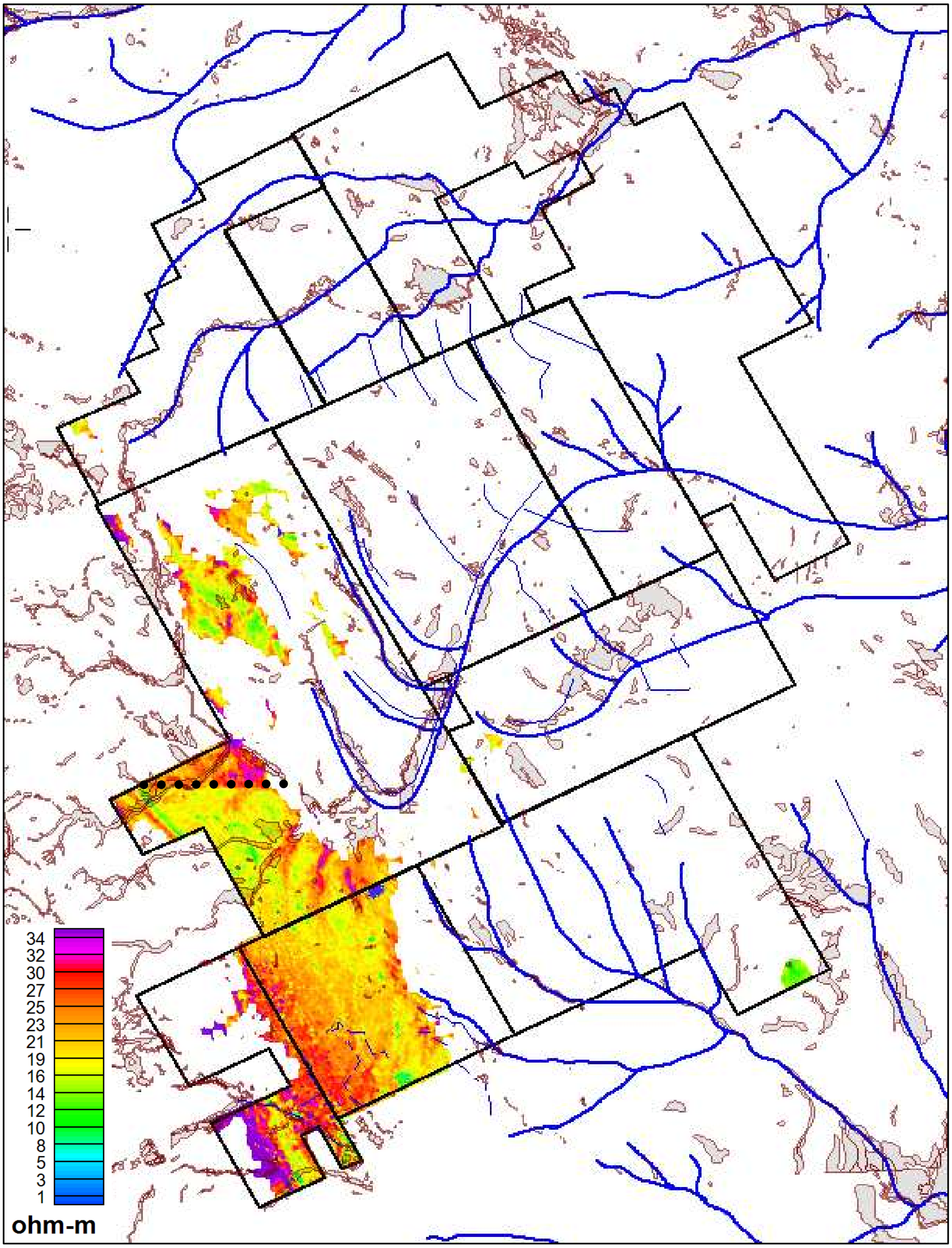

Figure 49: Terrain corrected depth slice at 1000 m elevation, showing the locations of the buried bedrock valleys (heavy blue lines), the meltwater channels (thin blue lines), and the sand and gravel deposits (outlined in brown).

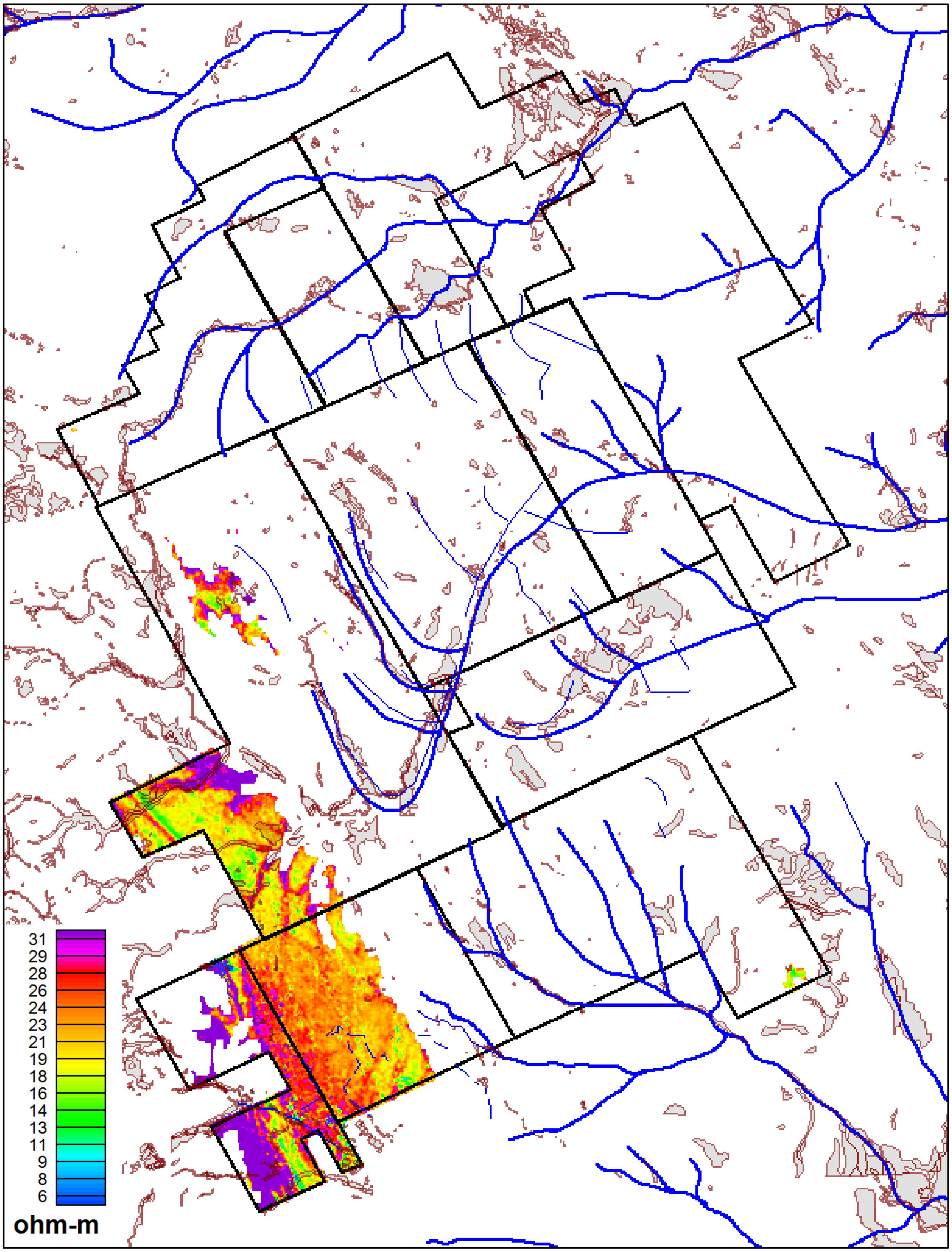

Figure 50: Terrain corrected depth slice at 1050 m elevation, showing the locations of the buried bedrock valleys (heavy blue lines), the meltwater channels (thin blue lines), and the sand and gravel deposits (outlined in brown).

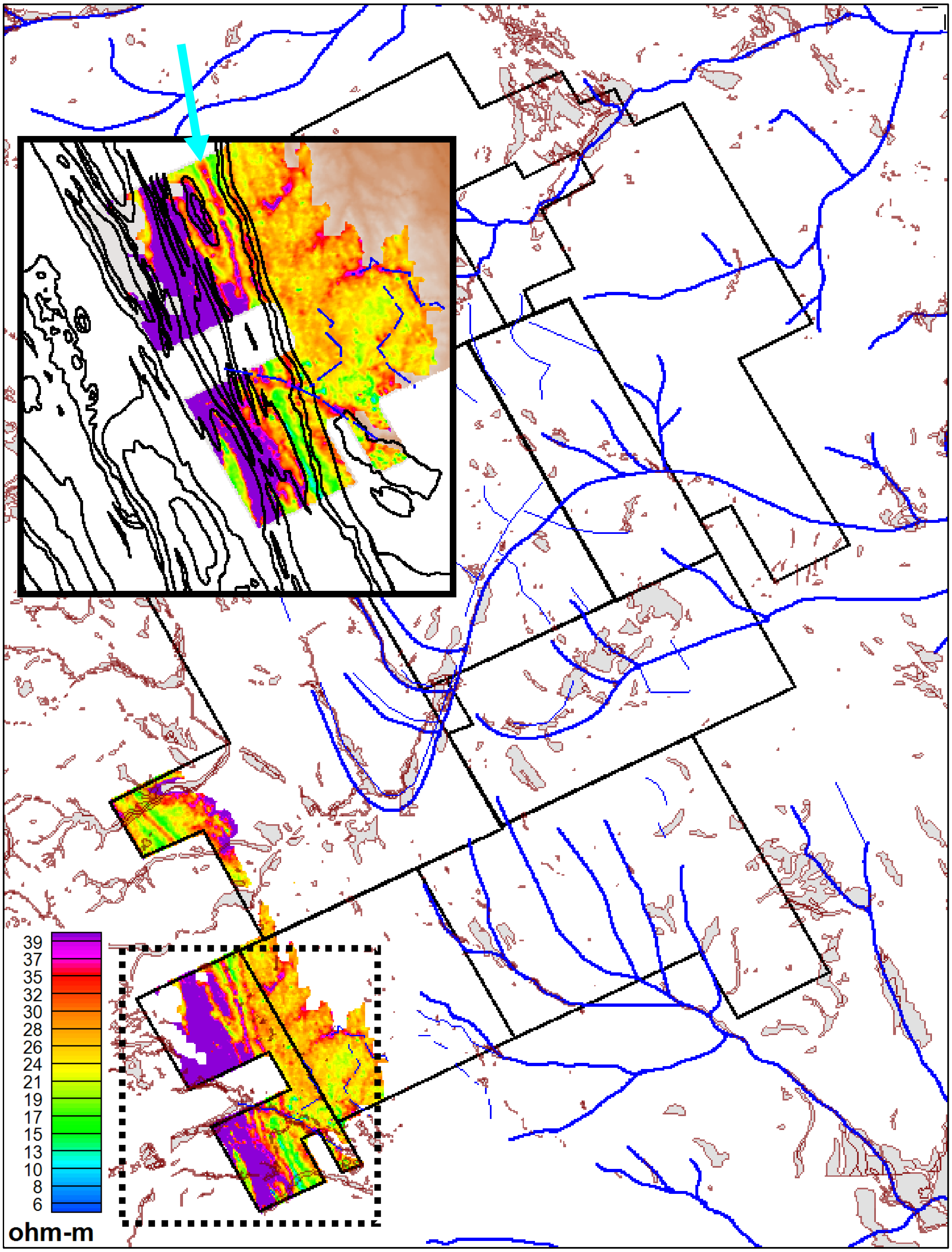

Figure 51: Terrain corrected depth slice at 1150 m elevation, showing the locations of the buried bedrock valleys (heavy blue lines), the meltwater channels (thin blue lines), and the sand and gravel deposits (outlined in brown).

Because the survey is so extensive, the area has been divided into three sections, northern, central and southern; to better discuss and show areas/features of interest. The black arrows shown in the next couple of figures indicate potential tributaries to the buried bedrock valleys. The DTM (Digital Terrain Model) is shown beside these images to emphasis the close correlation between the current topography and the EM data.

Northern section of the survey

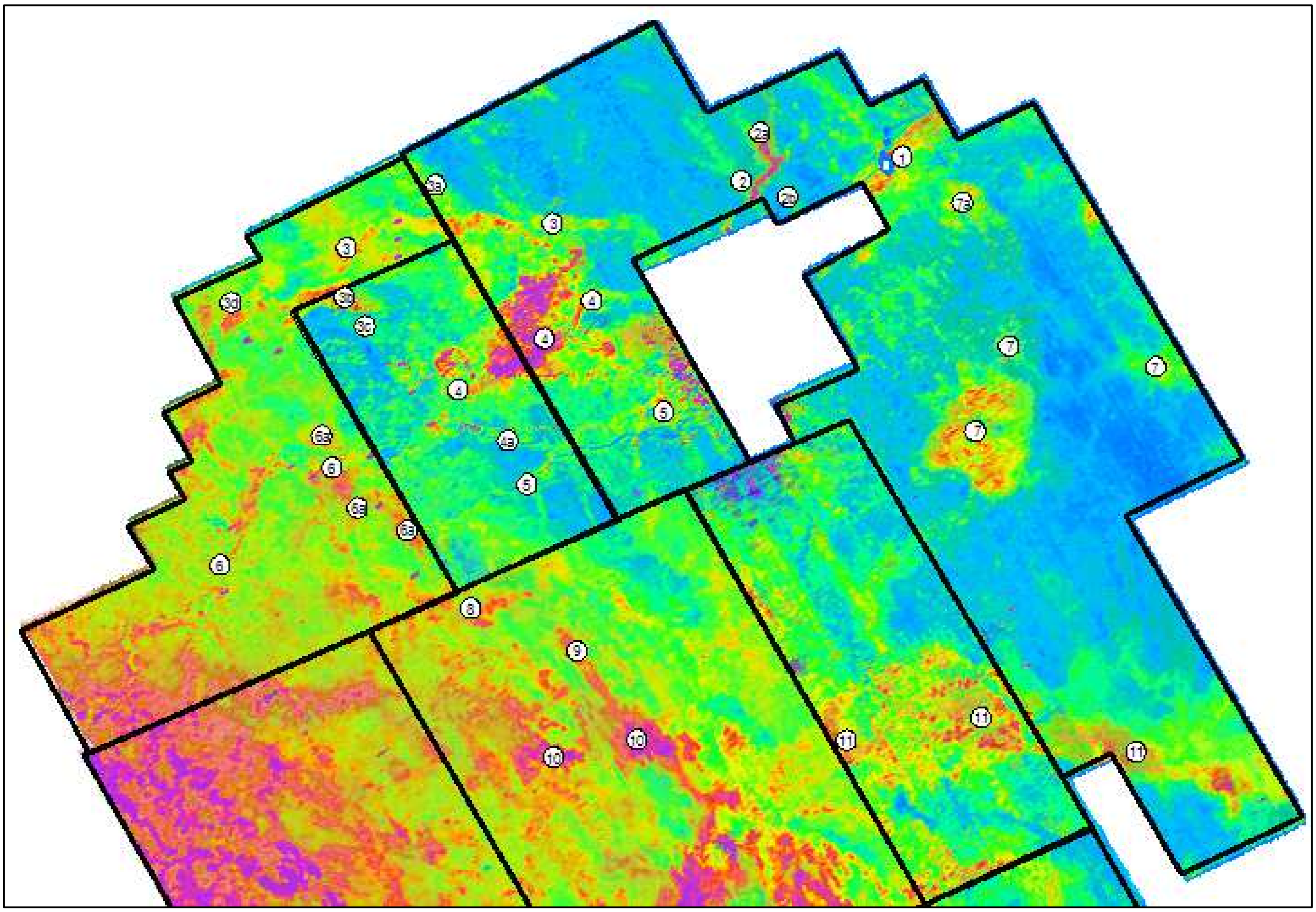

Image showing the location of the northern sections areas of interest

Figure 52 – 650 m elevation – The northern WNW structure mentioned previously as part of the Figure 47 discussion, is clearly visible at this elevation.

Figure 53 – 800 m elevation – the dashed line shown on the image was also shown and discussed earlier in the Figure 45 discussion, and the circular symbols overlie regions of elevated resistivity lying south of this trend.

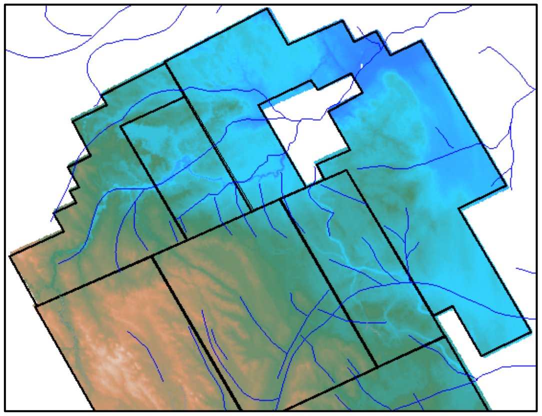

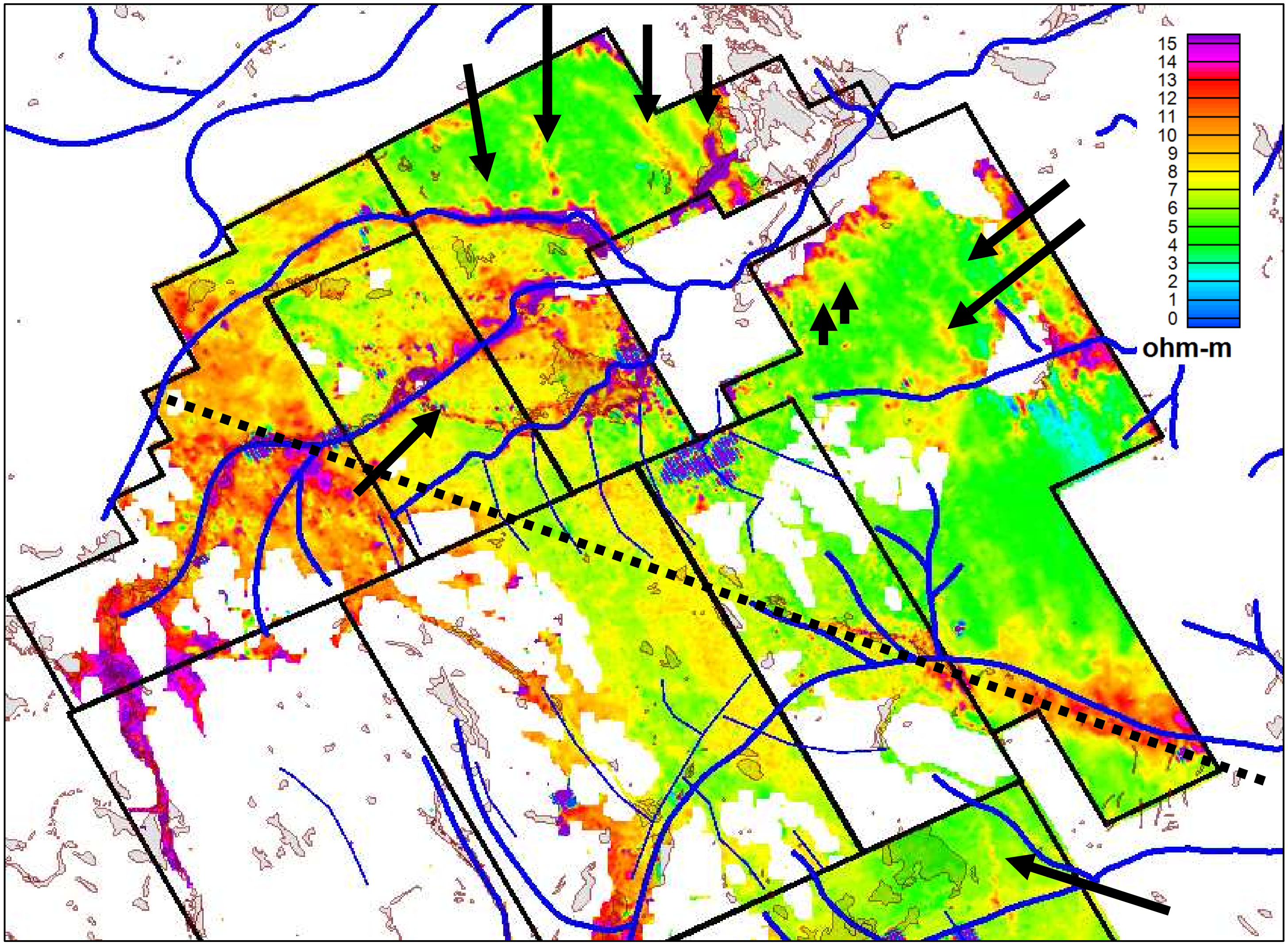

Figure 52: Northern part of the merged survey area. Terrain corrected depth slice at 650 m elevation, showing the locations of the buried bedrock valleys (heavy blue lines), the meltwater channels (thin blue lines), and the sand and gravel deposits (outlined in brown). The arrows point to possible tributaries or extensions from the buried bedrock valleys and meltwater channels. The dashed line indicates a potential trend in the gravel and sand deposits, and this feature may have some impact as well on the buried bedrock valleys. This trend can also potentially be seen in the magnetic data (see Figure 9).

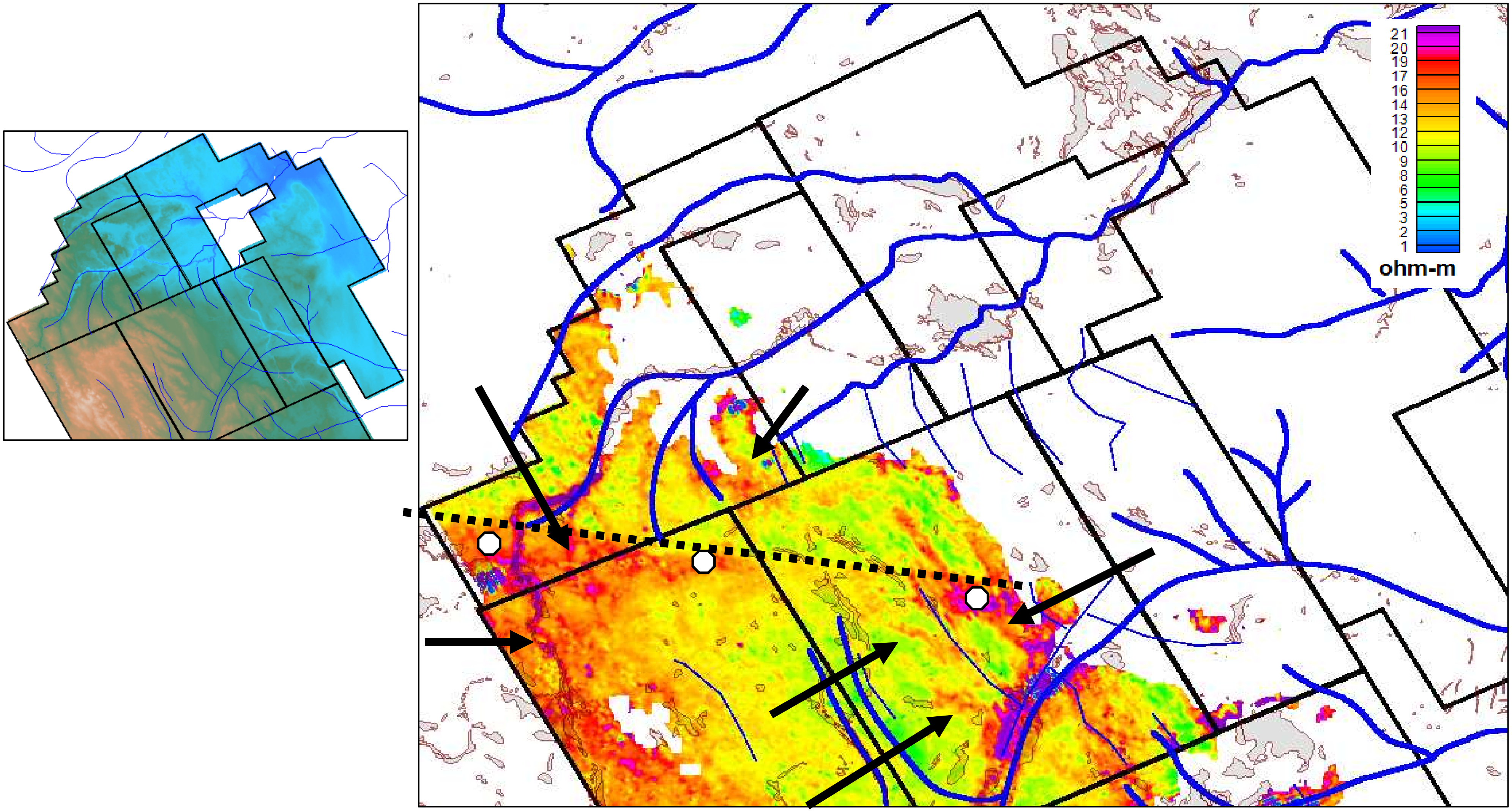

Figure 53: Northern part of the merged survey area. Terrain corrected depth slice at 800 m elevation, showing the locations of the buried bedrock valleys (heavy blue lines), the meltwater channels (thin blue lines), and the sand and gravel deposits (outlined in brown). The arrows point to possible tributaries or extensions from the buried bedrock valleys and meltwater channels. The circular symbols indicate area of elevated resistivity along a trend of possible interest.

Feature 1:

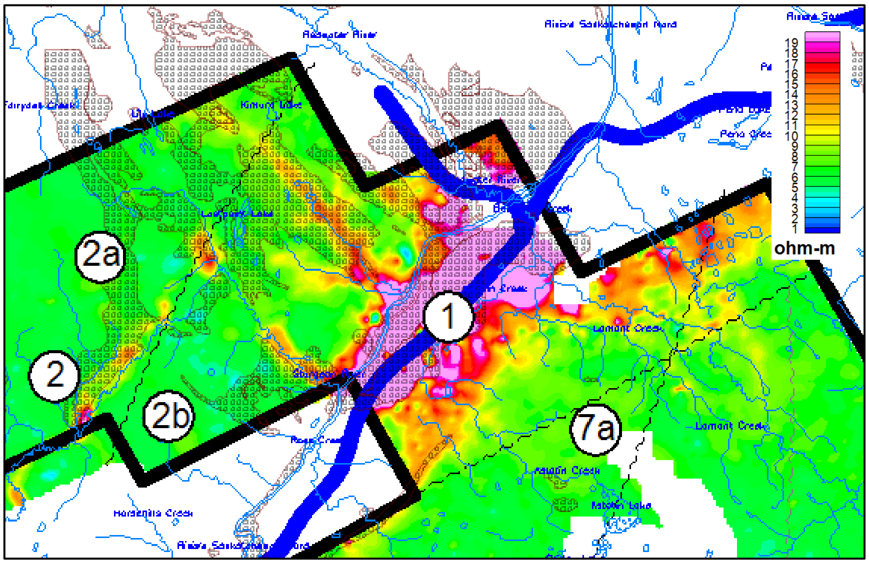

Figure 54: Terrain corrected depth slice at 600 m, showing the locations of the mapped buried bedrock valleys (heavy blue lines), the meltwater channels (thin blue lines), and the sand and gravel deposits (hatched area), and potential basement lineaments.

This selection is located on a mapped buried bedrock valley just south of the Riviere Saskatchewan Nord, and the EM data suggests several tributaries to the north. For the most part these correlate very well with sand and gravel deposits. A NE-SW potential lineament appears to correlate with the northern termination of the tributaries, along with a truncation of the sand and gravel deposits. The selection lies within an extensive low lying area.

Feature 2:

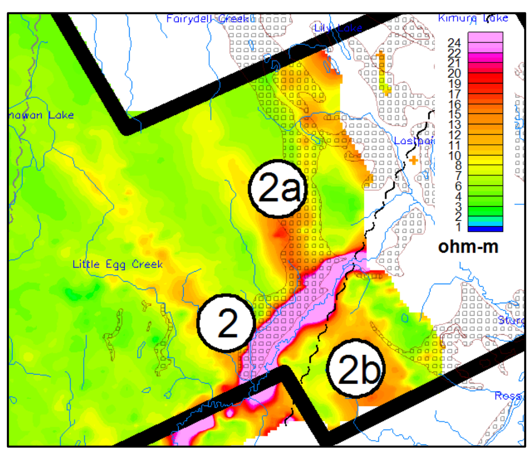

Figure 55: Terrain corrected depth slice at 650 m, showing the locations of the mapped sand and gravel deposits (hatched area) and potential basement lineaments.

The strongest response of this selection corresponds with mapped sand and gravel deposits. There are several possible "tributaries"; 2a lies to the north and also corresponds with sand and gravel. 2b lies to the southeast and is separated from 2 by the NE-SW potential lineament mentioned in Feature 1. Neither 2a nor 2b really correlate with current topography.

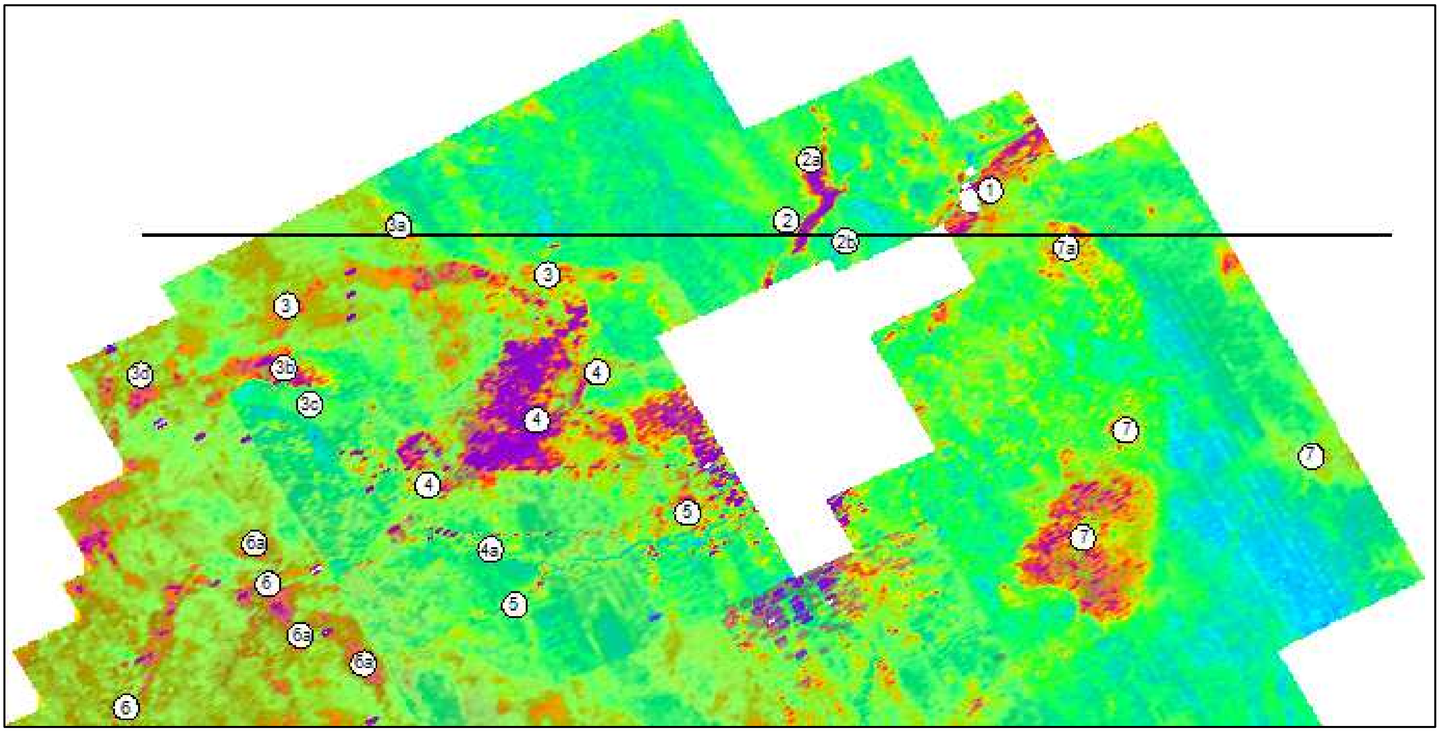

The image above is resistivity relative to surface at 0, 20, 30 and 60 m depth, with the surface grid being the most transparent. The horizontal line indicates the vertical slice that is shown in the 3D images. The top 3D image is relative to surface, the bottom 3D image is corrected for terrain. Features 1 and 2 area clearly seen.

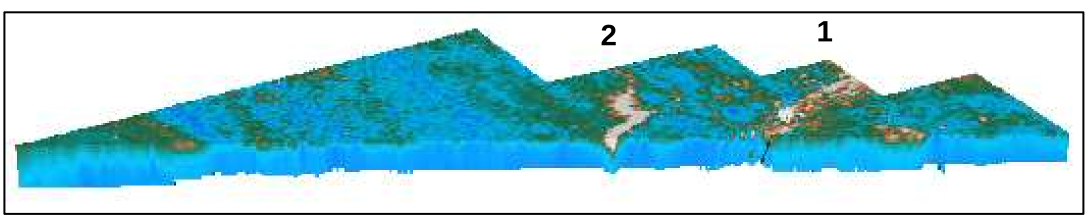

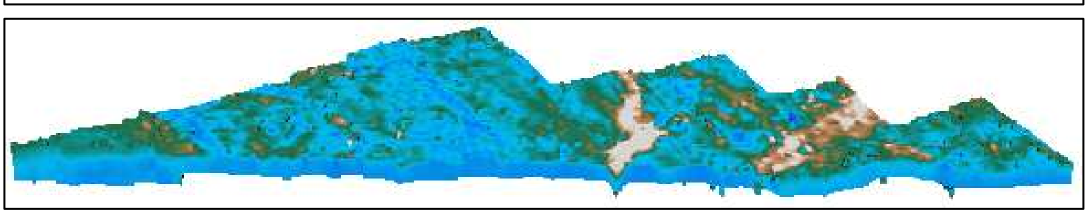

Feature 3:

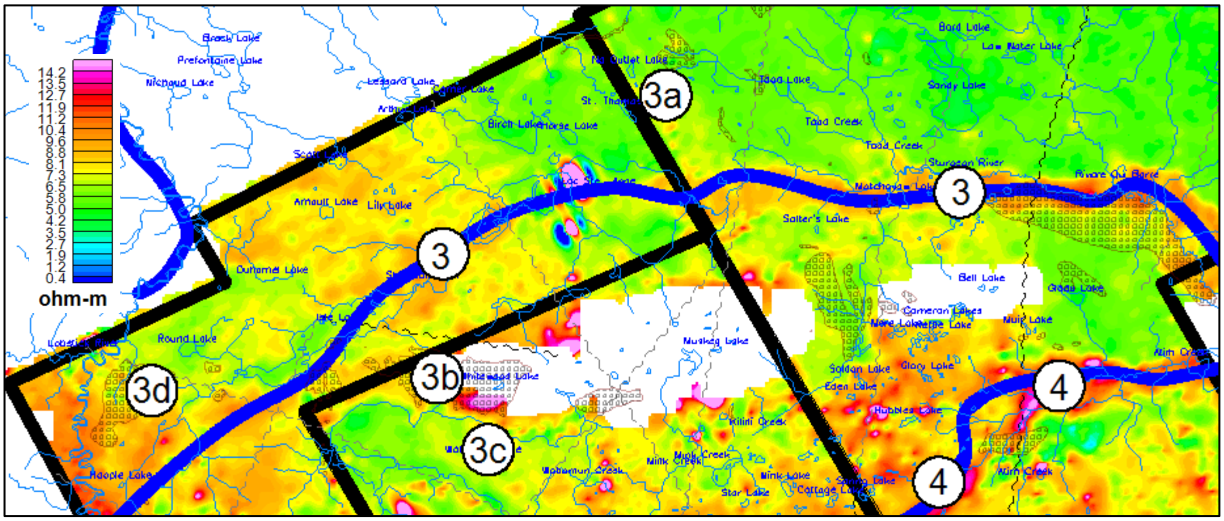

Figure 56: Terrain corrected depth slices at 620 m (above), 650 m (centre), and 680 m (bottom) showing the locations of the mapped buried bedrock valleys (heavy blue lines) and mapped sand and gravel deposits (hatched area) and potential basement lineaments.

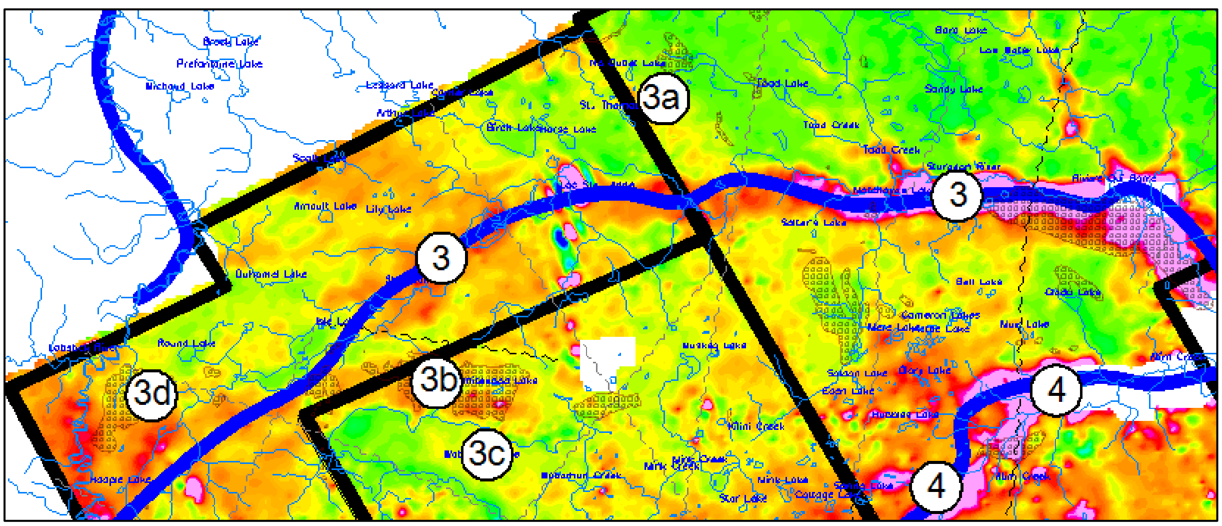

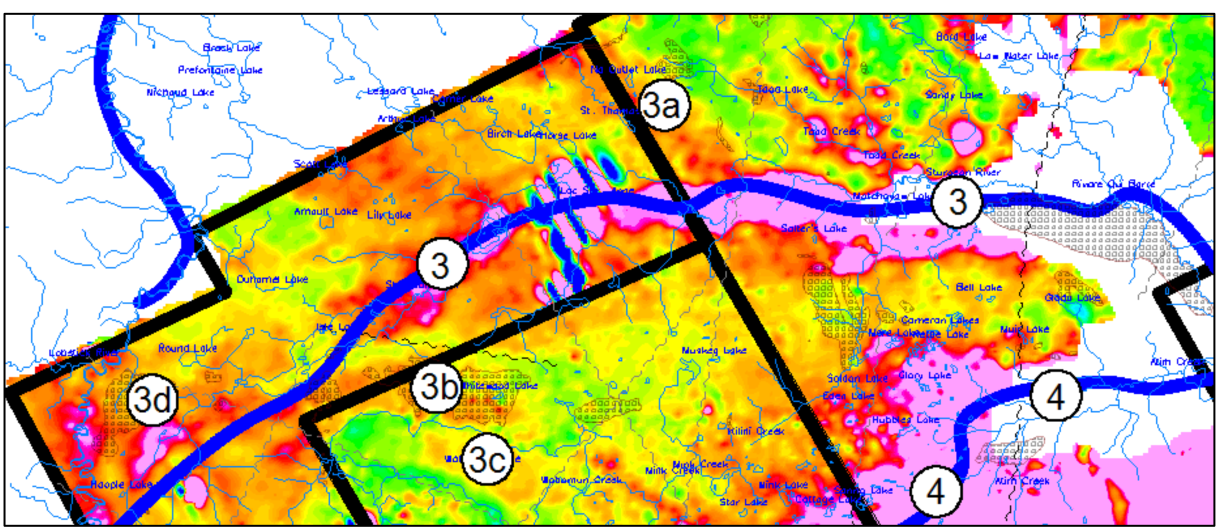

This selection follows a mapped buried bedrock valley. It is potentially fault controlled along sections of the feature as shown in Figure 56 on the previous page, and follows low-lying areas, but no specific current day river. The eastern section close to Edmonton closely corresponds with mapped sand and gravel deposits.

The elevated resistivities continue with the mapped bedrock valley to the western survey boundary; however the higher resistivities terminate at a possible basement lineament (see the bottom image o Figure 56) which passes through Isle Lake.

The area where the label 3a is located is a weakly resistive area, possibly branching from the buried bedrock valley, which does not appear to follow current topography. A broad expanse of area north of the western ③ label essentially between Duhamel Lake and the potential lineament which passes transects Lac Ste Anne also exhibits slightly elevated resistivities, which seem to persist to a greater depth than 3a.

The region of 3b lies south of a possible fault, and north of Wabamun Lake (shown also in Figure 44). It correlates with an area of mapped sand and gravel in elevated terrain.

The area of 3c lies directly to the south and is located within Wabamun Lake and exhibits slightly elevated resistivities in the east of the Lake, but quickly becomes more conductive with depth.

3d is located in a region of elevated resistivity, lying north of the mapped bedrock valley, the strongest response lies immediately west and south of the label and can identified from depth slices 650 to 750 m. A mapped area of sand and gravel deposits lies between these elevated responses.

Feature 4:

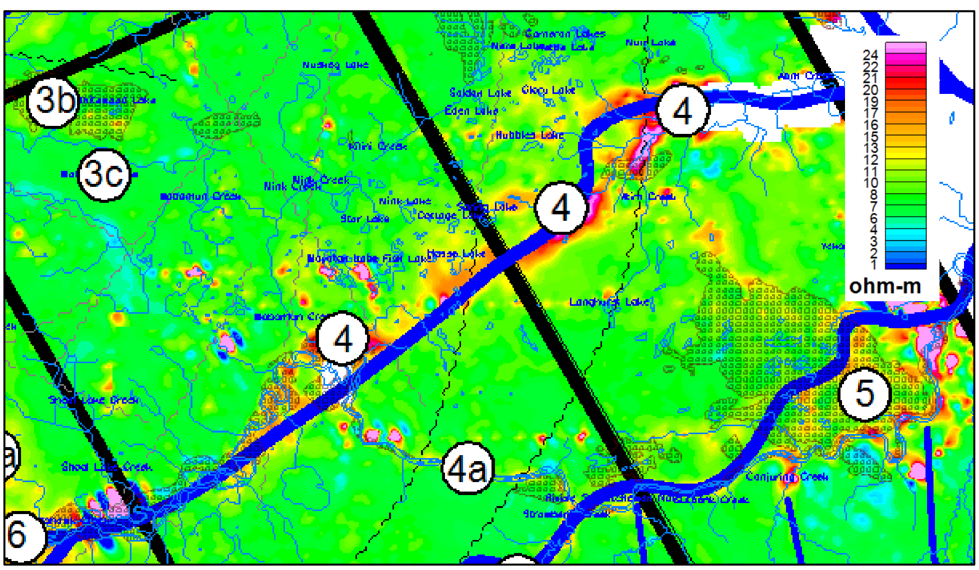

Figure 57: Terrain corrected depth slices at 650 m showing the locations of the mapped buried bedrock valleys (heavy blue lines), meltwater channels (thin blue lines), mapped sand and gravel deposits (hatched area), and potential basement lineaments.

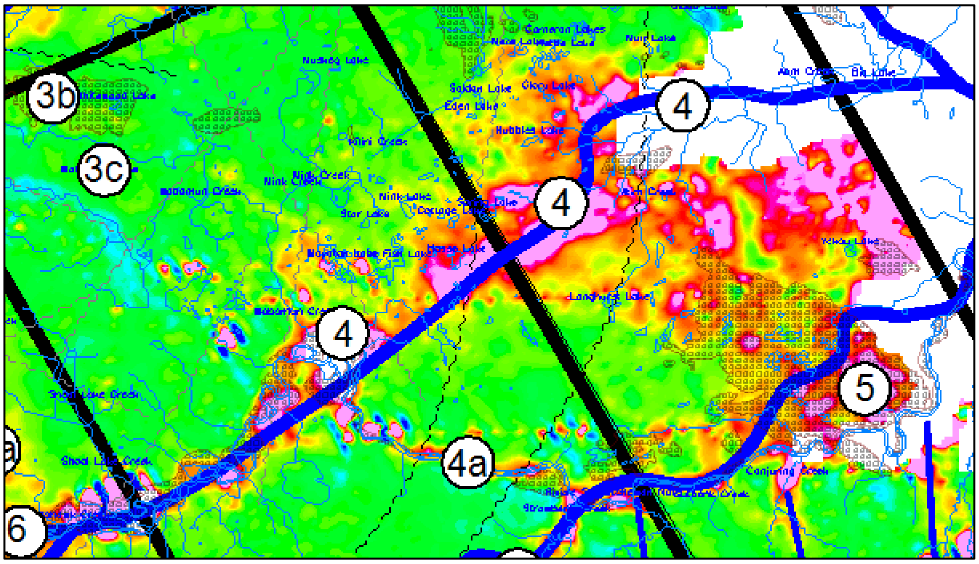

Figure 58: Terrain corrected depth slices at 680 m showing the locations of the mapped buried bedrock valleys (heavy blue lines), meltwater channels (thin blue lines), mapped sand and gravel deposits (hatched area) and potential basement lineaments.

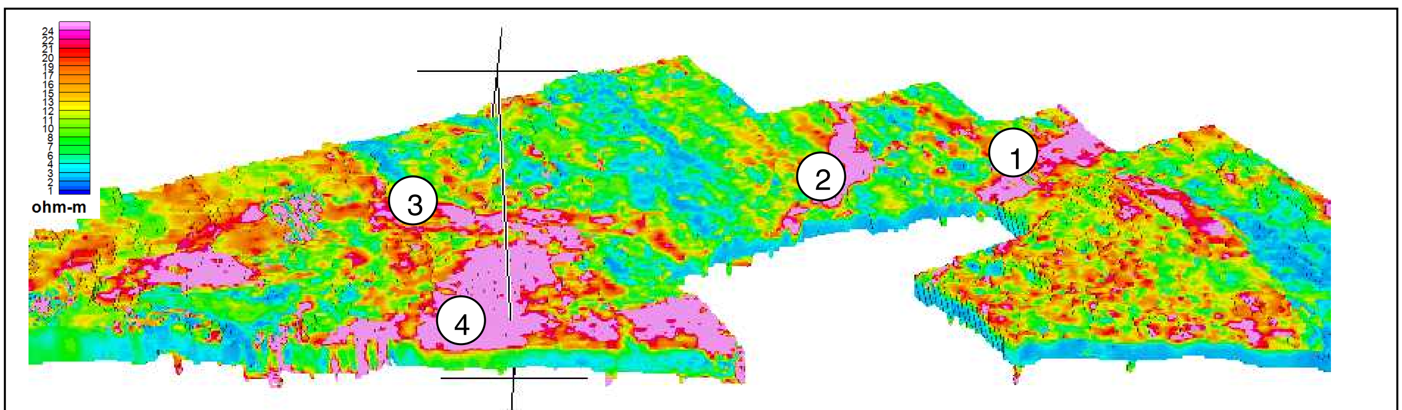

Figure 59: Slice through the terrain corrected 3D cube, limited to 800m elevation above and 700 m below. The crosshair is centred at the central ④ label in Figures 57 and 58.

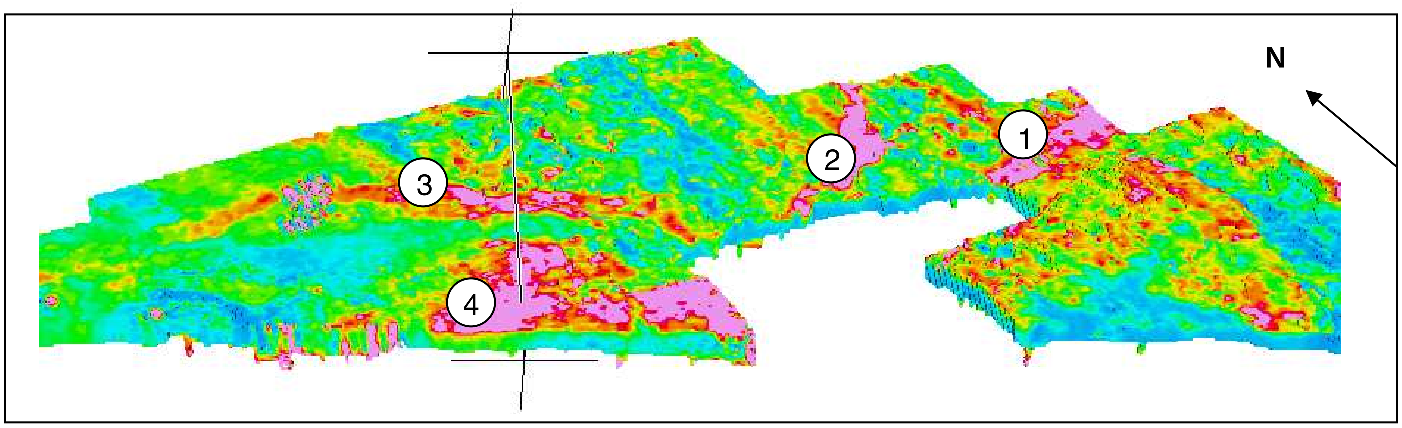

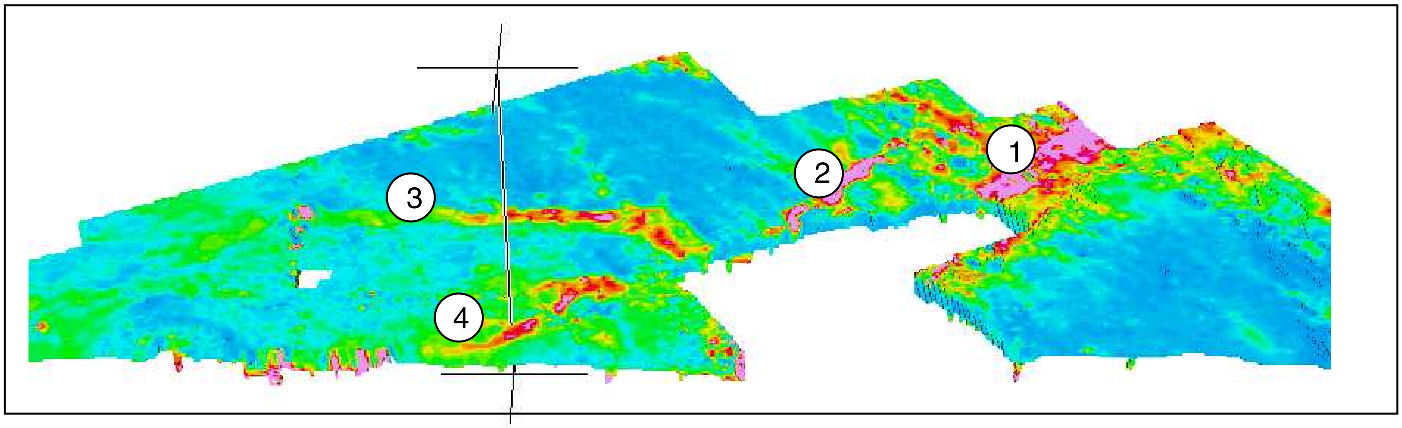

Figure 60: Slice through the terrain corrected 3D cube, limited to 650 m elevation above and 620 m below. The crosshair is centred at the central ④ label in Figures 57 and 58.

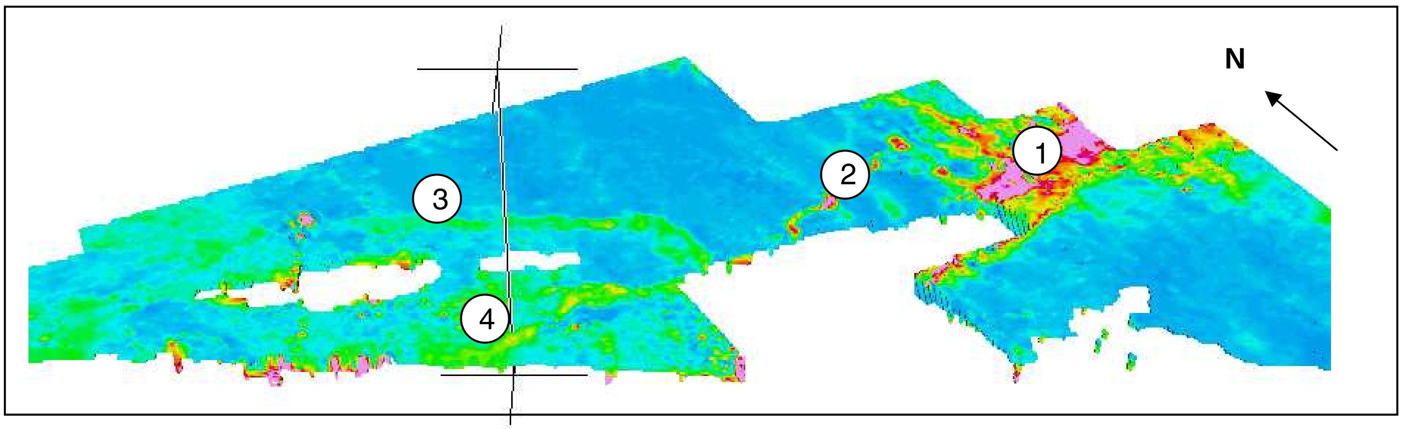

Feature 4 consists not only of the buried bedrock valley (from the survey border cutout over Edmonton to where it branches to become Feature 6) shown in Figures 57 and 58 but also, as shown in Figure 59, a region of highly resistive material to the north and east. Given the proximity to the city of Edmonton and the considerable culture within the vicinity, caution should be exercised when reviewing this data.

The depth slices through the terrain corrected 3D cube clearly indicate the bedrock valleys in the lower elevations.

The feature that is labeled as 4a follows a section of the Riviere Saskatchewan Nord and, although it is quite resistive near surface, it quickly returns to background levels. The section between the two potential NE-SW lineaments, exhibits some of the highest resistivities. The eastern of these lineaments seems to truncate the sand and gravel deposit lying to the east.

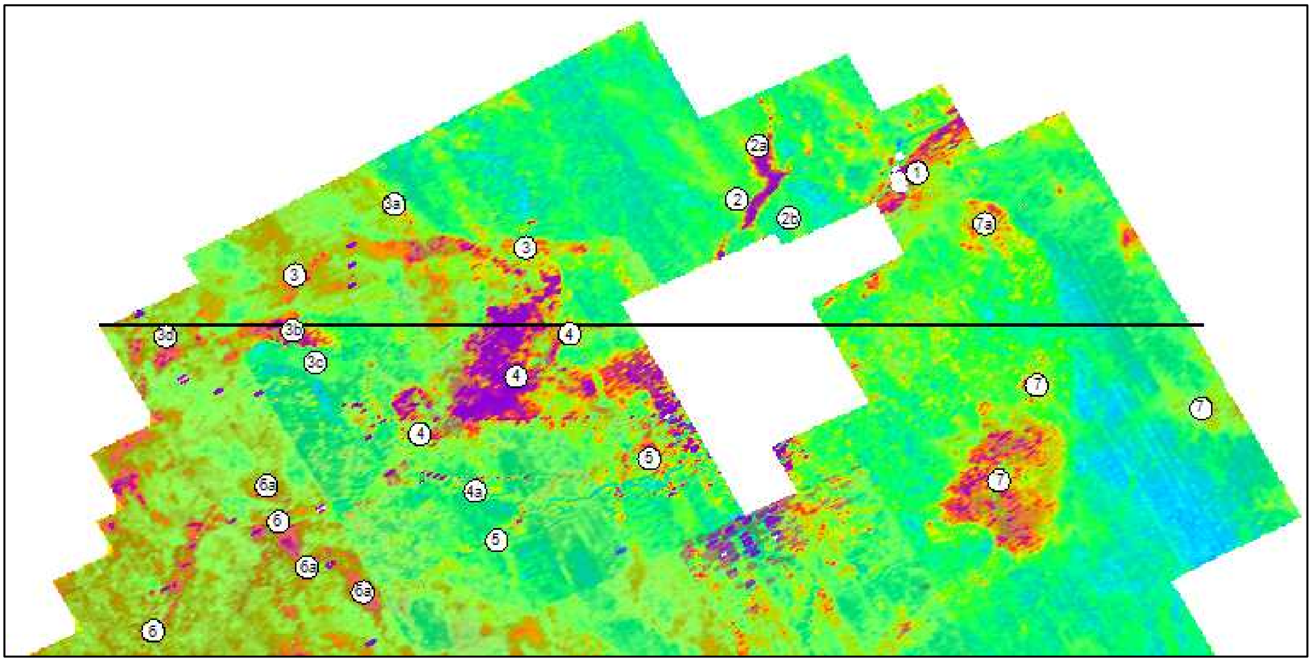

The image above is resistivity relative to surface at 0, 20, 30 and 60 m depth, with the surface grid being the most transparent. The horizontal line indicates the vertical slice that is shown in the 3D images. The top 3D image is relative to surface, the bottom 3D image is corrected for terrain. Features 3 and 4 area clearly seen.

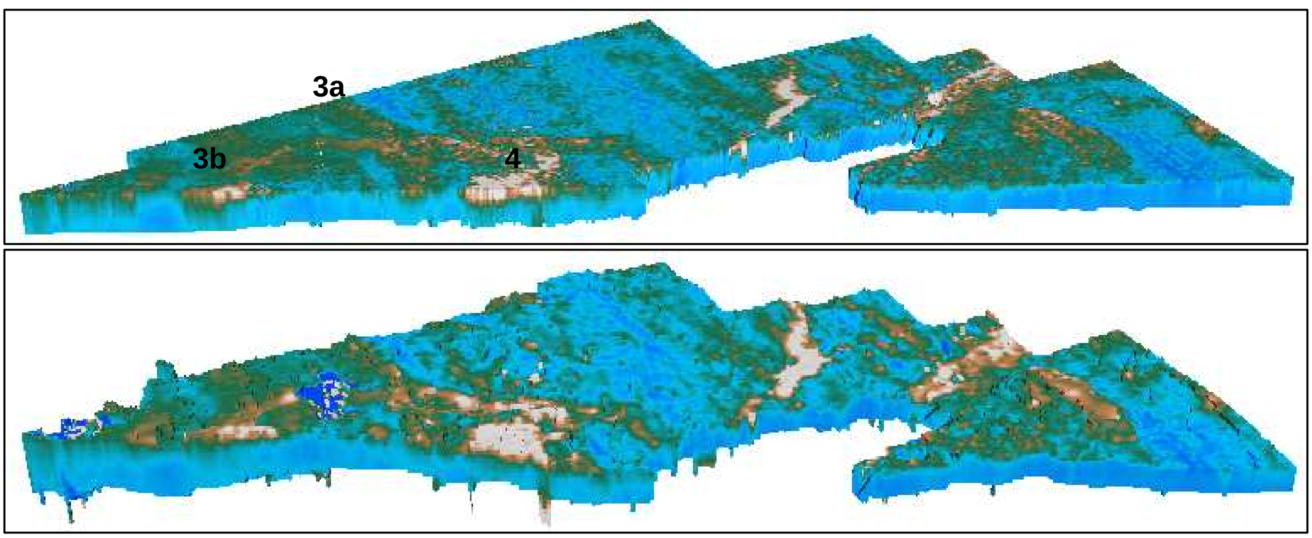

Feature 5:

This selection corresponds to the mapped location of a buried bedrock valley, lying WSW of Edmonton. As this area is in close proximity to Edmonton and its outlying areas, caution should be exercised when reviewing this data. The bedrock valley is mapped for a section to the north of the Riviere Saskatchewan Nord but then rejoins the river in the west.

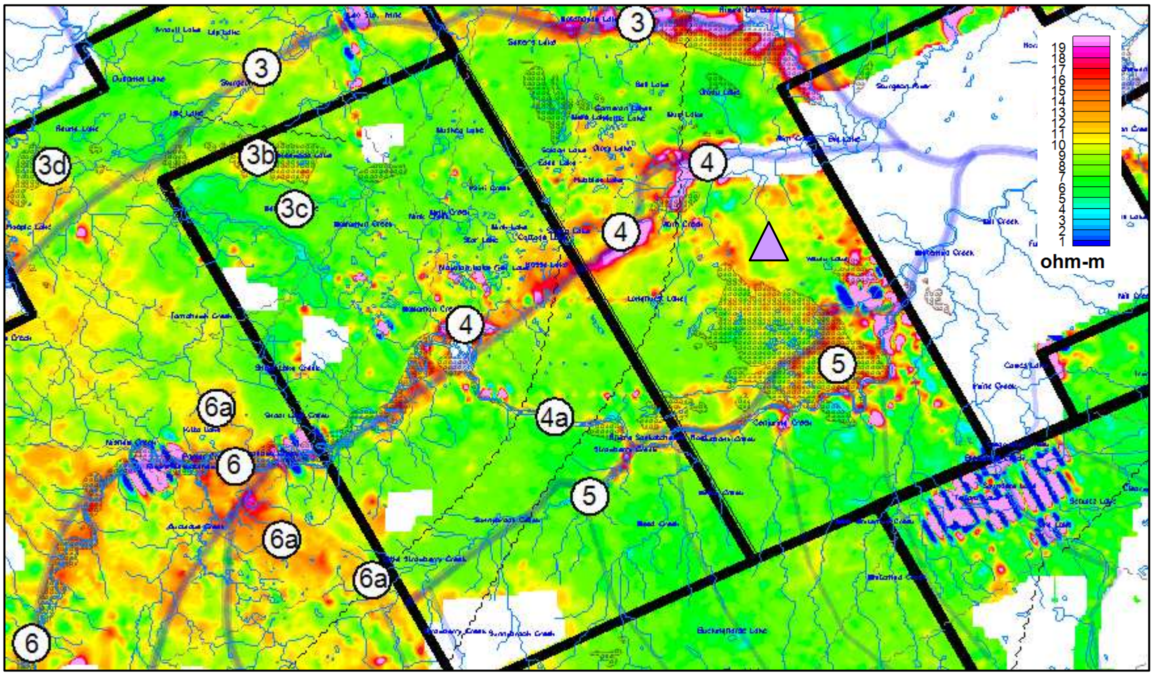

Figure 61: Terrain corrected depth slices at 650 m (above) and 600 m (below) showing the locations of the mapped buried bedrock valleys and meltwater channels (faded lines), mapped sand and gravel deposits (hatched areas), and potential basement lineaments.

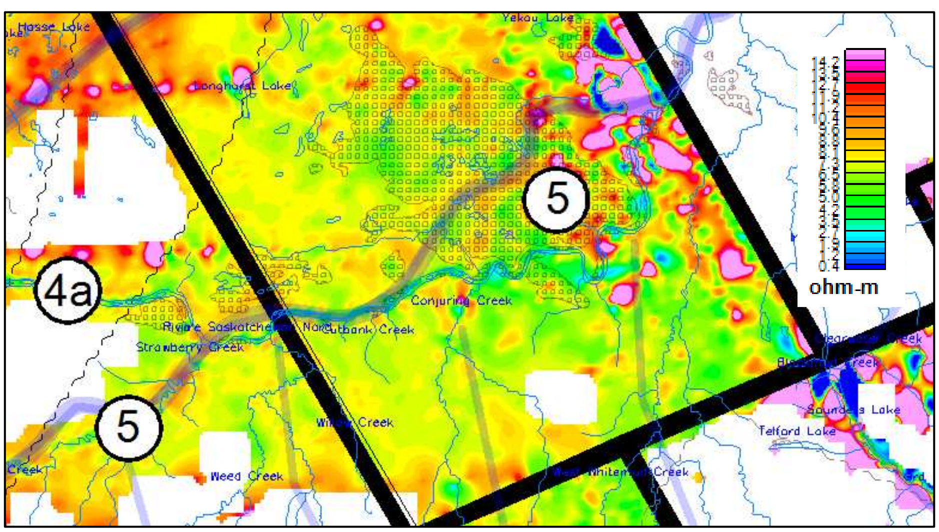

For a portion where the river and bedrock valley deviate, and for some distance further west, the EM data exhibits high resistivities near the surface (see the 650 m depth slice), but quickly becomes conductive by the 600 m depth slice (see also Figure 63).

Figure 62 below, shows the response of the bedrock valley at various elevations and several potential tributaries.

North of the eastern ⑤ symbol a broken area of high surface resistivity corresponds with a mapped region of sand and gravel deposit.
A triangle symbol in Figure 61 between bedrock valleys 4 and 5 suggests a potential lineament along the northern limit of the sand and gravel deposit.

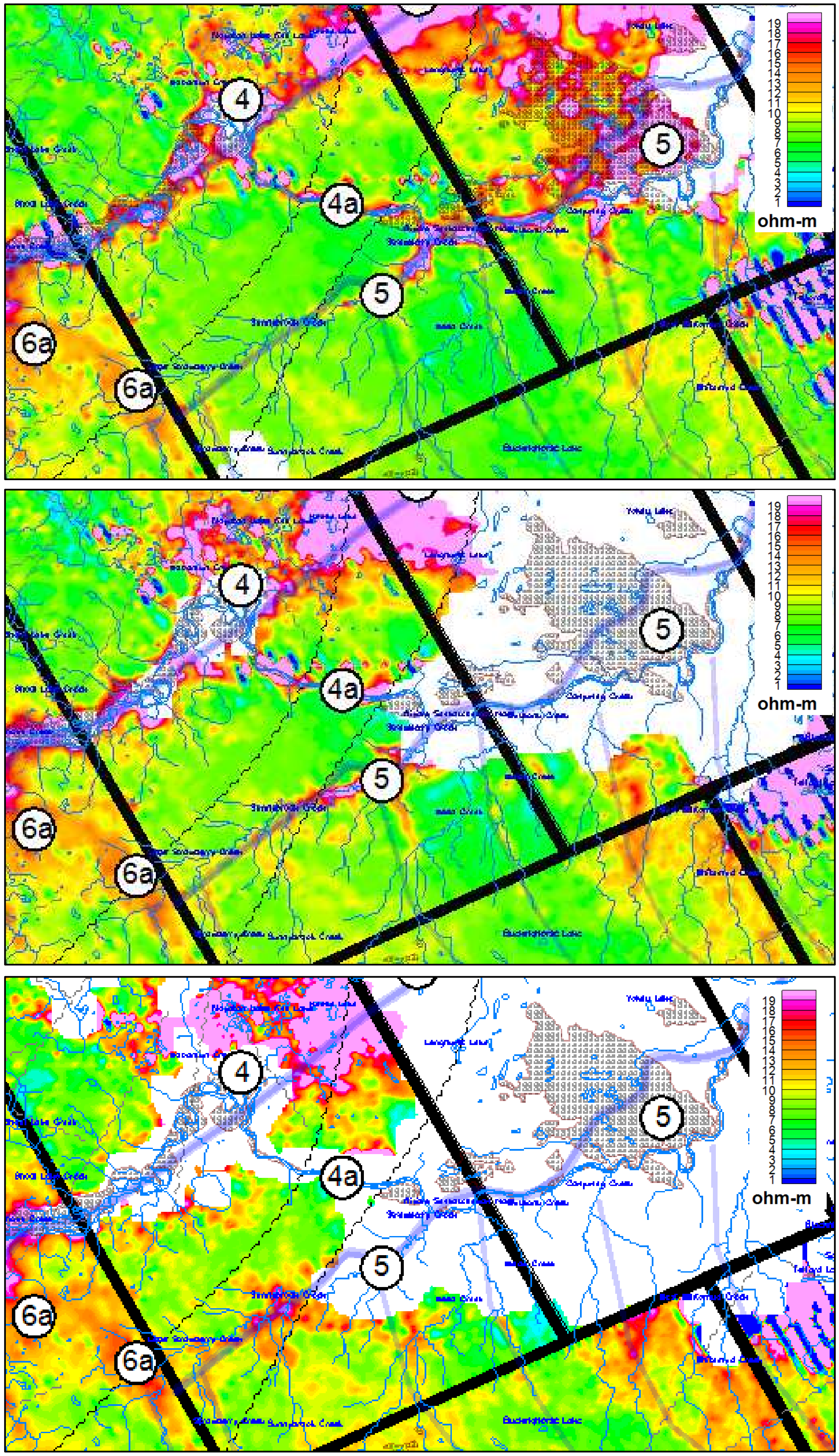

Figure 62: from top to bottom: Terrain corrected depth slices at 680 m, 700 m, and 720 m showing the locations of the mapped buried bedrock valleys, meltwater channels, mapped sand and gravel deposits (hatched area), and potential basement lineaments.

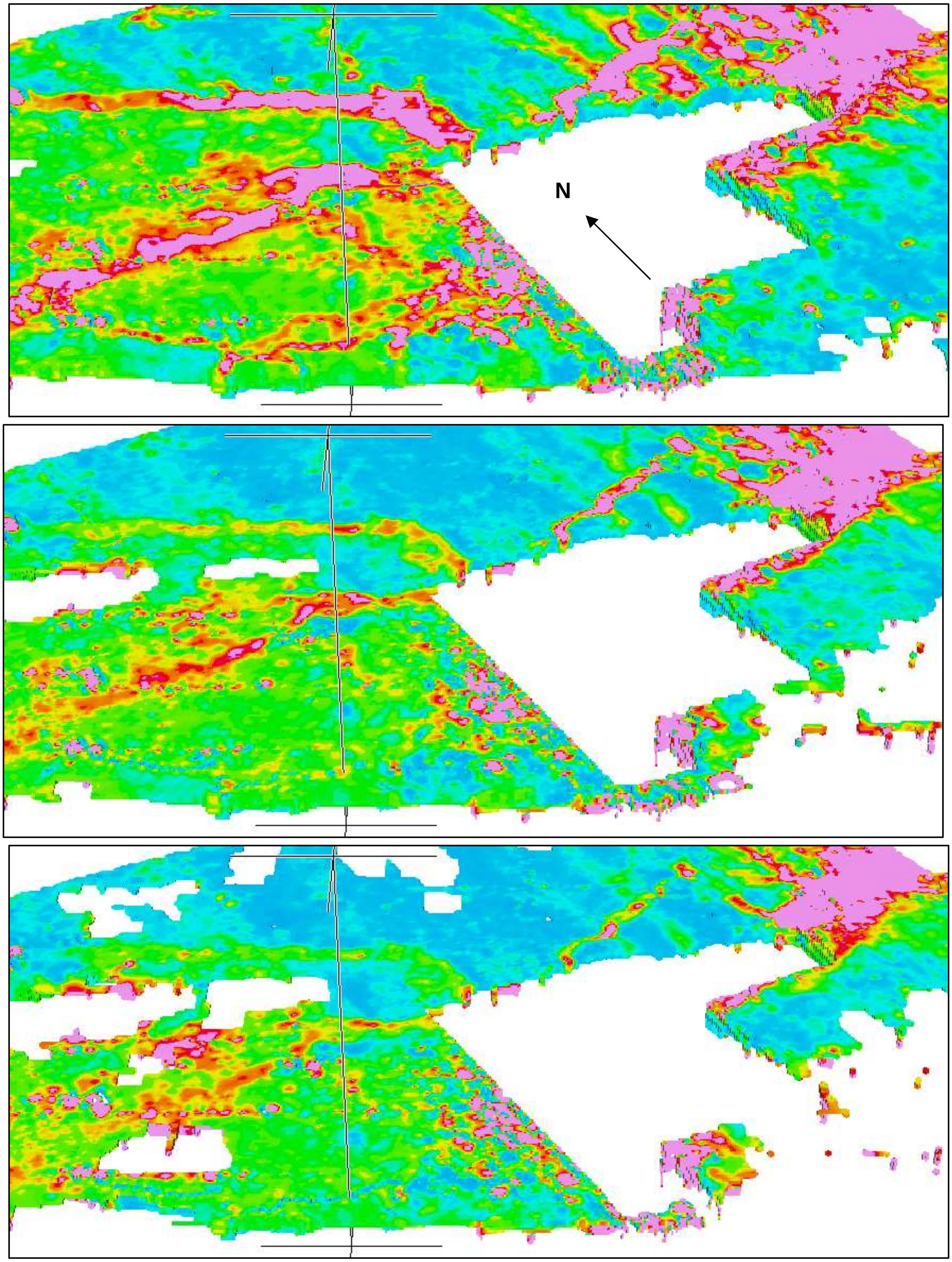

Figure 63: Slices through the terrain corrected 3D cube, limited to 650 m elevation (top), 620 m (centre), and 600 m (below). The crosshair is centred midway between the two ⑤ labels along the Rivere Saskatchewan Nord, south of the bedrock valley.

Feature 6:

This is where the bedrock valley of feature 4 branches to the south and southwest. The southwestern branch remains closely following the Riviere Saskatchewan Nord, whereas the southern branch although in the north lies within low terrain, further south the terrain becomes elevated.

The feature 6a extends north and southeast of the mapped bedrock valley and appears to be independent of the current topography. The northern section is moderately weak, and does not appear to extend to significant depth, whereas from the grids relative to surface there still seems to be some expression from the southern branch to 120 m depth. This southern region also lies between two of the structures seen in the magnetic data which are delineated in Figures 8, 9 and 41.

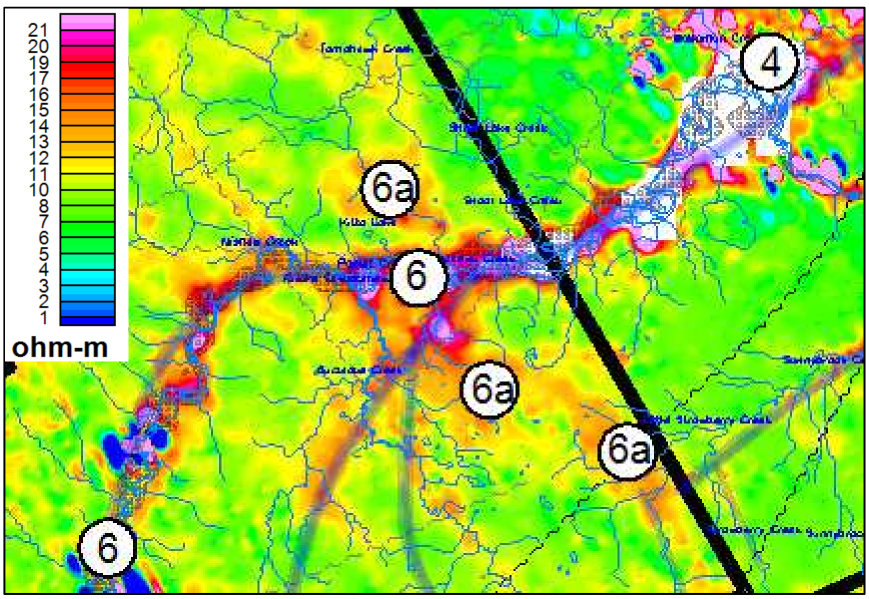

Figure 64: Terrain corrected depth slice at 700 m elevation (above) and the resistivity at 120 m below surface (below) showing the locations of the mapped buried bedrock valleys, meltwater channels, mapped sand and gravel deposits, and potential basement lineaments.

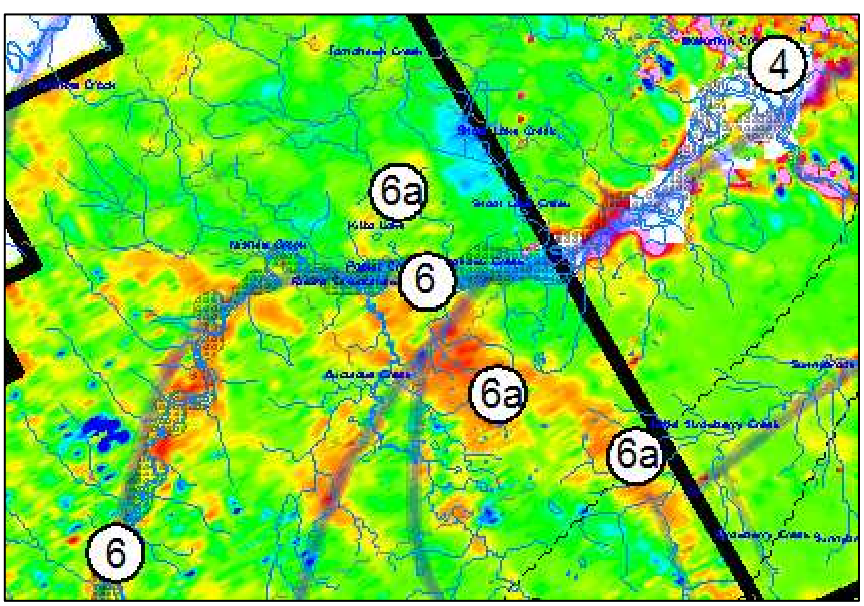

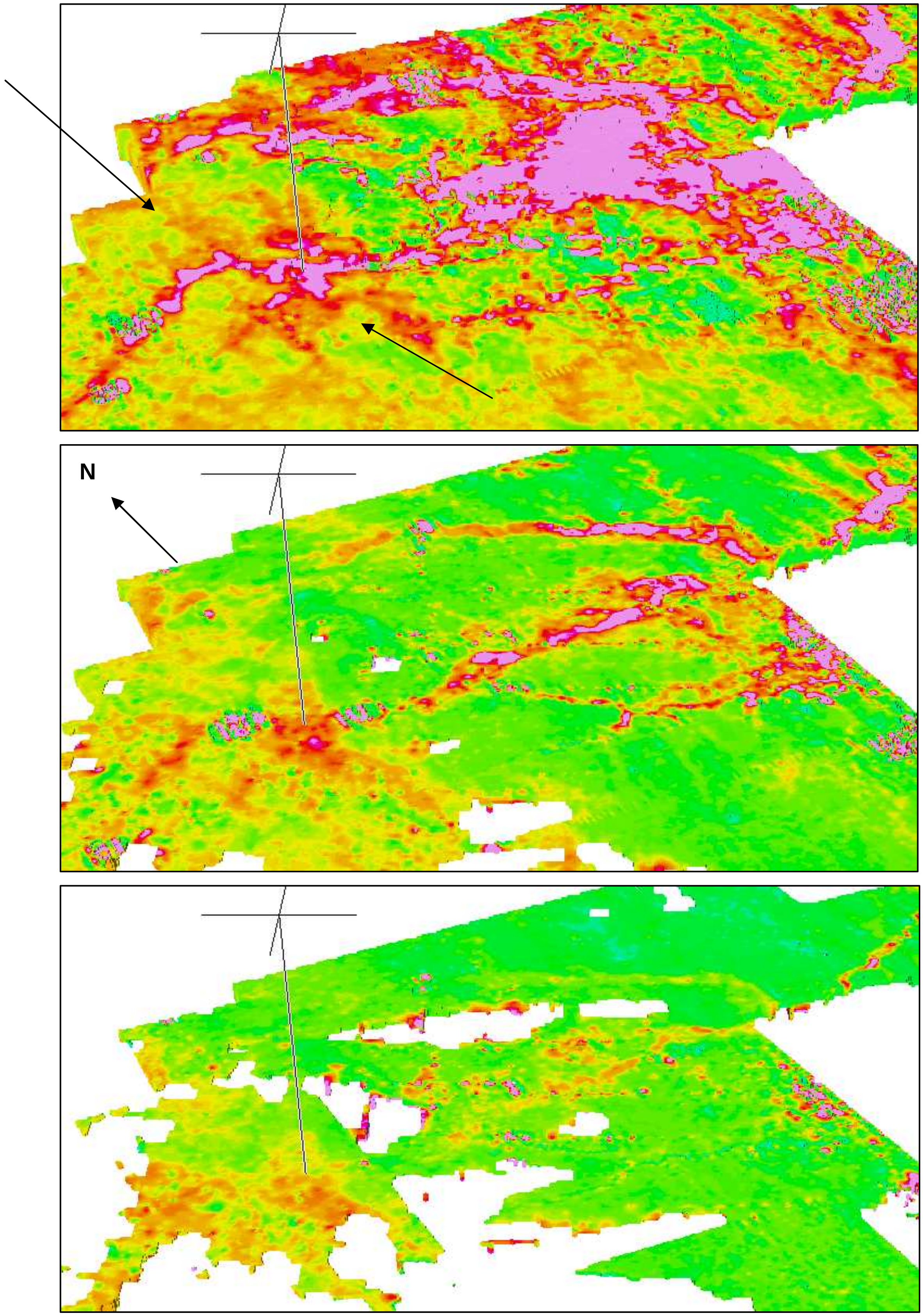

Figure 65: Slices through the terrain corrected 3D cube, limited to 740 m elevation (top), 660 m (centre), and 610 m (below). The crosshair is centred on the northern ⑥ label.

The top image in Figure 65 appears to indicate a potential fault (shown between the two arrows) however this is not seen in either the magnetic data or the digital terrain model.

Feature 7:

A near circular region of resistivity spanning north and south of the buried bedrock valley in Figure 66 likely extends weakly to the northeast, and then changes direction to north to join up with feature labeled as 7a. The trend also corresponds with elevated terrain and its eastern boundary corresponds with a mapped lithologic boundary between Horseshoe Canyon and Bearpaw Formations. With slices through the terrain corrected voxel to lower elevations, this area becomes more clearly defined as sinuous trends (see Figure 68).

The area where label 7a is located, in the near surface seems to correlate with feature 7 to the south however with depth (see Figure 69 the resistivity at 120 m below surface) 7a seems to be connected more with feature 1.

Figure 70 shows the buried bedrock valley extending WSW under Beaverhill Lake. The arrows in the image point to two more possible branches extending from the bedrock valley.

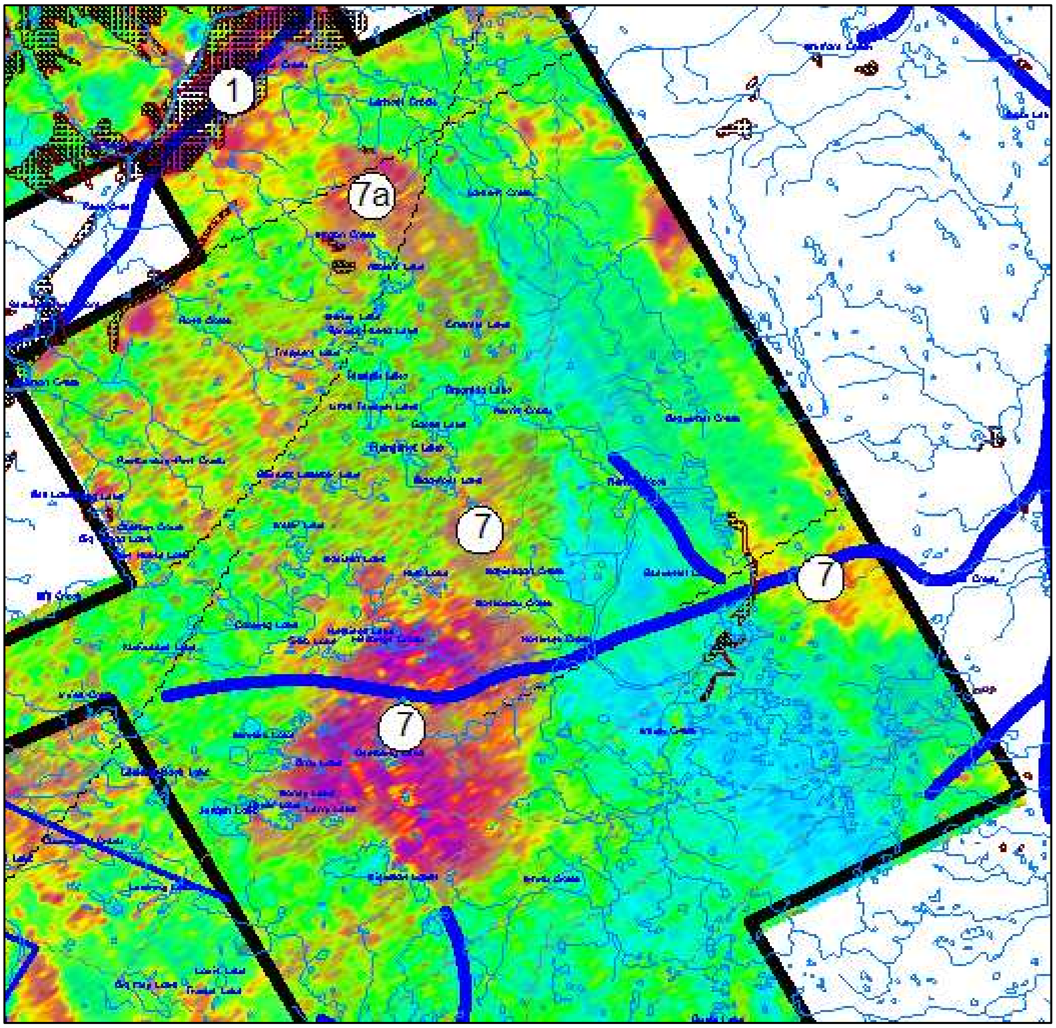

Figure 66: This image is resistivity relative to surface at 0, 20, 30 and 60 m depth, with the surface grid being the most transparent. The locations of the mapped buried bedrock valleys (heavy blue lines), meltwater channels (thin blue lines), mapped sand and gravel deposits (hatched area), and potential basement lineaments are also shown.

Figure 67: View from the top of the terrain corrected 3D cube.

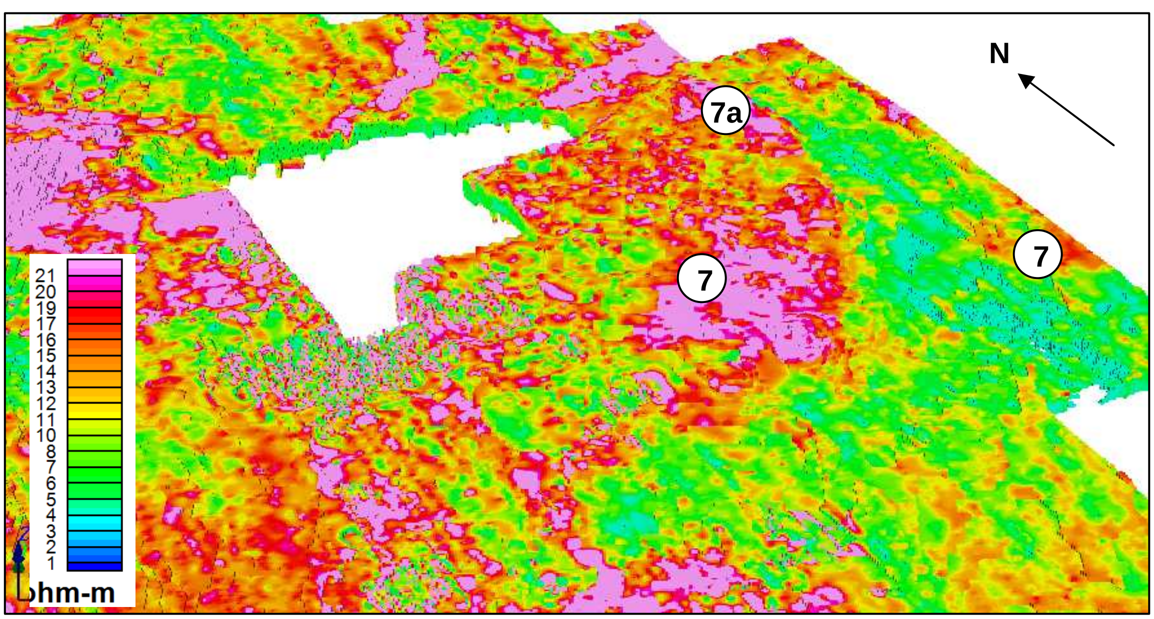

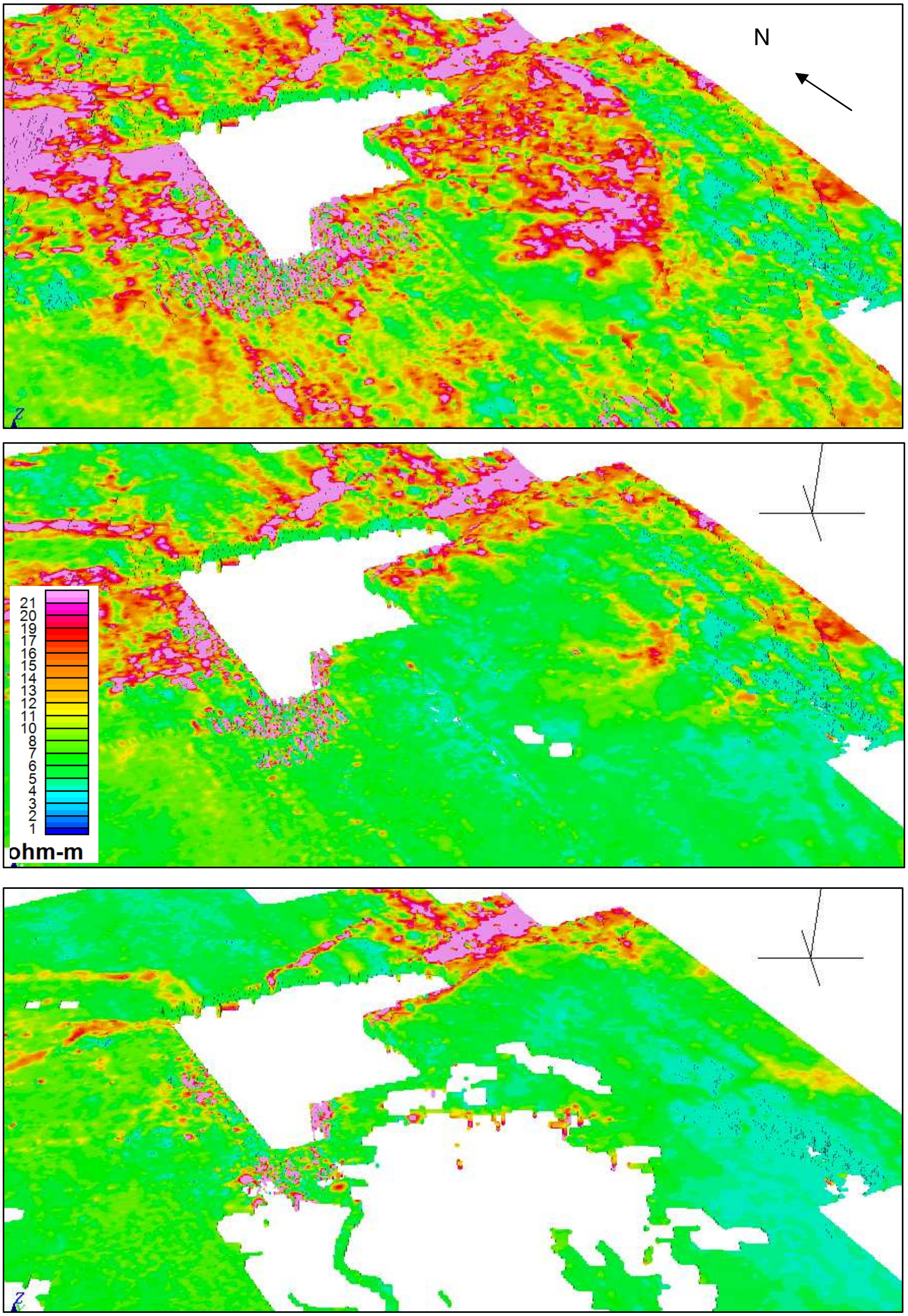

Figure 68: Slices through the terrain corrected 3D cube, limited to 730 m elevation (top), 670 m (centre), and 630 m (below).

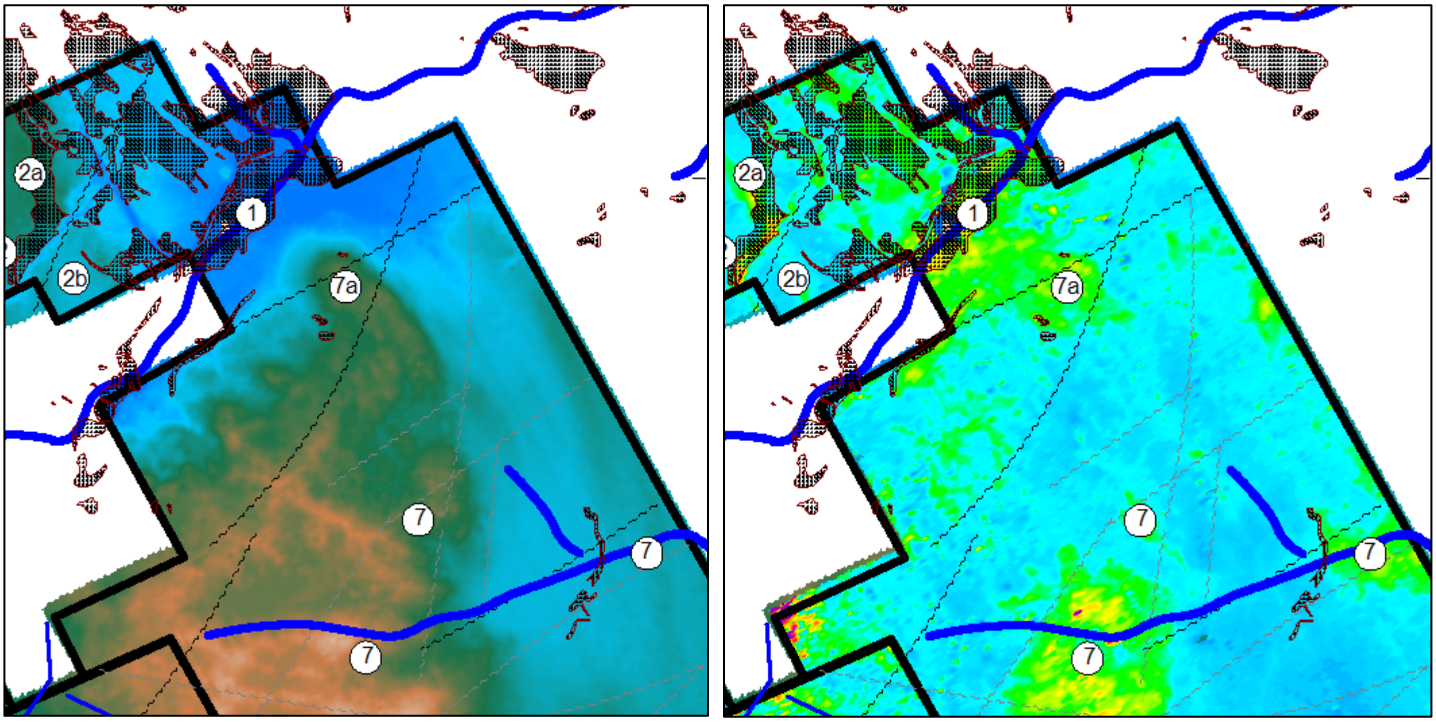

Figure 69: Digital Terrain model (left), resistivity below surface at 120 m depth (right). The images are overlain by the buried bedrock valleys (heavy blue lines) meltwater channels (thin blue lines), the sand and gravel deposits (hatched areas) and potential basement lineaments.

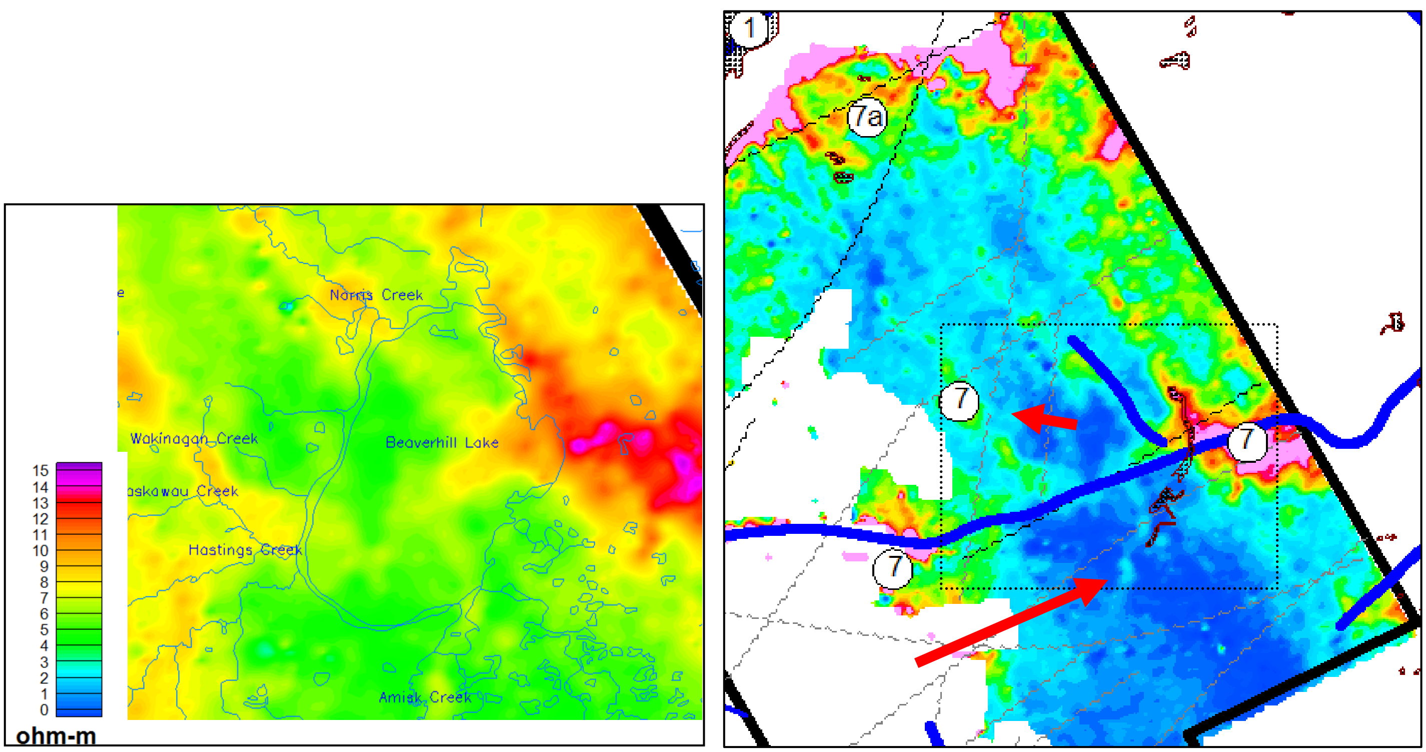

Figure 70: Resistivity at a 620 m elevation with different colour palettes. The location of the left image is shown as an outline on the right image.

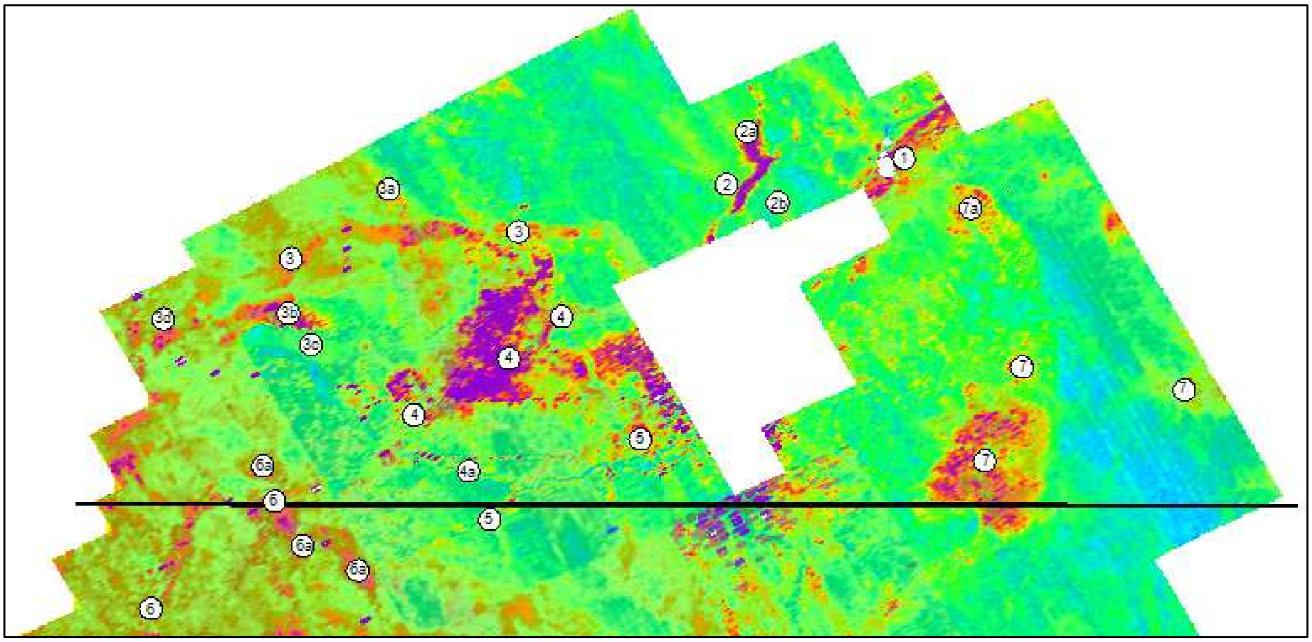

The image above is resistivity relative to surface at 0, 20, 30 and 60 m depth, with the surface grid being the most transparent. The horizontal line indicates the vertical slice that is shown in the 3D images. The top 3D image is relative to surface, the bottom 3D image is corrected for terrain. Features 6 and 7 are clearly seen however 5 is not that obvious except for in the terrain corrected image. Both images are looking to the north.

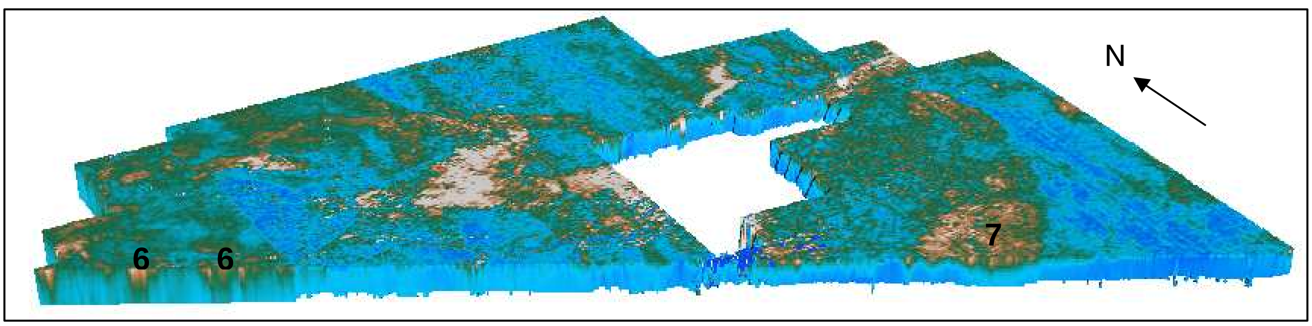

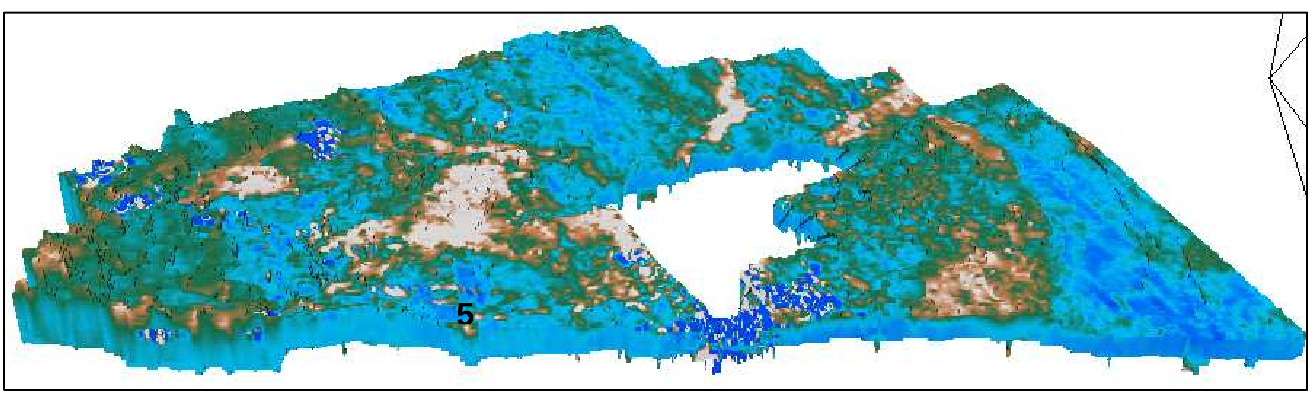

Feature 8:

Rather than a single feature, this is more a region of interest with, as seen below in Figure 71 this is an area of generally elevated resistivity which, from the vertical slices, do not appear to be just surficial responses.

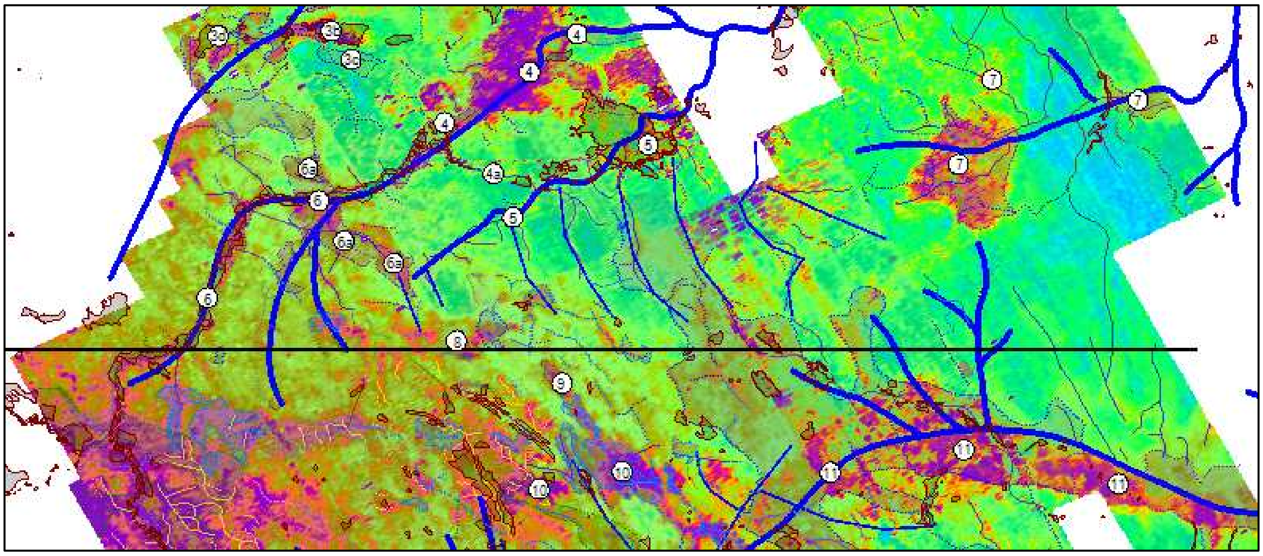

Figure 71: This image is resistivity relative to surface at 0, 20, 30 and 60 m depth, with the surface grid being the most transparent. The locations of the mapped buried bedrock valleys (heavy blue lines), meltwater channels (thin blue lines), mapped sand and gravel deposits (hatched areas), and the lineaments and areas of interest are shown.

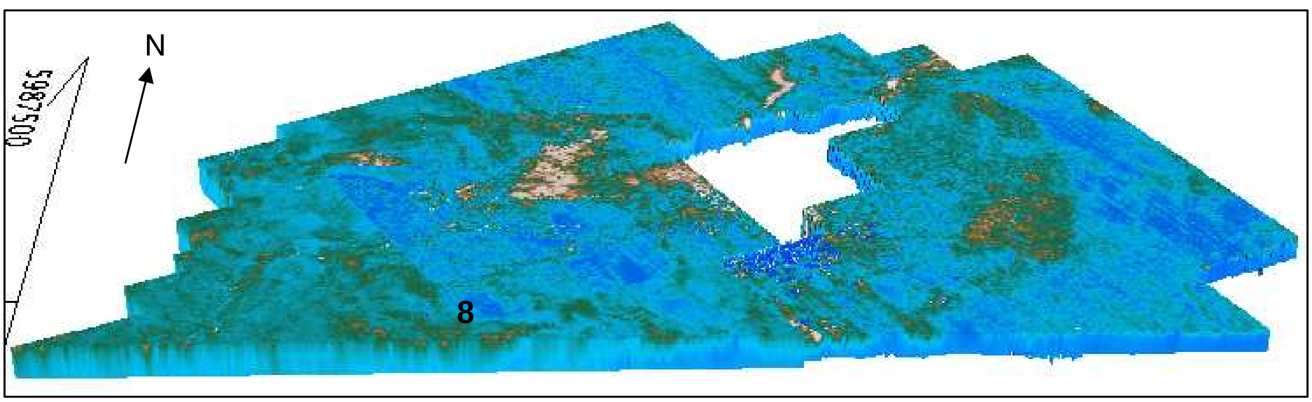

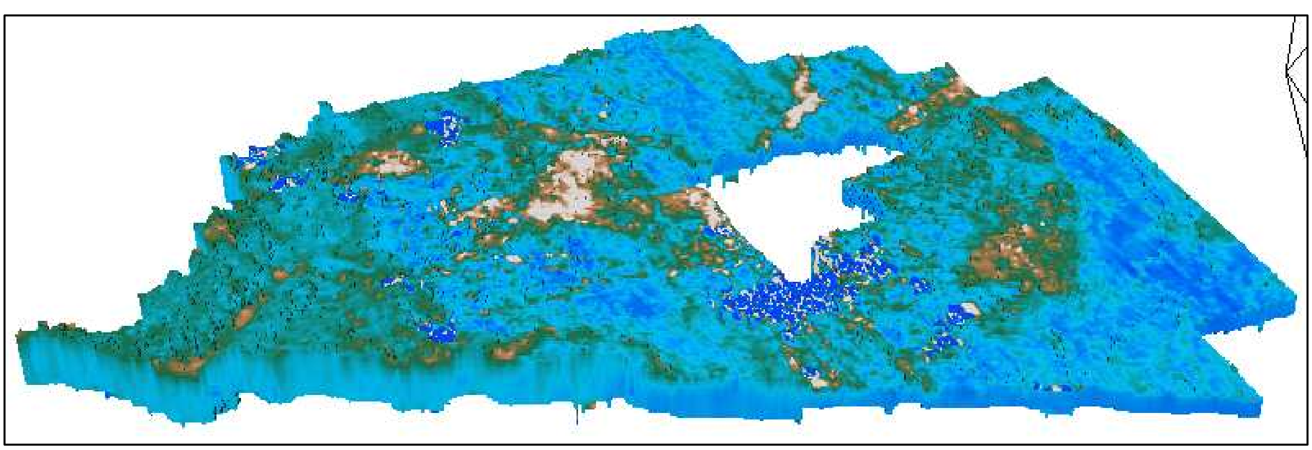

This feature lies within the same confined low lying area as feature 9, so this may be its northern extension.

Feature 9:

This is the Pigeon Lake trend that has been mentioned previously. From the image below it seems the trend continues for some distance to the south, through a large area of high resistivity (feature 10) to the northern end of the Red Deer buried bedrock valley.

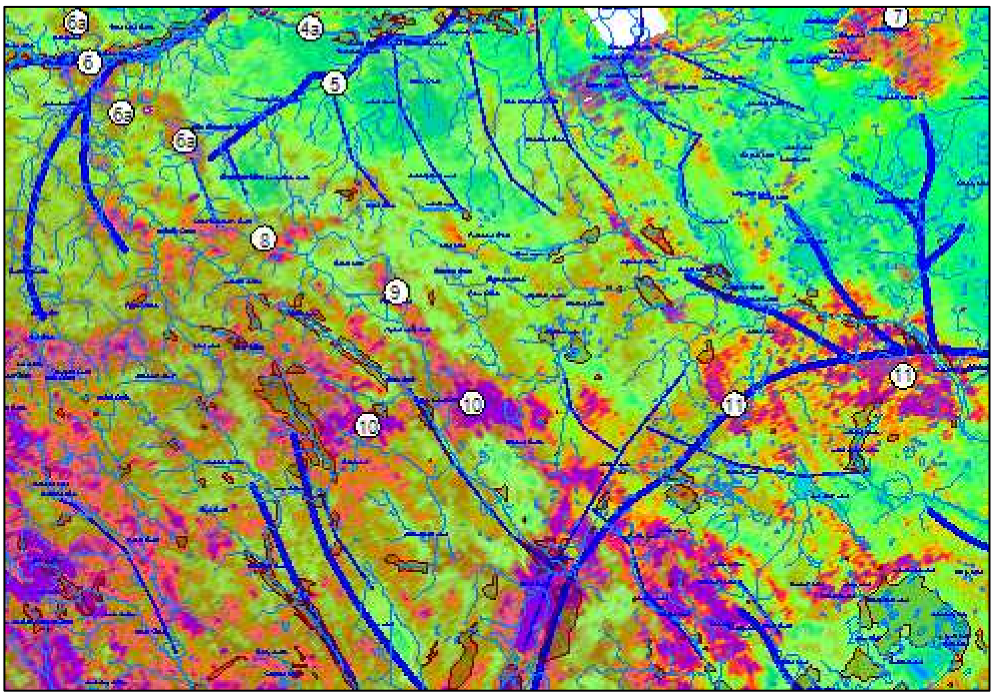

Figure 72: (above) this image is resistivity relative to surface at 0, 20, 30 and 60 m depth, with the surface grid being the most transparent. The locations of the mapped buried bedrock valleys (heavy blue lines), meltwater channels (thin blue lines), and mapped sand and gravel deposits (hatched areas) are shown; (below) vertical slice through the northern part of feature 9.

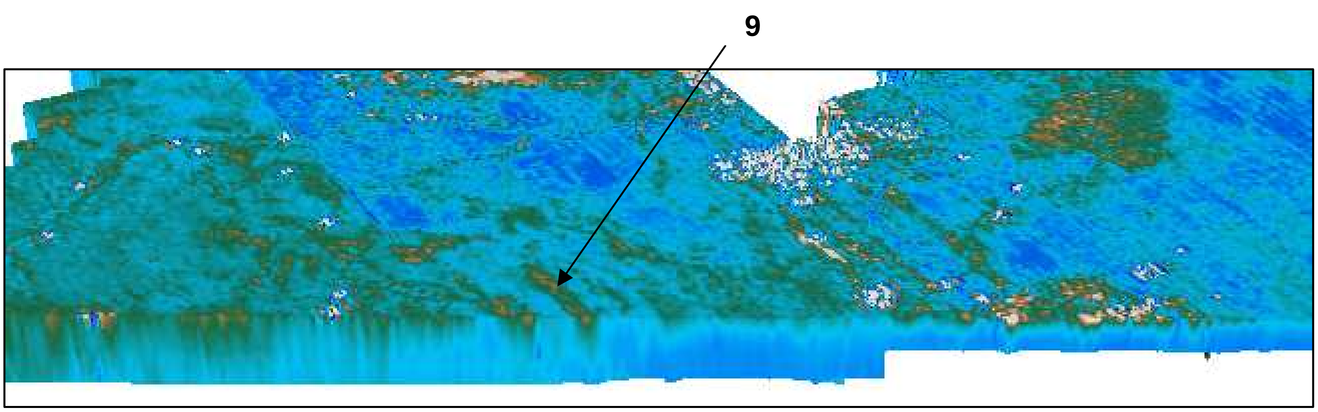

Features 10:

These points of interest (see Figure 72) relate to two larger areas of high resistivity, of which the southern limit appears to be fault controlled.

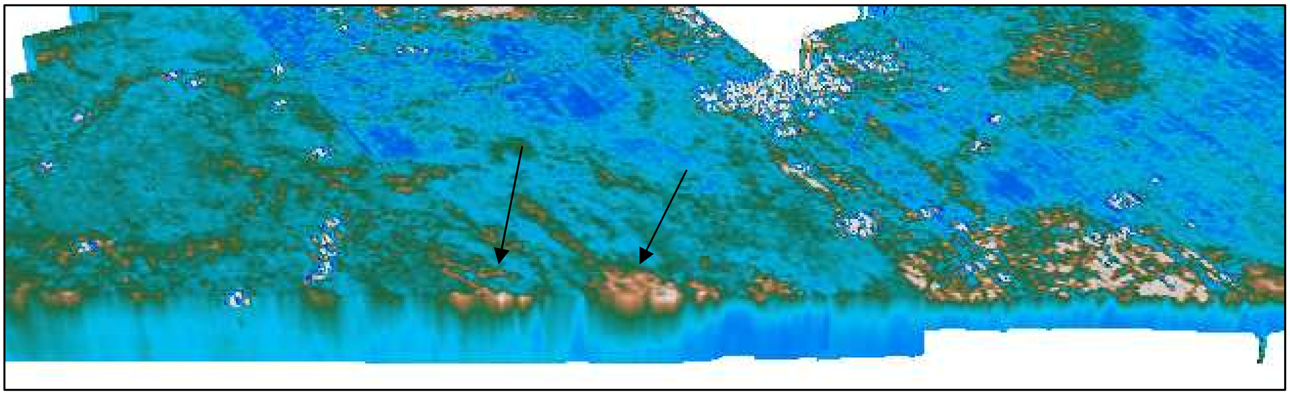

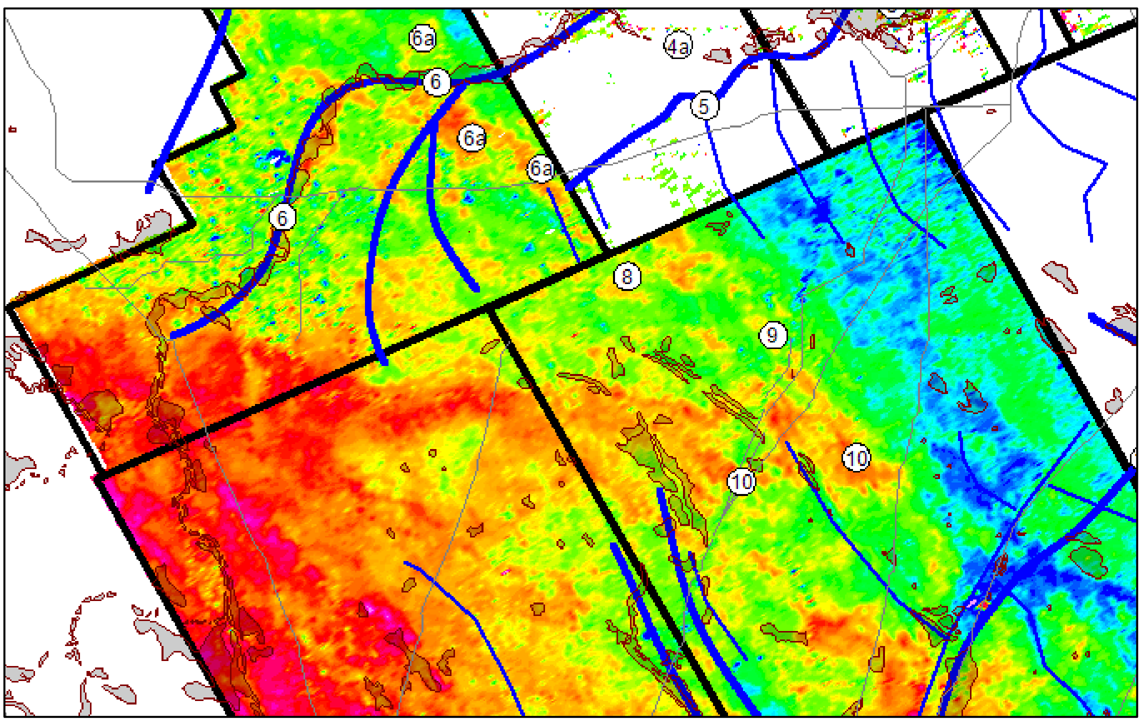

Figure 73: Vertical slice through feature 10 (above) and Resistivity at 120 m below surface (left) showing the location of pipelines, and (below) the terrain corrected depth slice at 850 m elevation, with the sand and gravel deposits (hatched areas).

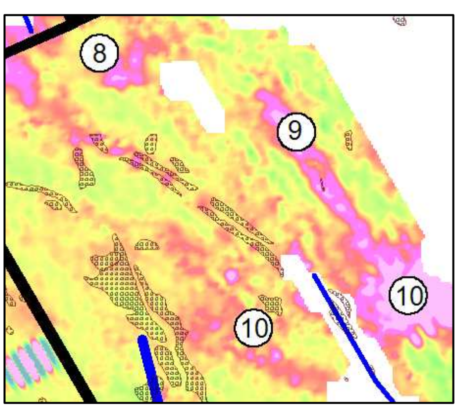

The Resistivity image at 120 m below surface in Figure 73, suggests that the western zone at least is an extension of the more resistive material to the west. It appears that perhaps a fault may separate, and perhaps offset, the two points of interest, or this may just be the response to a pipeline crossing the area (see Figure 73).

A weak lineament shown in Figure 73 at the 850 m elevation corresponds with mapped sand and gravel deposits.

Feature 11

This zone of interest (shown in Figures 71 and 74) is controlled in part by two large scale features (see Figure 41), bounding it to the north and south. This feature curves with the mapped bedrock valley to become part of the Red Deer bedrock valley. The south controlling fault also provides a truncation to several sand and gravel deposits along its length, and perhaps coincides with a slight change in direction of the bedrock valley and the Battle River. The northern structure is less clearly defined.

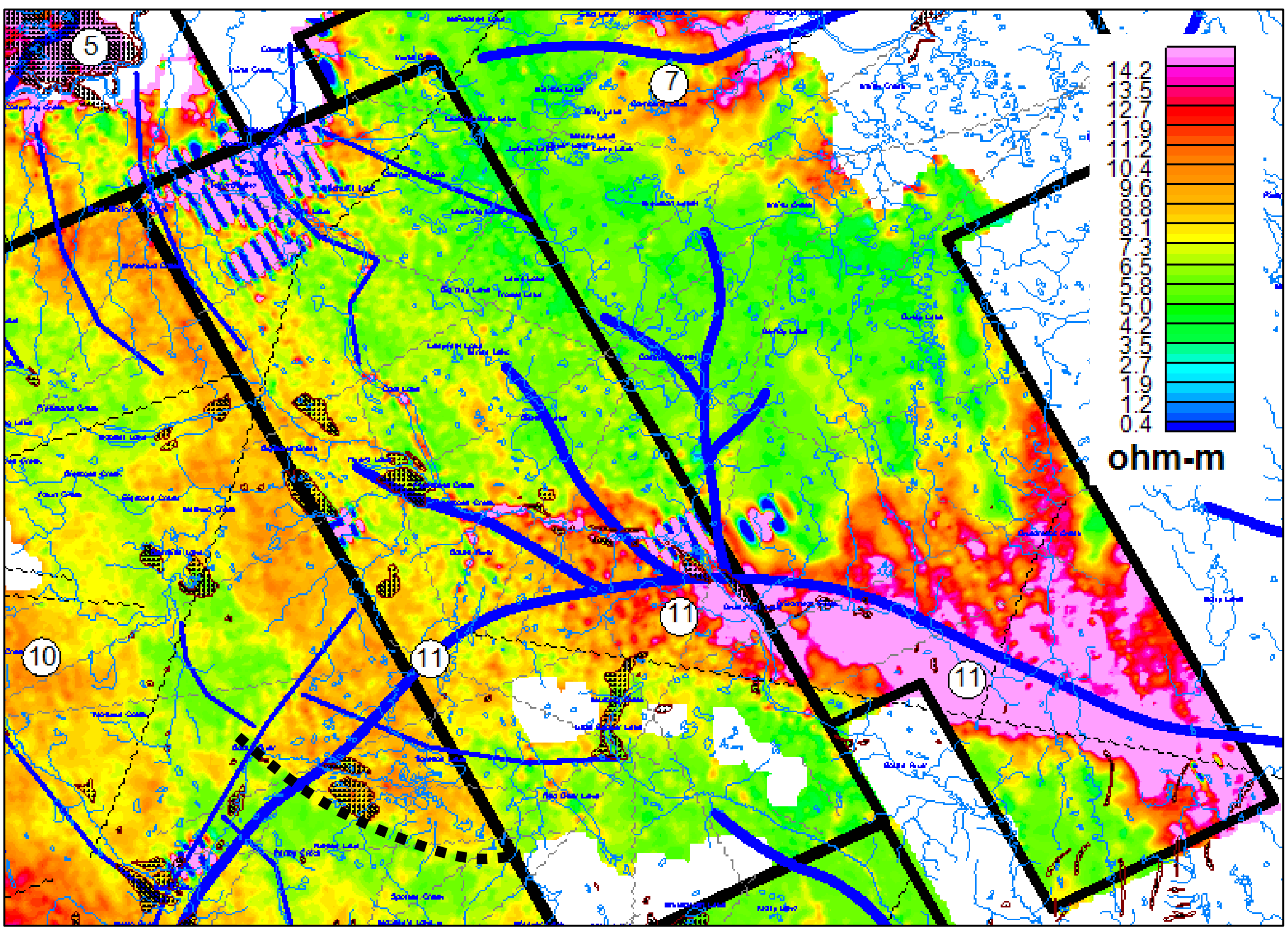

Figure 74: Resistivity at 680 m elevation. The bedrock valleys and meltwater channels are shown as heavy and thin blue lines respectively. Sand and gravel deposits are seen as hatched areas, and brown outlines, and potential faults are also shown.

The WNW trend of feature 11 seems to stop at the Battle River before changing direction (and showing a decrease in resistivity) to NNW-SSE. Although this feature follows the boundary between the 30 Hz and 90 Hz Geotem surveys, and there is a slight change in amplitude of the resistivity, the trend does continue over the boundary. Feature 11 is terminated in the south where the dotted line is shown in Figure 74. The trend continues towards the east as shown in Figure 77.

Figure 75 shows 3 triangles over slightly above background resistivity. The northernmost may indicate an ENE trend towards selection 7.

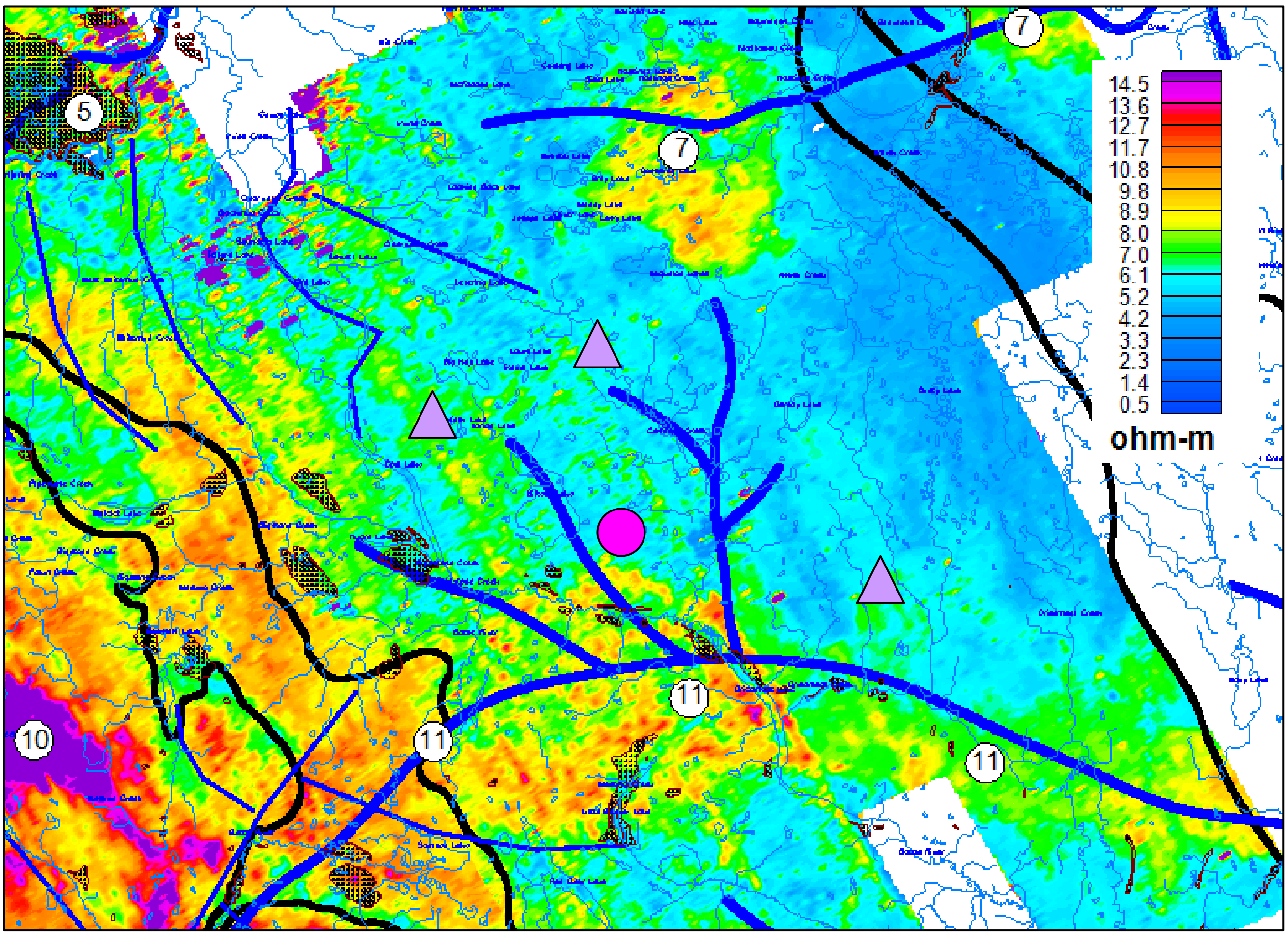

Figure 75: Resistivity depth slice at 60 m below surface, along with the bedrock valleys, meltwater channels and sand and gravel deposits, the lithologic boundaries are also displayed.

Both Figure 75 and the 3D cube image 40 m below surface in Figure 76 suggest sinuous trends which are relatively shallow (see the circular symbols in both Figures).

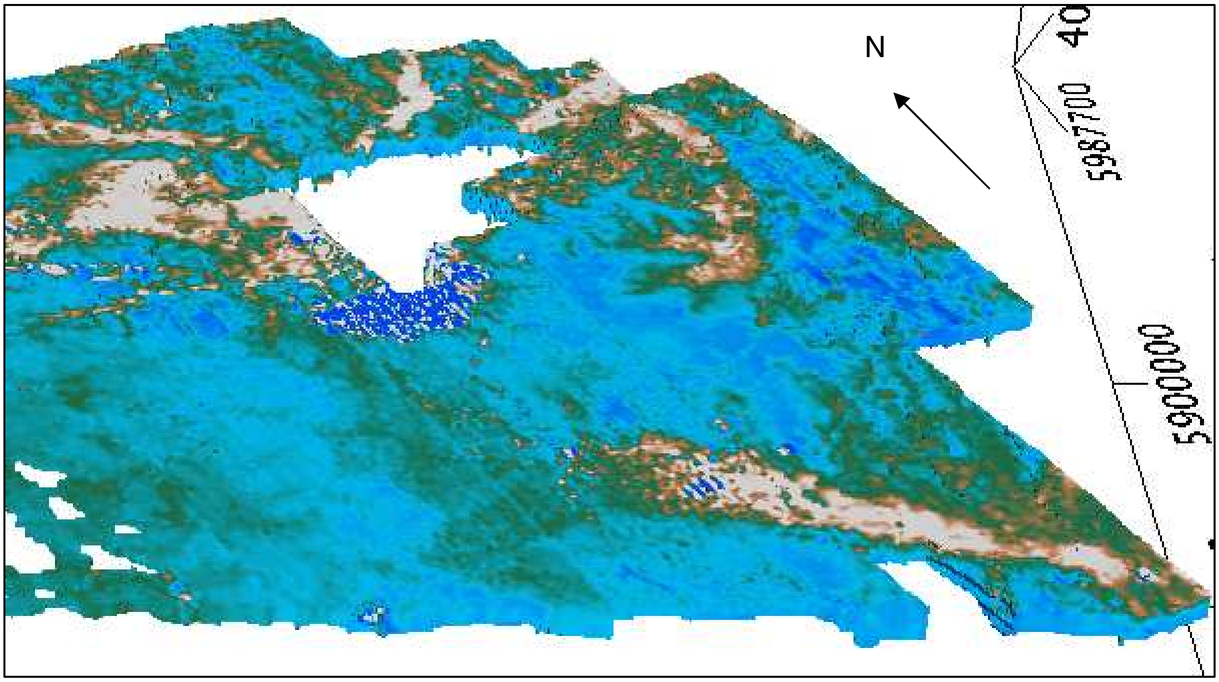

Figure 76: Slice through terrain corrected 3D cube showing the 405 to 710 m elevations (above) and the Resistivity 40 m below surface (below). Both images are looking to the north.

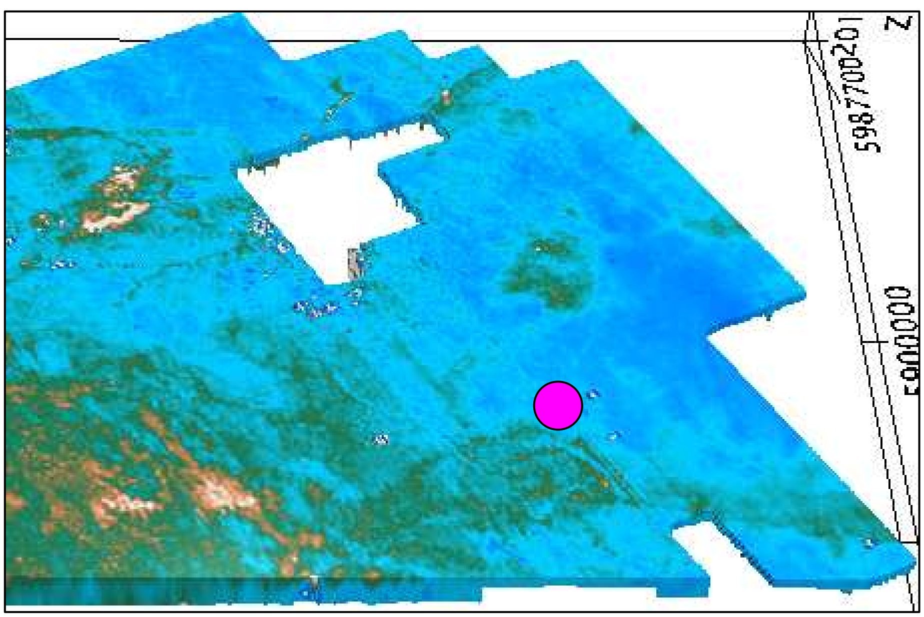

Central section of the survey

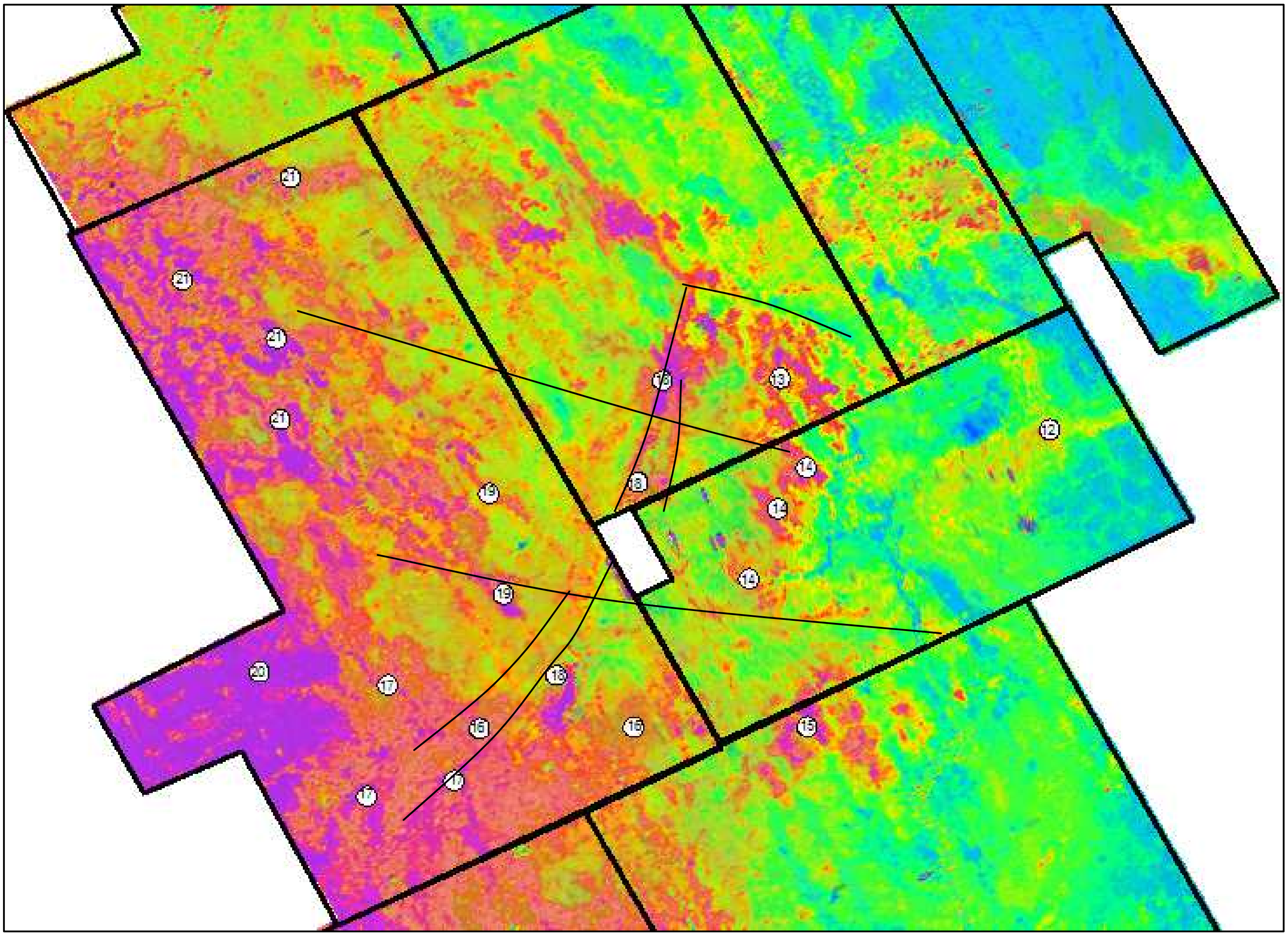

Image showing the location of the central sections areas of interest and several potential structures

Figure 77: - 750 m elevation – a heavy dotted line, indicates slightly elevated resistivity seen between two mapped buried bedrock valleys which continues east past the Red Deer valley. A weaker dashed line aligns with trends seen in the sand and gravel deposits and the buried bedrock valleys, and a heavy dashed lines shows a weak limit of resistivity.

Figure 78: - 800 m elevation - the dotted lines trending WNW-ESE are possible structures of interest and the curved dotted lines indicate regions of generally elevated resistivity.

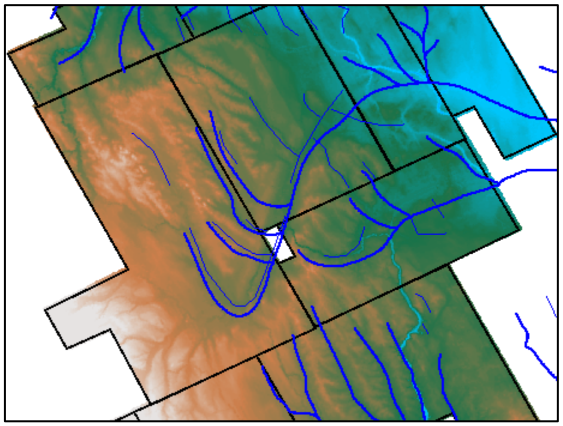

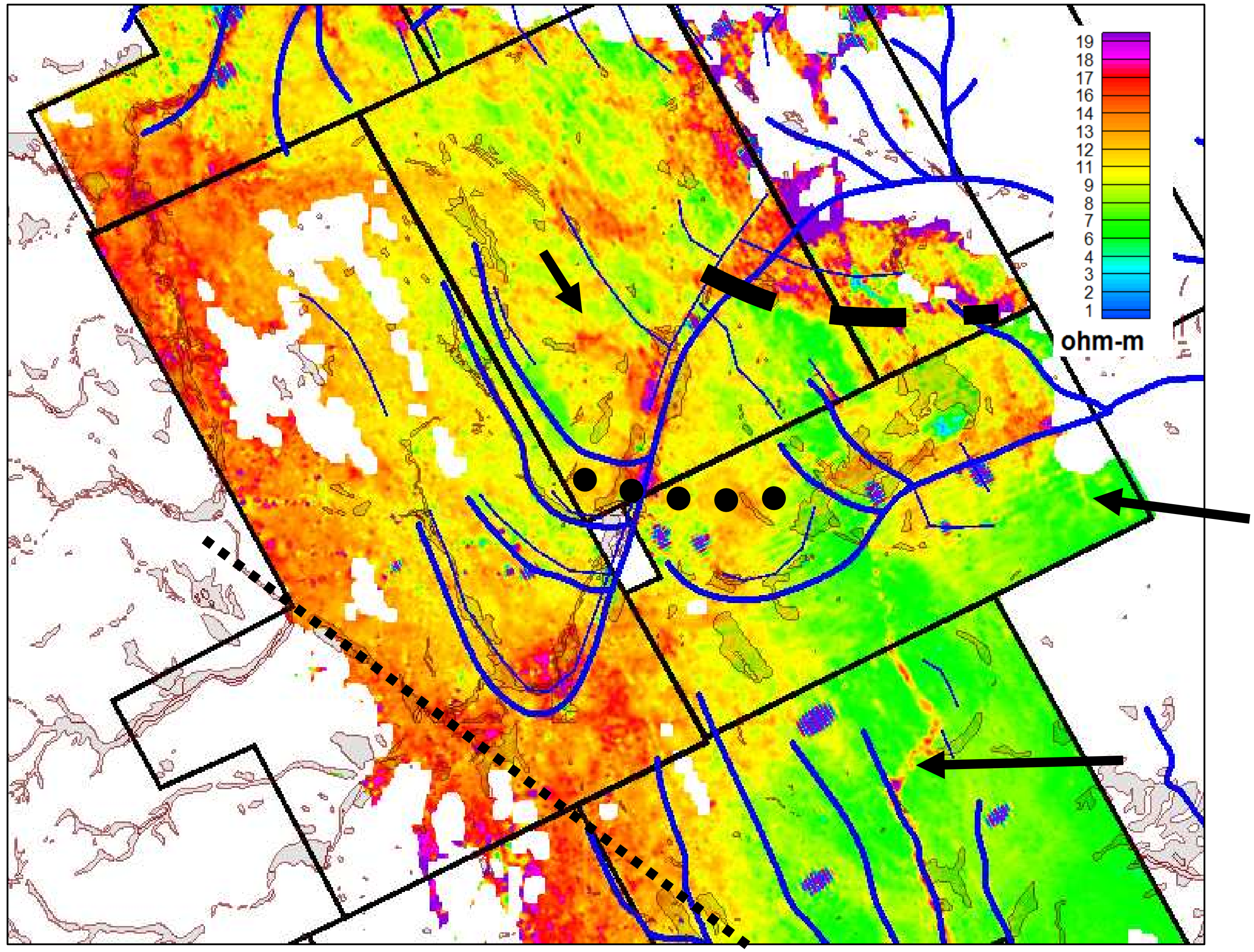

Figure 77: Central part of the merged survey area. Terrain corrected depth slice at 750 m elevation, showing the locations of the buried bedrock valleys (heavy blue lines), the meltwater channels (thin blue lines), and the sand and gravel deposits (outlined in brown). The arrows point to possible tributaries or extensions from the buried bedrock valleys and meltwater channels. The dashed line indicates a potential trend in the gravel and sand deposits as well as the buried bedrock valleys which can also be identified in the magnetic data (see Figure 9).

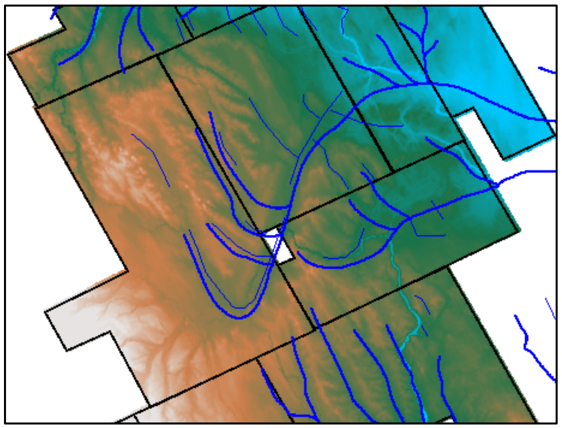

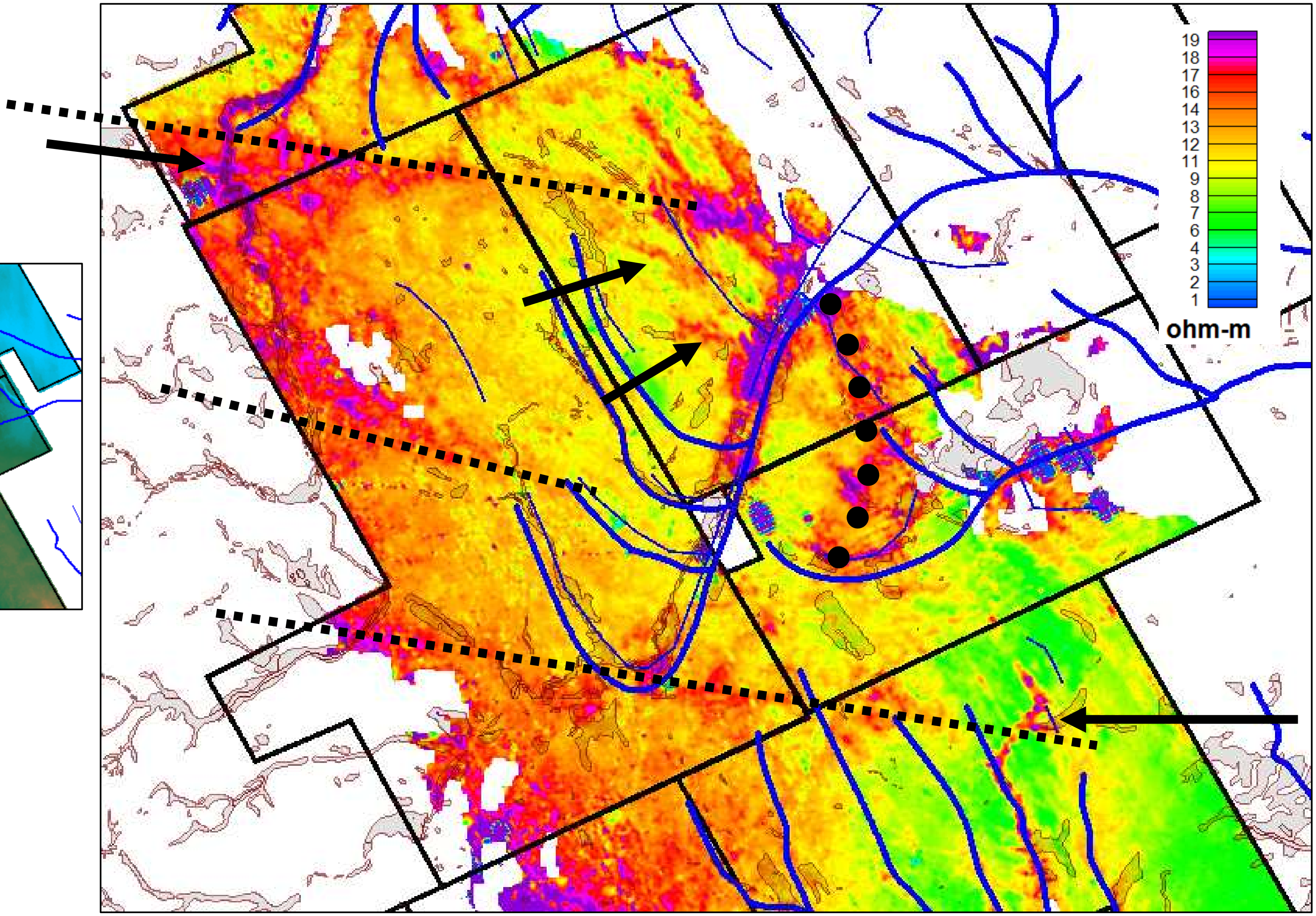

Figure 78: Central part of the merged survey area. Terrain corrected depth slice at 800 m elevation, showing the locations of the buried bedrock valleys (heavy blue lines), the meltwater channels (thin blue lines), and the sand and gravel deposits (outlined in brown). The arrows point to possible tributaries or extensions from the buried bedrock valleys and meltwater channels. The dotted lines trending WNW-ESE are possible structures of interest, and the curved dotted line indicates a region of generally elevated resistivity.

Feature 12

This feature follows a series of buried bedrock valleys. Several possible tributaries are shown above and below the mapped valleys (see the arrows in Figure 79). The weakly elevated responses appear to circle Buffalo Lake and a large deposit of sand and gravel. The bottom image in Figure 79 shows a triangle symbol where the resistive background changes direction from ENE to almost N-S. This corresponds with the extension of a potential structure shown in the image on page 84.

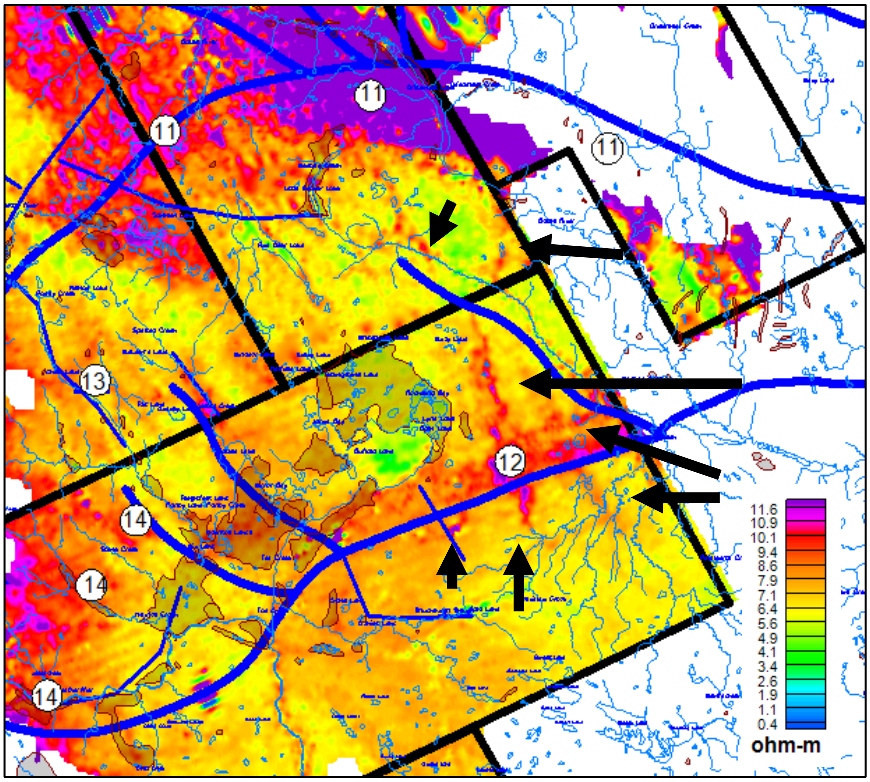

Figure 79: (above) - Terrain corrected depth slice at 700 m elevation, showing the locations of the buried bedrock valleys (heavy blue lines), the meltwater channels (thin blue lines), and the sand and gravel deposits (hatched areas); (below) – resistivity 30 m below surface.

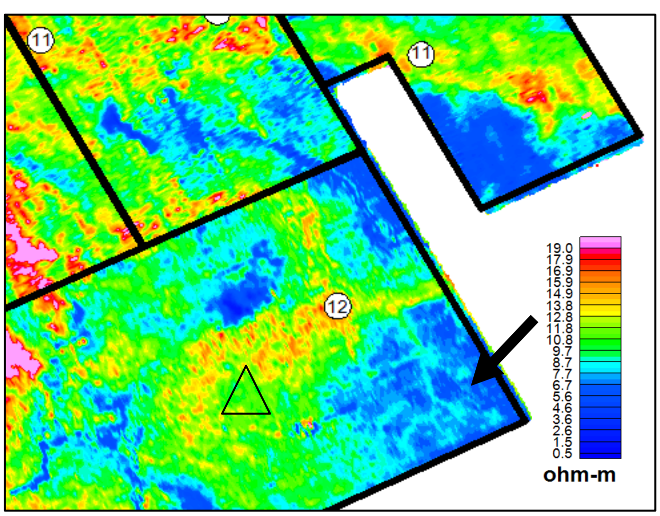

Features 13 and 14

Feature 13 refers to several weak near surface lineaments and a slightly more resistive zone. The zone seems to change direction slightly at a major WNW feature which has been mentioned in the report on several occasions to become selection 14. Above the structure the zone seems to trend almost N-S and below NE-SW. The southern portion still seems to show some expression 100 m below surface, whereas the northern portion is difficult to identify at this depth.

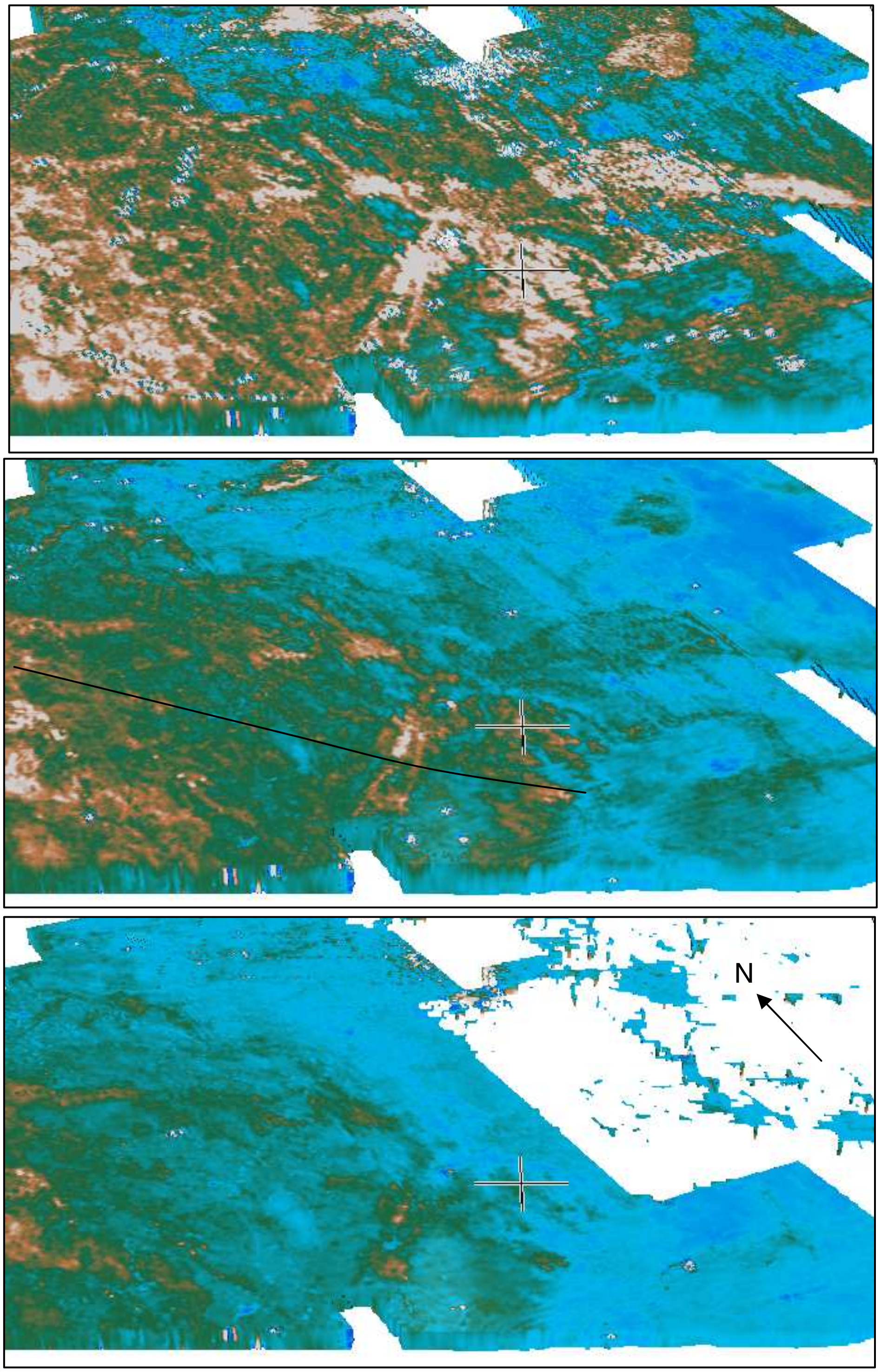

Figure 80: Sections through 3D cube relative to surface looking north. From top to bottom: 0 m, 40 m and 100 m below surface

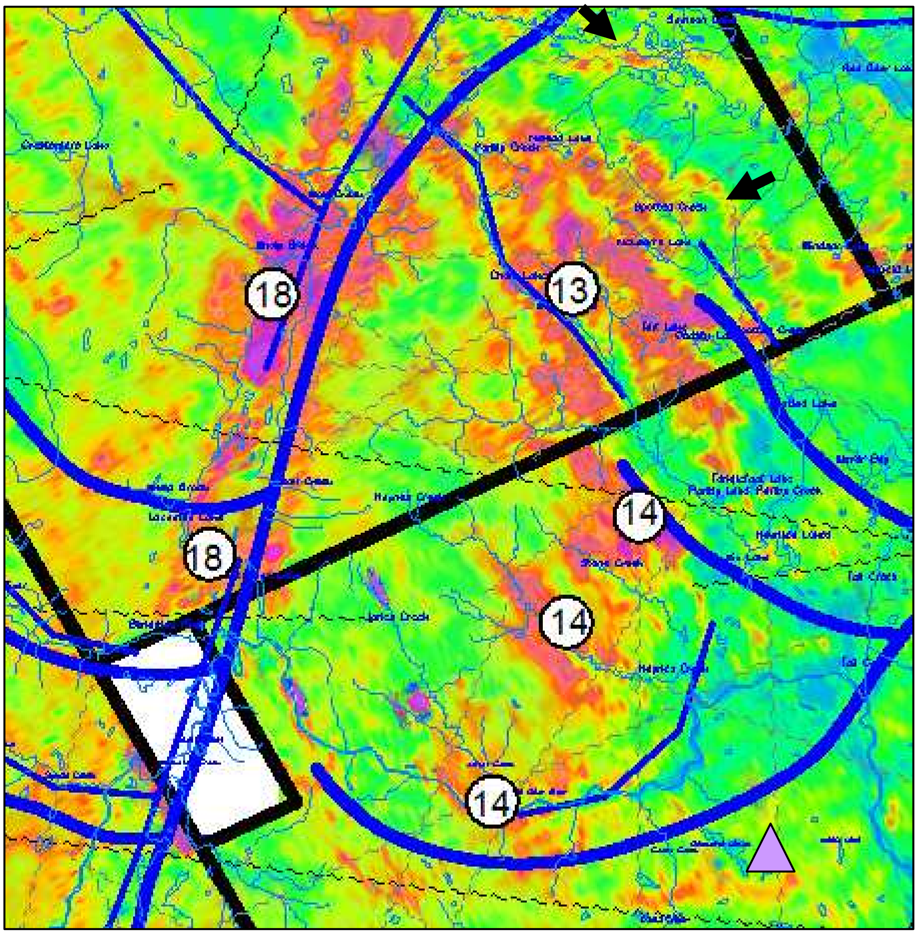

Figure 81: This image is resistivity relative to surface at 0, 20, 30, 60 and 90 m depth, with the surface grid being the most transparent; showing the locations of the buried bedrock valleys (heavy blue lines), the meltwater channels (thin blue solid and dashed lines), and the potential basement lineaments.

The features labeled 14 indicate areas of slightly increased resistivity between NNE-SSW striking potential basement lineaments. The two southern labels are located over low-lying areas and the responses return to the slightly elevated background response of feature 13 at approximately 70 m below surface, whereas the northern feature (also corresponding to the eastern mapped edge of a bedrock valley) still shows a response 100 m below surface.

The triangular symbol in Figure 81 shows a feature located near the WNW fault, which seems to be unrelated to topography. The arrows near the top of the image are weakly resistive features and the northernmost seems to parallel an E-W lineament. A potential lineament shown in the image on page 84 seems to indicate the northern extent of features 13 and 18, and at this point the NW striking feature 9 emerges to the north.

Features 13 and 14 apart from the more surficial component do not follow current day terrain.

Feature 15

This feature is bound by two potential NE-SW trending faults. It is similar in strike to selection 14,and may in fact be part of the same feature, as the major WNW feature which essentially separates these two zones, also appears somewhat to correlate with an offset in the mapped lithologies (see Figure 83).

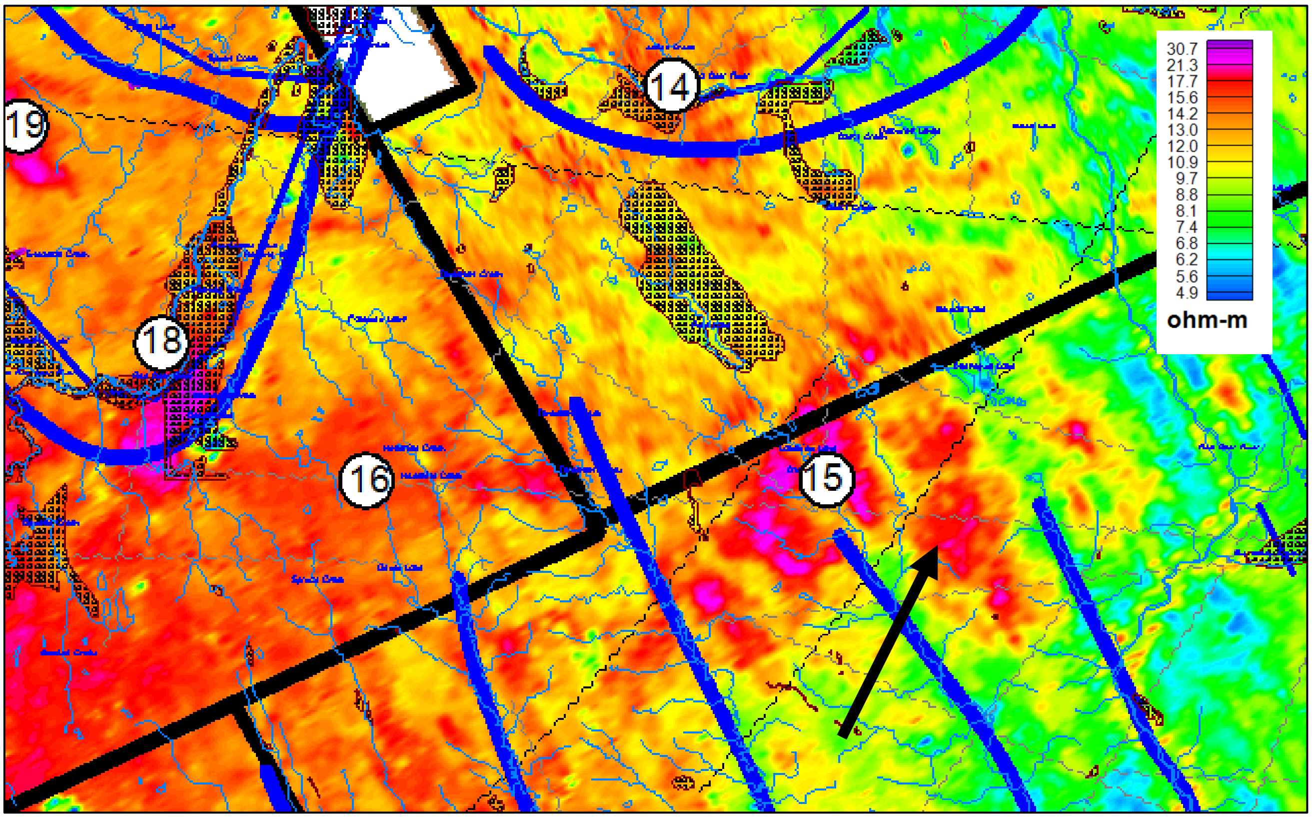

Figure 82: This image is resistivity relative to surface at 60m depth showing the locations of the buried bedrock valleys (heavy blue lines), the meltwater channels (thin blue solid and dashed lines), sand and gravel deposits (hatched areas) and the potential basement lineaments.

The eastern of the two NE-SW trending faults also seems to offset a slightly weaker potential extension of selection 15 (see the arrow in Figure 82 above). The selection lies in elevated terrain.

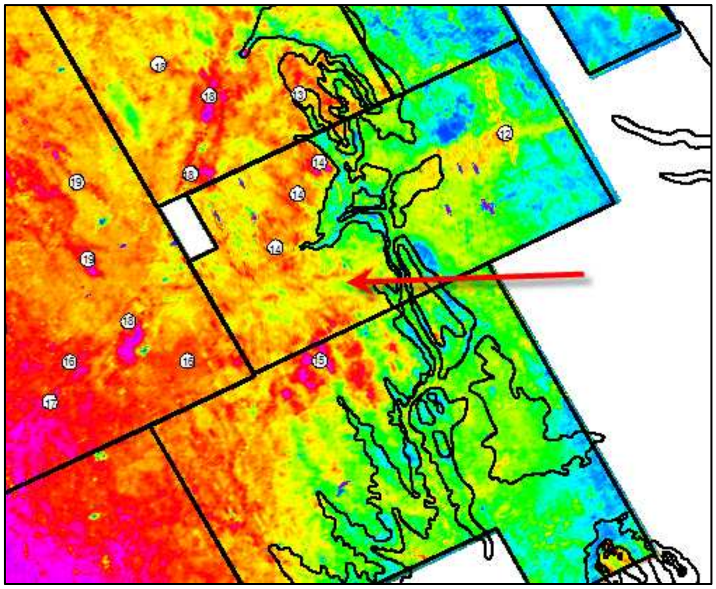

Figure 83: The image above is resistivity relative to surface at 60m depth showing the mapped bedrock lithology and the location of the potential WNW fault which essentially separates selections 14 and 15. The image below shows the 3D cube corrected for terrain limited to an elevation of 920 m. A potential EM lineament (this feature is very ambiguous in the magnetic data) shown below would also provide an offset for features 14 and 15 and the bedrock lithologies.

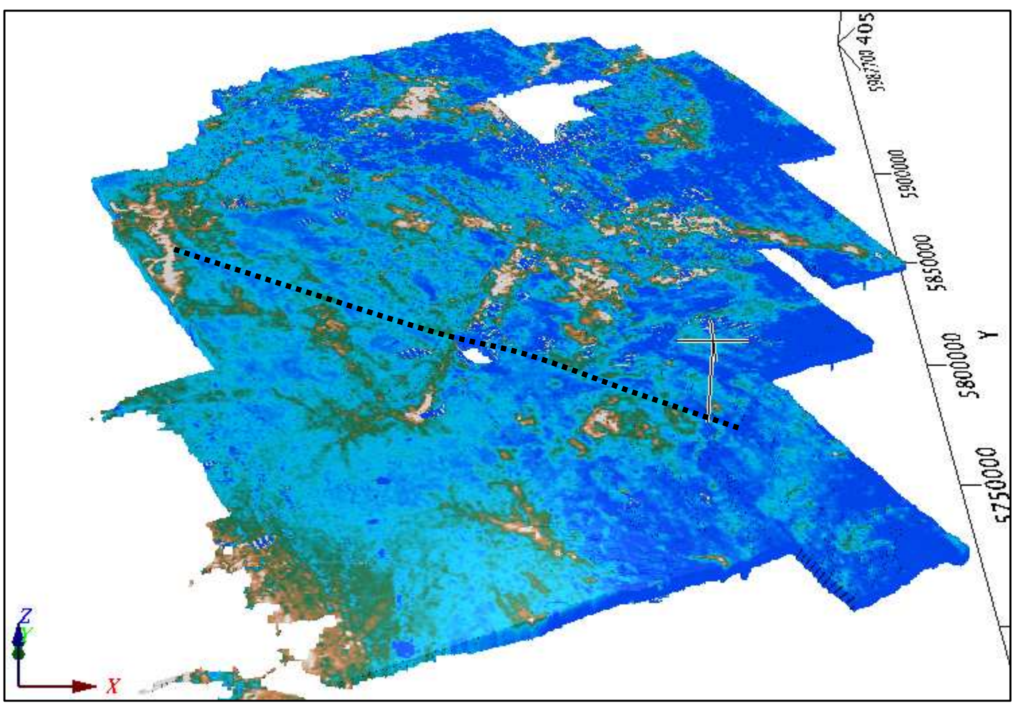

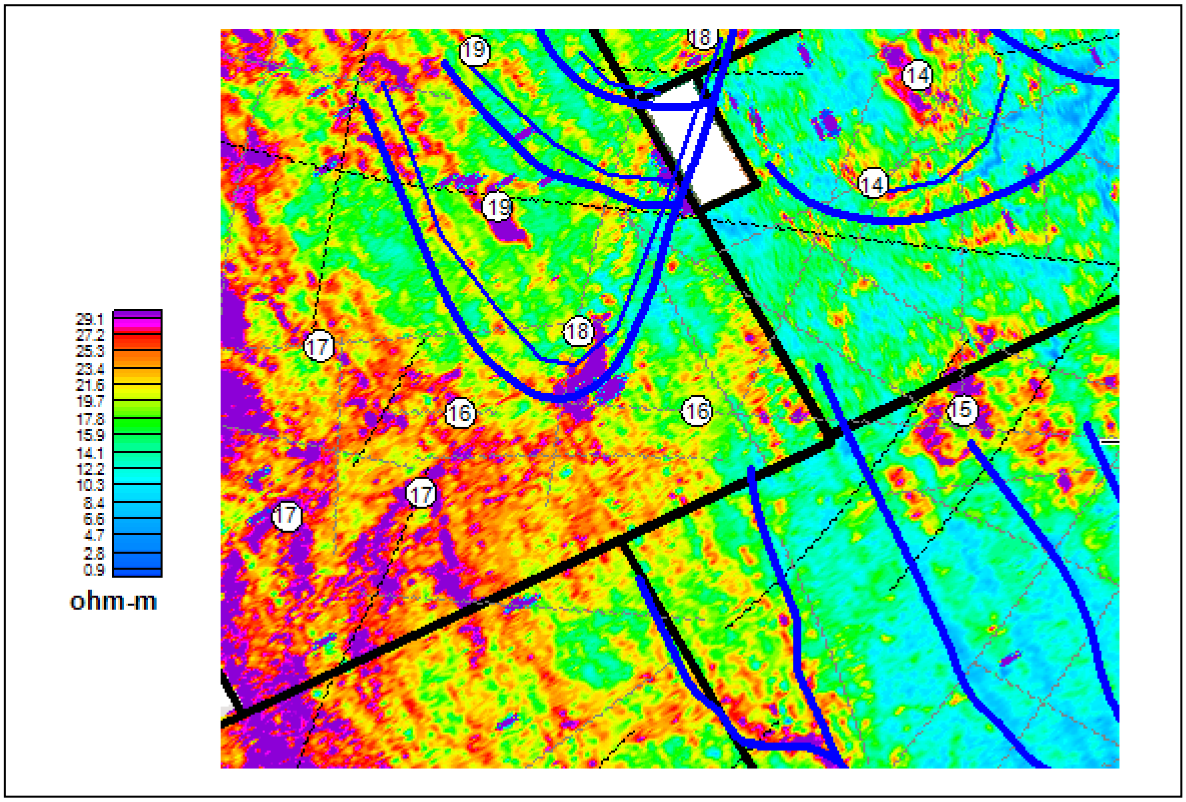

Figure 84: Resistivity relative to surface at 0 m below surface (above) and 120 m below surface (below) showing potential basement lineaments, and mapped buried bedrock valleys and meltwater channels.

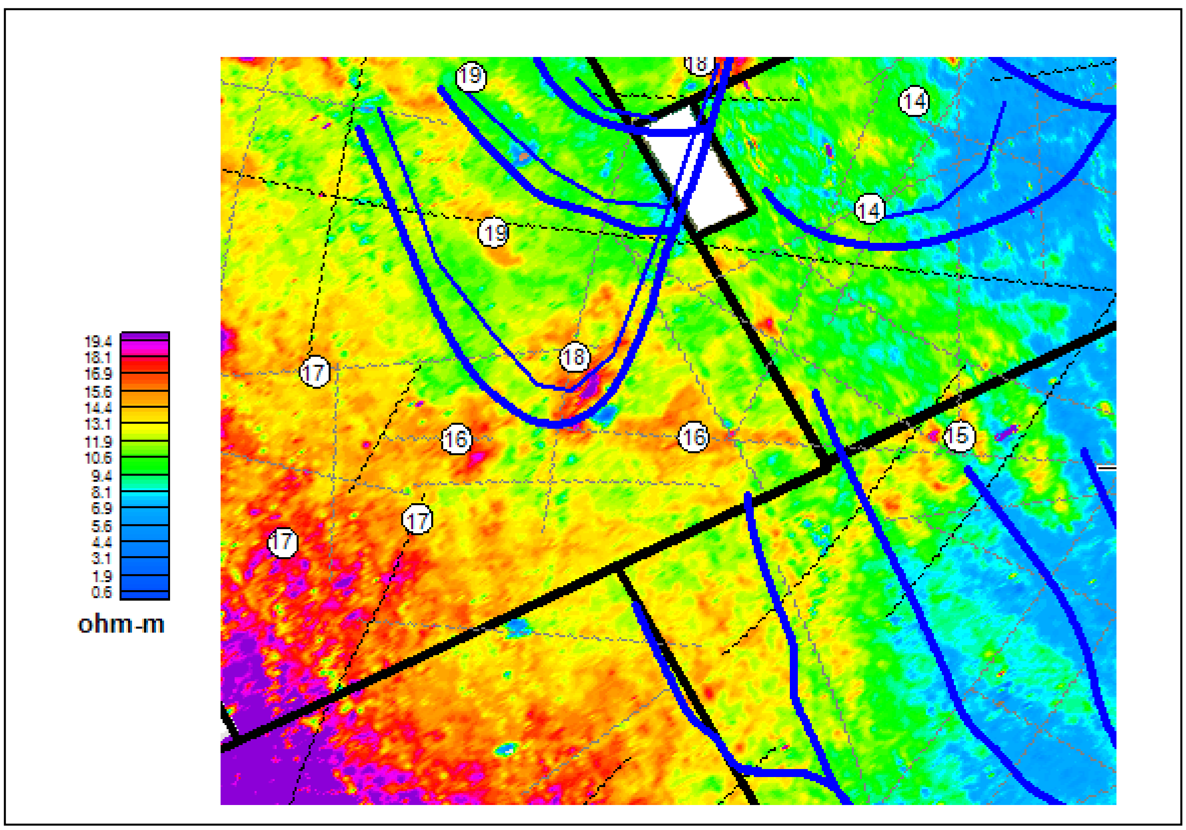

Features 16

This feature encompasses two areas along a potential WNW striking structure (the southern lineament shown in Figure 85), which also corresponds with the mapped southern boundary of the Red Deer buried bedrock valley. They do not standout as more isolated regions in the near surface (see Figure 84). The western label 16 is located over a region very similar in character to the region labeled 18 immediately to the northeast.

The eastern area of feature 16 is more elongated and follows the potential lineament. In fact in this area a number of weak features lie parallel with the lineament.

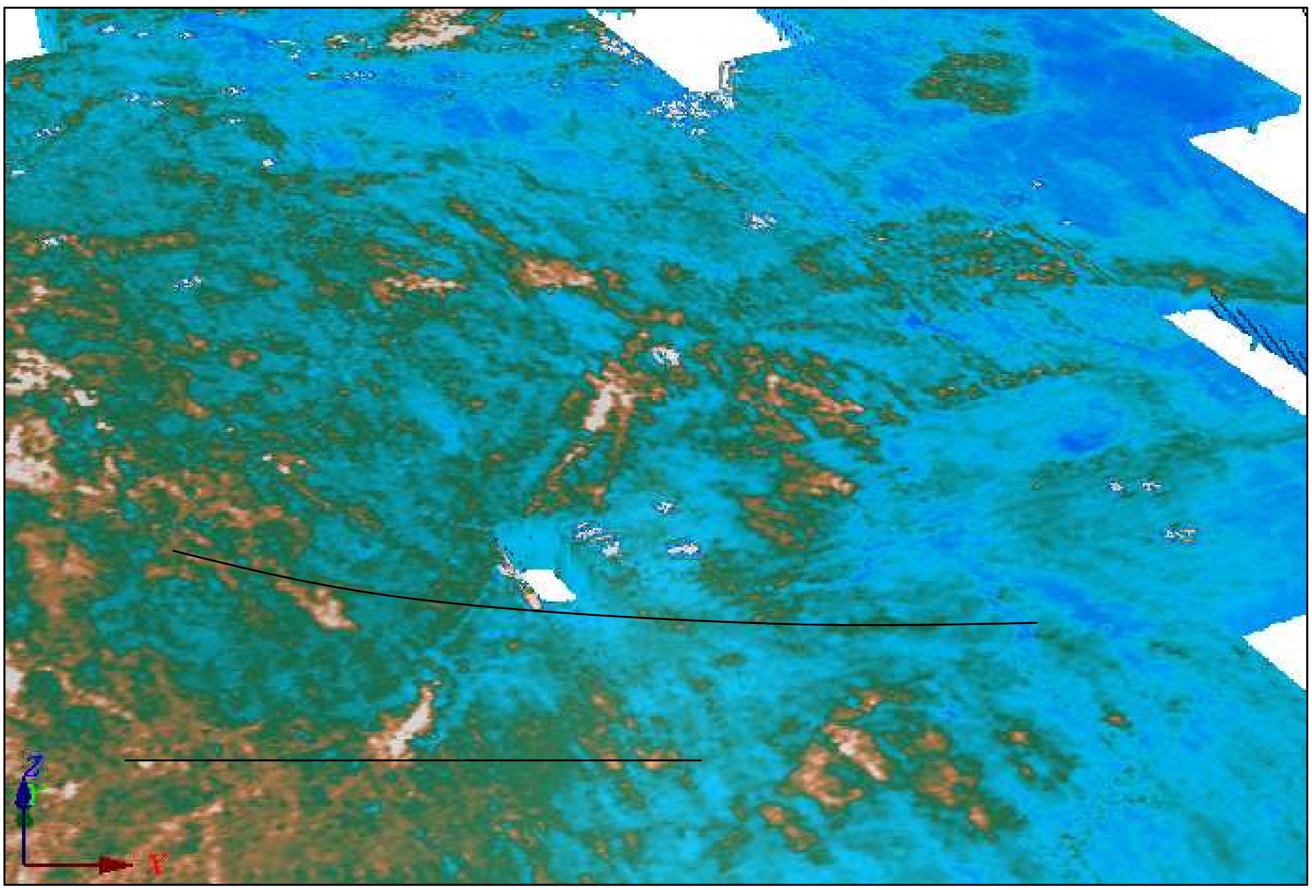

Figure 85: Sections through 3D cube relative to surface at 20 m depth looking north

Feature 17:

The top image in Figure 86 shows a close correlation between high resistivity values and the current day creeks and rivers. The bottom image shows that at 60 m depth, these features have all but disappeared, but several crosses are located on the image indicating regions of slightly elevated resistivity above background, which do lie adjacent to the current creeks and rivers.

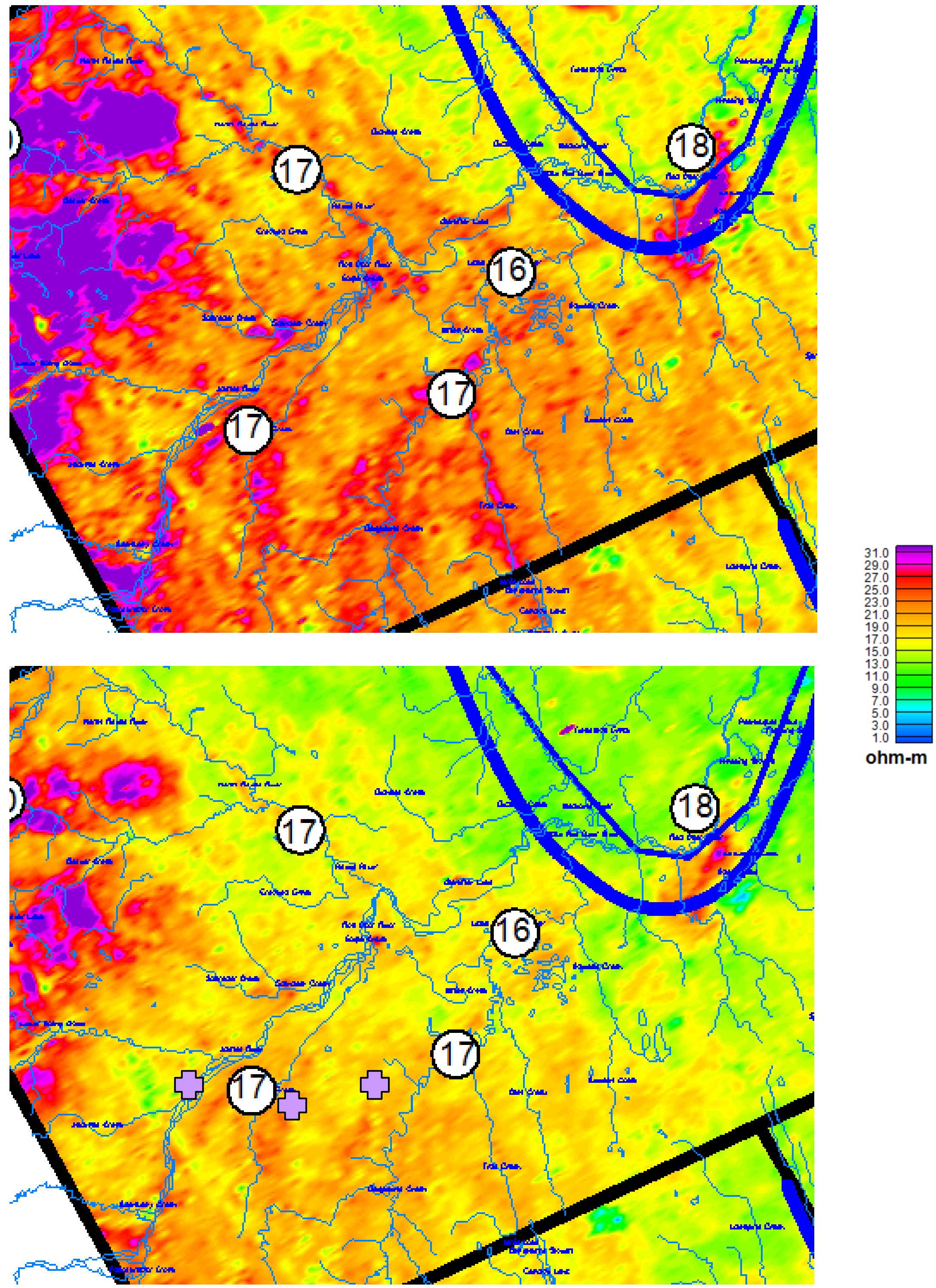

Figure 86: Resistivity relative to surface. At 20 m depth (top) and 60 m depth (bottom)

Features 18

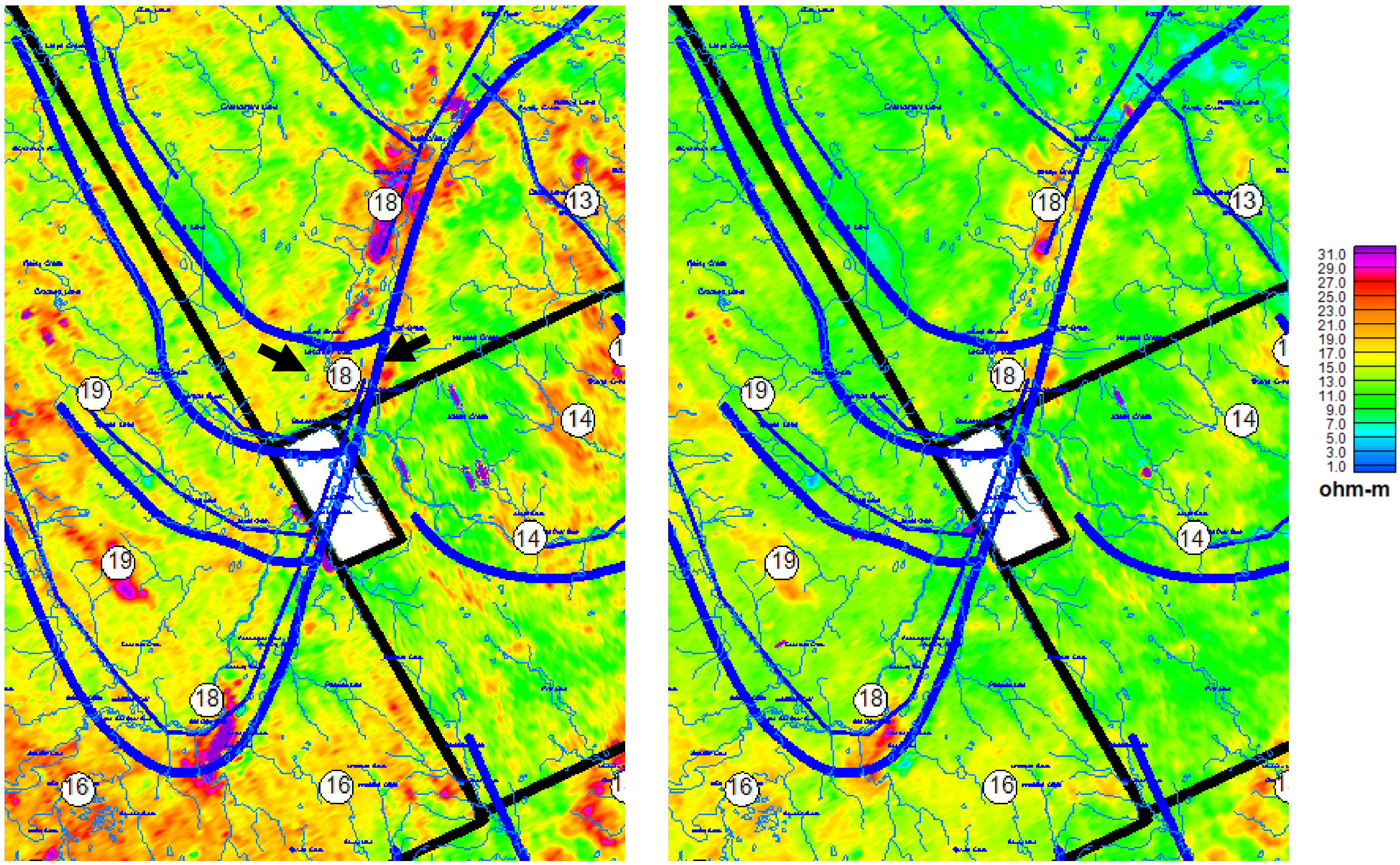

Figure 87: Resistivity relative to surface. At 20 m depth (left) and 60 m depth (right) showing the mapped buried bedrock valleys and meltwater channels.

The features labelled 18 include the extent of the Red Deer buried bedrock valley. The labels are located over regions which exhibit the strongest resistivity's from surface to depth. North of the city of Red Deer two sub parallel lineaments can be seen (shown by the arrows in Figure 87), and may be of some interest, however caution should be exercised when considering these features, as there is extensive culture in the area. Where the northern label is located on the image, the resistivity is likely controlled by the WNW trending structure which also potentially offsets selections 13 and 14 (see Figure 80).

Although not shown in the image above there is a very good correlation between the sand and gravel deposits and the features of selection 18.

The slices through the 3D cube (Figures 88 and 89) show the high resistivities of feature 18, continue to some depth.

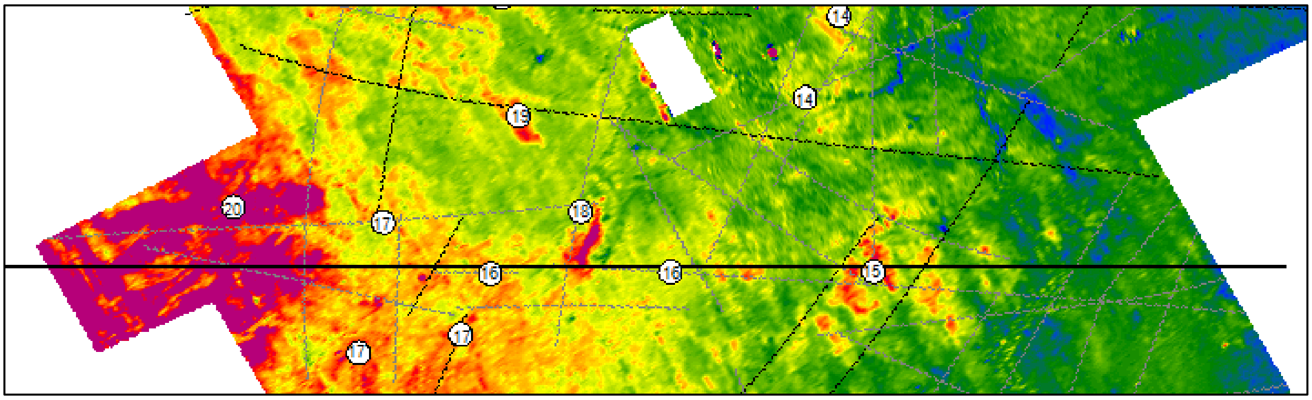

Figure 88: Resistivity relative to surface at 30 m depth (above); the horizontal line indicates the vertical slice that is shown in the terrain corrected 3D image below (looking to the north).

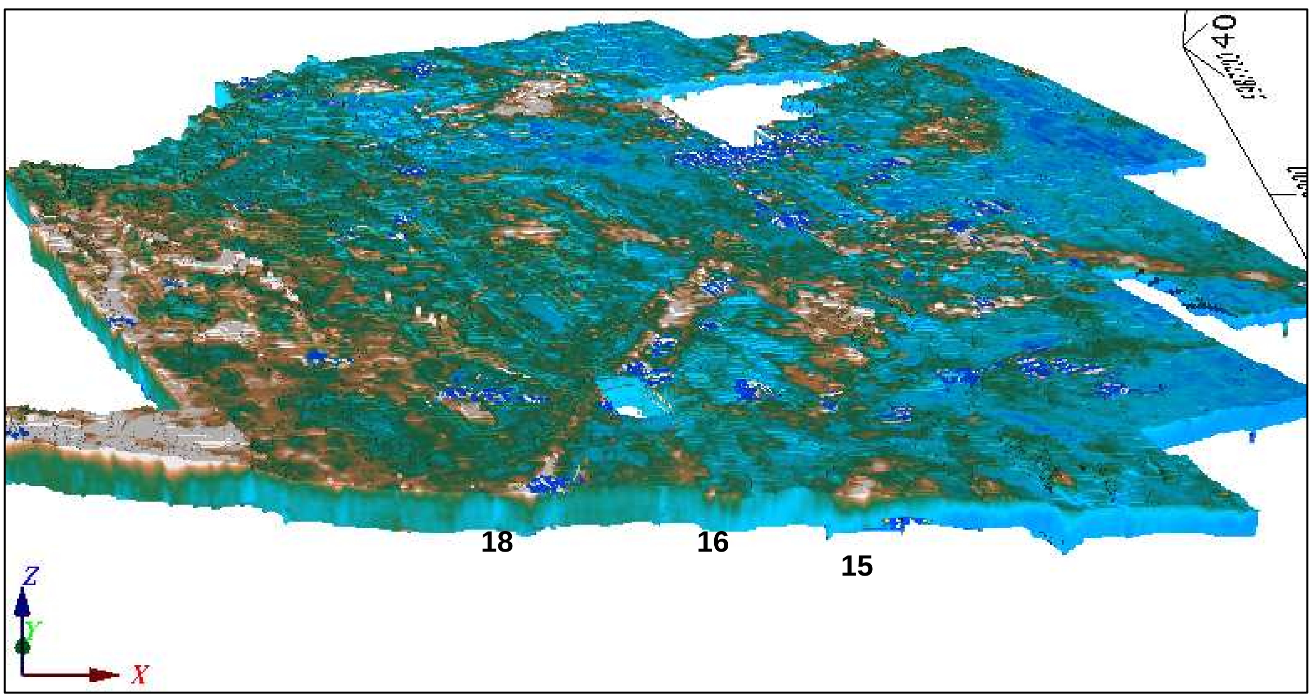

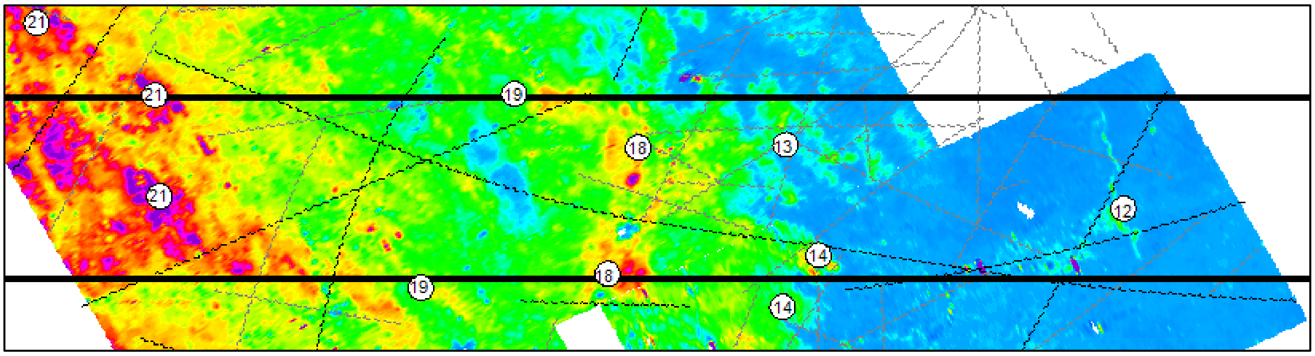

Figure 89: Resistivity relative to surface at 120 m depth (top); the horizontal lines indicate the vertical slices that are shown below. Both are terrain corrected 3D images (looking north), the top horizontal line is the central vertical slice

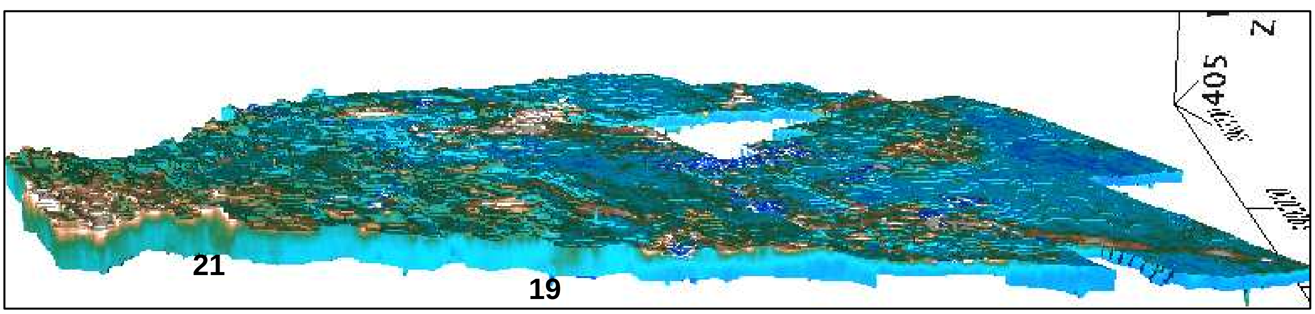

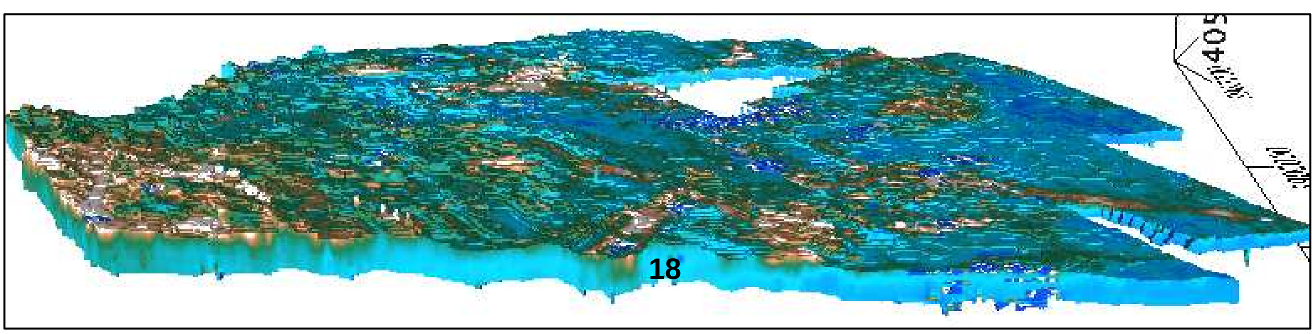

Features 19

The two southern features labeled 19 in Figure 90 below lie in close proximity to branches off the main Red Deer buried bedrock valley and correlate with elevated terrain. The southernmost feature strikes NW-SE between two buried bedrock valleys and is transected by a WNW trending structure; the highest resistivity's lie to south of this. The central feature lies immediately north of Sylvan Lake.

The northernmost feature is not apparent in the near surface but with depth can be seen as an area of elevated resistivity lying just to the northwest of the Red Deer buried bedrock valley, and the image of Figure 93 suggests it may be part of a potential tributary of the bedrock valley.

The triangular symbol in Figure 90, is located where the cross-section of two potential lineaments truncates a slightly elevated resistive feature aligned with a branch of the Red Deer valley and mapped sand and gravel deposits (see Figure 78).

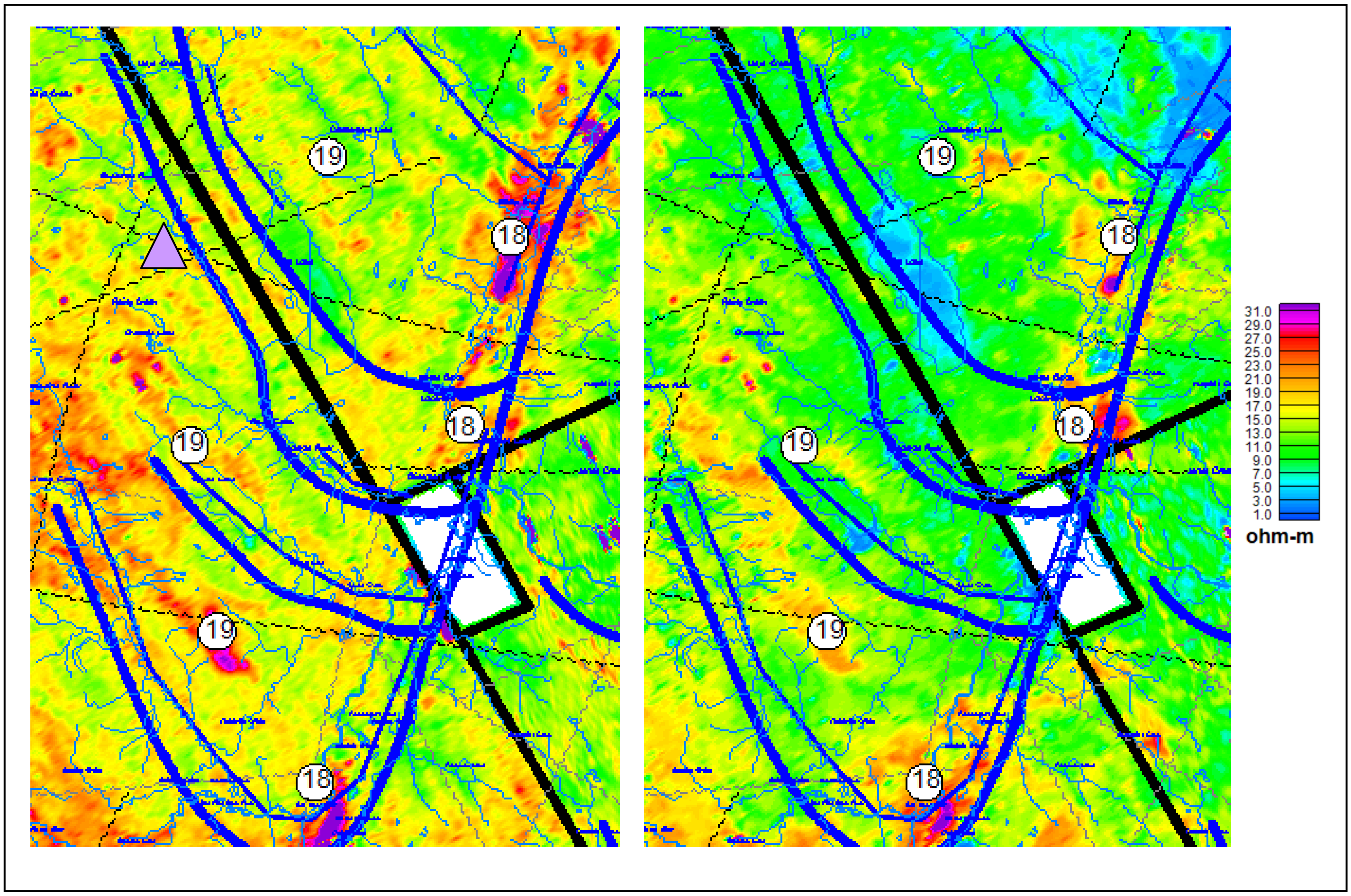

Figure 90: Resistivity relative to surface. At 20 m depth (left) and 120 m depth (right) showing the mapped buried bedrock valleys, meltwater channels and potential lineaments.

Feature 20

This point of interest is not a resistive lineament or zone, rather a structural element that controls the limits of (see the feature labeled 18) or offsets (see the arrow at label 17) various resistive features. The area surrounding the location of the label 20 is for the most part disturbed belt. Figure 93 suggests that, at the 900 m elevation at least, the higher elevations with depth lie north of this structure.

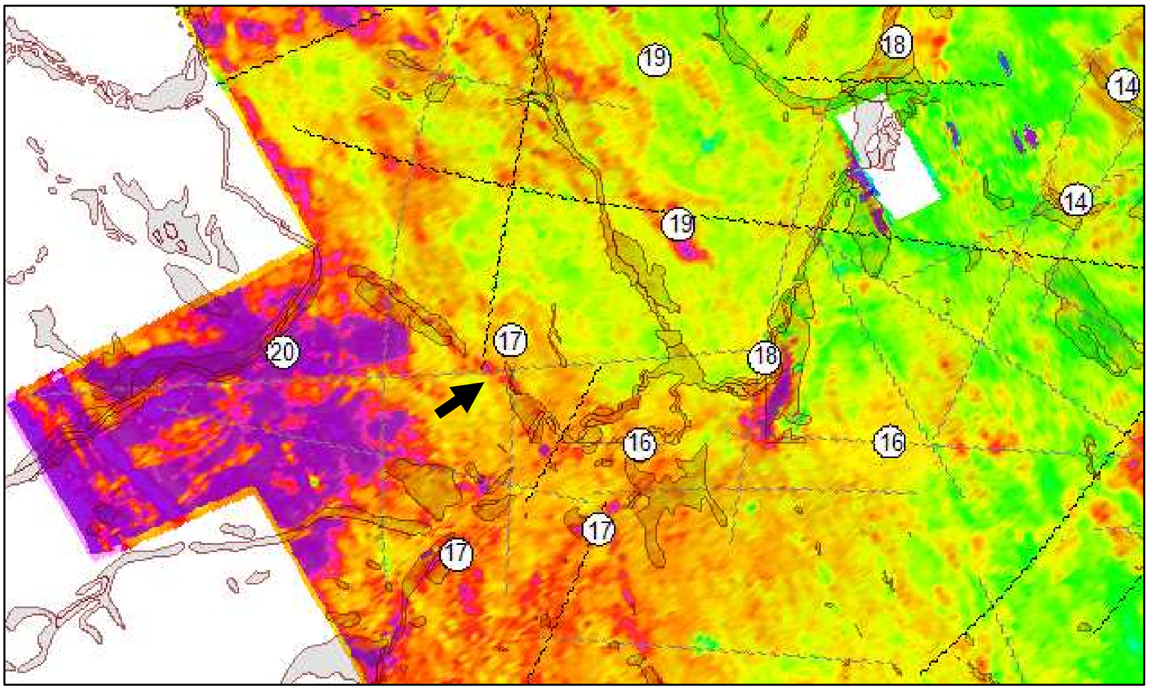

Figure 91: The image (above) is resistivity relative to surface at 20, 90, 120, and 160 m depth, with the 20 m grid being the most transparent; showing the locations of the potential basement lineaments and sand and gravel deposits (hatched areas). The image below is a slice through the 3D cube relative to surface, truncated at 180 m below surface.

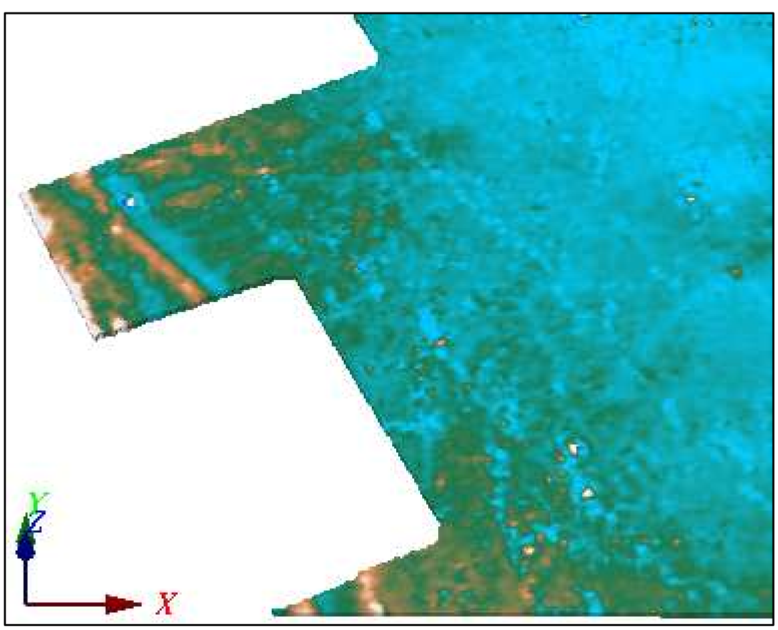

Feature 21

There are numerous resistive lineaments in this area, so, rather than a discussion on each feature, a general description will be made. The three southern labels of 21 (see Figure 92) are located at some of the strongest resistivity at depth lineaments, which are also seen along the western boundary. For the most part there is some correlation with the digital terrain model, be it elevated (the three southern label locations) or low lying regions (location of the northern label). The area seems to be strongly controlled by potential lineaments see figures to follow.

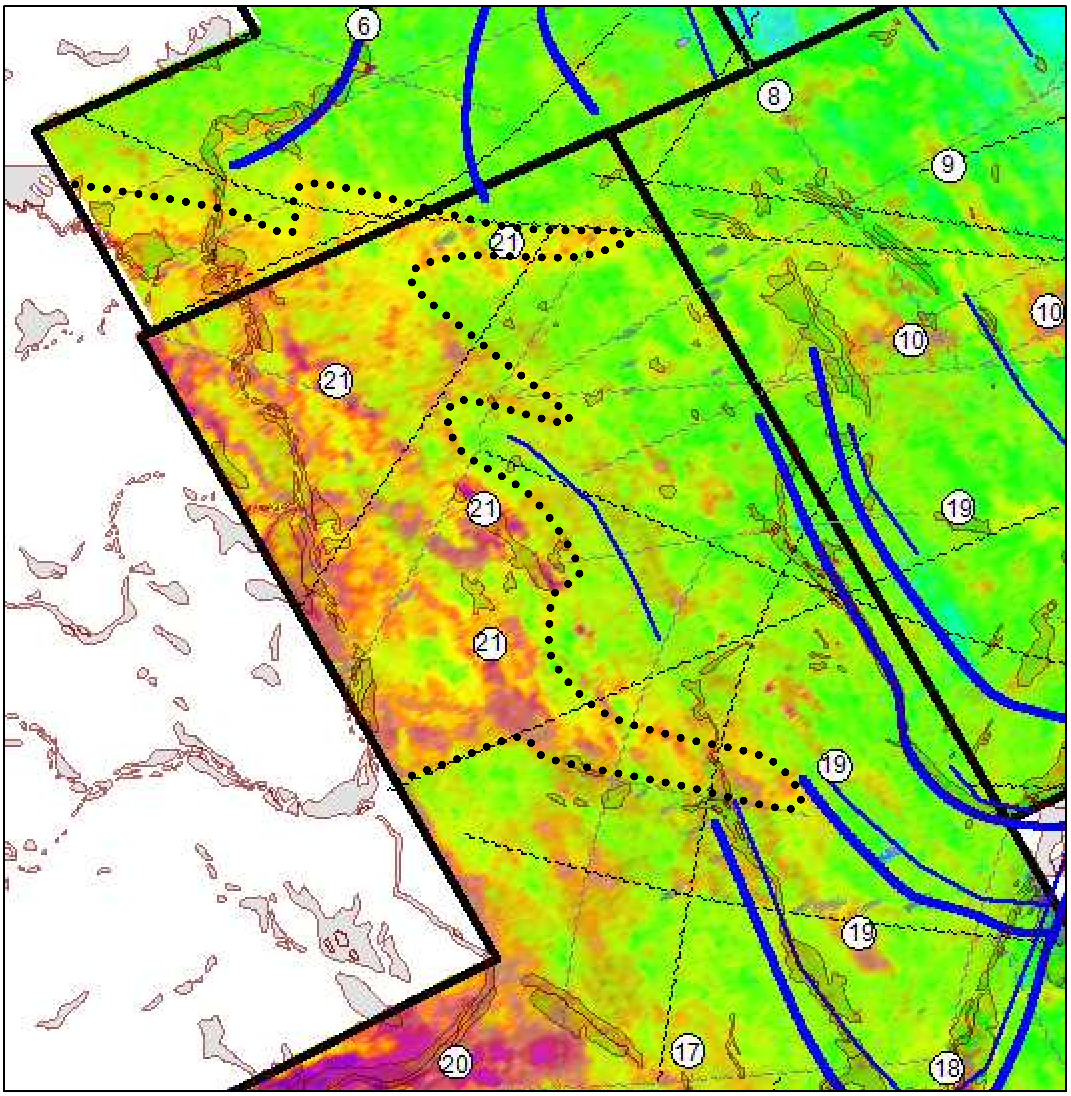

Figure 92: This image is resistivity relative to surface at 0, 60 and 120 m depth, with the surface grid being the most transparent; showing the locations of the buried bedrock valleys (heavy blue lines), the meltwater channels (thin blue solid and dashed lines), the sand and gravel deposits (hatched areas) and the potential basement lineaments.

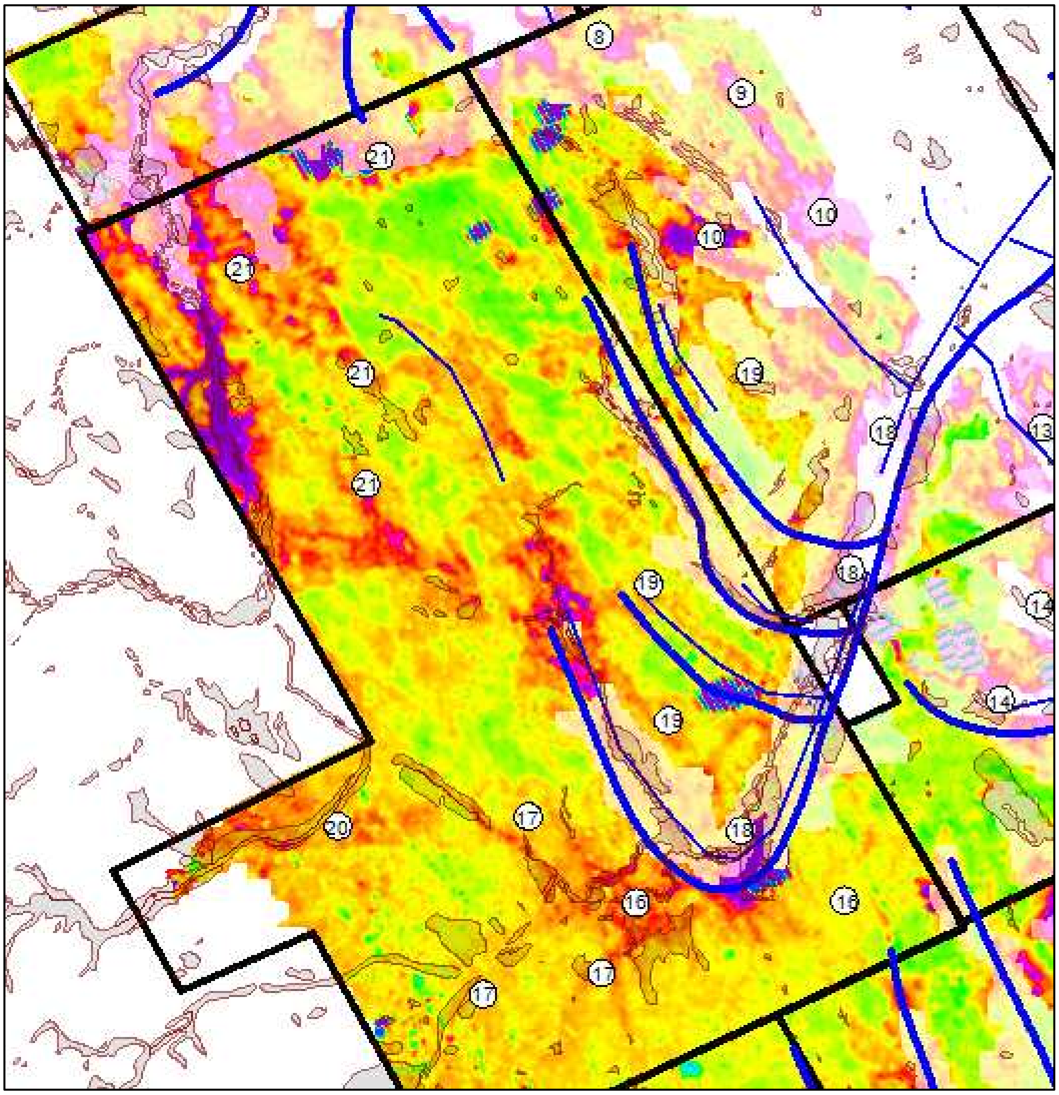

Figure 93: Terrain corrected depth slice at 920 m and 850 m elevations, with the 850 m elevation being transparent. The image shows the locations of the buried bedrock valleys (heavy blue lines), the meltwater channels (thin blue lines), and the sand and gravel deposits (hatched areas).

Southern section of the survey

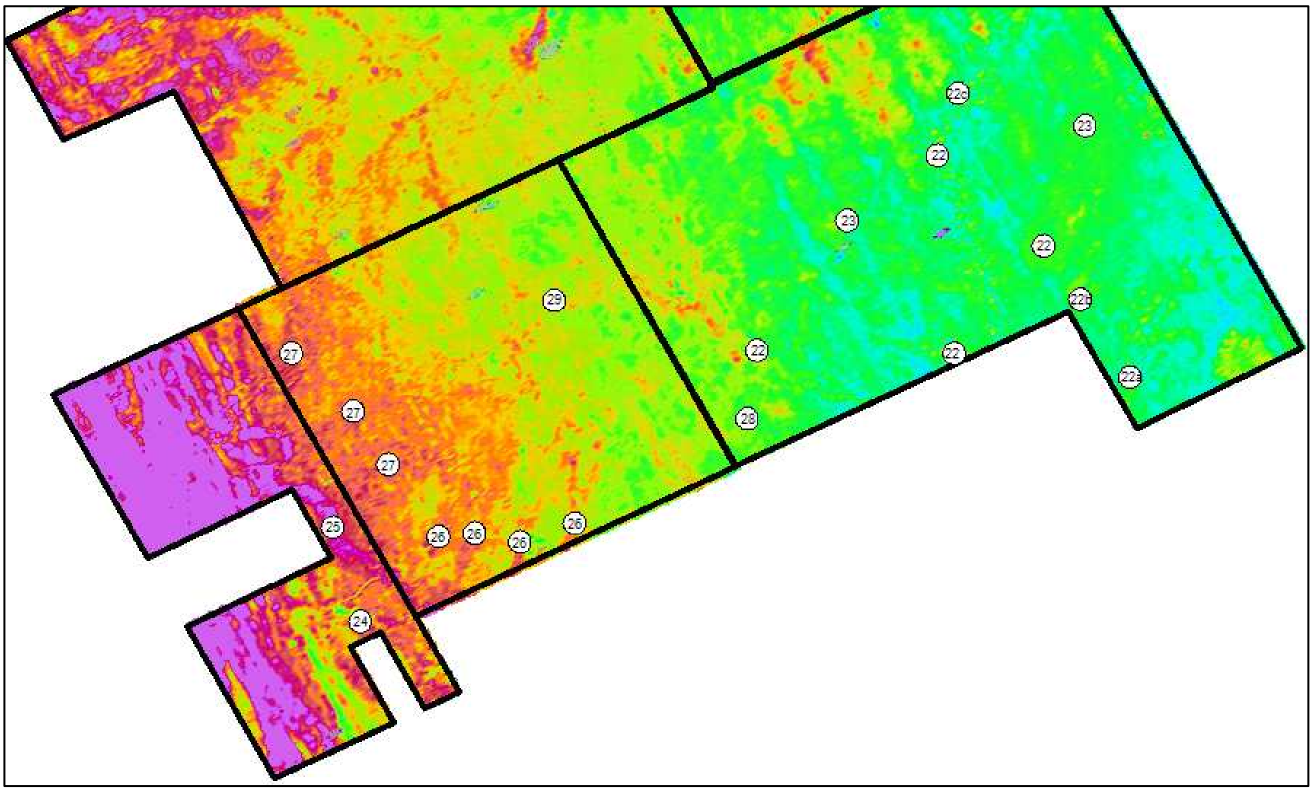

Image showing the location of the central sections areas of interest and several potential structures

Figure 94: - 800 m elevation – shows two areas of slightly elevated resistivity (between dashed lines) which are labeled as features 23. The arrows point to lineaments which may well be tributaries to buried bedrock valleys.

Figure 95: - 900 m elevation - The black dashed lines indicate potential trends in the gravel and sand deposits as well as the buried bedrock valleys which can also be identified in the magnetic data (see Figure 9). The arrows point to a possible branch from the bedrock valley tributary.

Figure 96: - 950 m elevation – the southern arrow points to a NE-SW trending feature which is part of the features of interest labeled as 26. The arrow is also the eastern edge of a NW striking slightly more resistive zone feature 25.

Figure 97 and 98: - 1100 and 1150 elevations respectively – these images show moderately good correlation with the mapped meltwater channels.

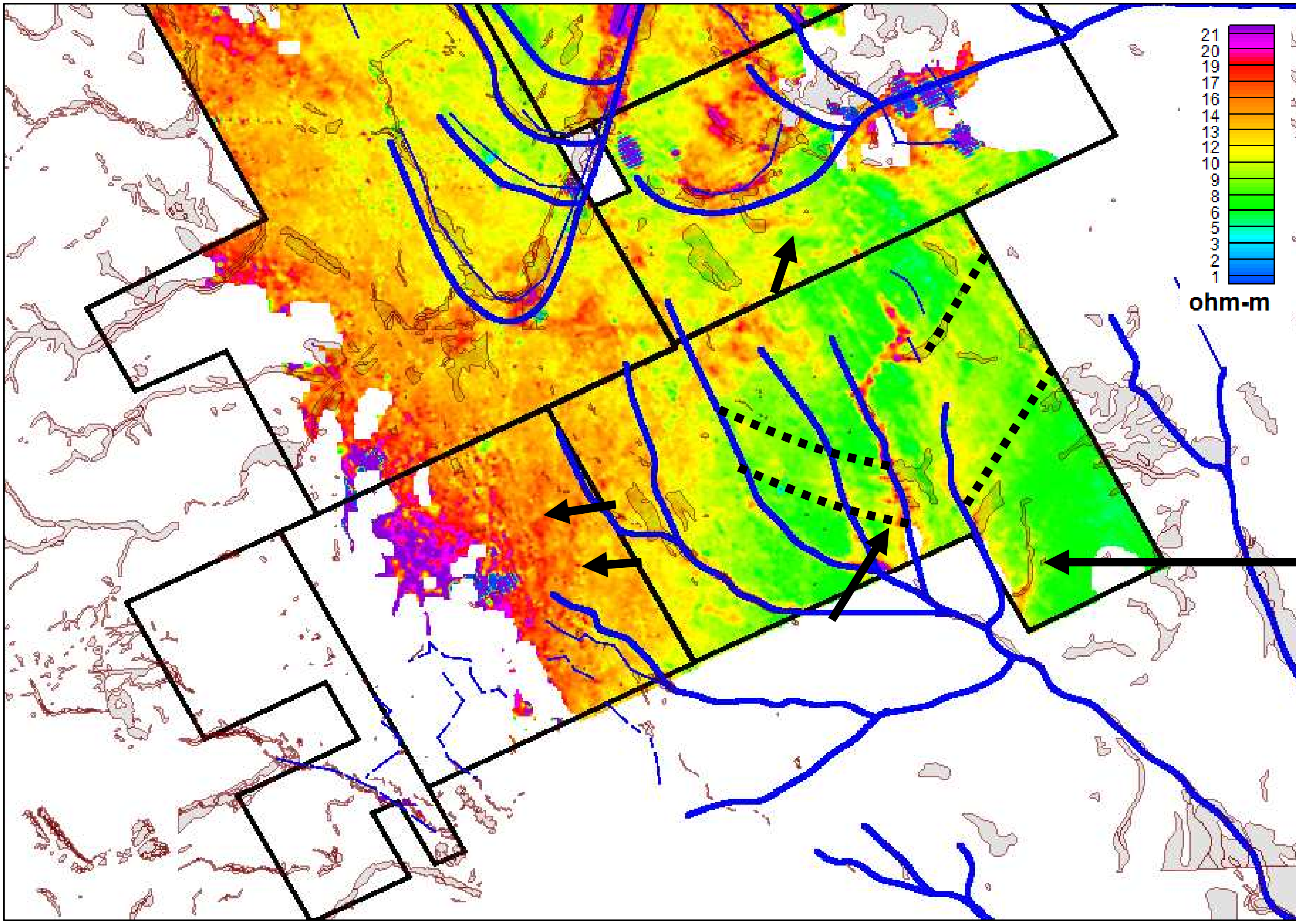

Figure 94: Southern part of the merged survey area. Terrain corrected depth slice at 800 m elevation, showing the locations of the buried bedrock valleys (heavy blue lines), the meltwater channels (thin blue solid and dashed lines), and the sand and gravel deposits (outlined in brown). The arrows point to possible tributaries or extensions from the buried bedrock valleys and meltwater channels. The region between the dashed lines indicates areas of slightly elevated resistivity.

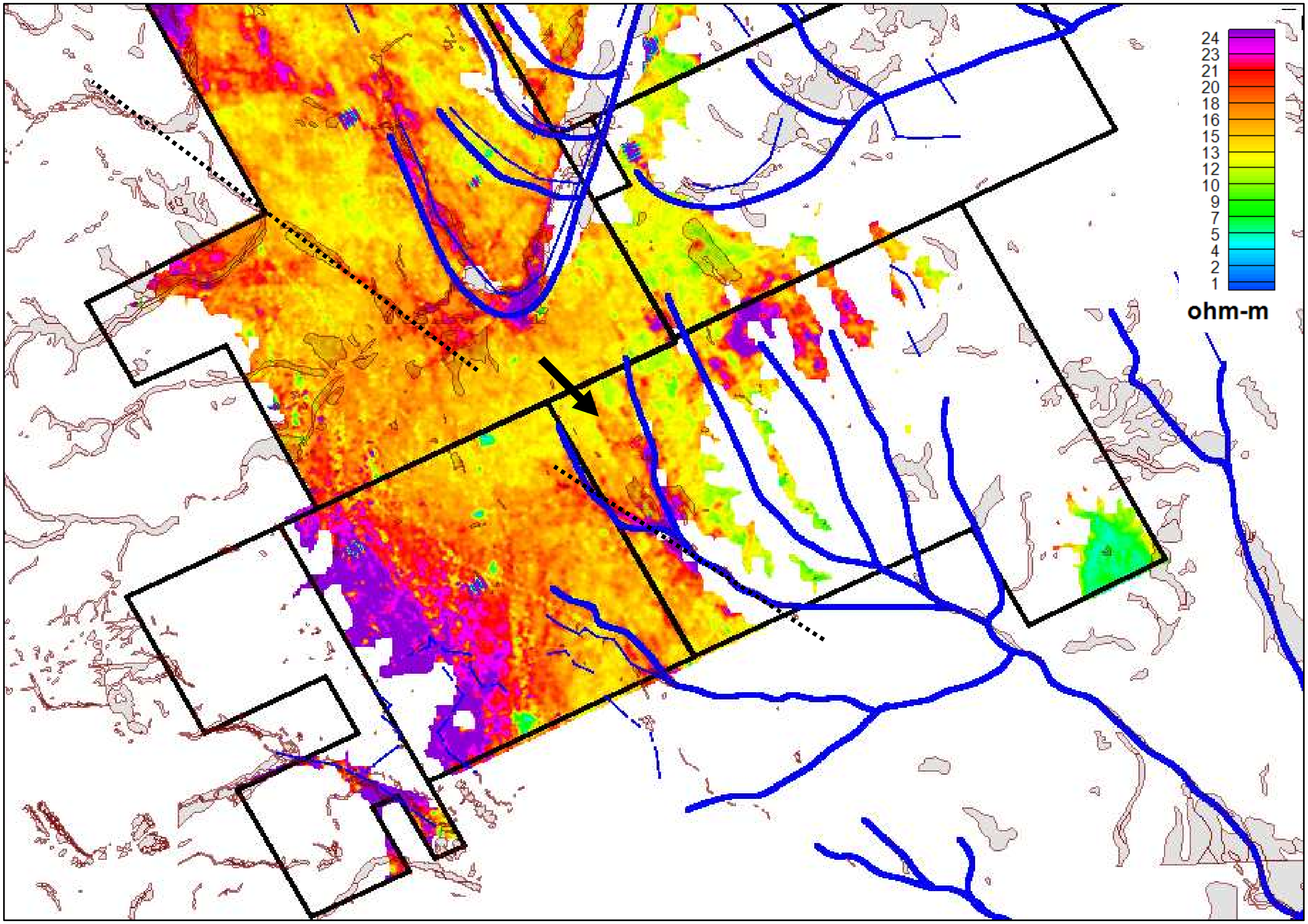

Figure 95: Southern part of the merged survey area. Terrain corrected depth slice at 900 m elevation, showing the locations of the buried bedrock valleys (heavy blue lines), the meltwater channels (thin blue solid and dashed lines), and the sand and gravel deposits (outlined in brown). The black dashed lines indicate a potential trend in the gravel and sand deposits as well as the buried bedrock valleys which can also be identified in the magnetic data (see Figure 9).

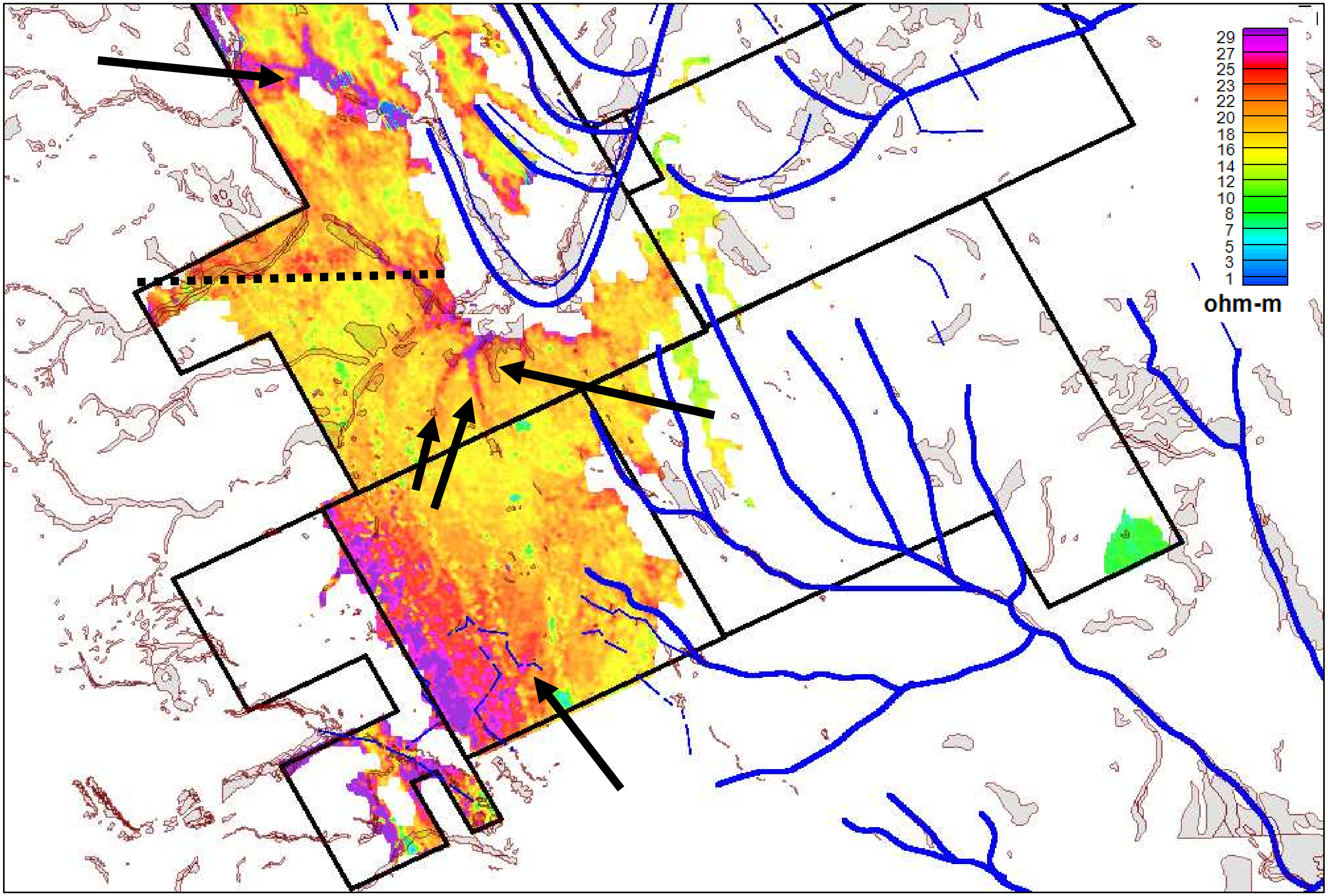

Figure 96: Southern part of the merged survey area. Terrain corrected depth slice at 950 m elevation, showing the locations of the buried bedrock valleys (heavy blue lines), the meltwater channels (thin blue solid and dashed lines), and the sand and gravel deposits (outlined in brown). The arrows point to a potential bedrock valley tributaries? The dashed line indicates a possible structure of interest since the region north of the lineament shows elevated resistivities.

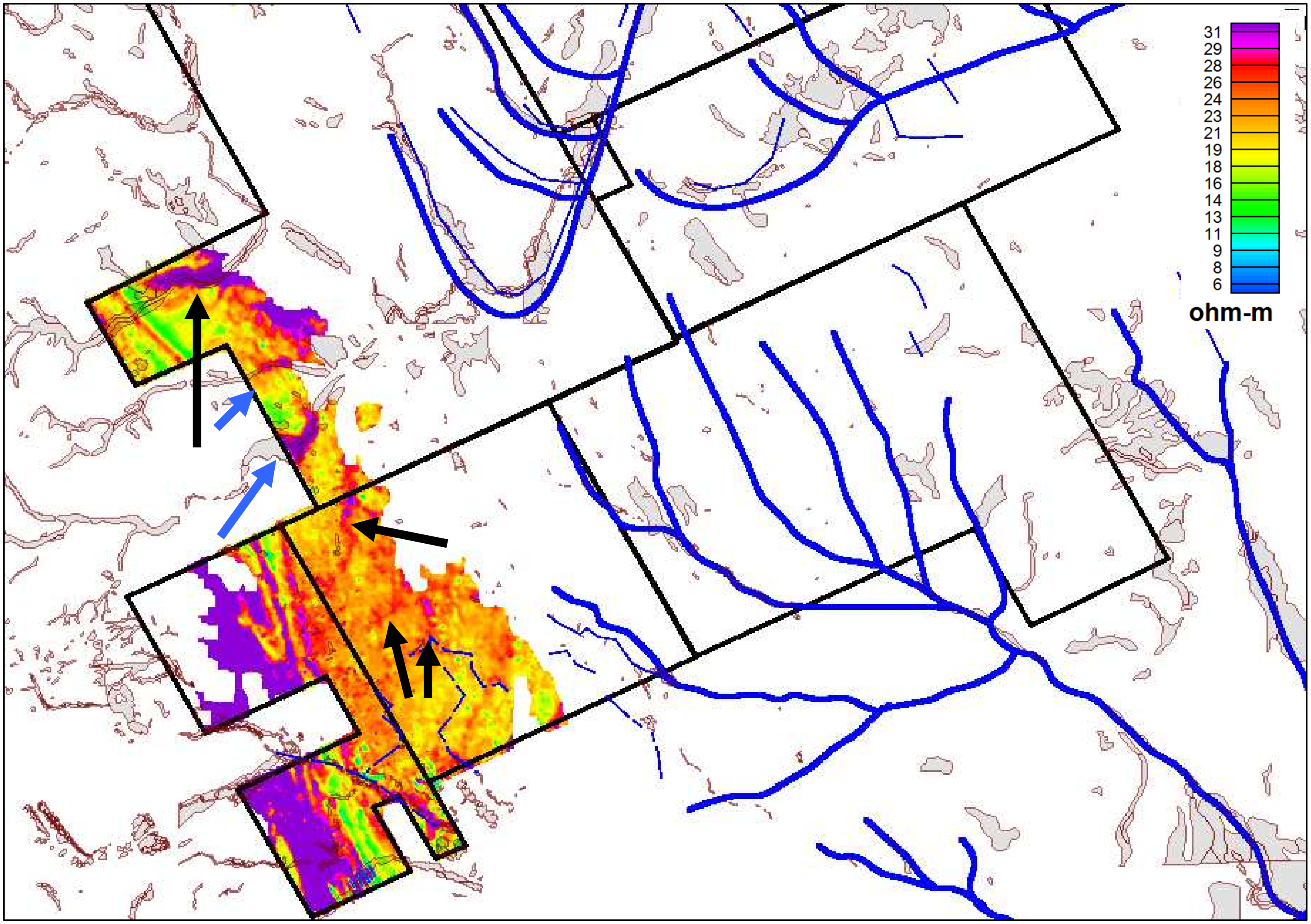

Figure 97: Southern part of the merged survey area. Terrain corrected depth slice at 1100 m elevation, showing the locations of the buried bedrock valleys (heavy blue lines), the meltwater channels (thin blue solid and dashed lines), and the sand and gravel deposits (outlined in brown). The black arrows point to an extension of the potential bedrock valley/ meltwater channel with tributaries shown in the previous Figure. The blue arrows show good correlation with the sand and gravel deposits.

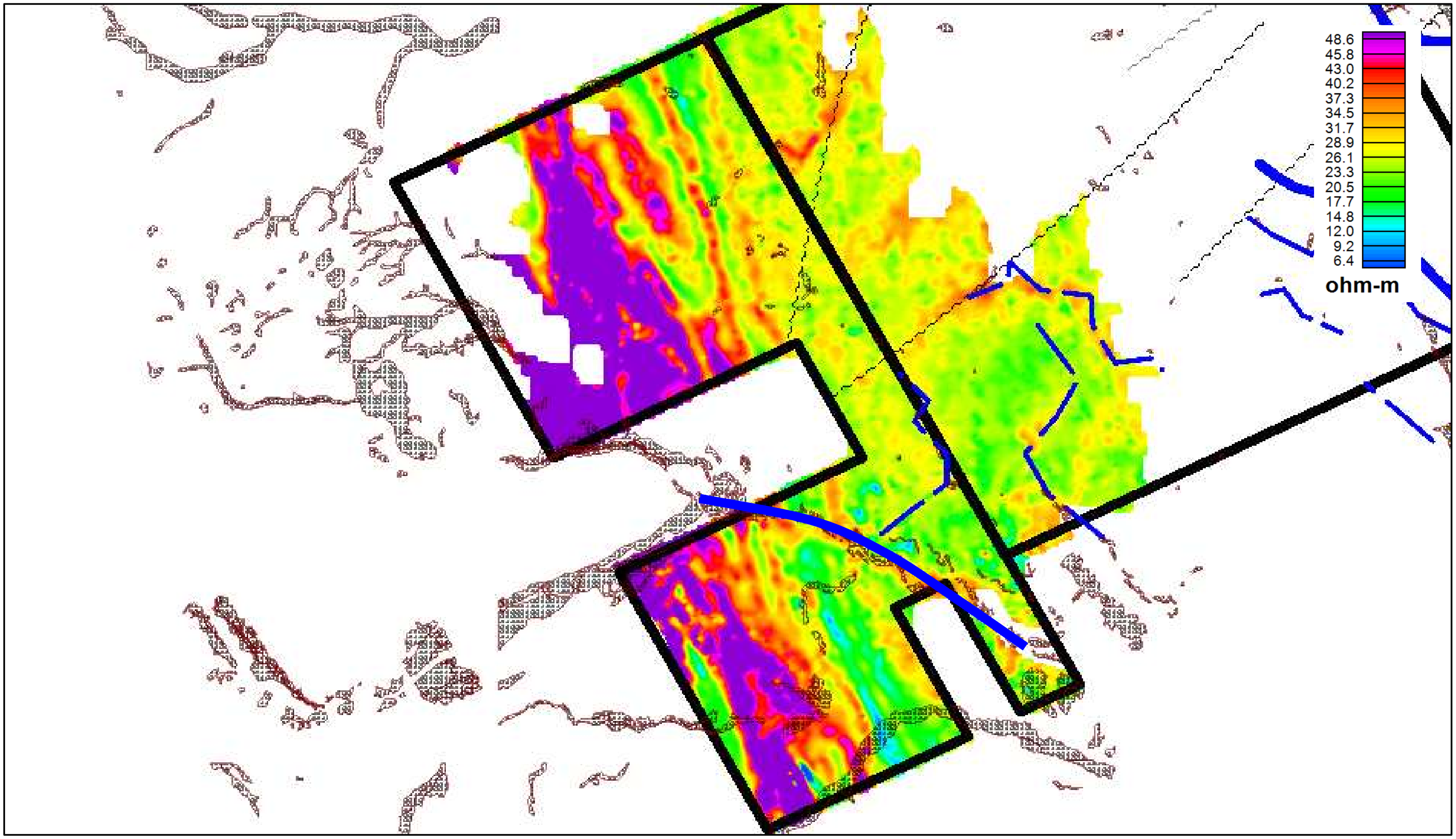

Figure 98: Southern part of the merged survey area. Terrain corrected depth slice at 1150 m elevation, showing the locations of the buried bedrock valleys (heavy blue lines), the meltwater channels (thin blue solid and dashed lines), and the sand and gravel deposits (outlined in brown and hatched areas).

Features 22

Features 22 (shown in Figures 99 and 100) are tributaries from a major mapped bedrock buried valley lying south of the survey. Those features labeled 22a, 22b and 22c are possible branches from these tributaries. 22a and 22b correlate reasonably well with mapped sand and gravel deposits. All of these tributaries and branches correlate with current day low-lying terrain.

22c shows a branch from the mapped tributary to follow the Red Deer River, and Big Valley Creek. Although the strongest resistivities along the Red Deer River are seen in this southern section the elevated resistive response continues north.

Potential lineaments appear to control the nature of the resistive data along the lengths of the bedrock valleys.

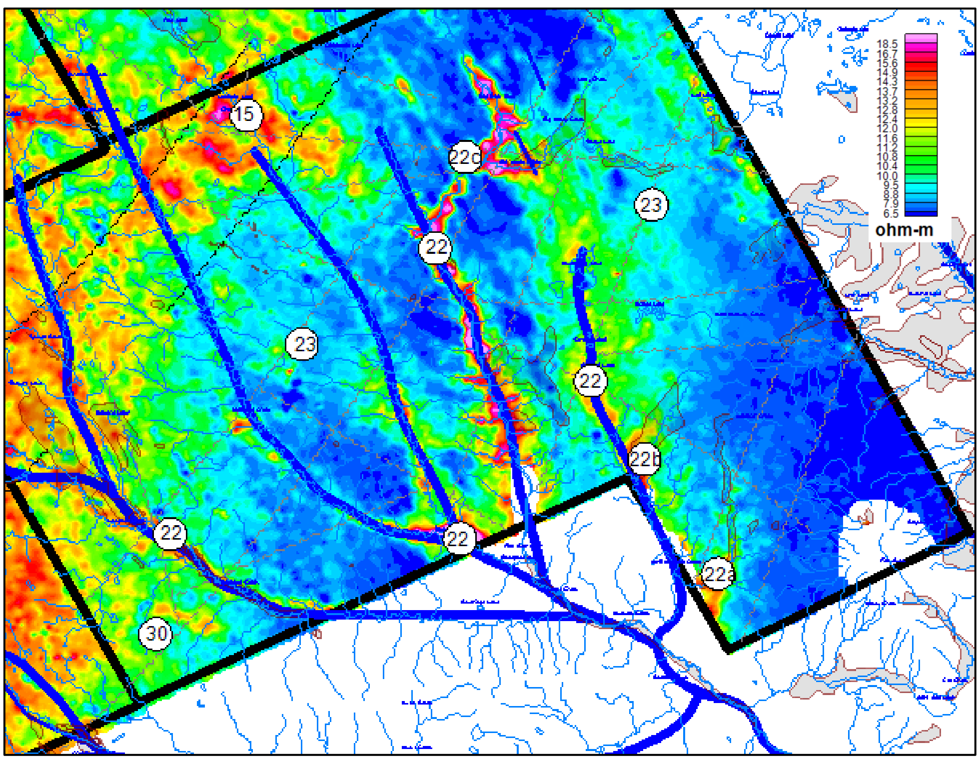

Figure 99: Resistivity at an elevation of 800 m, with potential basement lineaments, sand and gravel deposits and bedrock buried valleys.

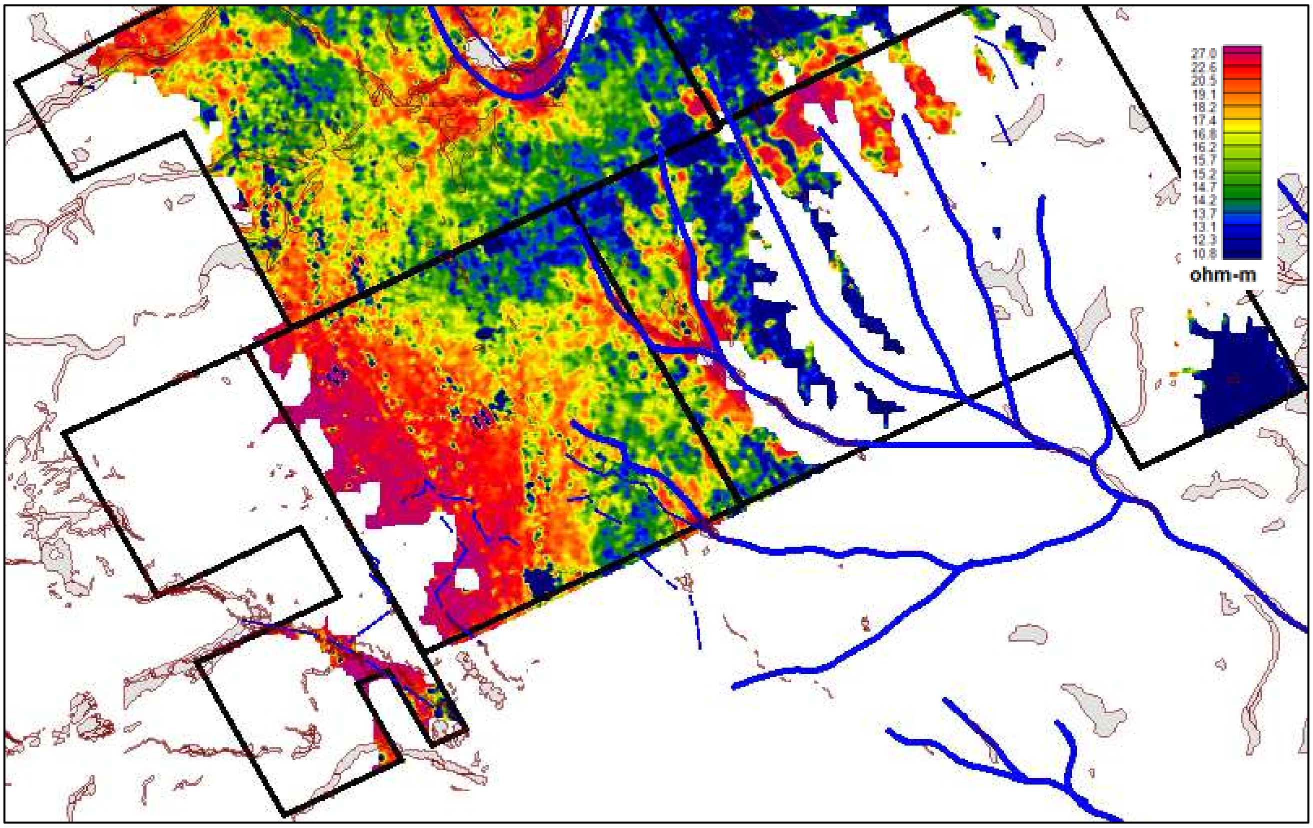

Figure 100: Resistivity at an elevation of 900 m, with potential basement lineaments, sand and gravel deposits and bedrock buried valleys.

Features 23

These features have been mentioned previously, and shown in Figure 94; they are simply areas of slightly elevated resistivity. The western region strikes NW-SE and does not follow current terrain. The eastern region essentially lies between two lengths of sand and gravel deposit, however as we see from the above image, the situation is obviously more complex. Still the elevated region is visible.

Feature 24

From the M.D. of Rocky View No. 44 Regional Groundwater Assessment, feature 24 correlates with the Calgary buried bedrock valley (Figure 98) and mapped sand gravel deposits lie along the feature.

Feature 25

The arrow in the left image of Figure 101 points to a NW-SE trending feature. This may just be unmapped disturbed belt lithology. The right image shows two possible structures, which are only tentatively seen in the magnetic data, which control resistivity backgrounds. The N-S structure suggests a possible sinistral offset, and the NNW trending structure shows the boundary between higher resistivity's to the west and lower resistivity's to the east.

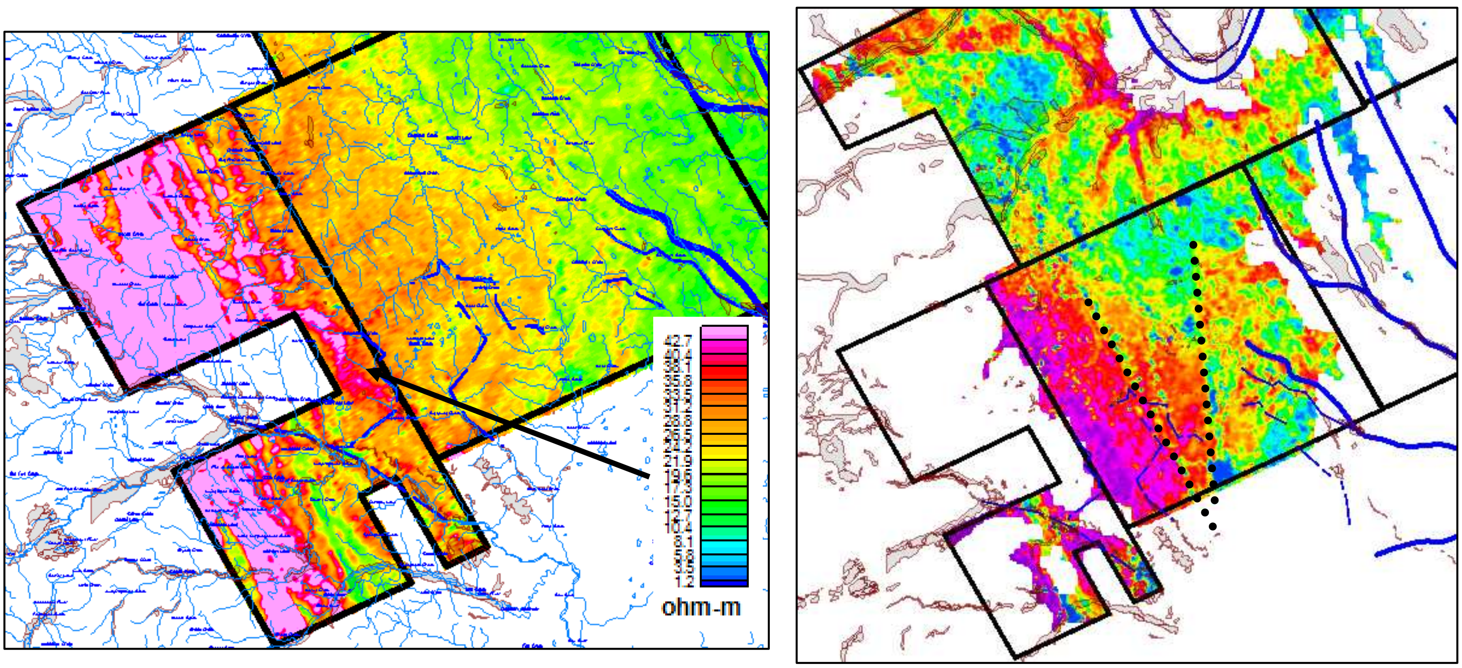

Figure 101: Resistivity relative to surface at 30 m depth (left) and Resistivity at 950 m elevation (right)

Features 26

These weak lineaments strike NE-SW and do not correlate with current topography.

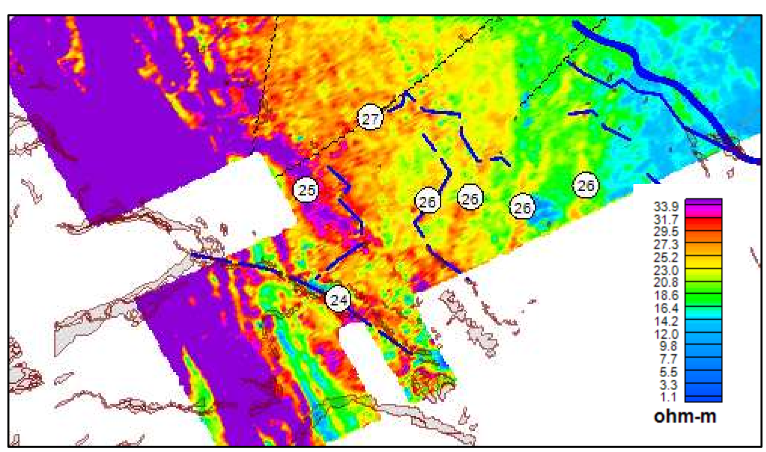

Figure 102: Resistivity relative to surface at 60 m depth

Features 27

These weakly elevated resistive regions (see Figure 103) correlate with current topography, and the river system is part of that from selection 17. However there does seem to be an area (see the right image) between the features where no elevation above background can be seen. The southern 27 location in the left image correspond with a meltwater channel and a NE-SW fault, and the northern 27 location seems to be bound to the east by a NNE structure.

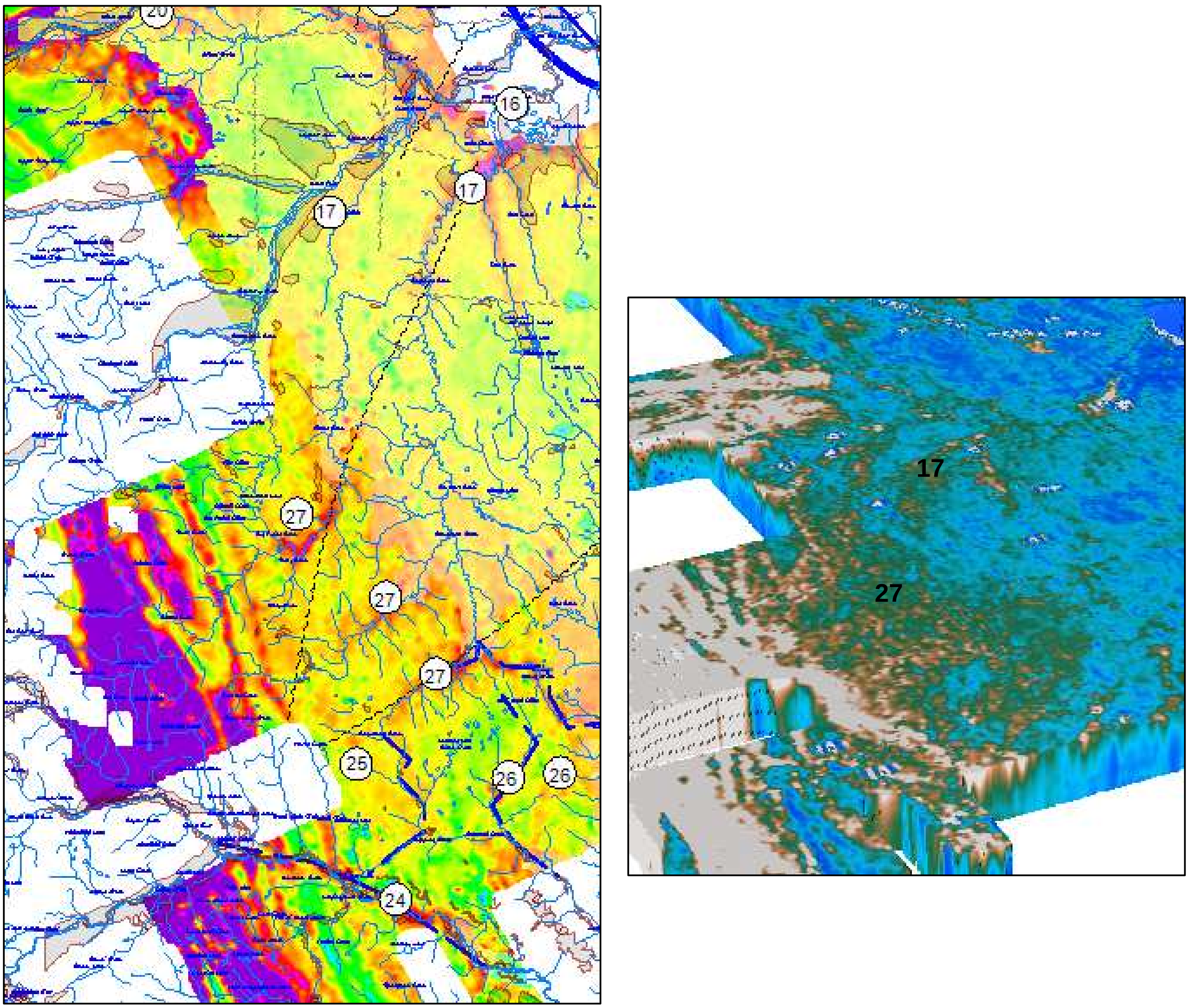

Figure 103: (left) terrain corrected depth slice at 1150 m and 950 m elevations, with the 950 m elevation being transparent. The image shows the locations of the buried bedrock valleys (heavy blue lines), the meltwater channels (thin blue lines), sand and gravel deposits (hatched areas) and potential lineaments; (right) 3D cube relative to surface at 0 m depth.

Features 28 and 29

These are quite weakly resistive features, which do not seem to be related to current topography.

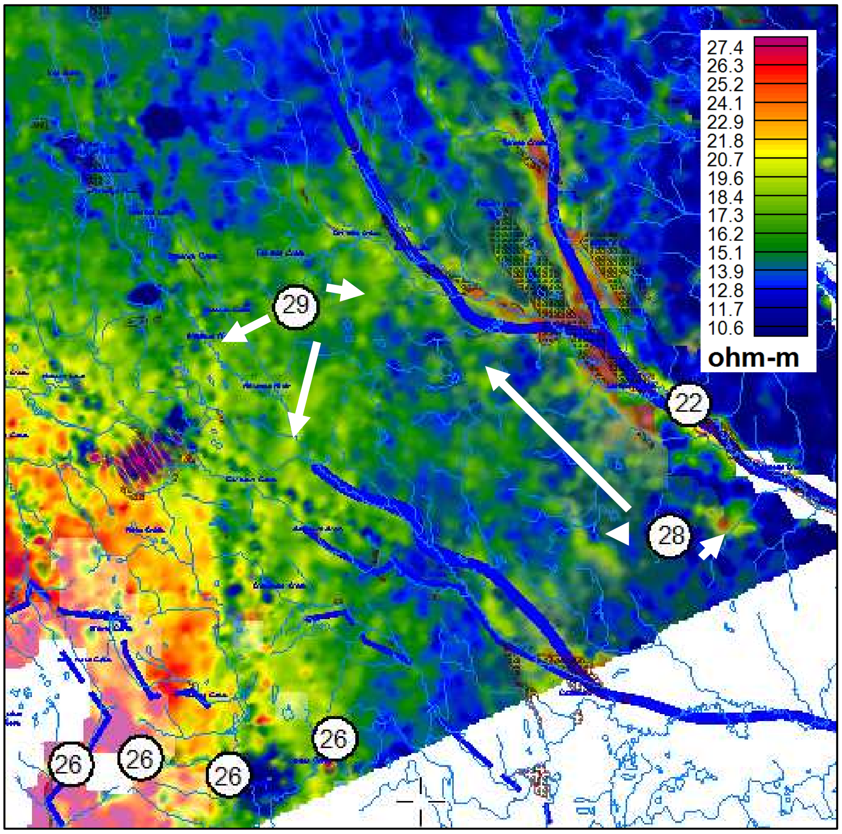

Figure 104: Resistivity corrected for terrain at elevations 900 and 850 m, with the 900 m elevation being slightly transparent. The bedrock valleys, meltwater channels and sand and gravel deposits are also shown.

CLOSING REMARKS

As mentioned previously because of the sheer volume of data in the complete survey area, only a small majority of features can be discussed. However this should not mean that the remaining features shown on the interpretation map should be discounted. Some extra slices through the 3D cubes have been included as "food for thought"…..

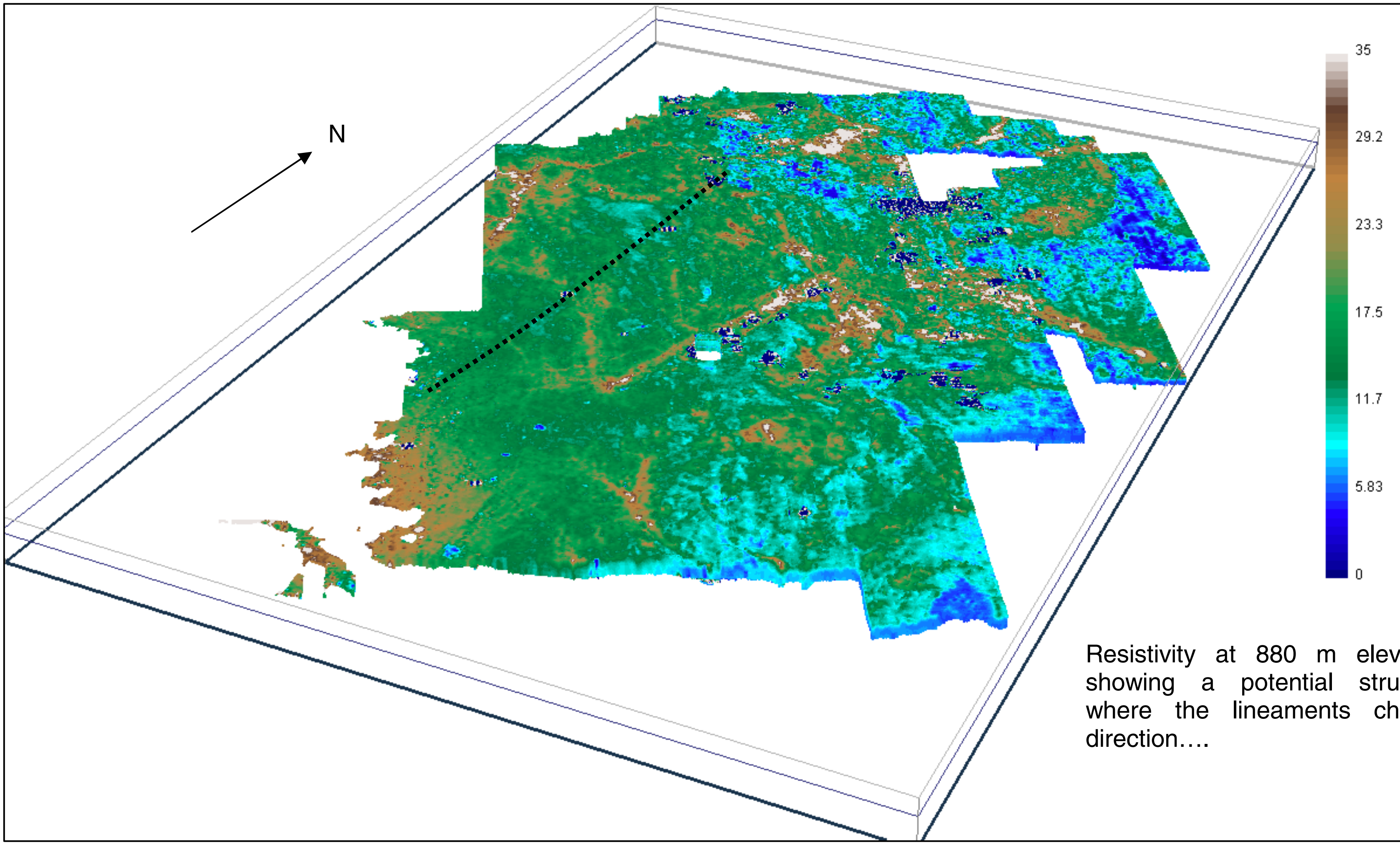

Resistivity at 880 m elevation showing a potential structure where the lineaments change direction….

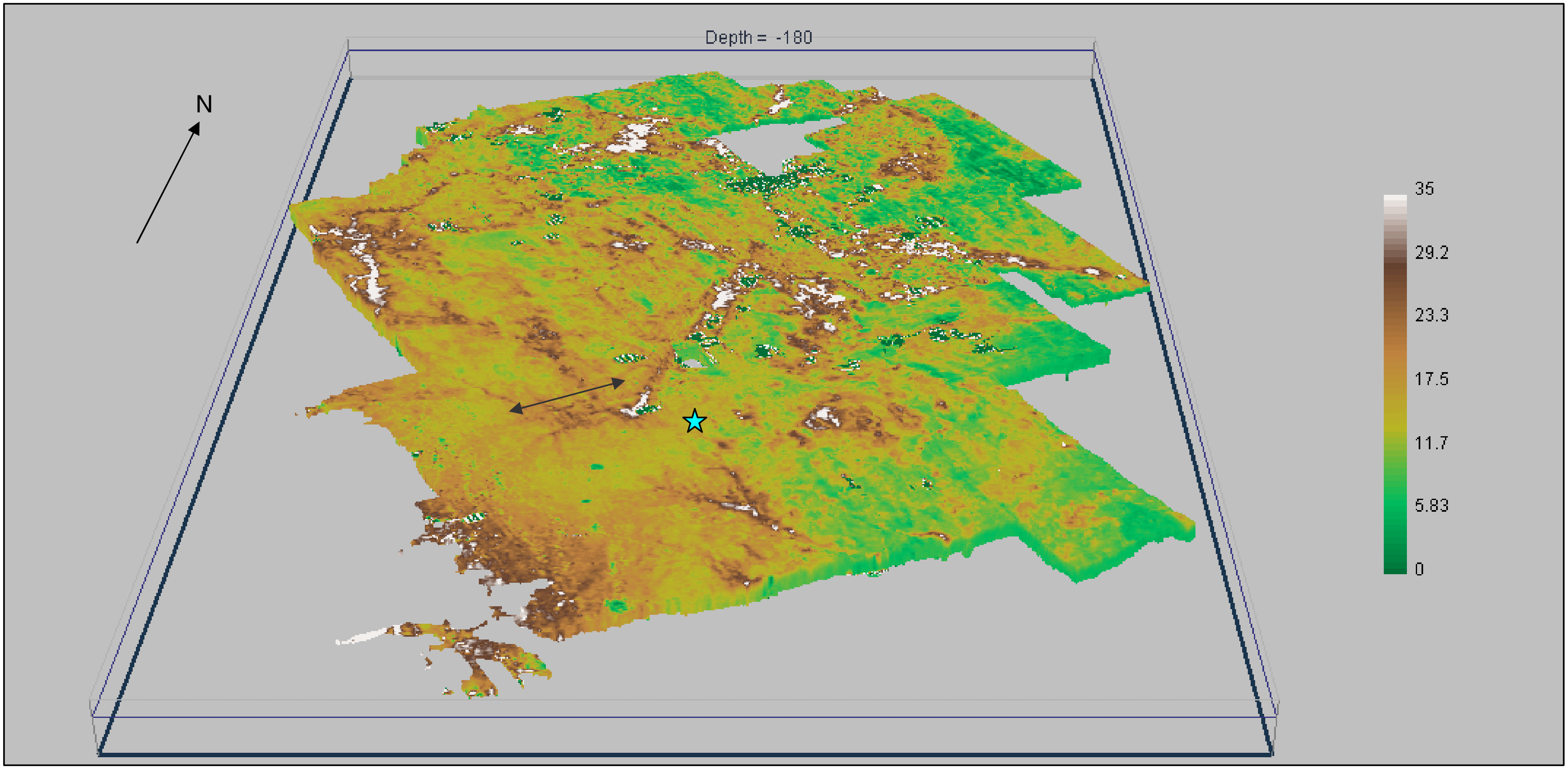

3D terrain corrected cube limited to an elevation of 920 m. Numerous lineaments can be seen extending from the Red Deer buried bedrock valley; to the southeast, towards another valley south of the area ☆; others trending approximately 70°

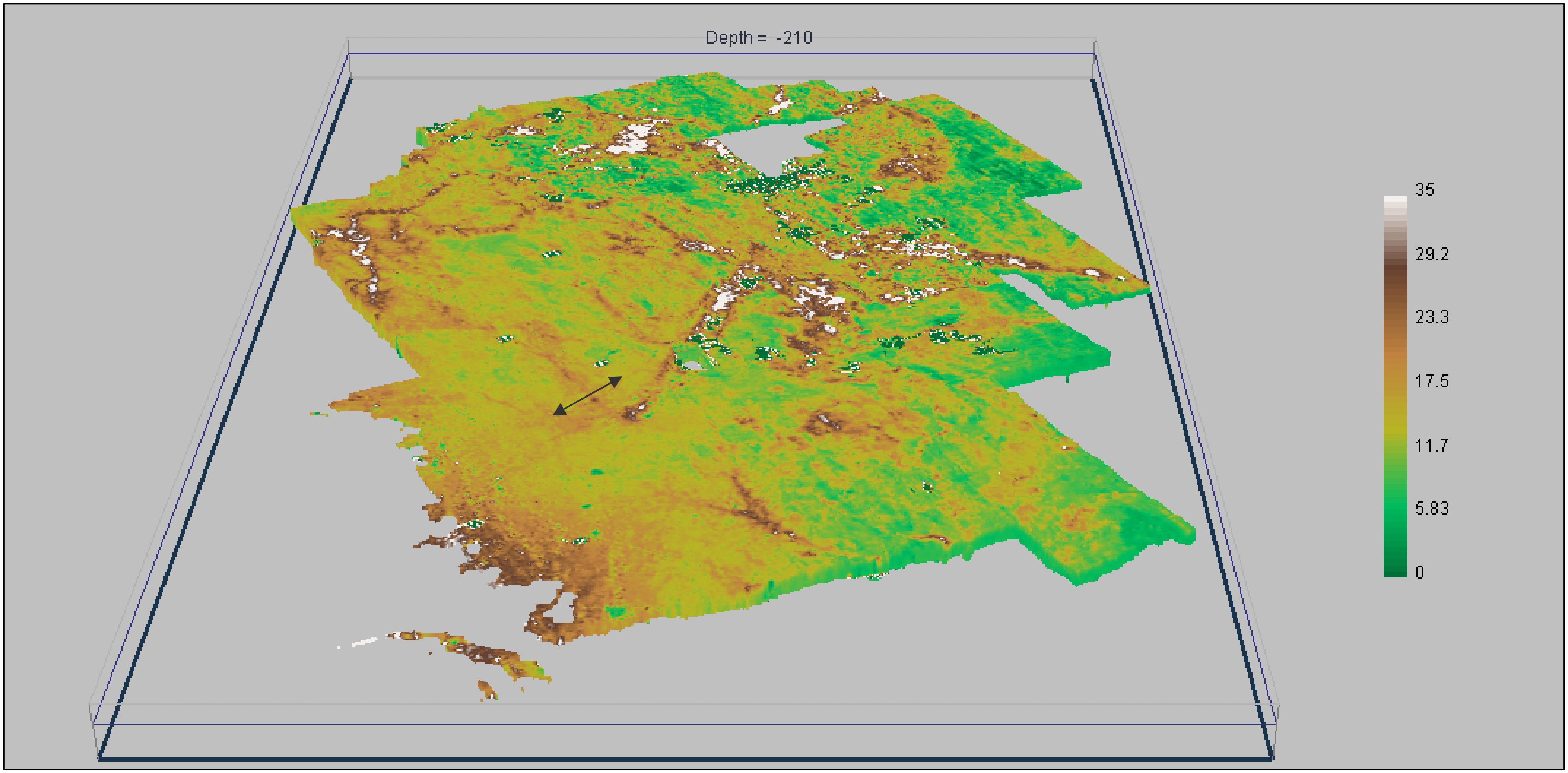

3D terrain corrected cube limited to an elevation of 890 m. At this elevation NE-SW trends can be seen extending from the southern NW striking tributary of the Red Deer buried bedrock valley

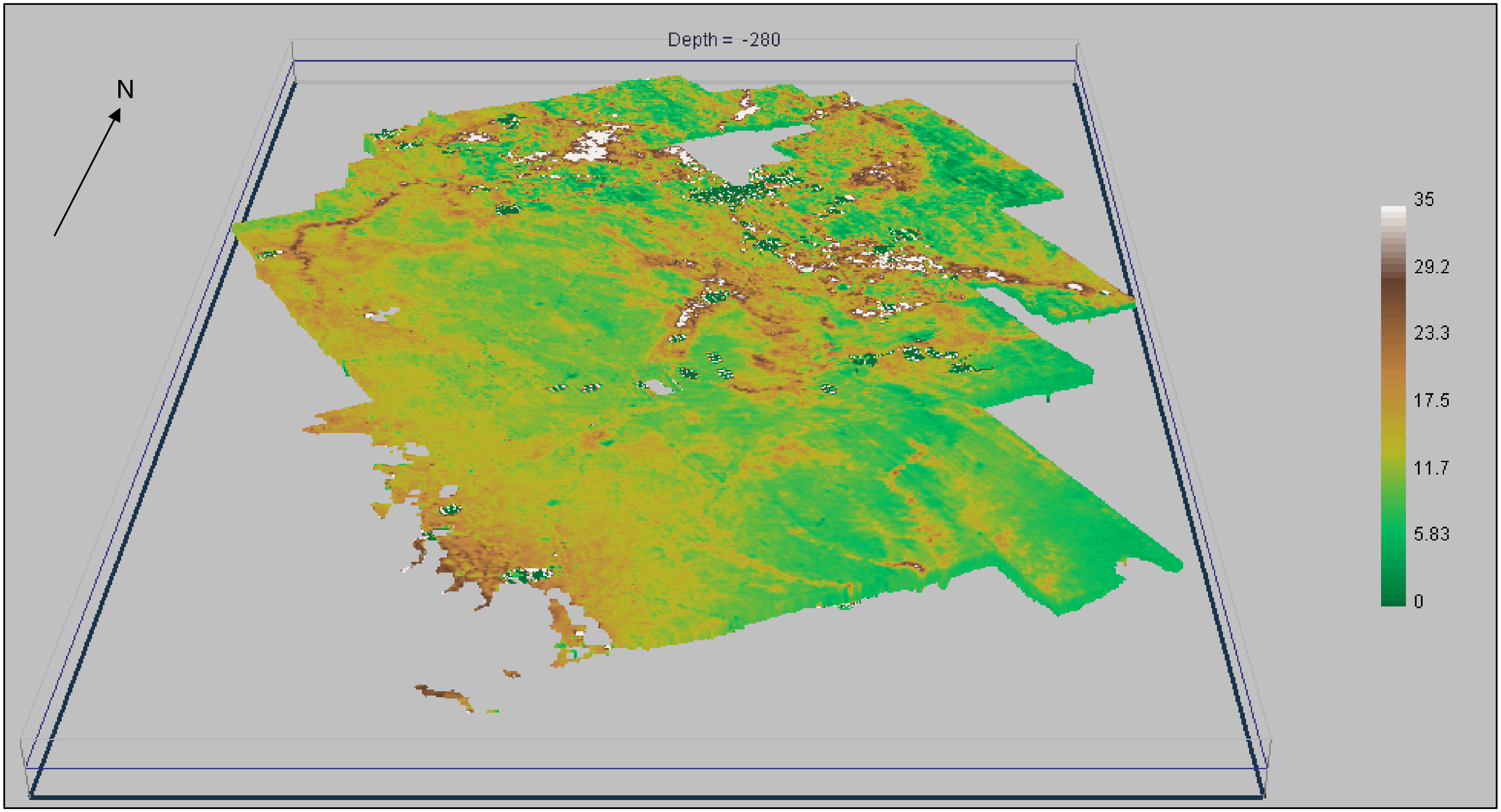

3D terrain corrected cube limited to an elevation of 820 m. The southern bedrock valleys are becoming more prominent.

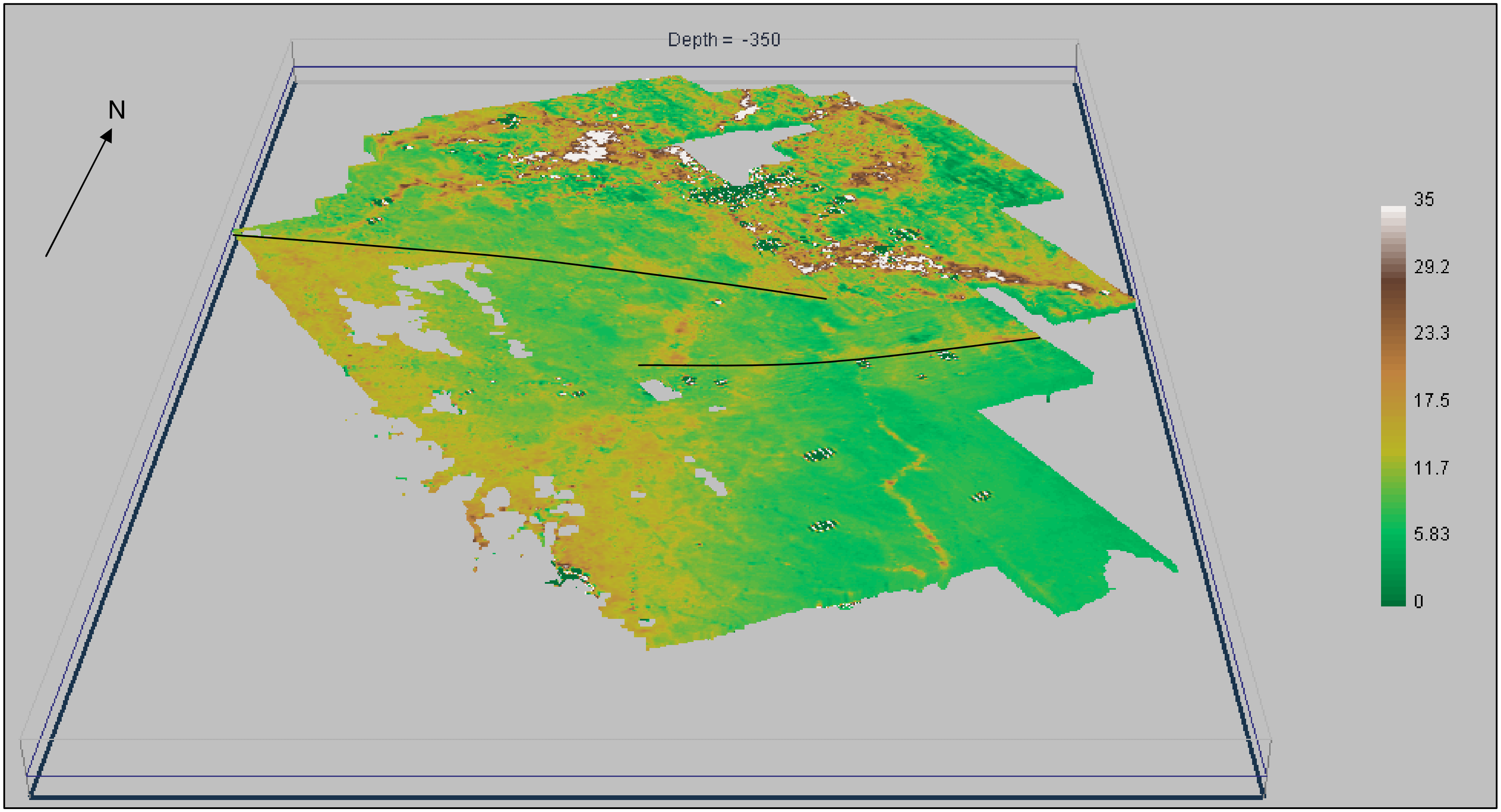

3D terrain corrected cube limited to an elevation of 750 m. Some of the trends mentioned previously in the report now begin to appear.

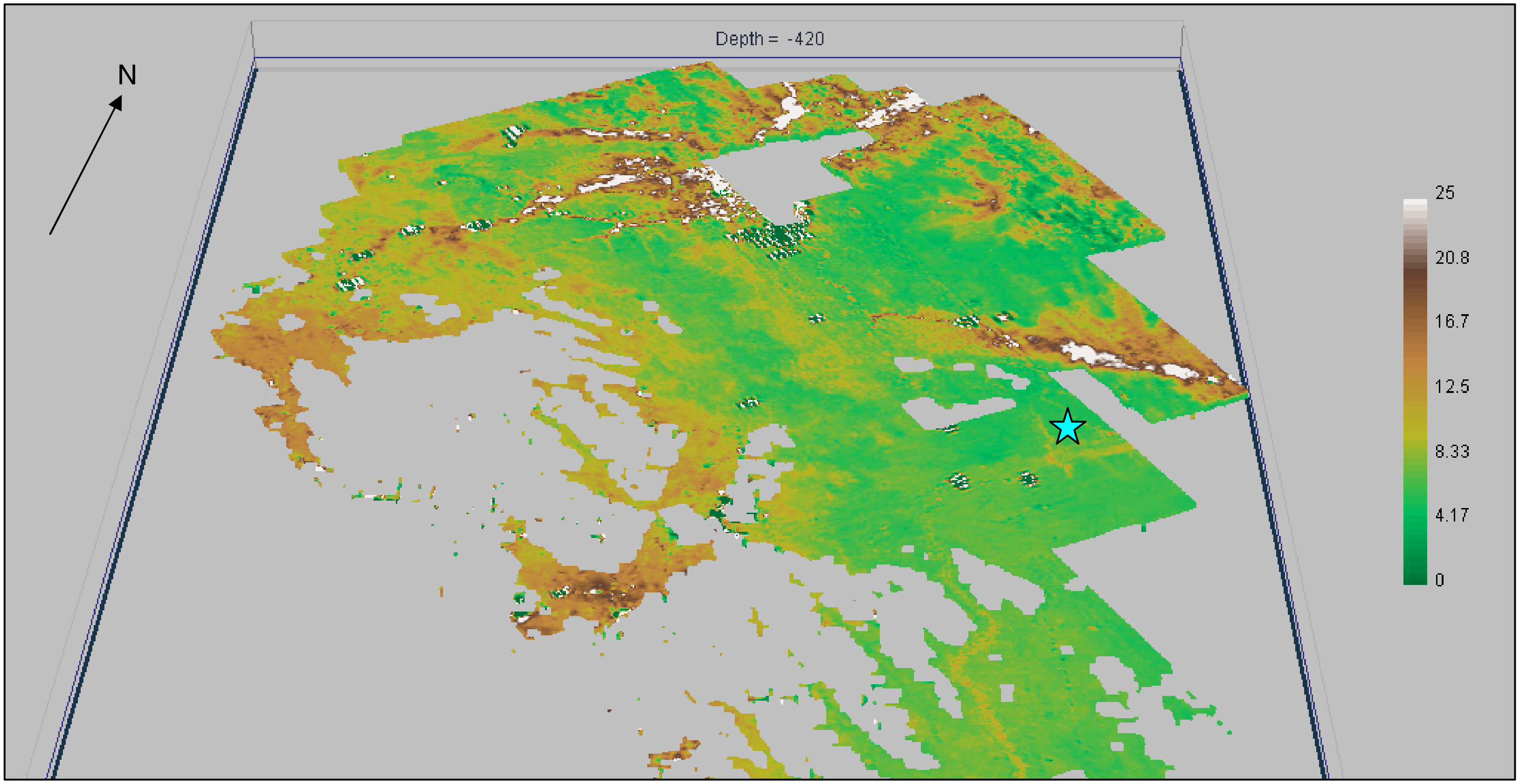

3D terrain corrected cube limited to an elevation of 680 m. A strong sinuous trend which is quite possibly an unknown tributary to a mapped bedrock valley is now emerging as are several weaker trends, striking NNW.

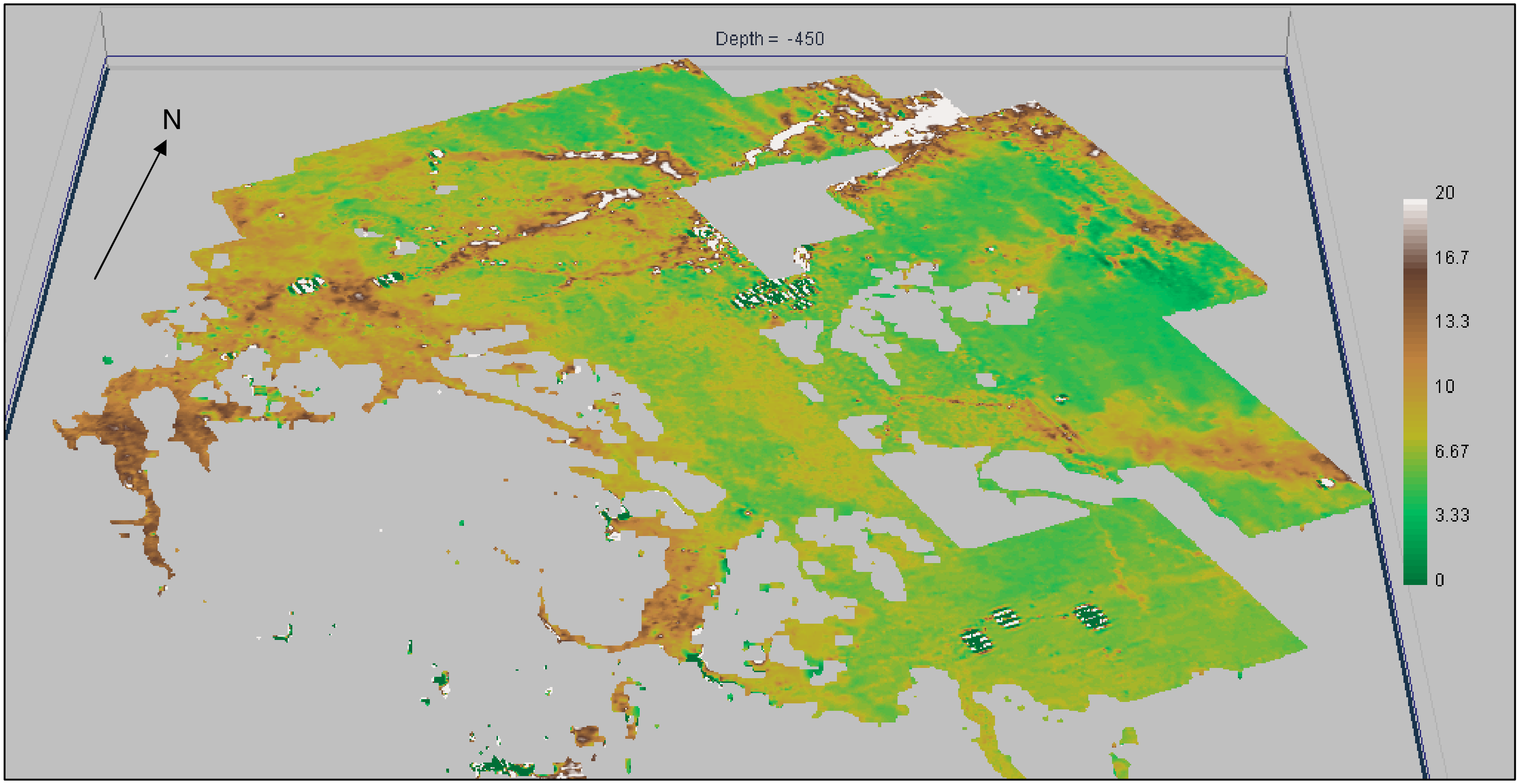

3D terrain corrected cube limited to an elevation of 650 m.

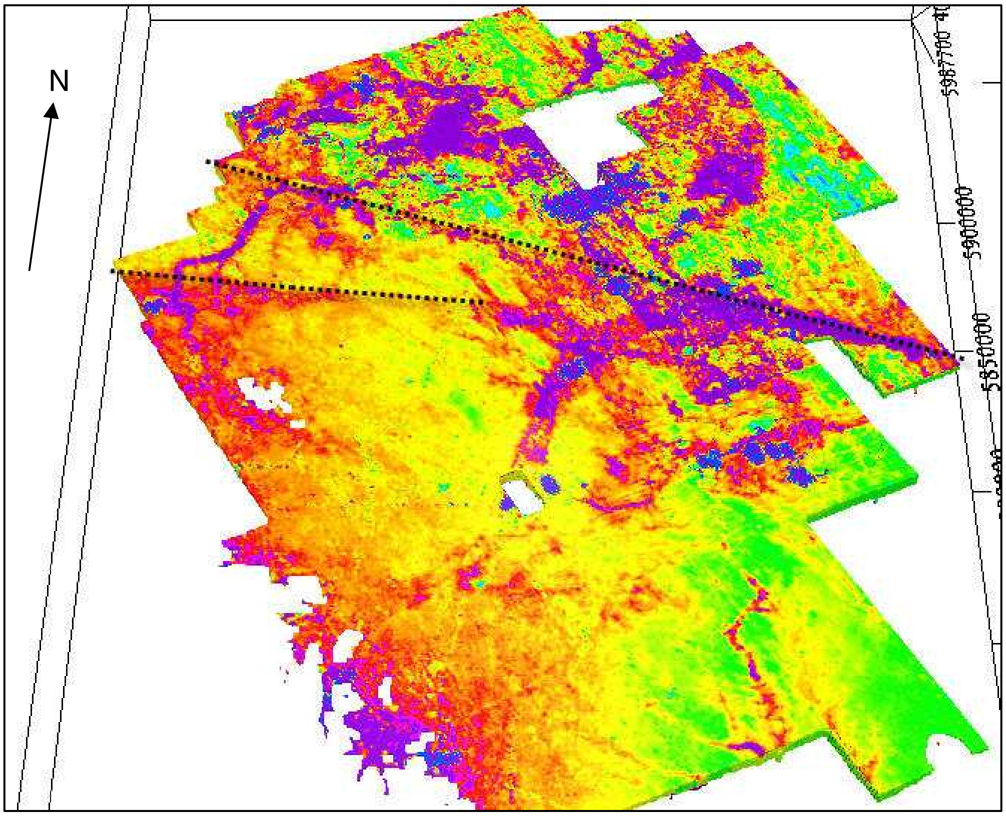

3D terrain corrected cube limited to an elevation of 800 m. Unlike the image on page 118, the southern trend in the image above, appears to strike north of what is feature 10, rather than to the south of it.

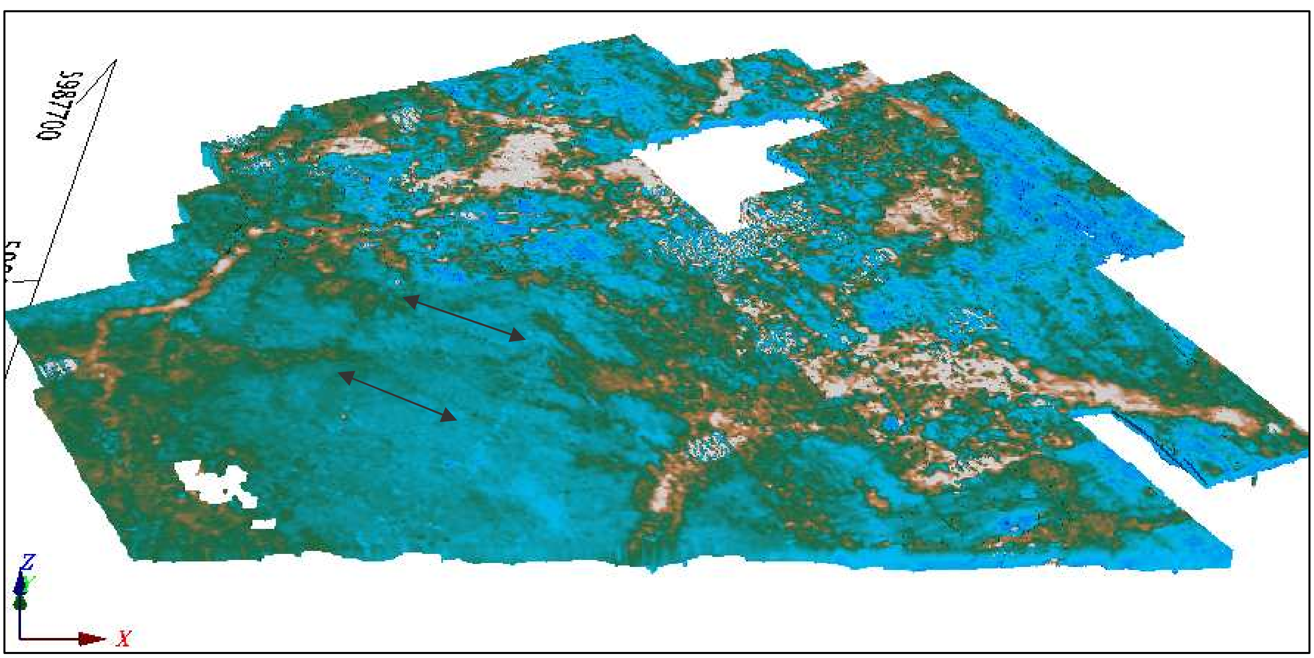

3D terrain corrected cube limited to an elevation of 800 m. Notice the several NW-SE trends

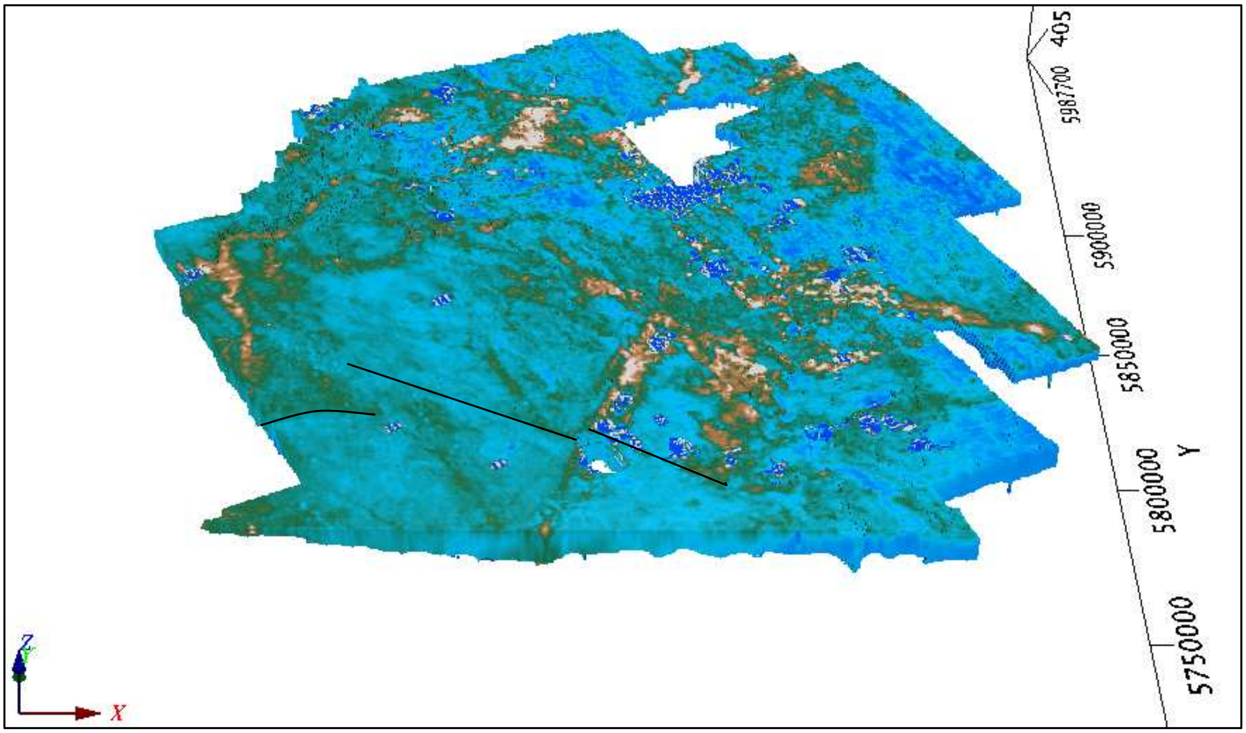

3D terrain corrected cube limited to an elevation of 880 m. Several trends mentioned previously in the report can be identified

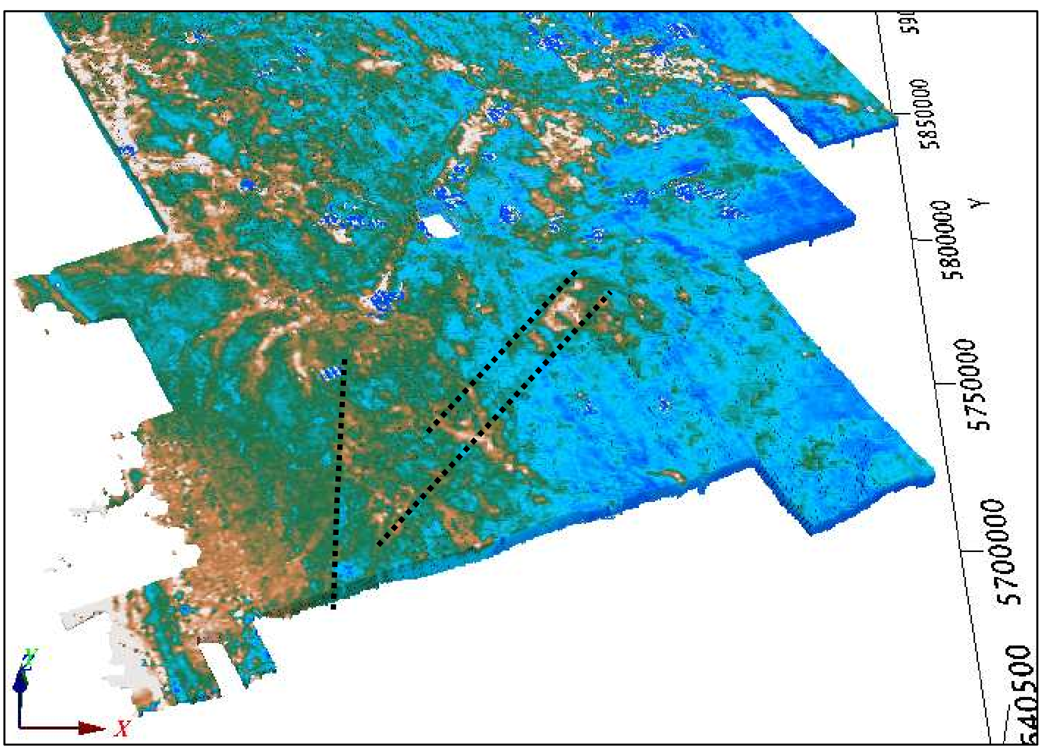

3D terrain corrected cube limited to an elevation of 1000 m. Several trends area seen

Appendix 2 – Geophysical Analysis of the Edmonton–Calgary Corridor

GEOPHYSICAL ANALYSIS OF THE EDMONTON – CALGARY CORRIDOR

Prepared for
Alberta Geological Survey
(ERCB)

For Consideration by
Laurence Andriashek, Steven Lyster, Shawn Slattery & Tony Lemay

Prepared by
TerraNotes Ltd.

April 14, 2010

Table of Contents

Table of Contents

Table of Contents

INTRODUCTION

PROJECT DESCRIPTION

This presents results of a multidisciplinary and collaborative project with the primary objectives of identifying, characterizing and mapping areas of interest for potential aquifers, establishing the relationship between Airborne Electromagnetic data (AEM) and test holes, assessing replicability of this type of surveys outside the Edmonton-Calgary Corridor.

SURVEY AREAS

Airborne Survey 2007-2009
Calgary Edmonton Corridor

The following Map displays the selected Test Holes in the proposed analysis area (Figure 1).

Data

Fugro GEOTEM (6 Datasets)
Fugro RESOLVE (1 Dataset)
12 bore holes

(All the datasets were provided by AGS.)

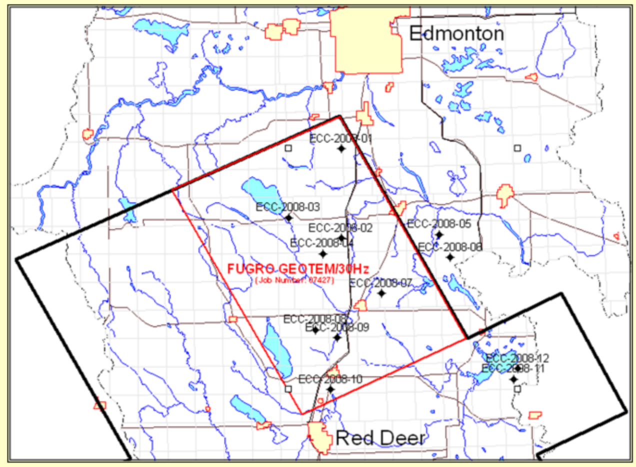

Figure 1. Selected Test Holes in the proposed analysis area (as provided by AGS).

OBJECTIVES

OBJECTIVES	WAS THIS OBJECTIVE ACHIEVED?
As per Agreement and following discussions at three meetings previously held with Mr. Andriashek and his colleagues, the project will attempt to achieve the following objectives:	
1. Calibrate regional Electromagnetic (GEOTEM) results with drill-hole logs.	Yes
2. Identify, characterize and correlate drill data with even faint GEOTEM/RESOLVE signatures of possible zones for aquifers. Characterize dominantly sand-based areas for primary aquifers above 200m.	Yes. For Grain size thresholds see recommendations.
3. Build the conductivity vs stratigraphic model for possible zones for aquifers around selected Test Holes.	Stratigraphic borders were geophysically mapped. Conductivity models were built but not related to stratigraphy as per discussions.

OBJECTIVES

OBJECTIVES	WAS THIS OBJECTIVE ACHIEVED?
4. Characterize Geometry and Edges of GEOTEM geophysical units vs test holes/known geology. Analyze boundaries of AEM geophysical vs geological units.	Yes
5. Select and characterize the GEOTEM properties that can be replicated in other areas – Criteria of Replicability.	Yes

Additional Objectives

Additional objectives were set during the discussions as the project evolved. All these additional objectives were achieved.

- Image resistive zones in the entire region, and relate them to specific lithologies such as sand and gravel.
- Image conductive zones in the entire region, and relate them to specific lithologies such as clay and mud.
- Differentiate the stratigraphic formations, especially the Paskapoo from the other formations.
- Amplify the weak anomalies coming from locally thick sand and gravel zones.
- Evaluate the resistive zones and characterize the source of the anomaly, including the superficial and cultural effects (to be completed with noise data and geophysical processing).
- Tie the drill-hole results with airborne electromagnetic results (Calibration and Flight Line Attributes Analysis.)
- Demonstrate the applicability and replicability of these techniques to other areas of Alberta where there is very little drill-hole information.

Executive Summary

- TerraNotes Ltd. analysed and interpreted the data and created maps to image the subsurface structures, features and trends within the ECC area. Resistive and conductive anomalies were delineated in the region, and some of those anomalies were related to the possible lithologies such as sand and gravel for resistive zones or clay and mud for conductive zones.
- Twelve resistive zones were delineated as regions of interest for potential aquifers within the Paskapoo formation.
- Four resistive zones were selected as regions of interest for potential aquifers within the Horseshoe Canyon / Scollard / Ardley / Battle formations.
- Five zones of interest for potential aquifers were identified and characterized based on a GEOTEM data calibrated against eight drill holes.
- We conclude that resistivity contrasts obtained from logging data between Paskapoo and other formations (Scollard, Ardley, Battle and Horseshoe Canyon) is sufficient to image with AEM.
- Frequency domain RESOLVE data was used to characterize the previously known aquifers and two intersecting aquifer regions were mapped at different depth levels.
- It was shown that GEOTEM amplification and calibration approaches can be used to provide resolution as high as Frequency domain RESOLVE does. These amplification and calibration approaches could be used to replace the FDEM data where FDEM data is not available.
- Amplified EM data can map the locally thick sand and gravel zones thicker than 9-10 metre.
- Relationship between surface topography and resistive zones was shown for some selected anomalies and we further showed how this relationship can be used to select potential aquifer zones.

Methods

- We have used our specific gridding techniques to grid both raw data and calculated products to eliminate the some local/cultural effects and the effect of large flight line spacing (~ 800 m).
- Preliminary imaging and mapping of the raw data set and their interpretation.
- Used our amplification techniques for EM anomalies to emphasize certain aspects of the EM anomalies. These aspects include amplifying the:
  1) near-surface
  2) mid-depth
  3) deeper
  4) local anomalies
  5) regional anomalies
  6) detailed edges
- We have adapted our 2D specific gridding techniques to 3D gridding algorithms to grid the Resistivity-Depth Imaging (RDI) dataset in 3D. Imaged the RDI data set as 3D volumes, isosurfaces of specific resistivity values, and as vertical and horizontal slices.
- We have used our procedures to include the real topography on the 3D images, which helped us evaluate the resistive and conductive zones.
- We have used our algorithms to tie the drill-hole data with AEM data and found criteria for calibration. This procedure was also used in imaging of detailed edges of the resistive and conductive anomalies.

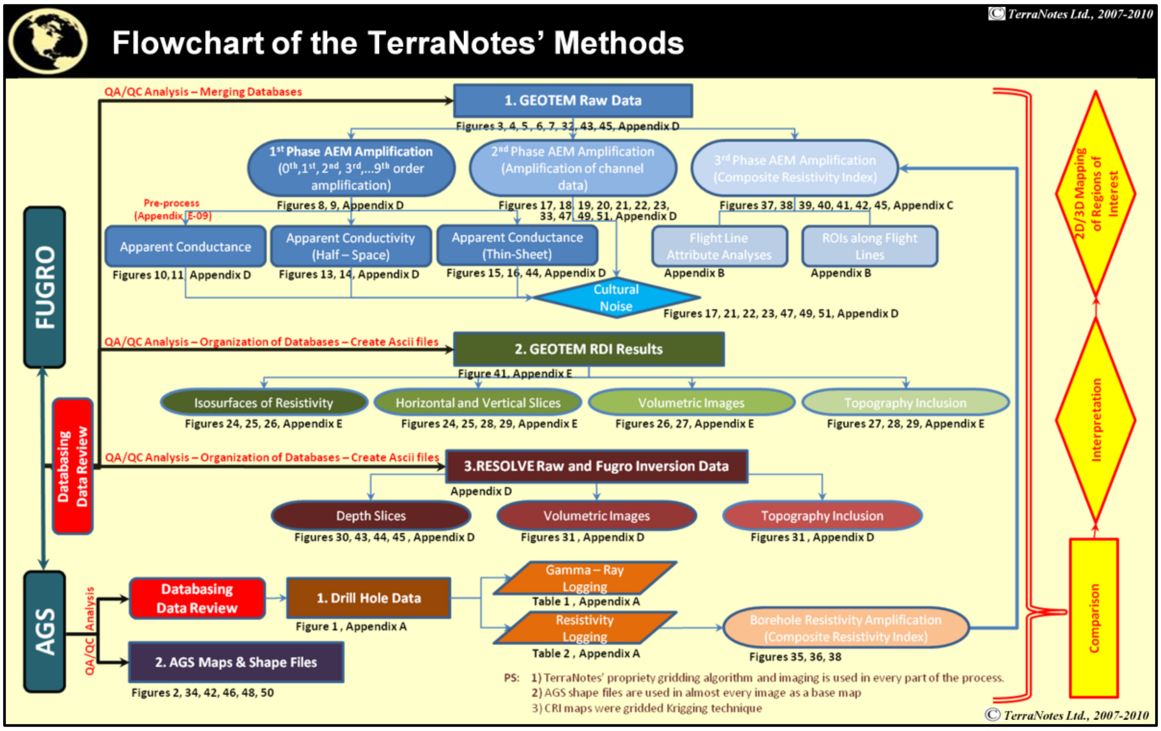
© TerraNotes Ltd., 2007-2010
Flowchart of the TerraNotes' Methods
QA/QC Analysis – Merging Databases
1. GEOTEM Raw Data
Figures 3, 4, 5, 6, 7, 32, 43, 45, Appendix D
1st Phase AEM Amplification (0th, 1st, 2nd, 3rd,...9th order amplification)
Figures 8, 9, Appendix D
2nd Phase AEM Amplification (Amplification of channel data)
Figures 17, 18, 19, 20, 21, 22, 23, 33, 47, 49, 51, Appendix D
3rd Phase AEM Amplification (Composite Resistivity Index)
Figures 37, 38, 39, 40, 41, 42, 45, Appendix C
Pre-process (Appendix E-09)
Apparent Conductance
Figures 10, 11, Appendix D
Apparent Conductivity (Half – Space)
Figures 13, 14, Appendix D
Apparent Conductance (Thin-Sheet)
Figures 15, 16, 44, Appendix D
Flight Line Attribute Analyses
Appendix B
ROIs along Flight Lines
Appendix B
Cultural Noise
Figures 17, 21, 22, 23, 47, 49, 51, Appendix D
FUGRO
QA/QC Analysis – Organization of Databases – Create Ascii files
2. GEOTEM RDI Results
Figure 41, Appendix E
Isosurfaces of Resistivity
Figures 24, 25, 26, Appendix E
Horizontal and Vertical Slices
Figures 24, 25, 28, 29, Appendix E
Volumetric Images
Figures 26, 27, Appendix E
Topography Inclusion
Figures 27, 28, 29, Appendix E
Databasing Data Review
QA/QC Analysis – Organization of Databases – Create Ascii files
3.RESOLVE Raw and Fugro Inversion Data
Appendix D
Depth Slices
Figures 30, 43, 44, 45, Appendix D
Volumetric Images
Figures 31, Appendix D
Topography Inclusion
Figures 31, Appendix D
AGS
QA/QC Analysis
Databasing Data Review
1. Drill Hole Data
Figure 1, Appendix A
Gamma – Ray Logging
Table 1, Appendix A
Resistivity Logging
Table 2, Appendix A
Borehole Resistivity Amplification (Composite Resistivity Index)
Figures 35, 36, 38
2. AGS Maps & Shape Files
Figures 2, 34, 42, 46, 48, 50
PS: 1) TerraNotes' propriety gridding algorithm and imaging is used in every part of the process.
2) AGS shape files are used in almost every image as a base map
3) CRI maps were gridded Krigging technique
2D/3D Mapping of Regions of Interest
Interpretation
Comparison
© TerraNotes Ltd., 2007-2010

How to Utilize This Report

- The format of this report has been created to allow for the practical use of the results and findings.
- Each page includes a map or an image with its related major findings.
- In appropriate cases, some geophysical assumptions and other relevant comments have been included.
- This report includes two parts: The main results and the appendices.
- The main results portion aims at presenting the most important findings, while the appendices include a large number of maps, images, tables and other items that have been used in our processes. The appendices can be used by the readers for further interpretations and evaluations. Due to its size (over 250 maps) the appendices are delivered in a hard disc drive. A list of the titles of the maps is provided at the end of this report.
- This report is formatted in pdf to allow the reader to zoom in the maps and expand the size up to 400 %.
- The 3D image presented in this report have been selected from a 3D rendering software that allows for the orientation in all directions and renders all depth and horizontal slices. Part of the deliverables for this project includes a viewer that will allow the reader to visualize the 3D imaging.

Main Findings

GEOTEM 2007-2009 ECC Survey

Main Findings

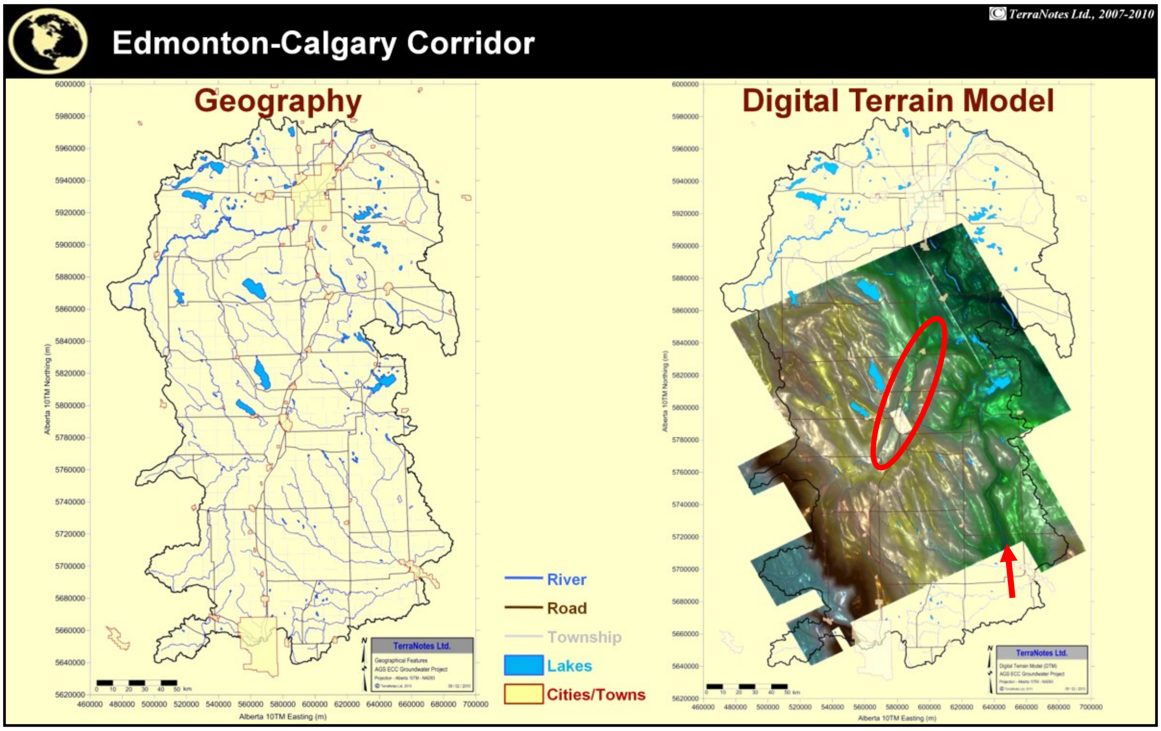

Figure 2. Geographical features of the ECC area (roads, rivers, lakes, urban areas provided by AGS).
Figure 3. Digital Terrain Model (DTM) map extracted from Fugro dataset provided to AGS.

➢The left panel shows the geographical features (i.e. Rivers, roads, lakes, cities/towns and townships) within the Edmonton-Calgary Corridor.
➢ These features are used in the following images as a reference (except for Townships).
➢ The right panel shows the Digital Terrain Model of the project area.
➢ This DTM map is validated with the SRTM dataset.

<u>Main Findings from these maps</u>

➢ The elevation increases as we go from east to west.
➢ Superficial valleys can be observed in many different directions.
➢ These valleys can be connected to subsurface channels as well. Red ellipse shows an example of an area around Red Deer. This area is situated where the RESOLVE data was collected.
➢ Red arrow indicates an example of a river course observed on a topography map. This zone can be used to cross-validate the source for linear resistive features that may indicate subsurface buried channels.

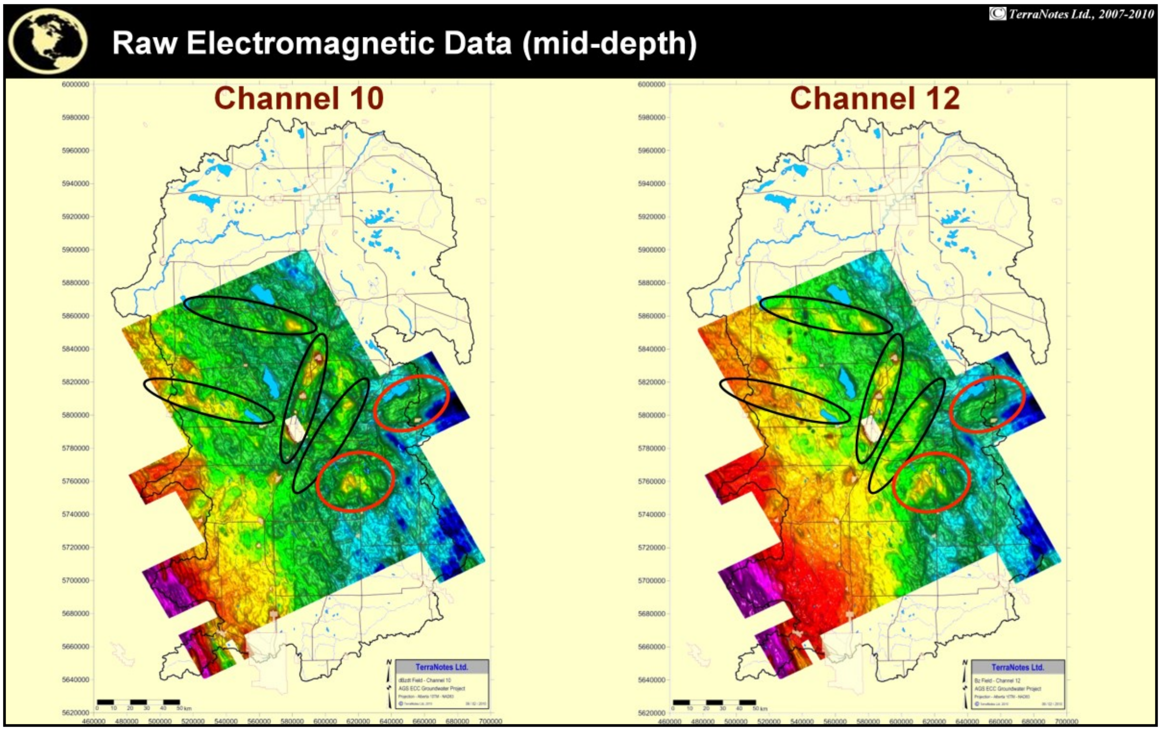

Figure 4. dBz/dt channel 10 data in pT/s (picoTesla/seconds).
Figure 5. Bz channel 12 data in fT (femtoTesla).

➢ This page shows the Z-component EM field data.
➢ These maps show the raw data from the Fugro dataset, and we try to test what we could get from the raw material without doing any further processing.
➢ In these maps red colour show the resistive zones where as blue colours show least resistive units. This convention was followed in all the figure in this report.
➢ The left panel is the channel 10 dBz/dt data that indicates mid-depth resistivity structures.
➢ The right panel is the channel 12 Bz field data that also indicate mid-depth but relatively deeper resistivity structures.

Main Findings from these maps

➢ Ellipses are drawn after a subjective interpretation done by TerraNotes staff.
➢ Black ellipses image continuous resistive trends that may indicate subsurface structures such as buried channels.
➢ Red ellipses show oval shape wide resistive anomalies in the region that may indicate aquifer lenses of higher porosity sands.
➢ We may divide the area into four regions.

1. Horseshoe Formation (blue - cyan)
2. Scollard Formation (cyan - dark green)
3. Paskapoo Formation (green - yellow - red)
4. Mountains (pink)

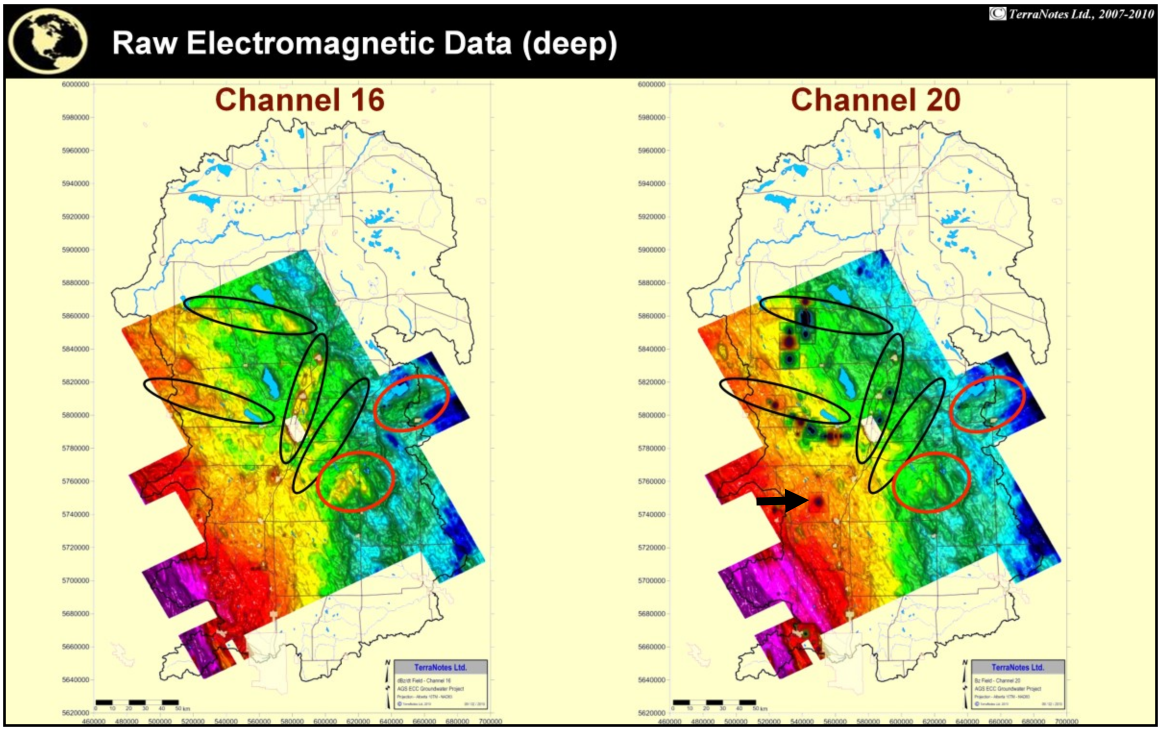

Figure 6. dBz/dt channel 16 data in pT/s (picoTesla/seconds).
Figure 7. Bz channel 20 data in fT (femtoTesla).

- The left panel is the channel 16 dBz/dt data.
- The right panel is the channel 20 Bz field data .
- This page also shows the z-component raw EM field data, but deeper than Figure 4 and 5.

Main Findings from these maps

- Both maps indicate the same resistive anomalies.
- Black ellipses image continuous resistive trends that may indicate subsurface structures such as buried channels.
- Red ellipses show oval shape wide resistive anomalies in the region that may indicate aquifer lenses of higher porosity sands.
- Black arrow on the right panel shows an example of noisy areas in the deepest channel. Those circular noise anomalies are interpreted as Towns and microwave towers. Noise source data is needed to engage a geophysical processing to remove their effect.

Geophysical Assumptions and Comments

- Cultural facilities (e.g. Towns, pipelines, microwave towers, ... etc) introduce a significant noise to the electromagnetic data. This is more visible in the later channels of raw data, where signal to noise ratio is much smaller than the earlier data. Eliminating these effect without noise source data would cause losing the AEM signals as well. Thus, we delineated these areas and did not include them in the polygon aquifer interpretation. Please see pages 22-24.

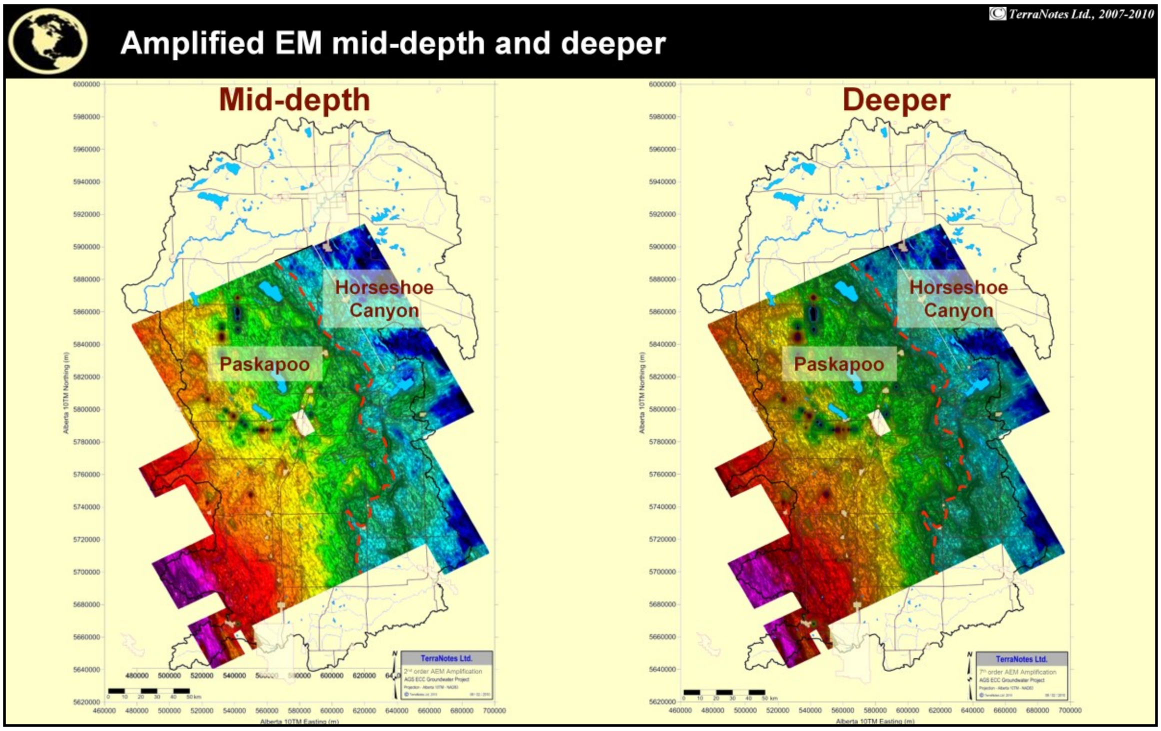

Figure 8. 2nd order EM amplification map (A.m/s^2)
Figure 9. 7th order EM amplification map (A.m/s^7)

➢ This part is the first phase of the EM processing done by TerraNotes staff. The amplification done at this stage amplifies the mid-time and late-time EM data using all the channels starting from the half of on-time (3-20), to test if we could differentiate the mid-depth and deeper resistivity distribution.
➢ This page compares the two amplified EM data.
➢ The left panel shows the mid-depth and the right panel shows the deep resistivity structure.

Main Findings from these maps

➢ The overall resistivity structure is same in both maps.
➢ Red dashed line shows the interpreted western border of the low resistivity anomaly (cyan and blue colours) extracted from the amplified EM data.
➢ Red dashed line is generally coincident with the eastern edge of the Paskapoo Formation, seen in the bedrock geology map of Alberta (AGS map 336).
➢ The geophysical signature of the Horseshoe Canyon, Scollard and Battle formations are low resistive in comparison to the more resistive Paskapoo formation. Thus, Paskapoo formation can be differentiated from other formations in the ECC.

Geophysical Assumptions and Comments

➢ Statistical work done on the resistivities from 12 boreholes revealed that Paskapoo is more resistive than Horseshoe Canyon, Scollard, Ardley and Battle. This study also suggest that geophysical differentiation among Horseshoe Canyon, Scollard, Ardley and Battle is not possible. Please see "Recommendations" page at the end of this report to see a method That may differentiate Horseshoe Canyon, Scollard, Ardley and Battle formations.

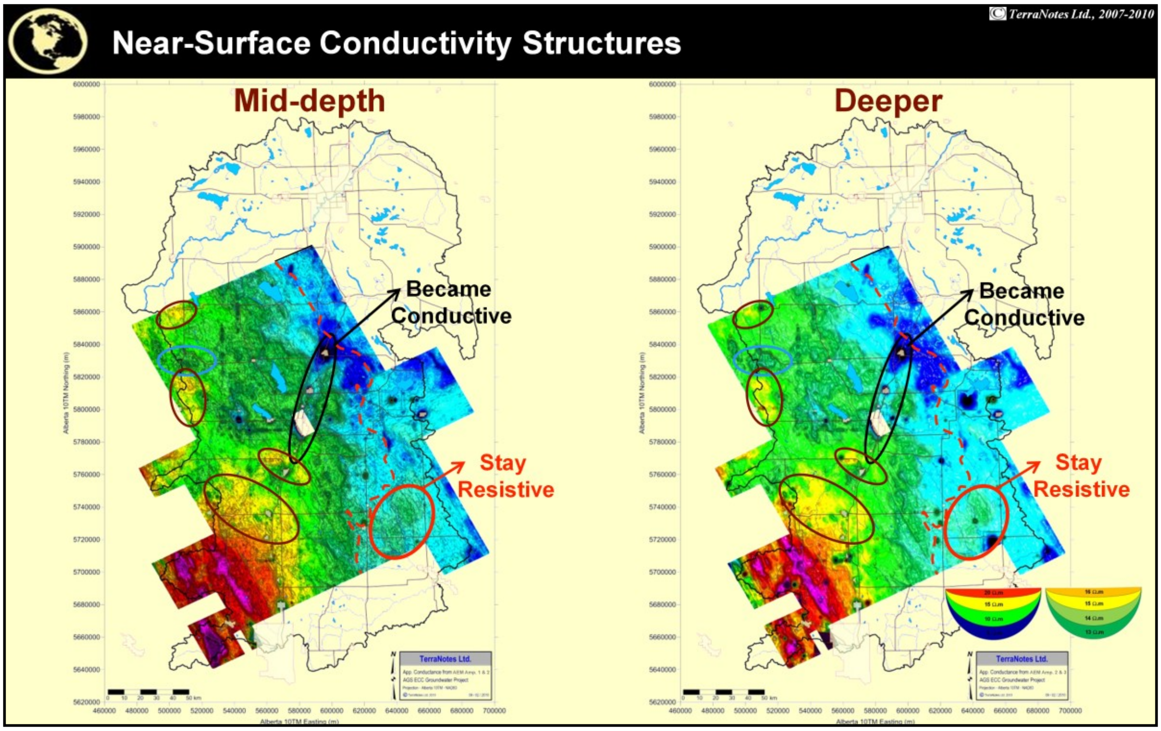

Figure 10. Apparent Conductance (S) map extracted from 1st and 2nd order EM amplification data.
Figure 11. Apparent Conductance (S) map extracted from 2nd and 3rd order EM amplification data.

➢ Apparent conductance (conductivity of a volume) maps were calculated from consecutive amplified EM calculations indicating resistivity structures from different relative depth levels. This is done to evaluate and highlight the differences between two consecutive orders of amplified EM data (e.g. 1 and 2 (Figure 10) and 2 and 3 (Figure 11).
➢ The left panel shows the apparent conductance of near-surface to mid-depths
➢ The right panel shows the apparent conductance from deeper depths.

<u>Main Findings from these maps</u>

➢ Black ellipse shows the resistive paleovalley NE of Red Deer as a conductive trend in this type of maps (please compare them with Figures 4 -9).
➢ Moreover, the NE to E of the Northeastern end of the paleovalleys becomes more conductive.
➢ Red ellipse shows the resistive pocket in the SE corner that was also resistive in the previous EM maps (please compare them with Figures 4 -9).
➢ The region with black ellipses indicates a resistive zone where its resistivity decreases very quickly with depth.
➢ The region with red ellipse indicates a weaker resistive zone where its resistivity decreases slowly with depth.
➢ Blue ellipse shows similar region to black ellipse region.
➢ Dark red ellipses show similar regions to red ellipse region.
➢ Please see Figure 12 for more details about the sample subsurface models

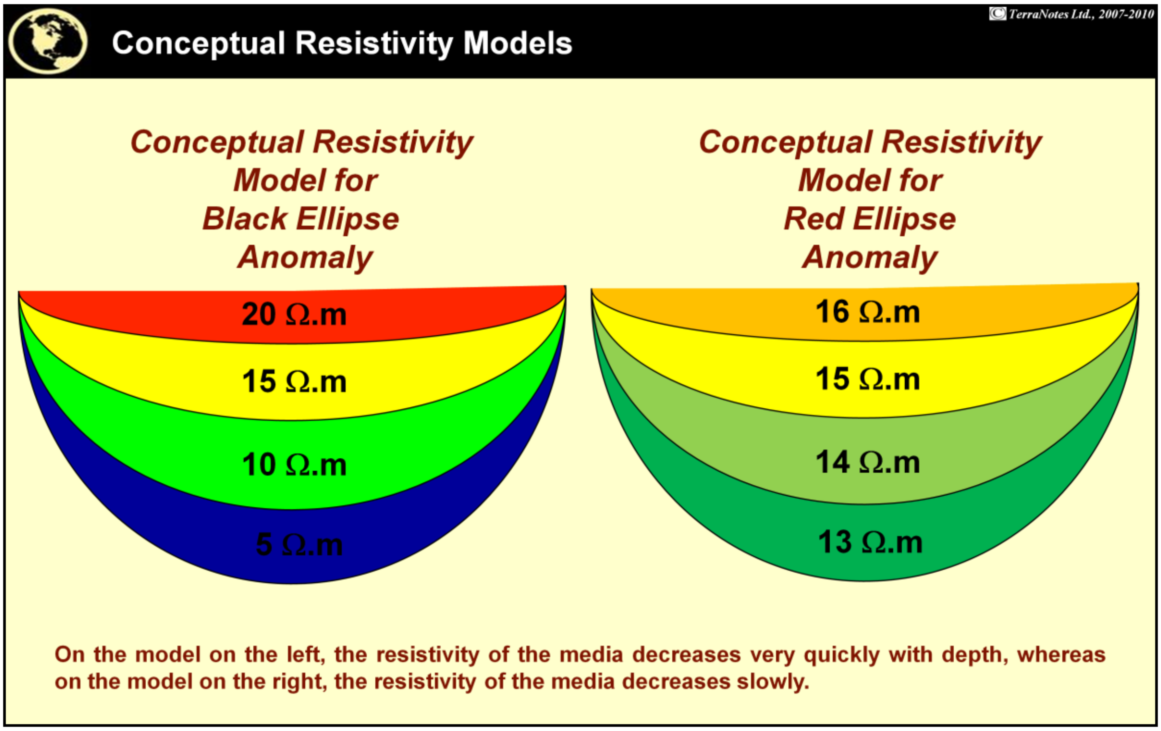

Figure 12. Left panel: Conceptual model of Black ellipse seen in Figures 10 and 11. Right panel: Conceptual model of Red ellipse seen in Figures 10 and 11. Units in this conceptual model is not same as the Figures 10 and 11.

➢ This page shows the constructed sample subsurface models of the anomalies indicated with black ellipse (blue anomaly) and red ellipse (green anomaly) in the previous page.

Main Findings from these maps

➢ Black ellipse area (Figure 10 and 11) shows a resistive anomaly where its resistivity decreases very quickly with depth.
➢ Red ellipse area (Figure 10 and 11) shows a weaker resistive anomaly where its resistivity decreases slowly with depth.
➢ The topographical features were the same in the anomalies on the previous page. There might not be any relationship between topography and the difference in those anomalies.

Geophysical Assumptions and Comments

➢ This model is solely based on resistivity variation and it does not include any topography effects. High and dry topographical region may also show such differences. This illustrates the importance of integrating topography in the interpretation.

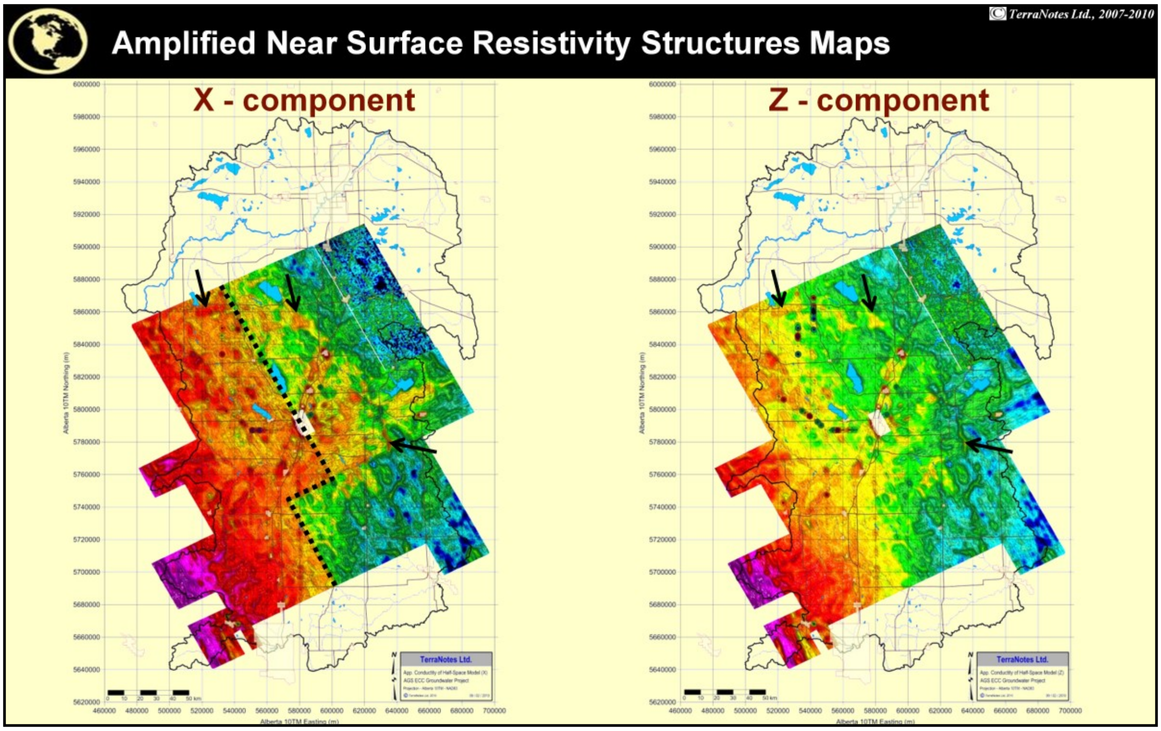

Figure 13. Apparent conductivity of a half-space model of X-component amplified EM data (Siemens/metre (S/m)). Red colours denote low conductance and blue colours denote high conductance.

Figure 14. Apparent conductance of a half-space model of Z-component amplified EM data (Siemens/metre (S/m)). Red colours denote low conductance and blue colours denote high conductance.

- A modelling study is applied to the amplified EM data calculations.
- In this page, a half-space model is fit to the X and Z component amplified field.
- This analysis is design to highlight the local resistivity zones. But it also shows the regional resistivity distribution.

<u>Main Findings from these maps</u>

- X- component data is useful to interpret high resolution details about the isolated resistivity anomalies.
- Black arrows show examples of isolated resistive features and trend that are more visible in the X-component.
- X-component is useful to locate local resistive structures but not for regional anomalies. Because there is a shift between different datasets in the X-component (e.g. Dashed black line) and the regional anomalies are not very visible.
- After requesting Fugro to provide re-levelled Z- component data, we obtained a higher resolution image of the paleovalleys and possible aquifers in a regional scale.
- This process also highlighted the cultural features.

<u>Geophysical Assumptions and Comments</u>

- This calculation assumes a half-space earth model, and reflects the near-surface resistivity variation.

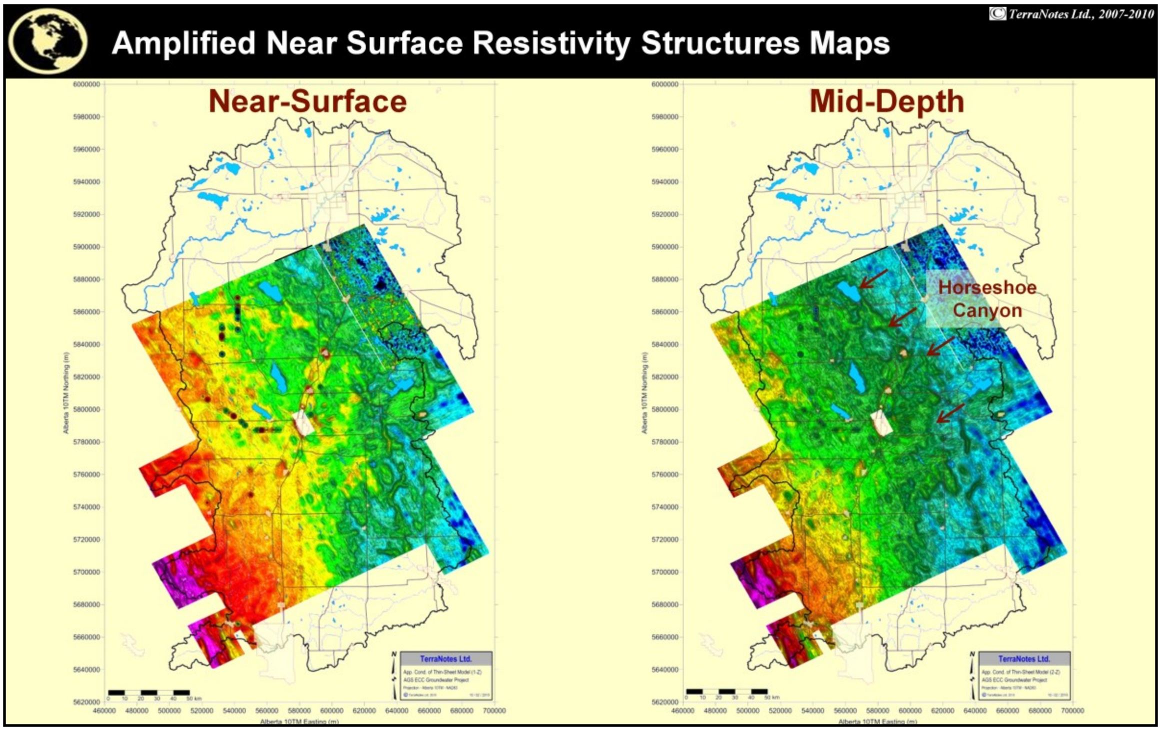

Figure 15. Apparent conductance of a thin-sheet model of 1st order Z-component amplified EM data (Siemens (S)). Red colours denote low conductance and blue colours denote high conductance.
Figure 16. Apparent conductance of a thin-sheet model of 2nd order Z-component amplified EM data (Siemens (S)). Red colours denote low conductance and blue colours denote high conductance.

➢In this page, a thin-sheet model is fit to the Z component amplified EM data and apparent conductance is calculated.
➢ The left panel represents the near surface and the right panel represents the mid-depth conductance structure.

Main Findings from these maps

➢ We can see that the conductive Horseshoe formation dips to the west as we go deeper.
➢ Red arrows shows the dipping direction of the Horseshoe formation, especially in the northern part.

Geophysical Assumptions and Comments

➢ This calculation assumes a thin-sheet earth model, and reflects the near-surface to mid-depth resistivity variations.

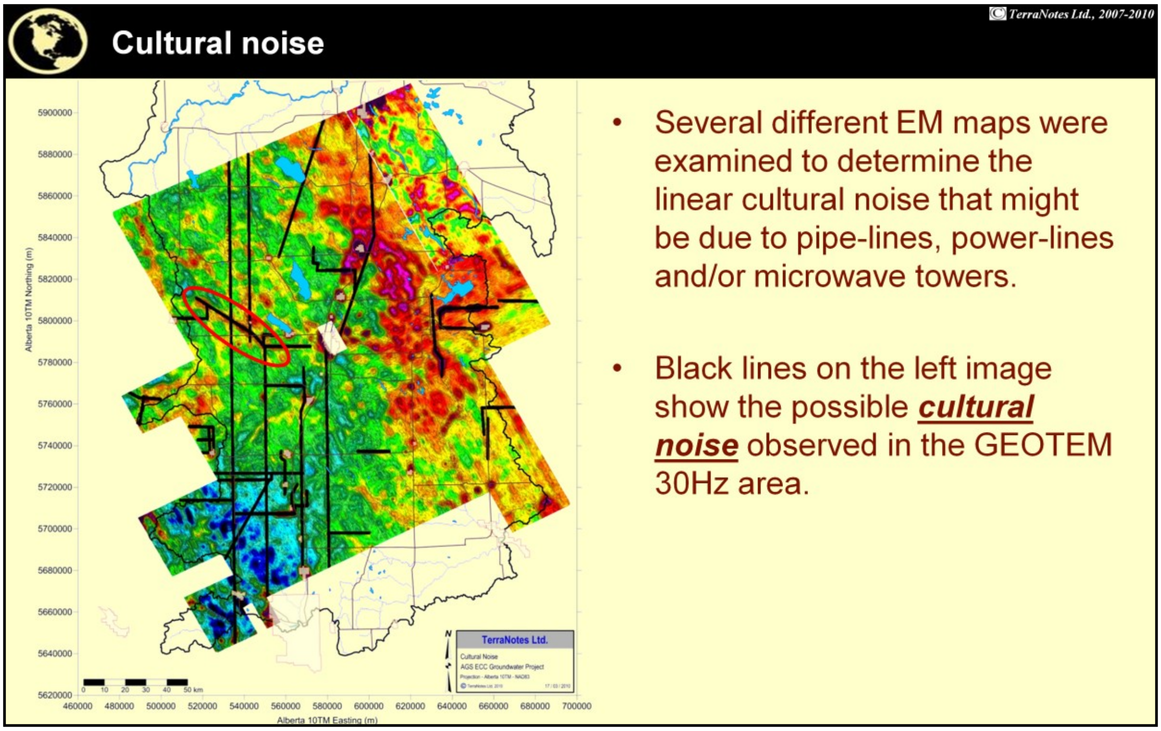

Figure 17. The amplification map (s) that is used in selecting the higher resistivity anomalies.

This amplification method uses the raw Electromagnetic data (usually off-time channels) and it is different from the one that was introduced in Figures 8 – 9. This method is used to highlight more local geophysical anomalies and it is a cross-validation method of the results from the other amplification methods. This method is also effective for deeper anomalies.

The amplification used in this figure also amplifies the cultural effects that are considered as Cultural Noise and it helps to delineate the locations of Cultural Noise.

Main Findings from these maps

➢ Local anomalies that may indicate cultural noise were visually located from this map and from several other similar maps.
➢ Black lines indicate the locations of these determined possible cultural noise.
➢ In some areas, there are wider linear resistive trends than those black lines, which may also indicate that the facility was constructed on a resistive lithology.
➢ Red ellipse shows such an area with wider linear resistive trends than the black line.

Geophysical Assumptions and Comments

➢ This method amplifies the local resistivity anomalies and it works better on resistive
➢ Cultural facilities (e.g. Towns, pipelines, microwave towers, ... etc) introduce a significant noise to the electromagnetic data. This is more visible in the later channels of raw data, where signal to noise ratio is much smaller than the earlier data. Eliminating these effect without noise source data would cause losing the AEM signals as well. Thus, we delineated these areas and did not include them in the interpretation. Please see pages below.

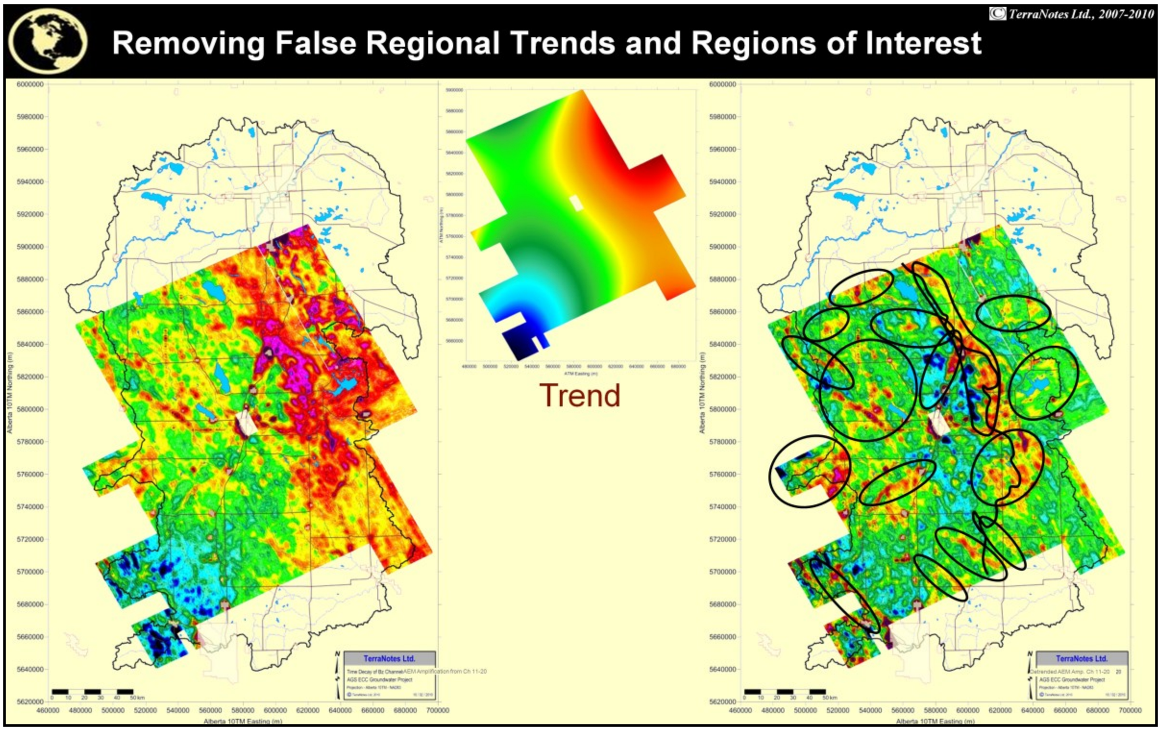

Figure 18. The results of a second phase AEM amplification method, expressed as unit of time (seconds (s)). This method was applied to highlight and select the local resistive anomalies. The red denote high resistivity units and blue denote low.
Figure 19. Regional trend (s) that was extracted from Figure 18.
Figure 20. Detrended amplification map (s) that was obtained by removing the trend illustrated in Figure 19 from the data illustrated in Figure18

Main Findings from these maps

- Figure 18 shows true local anomalies but false regional anomalies due to very conductive nature of the ECC.
- The false regional trend (Figure 19) was removed from Figure 18 to eliminate possible confusion.
- Resistive and conductive zones are more prominent in the detrended amplification map (Figure 20).
- We found 16 regions of interest on the detrended map (Figure 20) represented by the thick black ellipses.

Geophysical Assumptions and Comments

- Detrending is a technique whereby we can remove the artefact (previously defined in pages above) in the background by finding a polynomial trend and remove it from the data. The right panel shows the regional trend removed amplification map.
- The focus is on the local resistive and conductive zones and the background resistivity is assumed to be constant on the right panel.

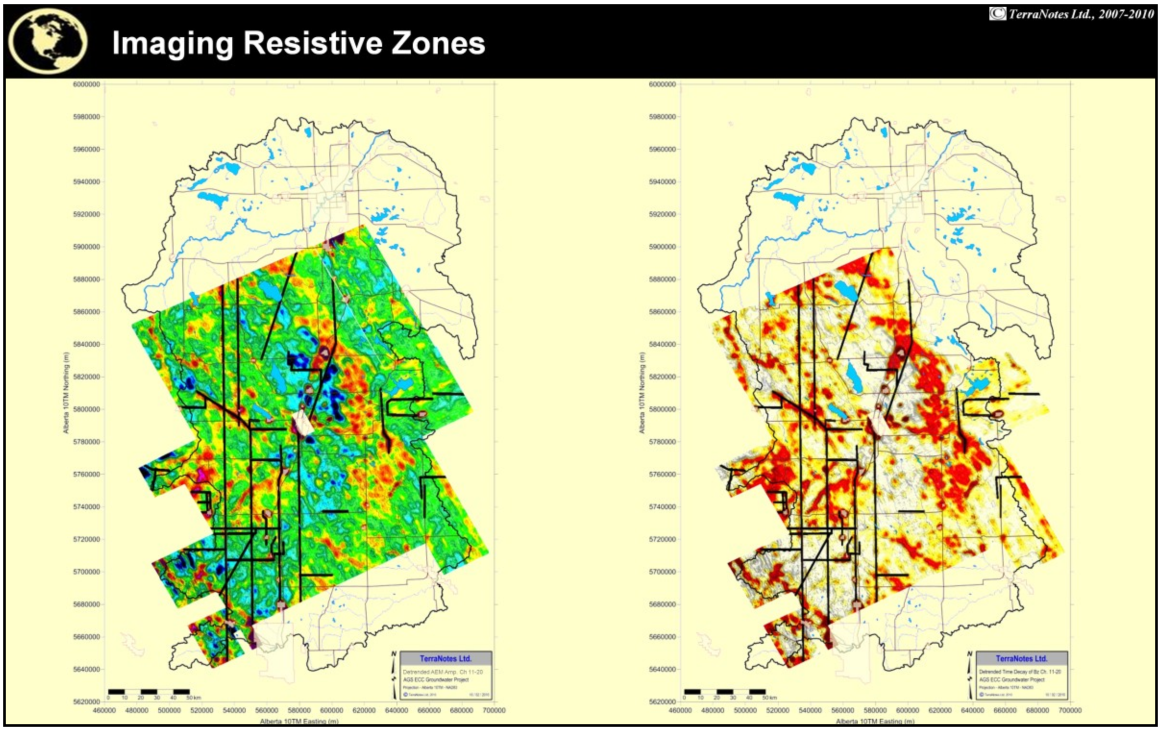

Figure 21. The detrended amplification map (s) with conductive and resistive anomalies. Cultural Noise defined in Figure 17 were overlaid on Figure 20 to get Figure 21.
Figure 22. The same map (s) with different colour scheme to emphasize the resistive anomalies only.

<u>Main Findings from these maps</u>

➢ Black lines on Figure 21 and Figure 22 indicate cultural noise and were not selected as Regions of Interest (ROI).
➢ Resistive and conductive zones are more prominent in the detrended amplification map (Figure 21).
➢ Conductive anomalies on Figure 21 may indicate clay and/or mud rich lithologies.
➢ Resistive anomalies (Figure 22) may indicate sand and gravel rich lithologies that may represent potential aquifers.
➢ Thus we focused only on the resistive zones (Figure 22).
➢ Red in Figure 22 shows high-resistivity anomalies, yellow denotes mid-resistivity.

<u>Geophysical Assumptions and Comments</u>

➢ Regional resistivity trend were removed from both map, and only local anomalies are shown.
➢ Only resistive anomalies are shown with colours in Figure 22.
➢ The differences between each zone could be due to differences in 1) geologic unit thickness 2) grain sizes, 3) porosity, 4) stratigraphy, 5) topography and/or 6) water geochemistry or other geological factors.

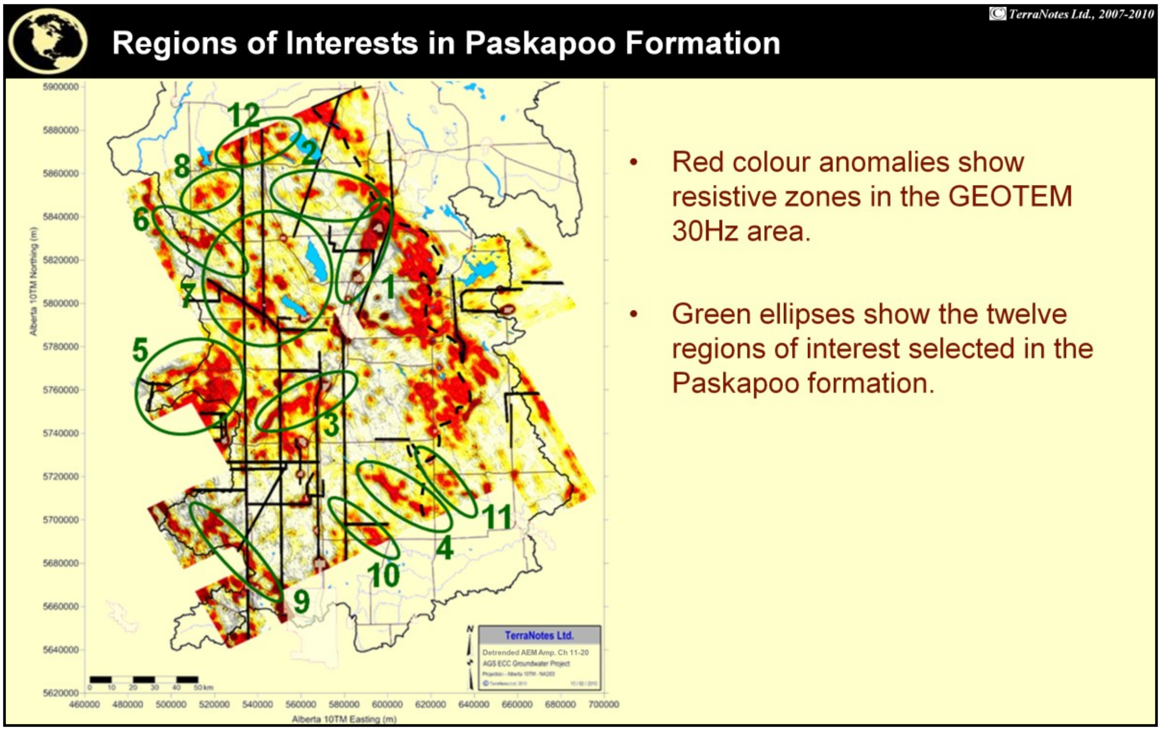

Figure 23. Regions of Interest at the ECC area (map unit is seconds).

➢ This page shows the detrended amplification map of the raw electromagnetic data with emphasized resistive anomalies.

<u>Main Findings from these maps</u>

➢ Red colour anomalies show the resistive zones of interest.
➢ Black lines indicate the locations of possible linear cultural noises such as pipelines, powerlines, microwave towers and ... etc.
➢ Green ellipses show the regions of interest that may represent potential aquifers.
➢ Black dashed line indicates the transition zone between Horseshoe Canyon and Paskapoo formations. The strong resistive anomaly at this location could also be due to the quick change of lithology and associated resistivity.

<u>Geophysical Assumptions and Comments</u>

➢ Regional resistivity trend were removed from the map above , and only local high resistivity anomalies are shown.
➢ The differences between each zone could be due to differences in 1) geologic unit thickness 2) grain sizes, 3) porosity, 4) stratigraphy, 5) topography and/or 6) water geochemistry or other geological factors.

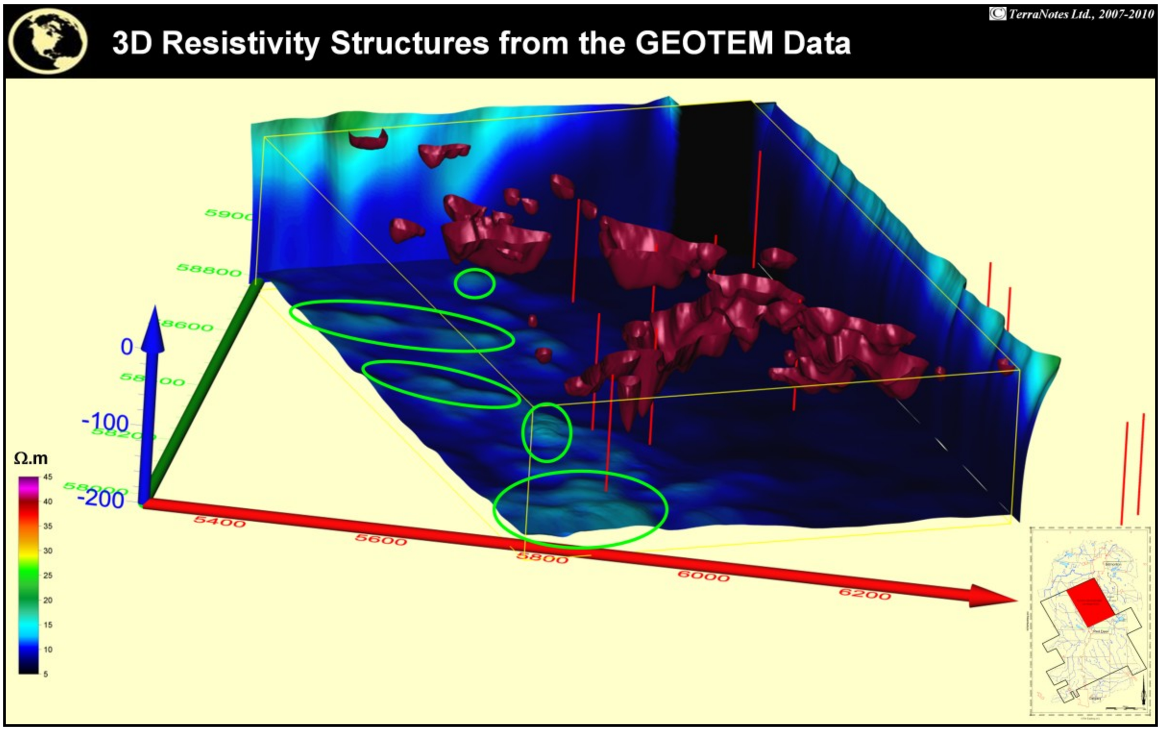

Figure 24. 3D Resistivity Structures from the GEOTEM RDI data.

➢ This image maps in 3D the first GEOTEM set of RDI data (Fugro 07427-30 Hz) collected in 2007 covering 8 of the 12 drill holes.
➢ This image shows the isosurface of the 20 Ω.m with the dark red volumes and color ranges on the scale varying from 5 to 45 Ω.m.
➢ The bottom of the image is one of 101 depth slices (every 2 m),
➢ The back wall of the image is one of the 480 NE-SW vertical slices (every 800 m)
➢ The right wall of the image is one of the 317 NW-SE vertical slices (every 800 m).
➢ Red lines show the locations of the 12 drill-holes (with 4 drill holes outside of the selected area for this image.)

Main Findings from these maps
➢ The dark red volumetric image delineates the NE-SW trending Red Deer Valley and the intersecting NW-SE trend indicating favourable resistivity zone for aquifers.
➢ The distance of the boreholes from the resistive volumes can be measured from these pictures as well.
➢ This imaging technique also allow us to change the resistivity limit of the isosurface to make the full interpretation.
➢ Green ellipses show the resistive zones and trends at the deepest interpretation level (~200 m), that may indicate sand lenses and deep channels.
➢ Note that real topography is not involved in these images.

Geophysical Assumptions and Comments
➢ The Fugro calculations of the Resistivity Depth Imaging (RDI) give smoothed resistivity variations.
➢ This image has been selected from a 3D rendering software that allows for the orientation in all directions and renders all depth and horizontal slices. Part of the deliverables for this project includes a viewer that will allow the reader to visualize the 3D imaging.
➢ Vertical Exaggeration is 100.

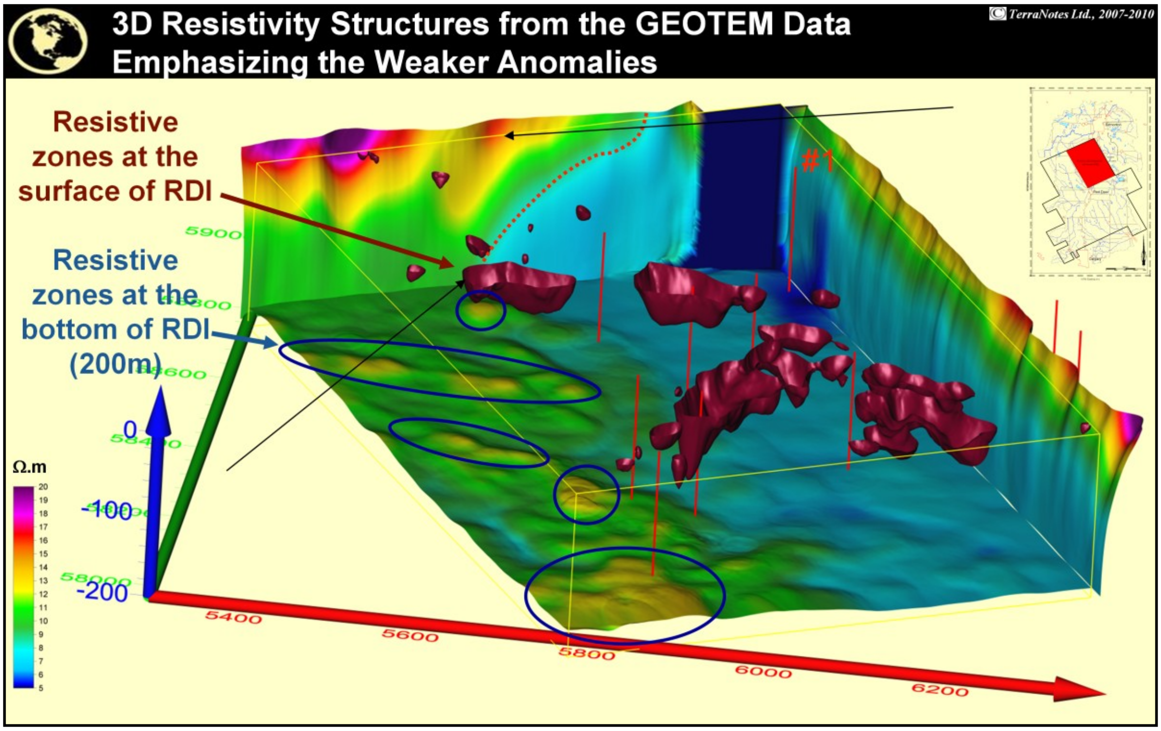

Figure 25. 3D Resistivity Structures from the GEOTEM RDI data.

- This map is the same as the previous map
- This image shows the isosurface of the 20 Ω.m with the dark red volumes and color ranges on the scale varying from 5 to 20 Ω.m.
- The bottom of the image is one of 101 depth slices (every 2 m),
- The back wall of the image is one of the 480 NE-SW vertical slices (every 200 m)
- The right wall of the image is one of the 317 NW-SE vertical slices (every 200 m).
- Red lines show the locations of the 12 drillholes (with 4 drill holes outside of the selected area for this image.)

Main Findings from these maps

- The dark red volumetric image delineates the NE-SW trending Red Deer Valley and the intersecting NW-SE trend indicating favourable resistivity zone for aquifers.
- Blue ellipses show the resistive zones and trends at the deepest interpretation level (~200 m), that may indicate sand lenses and deep channels.
- Red dotted line indicates the transition zone between the Horseshoe Canyon and Paskapoo formations that may include the Scollard and Battle formations.
- The dipping angle of the Horseshoe Canyon, Scollard and Battle formations can be evaluated from the NE-SW sections (red dotted line).
- Drill Hole number 1 (#1) is located in the most conductive zone, which did not show any aquifers.
- The geometry of the transition zone at depth can be also evaluated from the depth slices.
- NW-SE slices (parallel to the flight line) are good indicators of how the resistivity changes with depth.

Geophysical Assumptions and Comments

- The Fugro calculations of the Resistivity Depth Imaging (RDI) give smoothed resistivity variations.
- Note that real topography is not involved in these images.
- This image has been selected from a 3D rendering software that allows for the orientation in all directions and renders all depth and horizontal slices. Part of the deliverables for this project includes a viewer that will allow the reader to visualize the 3D imaging.
- Vertical Exaggeration is 100.

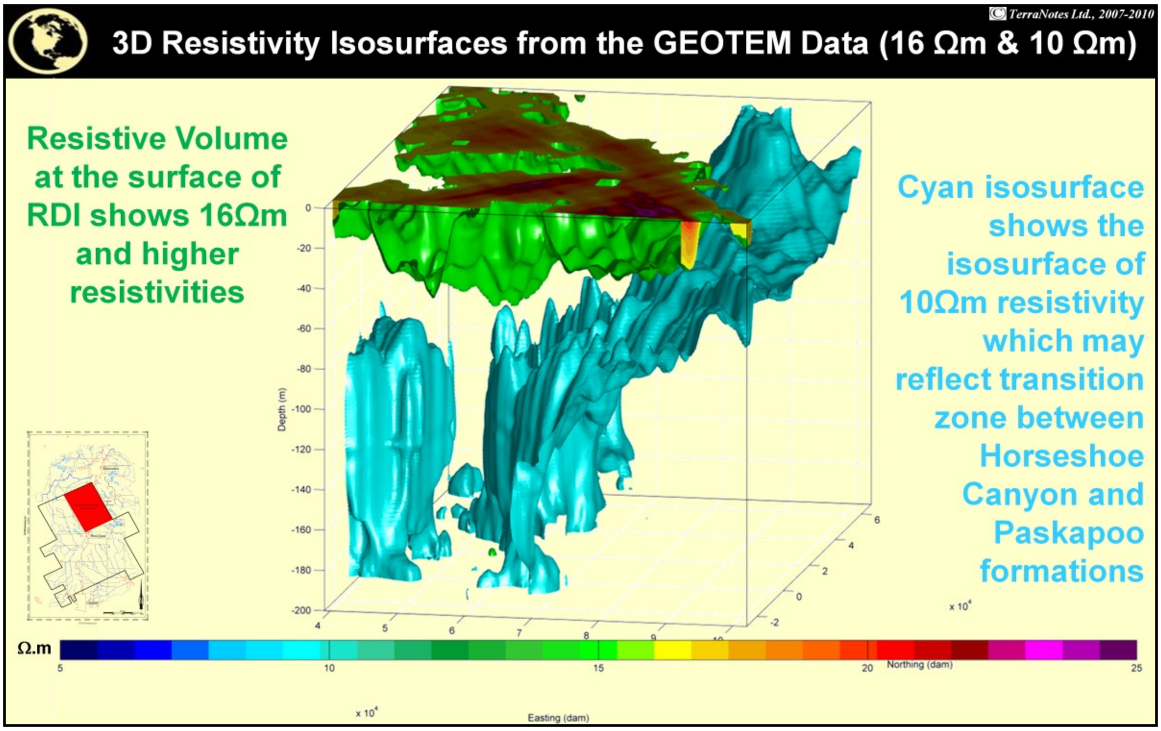

Figure 26. 3D resistivity isosurfaces (16 Ωm [green] and 10 Ωm [cyan]) from the GEOTEM RDI dataset.

➢ This map shows the high resolution variation of the high resistivity volume with depth.

Main Findings from these maps

➢ The Green structure on this map shows the volume of the resistive zones of 16 Ω.m and higher. Yellow, red, pink contours complete the 16 Ω.m isosurface as a volume of higher resistivity zone.
➢The Cyan structure is an isosurface of the 10 Ω.m resistivity in the east that could be a representative of a transition zone between Horseshoe Canyon and Paskapoo formations including Scollard and Battle formations.
➢ Cyan isosurface (10 Ω.m) in the west could be clayey and shaly part of Paskapoo formation.

Geophysical Assumptions and Comments

➢ The Fugro calculations of the Resistivity Depth Imaging (RDI) give smoothed resistivity variations.
➢ This image has been selected from a 3D rendering software that allows for the orientation in all directions and renders all depth and horizontal slices. Part of the deliverables for this project includes a viewer that will allow the reader to visualize the 3D imaging.
➢ Matlab is used for the computations and the imaging.
➢ Vertical Exaggeration is 100.

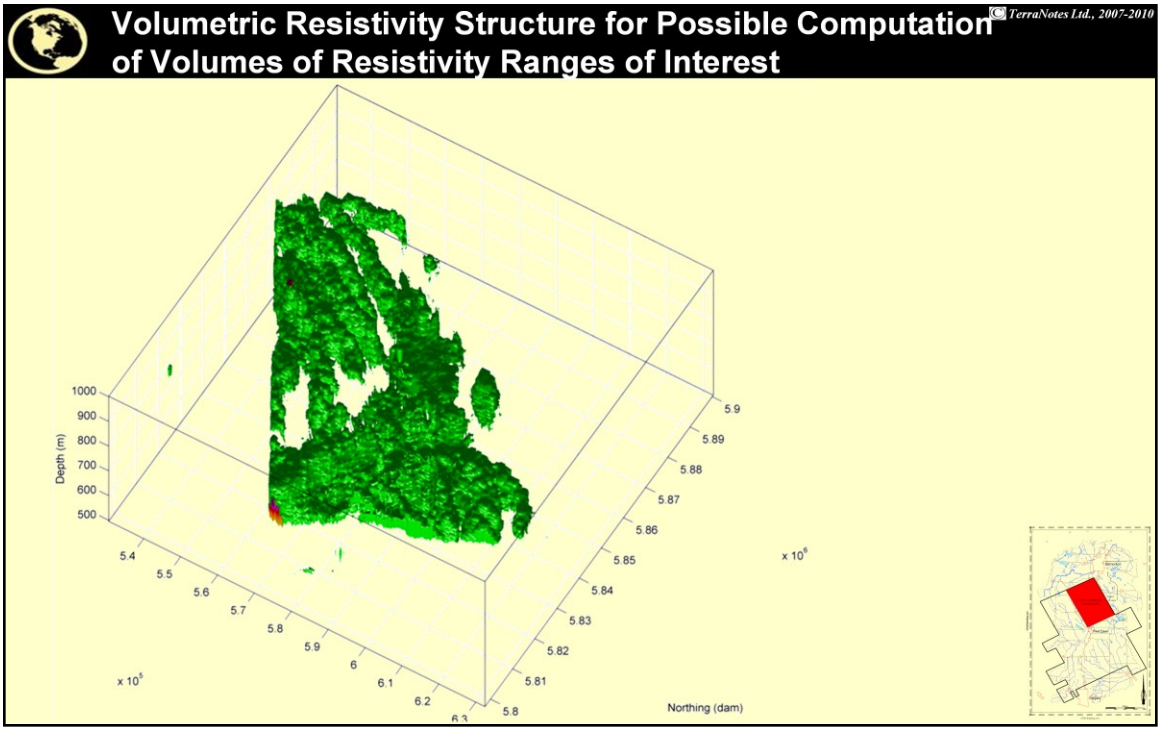

Figure 27. 3D volumetric resistivity structure (> 14 Ω.m) from the GEOTEM RDI dataset.

➢ The 3D rendering (of which this map is an excerpt) shows the volume of the resistive zones of a 14 Ω.m and higher, including the topography.

Main Findings from these maps

➢ This map shows the relatively high resistive zones (> 14 Ω.m) as a voxel image with topography.
➢ It is possible to relate the topography with the resistive zones using this technique.
➢ It is also possible to change the limit of the resistivity for volumes as required.
➢ With this technique we can calculate the volume of the selected resistivity range (e.g. > 14 Ω.m or 14 Ω.m - 24 Ω.m.)

Geophysical Assumptions and Comments

➢ We assume the resistivity of the air as 0 Ω.m to complete the volumes parallel to the real surface topography.
➢ Matlab is used for the computations and the imaging.
➢ Vertical Exaggeration is 100.

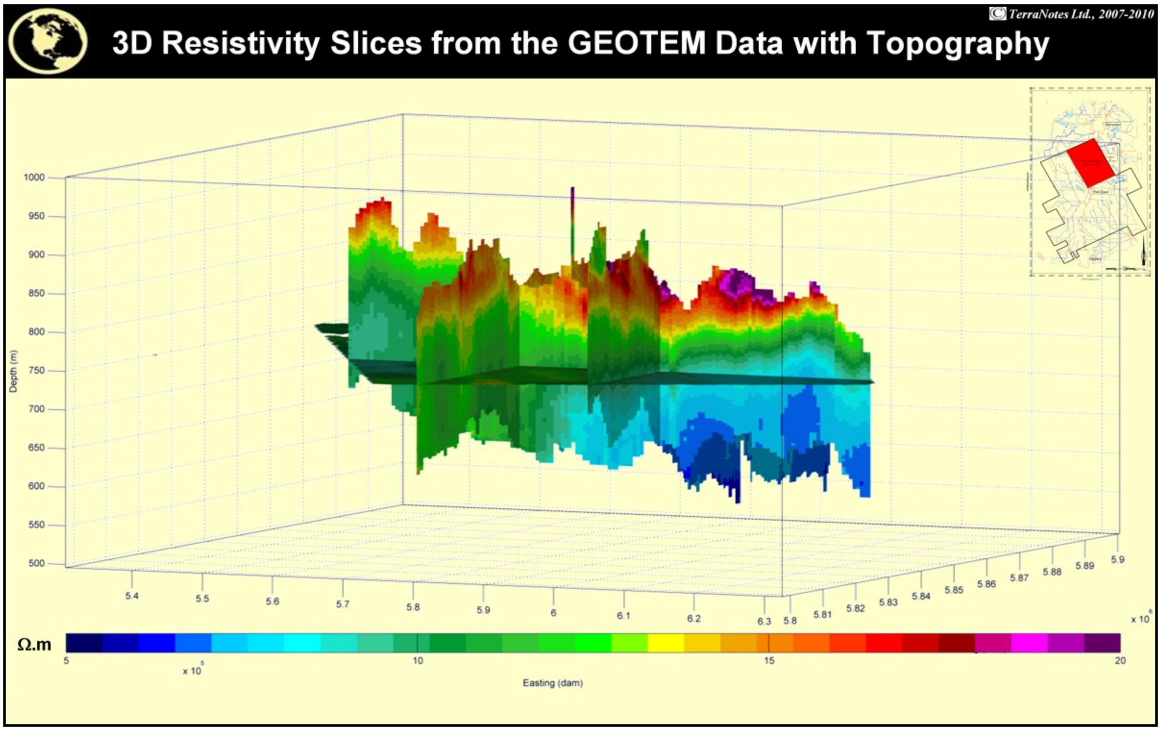

Figure 28. 3D resistivity slices from the GEOTEM RDI dataset including the real surface topography.

➢ This map shows the depth slices combined with the N-S, E-W slices for the first 200 metres of the subsurface. Resistivity values are represented with the colors for the first 2007 GEOTEM survey. The 3D rendering includes the real topography.

<u>Main Findings from these maps</u>

➢ With this technique it is possible to relate topography highs and lows with the resistive and conductive units at the desired location.
➢ Coincident resistivity highs and topography highs may be eliminated as they may not be related to an aquifer.
➢ Coincident resistivity highs and topography lows may be selected as they are thought to reflect the potential aquifers.
➢ Matlab is used for the computations and the imaging.
➢ Vertical Exaggeration is 100.

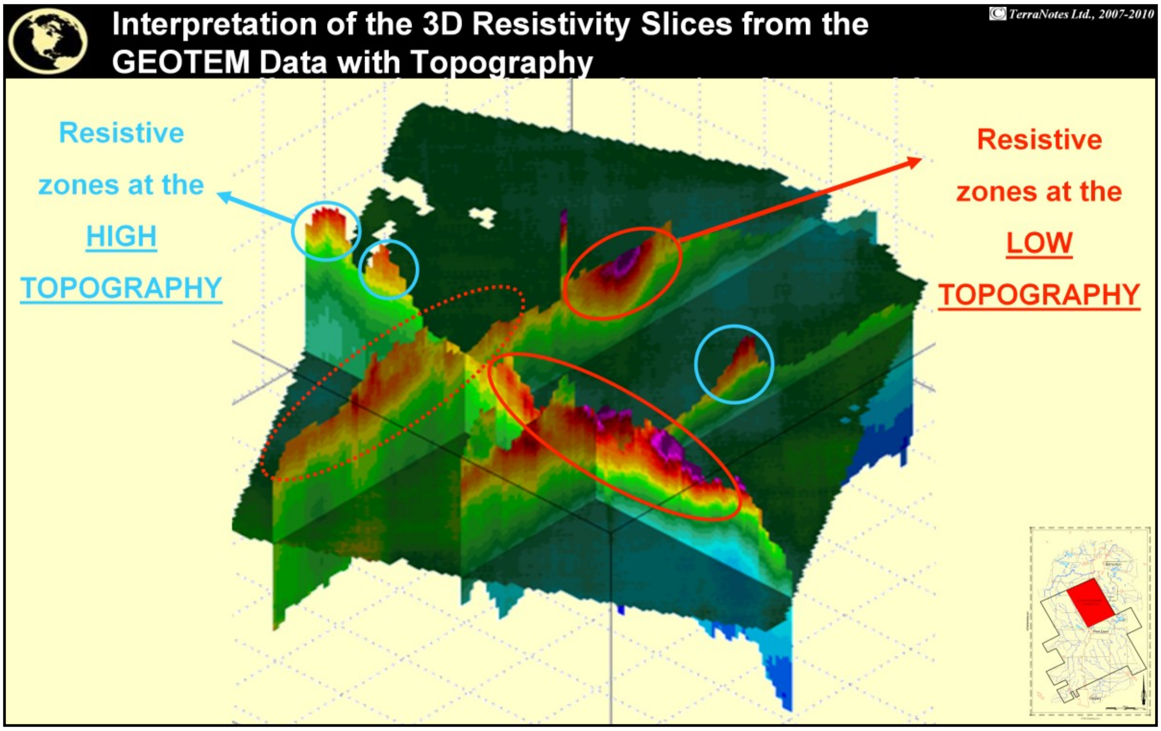

Figure 29. Relationship between the high resistivity units and surface topograpy.

- This map shows a different angle view version of the previous map.
- This map shows the depth slices combined with the N-S, E-W slices for the first 200 metres of the subsurface. Resistivity values are represented with the colors for the first 2007 GEOTEM survey. The 3D rendering includes the real topography.

Main Findings from these maps

- With this technique it is possible to relate topography highs and lows with the resistive and conductive units at the desired location.
- Coincident resistivity highs and topography highs may be eliminated as they may not be related to an aquifer.
- Cyan ellipses show areas with high resistivity and high topography.
- Coincident resistivity highs and topography lows may be selected as they are thought to reflect the potential aquifers.
- Red ellipses show areas with high resistivity and low topography.
- Matlab is used for the computations and the imaging.
- Vertical Exaggeration is 100.

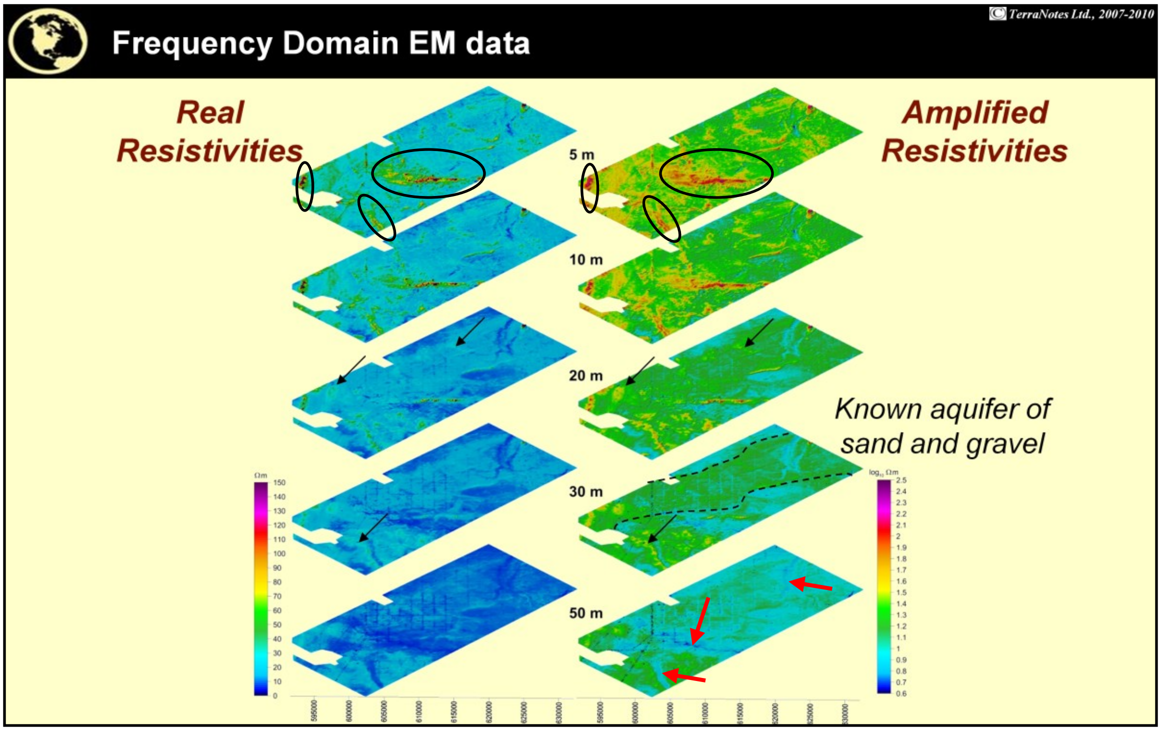

Figure 30. Depth slices from the Fugro's inversion results of the RESOLVE data set.

- This page shows the Fugro's inversion results of the RESOLVE data set (Fugro 07716 Frequency Domain Electromagnetic (FDEM) data).
- The left panel shows the resistivities of the inversion results.
- The right panel shows the amplified values of the same resistivity results.

Main Findings from these maps

- Resistivity of the medium decreases with depth in both panels.
- Black ellipses show high resistivity channels at near surface in the NW-SE direction.
- Continuation of these high resistivity channels (black ellipses) with depth is more visible with the amplification techniques (right panel.)
- Black arrows show the weak local resistivity highs at depth and how they are amplified in the right panel.
- Dashed lines at 30 m depth delineates the NE-SW trending channel which is also more visible in the right panel.
- Red arrows indicate the conductive channels at depth.

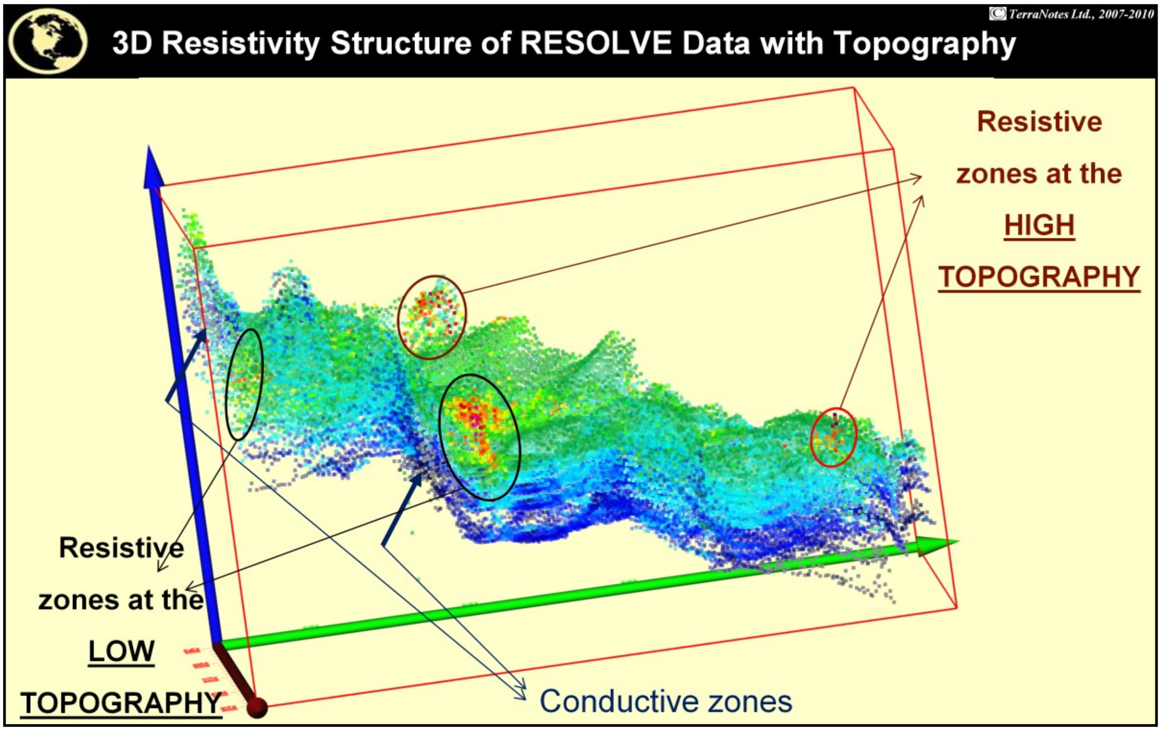

Figure 31. Scatter plot of the 3D resistivity structure of RESOLVE data including surface topography extracted from the airborne survey (Ω.m).

- This page shows the subsurface resistivity structure of the first 50 metres including the surface topography.
- This map shows the 3D view of the amplified RESOLVE data that is shown in the right panel on the previous page. Red colour shows the resistive zones and blue colour shows conductive zones.

Main Findings from these maps

- The resistivity of the medium decreases with depth.
- Black ellipses show the most resistive anomalies located at the valleys that could be related to aquifer channels.
- Red ellipses show the resistive anomalies related the high topography zones.
- Blue arrows show the conductive hills around two resistive valleys (black ellipses).
- Vertical Exaggeration is 100.

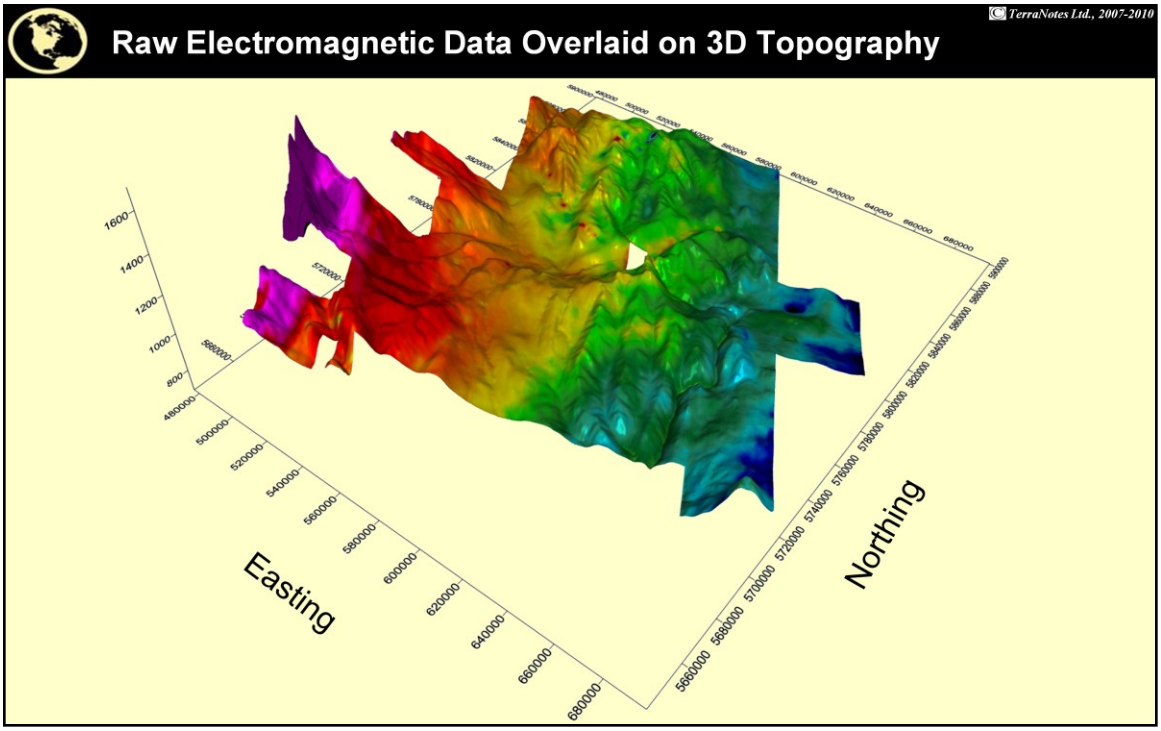

Figure 32. Raw electromagnetic data (fT) overlaid on 3D surface topography extracted from the GEOTEM survey.

➢ This page shows the raw electromagnetic data (Bz channel 16) overlaid on top of the surface topography.

Main Findings from these maps

➢ This map illustrates the variation of resistivity with the topography.

Geophysical Assumptions and Comments

➢ This raw data map illustrates how important it is to use a number of geophysical processing and amplification techniques to extract the details necessary for higher order interpretation.

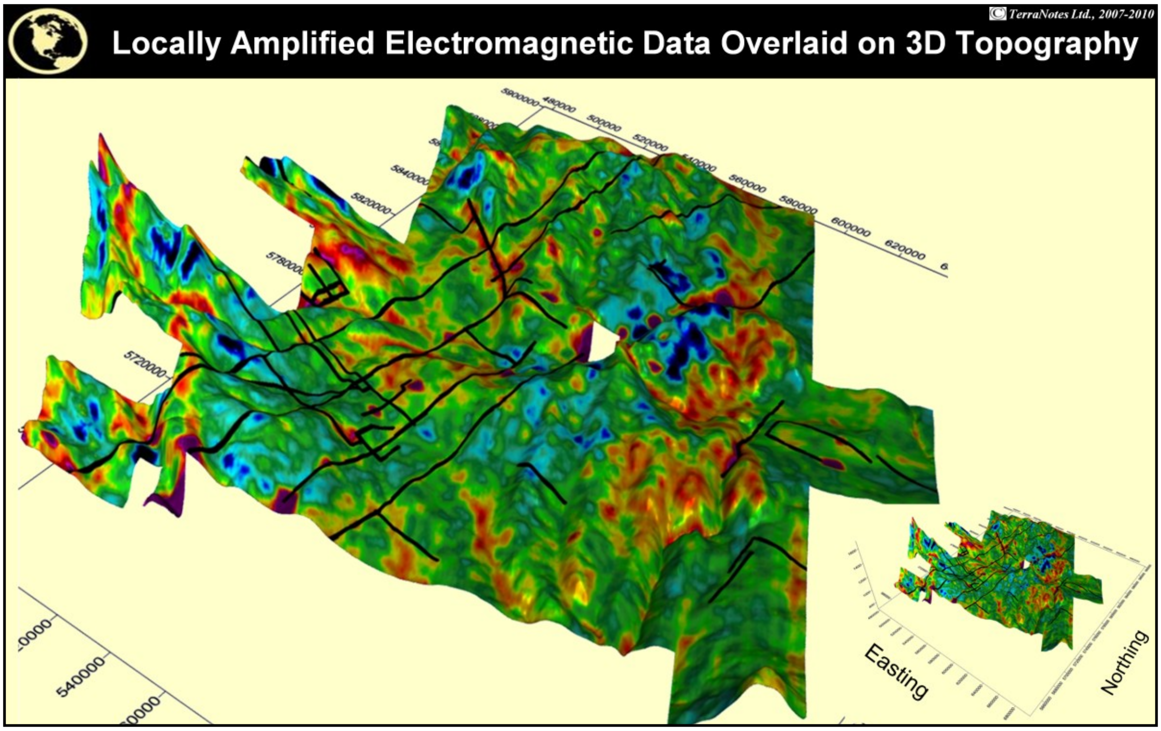

Figure 33. Locally amplified electromagnetic data (s) and linear cultural noise overlaid on 3D surface topography extracted from the GEOTEM survey.

➢ This page shows the detrended amplified electromagnetic data to delineate the local anomalies overlaid on top of the surface topography.

Main Findings from these maps

➢ This map provides only the local variations in resistivity overlaid on top of the surface topography.
➢ Red anomalies represent the high resistivity zones.
➢ Blue anomalies represent the low resistivity zones.
➢ Black lines show possible linear cultural noise.

Geophysical Assumptions and Comments

➢ Regional resistivity trend were removed from the map, and only local anomalies are shown.
➢ The differences between each zone could be due to differences in 1) geologic unit thickness 2) grain sizes, 3) porosity, 4) stratigraphy, 5) topography and/or 6) water geochemistry, and possibly other geological reasons.

Delineating zones of interest for aquifers using boreholes–calibrated GEOTEM

Delineating Zones of Interest for Aquifers Using Borehole–Calibrated GEOTEM Data

Objectives

The main objective was to calibrate GEOTEM using drill holes loggings. The following task groups were undertaken to:

1. review and statistically analyze the 12 down-hole logging data
2. apply the Composite Resistivity Index to calibrate GEOTEM using down-hole loggings
3. map the calibrated GEOTEM response
4. delineate and characterize zones of highest interest for aquifers
5. assess results

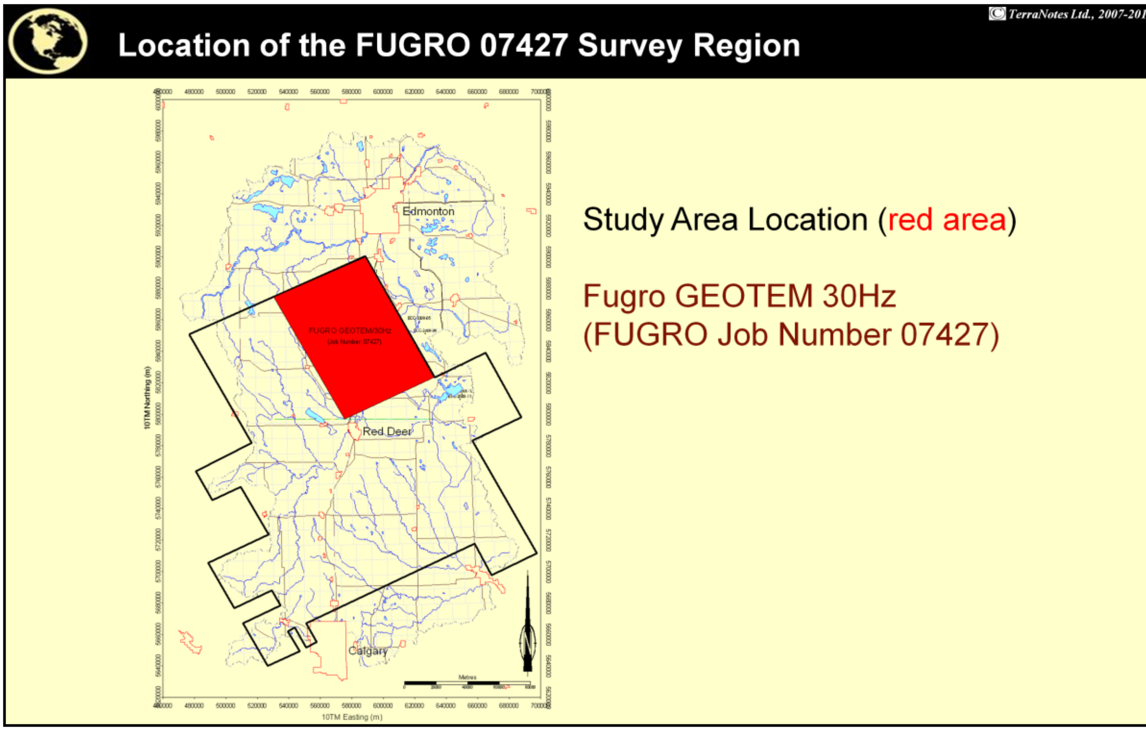

Figure 34. Location of the FUGRO 07427 survey region.

➢ The coverage area for the calibration corresponds to the area where 8 of the bore holes are located.

Summary of Statistics of 12 Borehole Gamma Loggings

GR in API

Borehole ID	Paskapoo				Scollard (+Ardley)				Battle				Horseshoe Canyon			
	Minimum	Maximum	Median	Std. Dev.	Minimum	Maximum	Median	Std.Dev.	Minimum	Maximum	Median	Std.Dev	Minimum	Maximum	Median	Std.Dev.
ECC2008-001													23.9	183.8	**101.4**	22.858
ECC2008-002					1.3	205.9	106.7	32.815	90.3	266.2	134.2	32.268	36.8	172.3	**111.6**	28.475
ECC2008-003	33.2	191.8	76.6	28.43	14.6	203.7	124	25.389								
ECC2008-004	37.6	157.7	76.2	13.501	14.6	221.4	116	29.796								
ECC2008-005													20.2	178	**104.7**	19.684
ECC2008-006													43.6	212.1	**86.9**	17.337
ECC2008-007	41	107.6	57.8	10.806	44.9	142.8	89.7	18.629	76.8	199.2	114.55	29	-6.4	142.8	**93**	15.859
ECC2008-008	31	269.7	73.5	31.878	53.3	131.6	84.6	16.798								
ECC2008-009	34.9	113.2	61.7	13.325	46.6	194.2	101.4	20.159								
ECC2008-010	40.6	236.8	89	27.926	72.9	182.6	131.6	23.9								
ECC2008-011													65.8	181.3	**120**	15.618
ECC2008-012													52.2	169.7	**114.2**	17.687

Note:
GR - Gamma logging

Table 1. Summary of statistics of 12 borehole gamma loggings

The table summarizes the most relevant statistical results of 12 boreholes Gamma Loggings (GR) for the stratigraphic formations, namely: Paskapoo, Scollard (including Ardley and Battle) and Horseshoe Canyon. The stratigraphic formations were identified and classified by AGS.

Main points derived from the table:

- Paskapoo formation has the lowest level of GR response.
- Battle formation features the highest level of GR response.
- The standard deviations of Battle are also higher than other formations, which suggests that the distributions of clay/shale/mud in Battle formation are strongly heterogeneous in depths OR that clay-contents in the formation behave differently in gamma radioactivity.
- The GR standard deviations of Horseshoe Canyon formation in both BH#011 and BH#012 are smaller than those in other 8 boreholes. This may reflect that the clay/shale/mud in the southern region is more homogeneous than that in the northern region.
- For the detailed statistical results of logging data corresponding to each stratigraphic formations, please see appendix A-1.

Summary of Statistics of 12 Borehole DG Resistivity Loggings

DG Resistivity in Ohm*m

Borehole ID	Paskapoo				Scollard (+Ardley)				Battle				Horseshoe Canyon			
	Minimum	Maximum	Median	Std. Dev.	Minimum	Maximum	Median	Std.Dev.	Minimum	Maximum	Median	Std.Dev	Minimum	Maximum	Median	Std.Dev.
ECC2008-001													1	338.7	**13.7**	19.14
ECC2008-002					9.9	297	**18**	42.755	11.2	17.5	**12.8**	1.376	9.5	233.3	**18.9**	18.681
ECC2008-003	8.4	220.7	**28.6**	15.375	6.6	357.7	**16.2**	42.662								
ECC2008-004	9.9	342.1	**41.2**	19.114	5.8	389	**15.1**	49.69								
ECC2008-005													6.8	177.8	**10.9**	11.547
ECC2008-006													5.2	52.1	**13.9**	6.246
ECC2008-007	2.5	51.3	**28.9**	7.82	6.9	24.5	**12.8**	3.793	5.4	11.6	**7.2**	0.728	4.9	97.8	**10.7**	5.302
ECC2008-008	6.1	171.9	**23.2**	15.983	11.5	46.8	**14.2**	3.515								
ECC2008-009	2.3	200.1	**26.8**	18.763	7.5	92.5	**13.1**	8.5								
ECC2008-010	6.1	383.5	**26.5**	24.363	8.8	152.4	**16.1**	11.91								
ECC2008-011													5.6	69.2	**12.7**	5.597
ECC2008-012													3.5	153.4	**12.4**	8.601

Note:
DG – Deep Guard resistivity logging

Table 2. Summary of statistics of 12 borehole Deep Guard (DG) resistivity loggings

The table summarizes the most relevant statistical results of 12 boreholes Deep Guard (DG) resistivity loggings for stratigraphic formations, namely: Paskapoo, Scollard including Ardley, Battle and Horseshoe Canyon.

Main points derived from the table:

- Paskapoo formation has the highest level of DG resistivity.
- Battle formation features the lowest level of DG resistivity.
- Regionally, the DG resistivity of Horseshoe Canyon is lower than that of Scollard including Ardley.
- The standard deviations of Scollard in ECC2008-02, ECC2008-03 and ECC2008-04 are highest in comparison to others. It suggests that geoelectrical properties of Scollard are severely heterogeneous in the region of these boreholes.

For the detailed statistical results of logging data for each stratigraphic formations, please see appendix A-1.

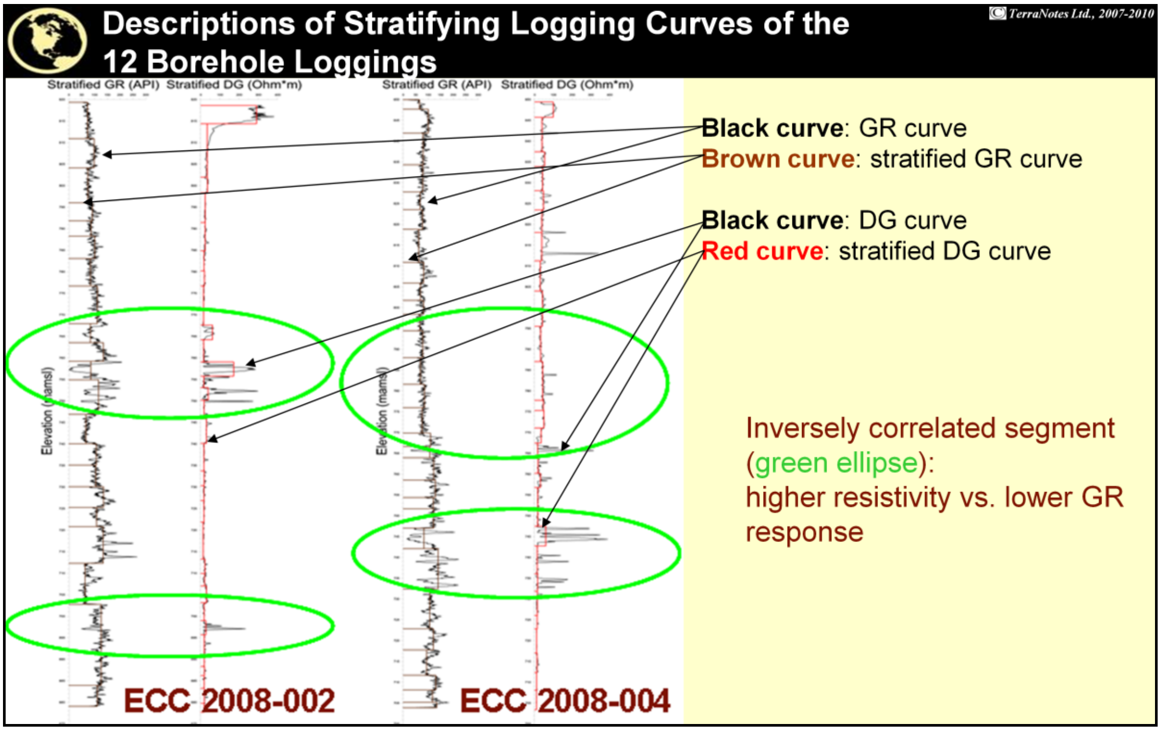

Figure 35. Gamma-ray and resistivity logs of the boreholes ECC2008-02 and ECC2008-04.

Specifications for stratifying the logging curves

- The minimum thickness of layer was specified as 2m. This thickness was set up after a series of experimentations using 0.2m, 0.5m, 1.0m and 2.0m.
- This minimal thickness is a compromise taking into account both vertical resolutions of down-hole loggings (high) and GEOTEM (low) for the purpose of calibration.
- Inflection points on smoothed DG curves, as picks of layers, were identified and recorded with respect to elevations.

Note: For ECC 2008-02 and ECC 2008-04, the curves of Sonic (DeltaT), Density Porosity (PORden) and Short Guard resistivity (SG) have also been stratified to assure that the minimal thickness is also applicable to other types of down-hole loggings and it can be used in further work in the future.

Main points derived from the logging curves:

The analysis of GR and DG logging data in both ECC2008-02 and ECC2008-04 demonstrates that:

- There is a clearly inverse correlation between GR response and DG resistivity, especially on high resistivity layers. This correlation could provide more information, even some quantitative relationships between DG resistivity and GR responses and classification in term of lithologies. Thus, this can be done as a further work in the future.
- It is noted that the GR response contrasts (a) between mudstone and adjacent layers (b) between coal and adjacent layers are significant, while the GR contrasts between other layers are not clear, i.e. siltstone, fine sandstone and medium sandstone.
- This observation about GR contrasts would suggest that (1) the formations intersected by the boreholes consist mostly of thin layers (<2m) of clay/shale/mud content, and (2) Using GR to identify and classify the lithologies should be incorporated with other down-hole loggings.

Application of the Composite Resistivity Index (CRI)

Objective: To calibrate AEM using drill holes loggings.

Solution: We apply a technique that we called **Composite Resistivity Index** (**CRI**) for Drill Holes and GEOTEM

Definitions:

Calibration: To assess/adjust the GEOTEM response against the **true values** calculated from drill holes loggings

CRI: CRI is a composite measure of the geological formations' ability to resist electrical current. This measure allows for the calibration between GEOTEM decay response and the known lithologic-resistivity data in borehole.

Process:

Calculate both CRI: We calculated both **Drill Holes CRI** and **GEOTEM CRI**

Calibrate GEOTEM: We used Drill Holes CRI to calibrate GEOTEM CRI for each flight line crossing the corresponding drill holes.

Assess Quality of Calibration: We then assessed the consistency between Drill Holes Results and GEOTEM CRI for each flight line around 8 drill holes.

Geophysical Assumptions and comments

- **The model of resistivity layer-cake**: an idealized model of superimposed horizontal homogeneous layers having constant resistivities in each layer below the half-space.
- The Borehole CRI was calculated based on the model of resistivity layer-cake. In the calculation of Borehole CRI the geometric factors are assumed to be 2.0 for each layers. The Borehole CRI numbers, shown in Figures 36 and 38 are the products of actual CRI values and assumed geometric factor (please refer to Figures 36 – 38 – 40 and their notes for further information).
- The GEOTEM CRI was calculated using GEOTEM decays. It is also based on the model of resistivity layer-cake;
- The resistivity logging data may be incomplete due to failing to collect data in superficial layers.
- Both logging data and GEOTEM data do not allow us to establish an mathematic function for exact calibration. However, a statistical relation can be built.
- Based on these assumptions, the results are not exact, however in practicality they are sufficient to calibrate the GEOTEM.

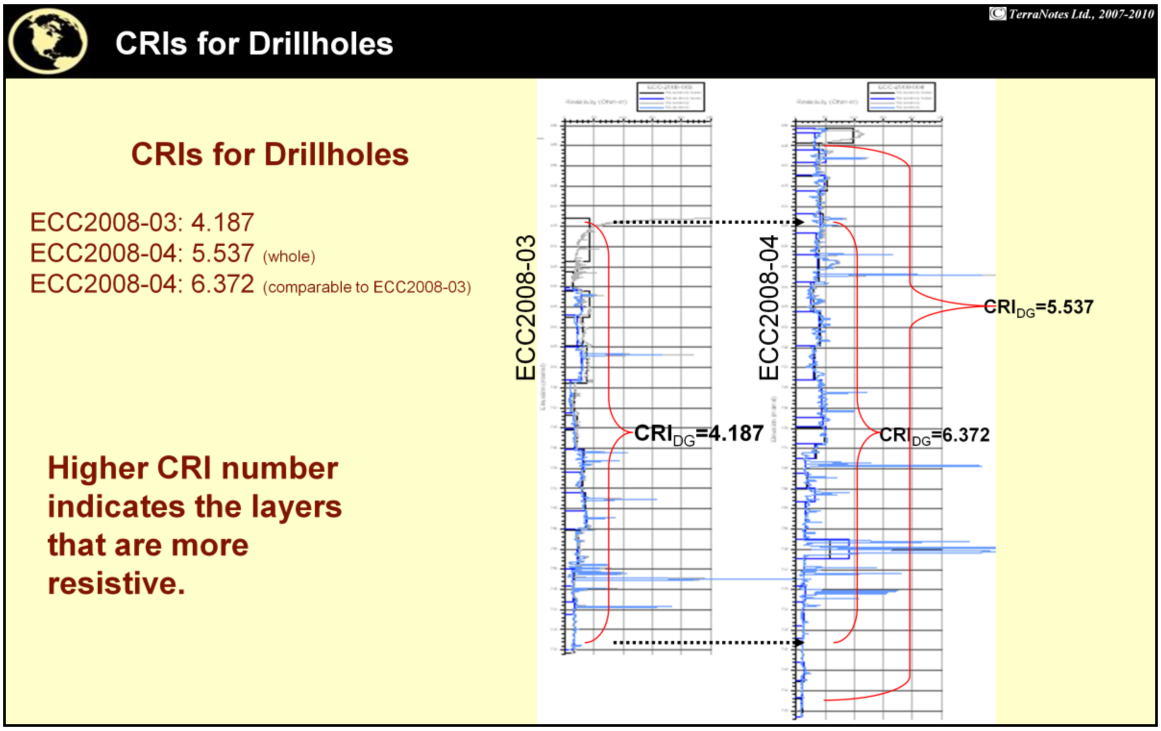

Figure 36. Composite Resistivity Indices calculated using DG resistivity of the boreholes ECC2008-003 and ECC2008-004.

CRI is a weighted average index which includes variables such as layers' resistivities & thicknesses and EM Amplitudes from GEOTEM 30 Hz data. EM Amplitudes are assumed to be inversely proportional to the square distance to the layers.

Calculation of CRI for 8 boreholes has been done using each stratified DG resistivity data. For sake of the report's space, we present the two boreholes' CRI in this section. All other borehole plots and tables including the calculated CRIs are in Appendix A-1.

Main Findings from the image:

- DG/SG resistivity measurements show that formations at ECC2008-04 are more resistive than those at ECC2008-03. Higher CRI number indicates more resistive layers/formations.
- CRI at ECC2008-04 = 5.537 for the segment from 845.72m to 708.08m of elevation.

  CRI at ECC2008-04 = 6.372 for the segment from 837.45m to 736.03m of elevation (this segment is comparable to that of ECC2008-03).
- CRI at ECC2008-03 = 4.187 for the segment from 836.93m to 738.81m of elevation.
- CRI at ECC2008-04 > CRI at ECC2008-03.
- CRI calculations show the layers at ECC2008-04 are more resistive than those at ECC2008-03.
- The results from CRI calculations are consistent with down-hole loggings.
- CRI is a practical tool that can be used for evaluating the integrated resistivities of layers
- Similar consistency of results has been determined for the other bore holes that are not presented in this section.

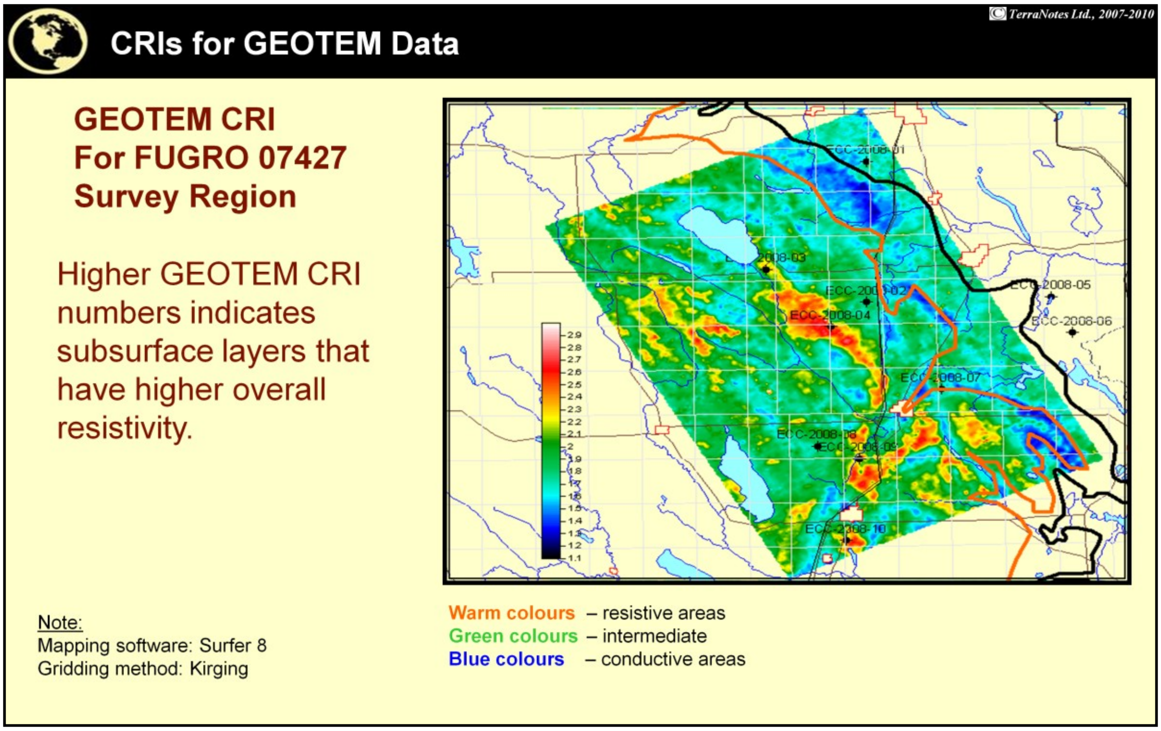

Figure 37. Composite Resistivity Indices of the GEOTEM data (no units for CRI).

In the GEOTEM CRI map above, the resistivity features are regionally consistent with existing boundaries of Paskapoo, Scollard and Horseshoe Canyon based on regional geology.

GEOTEM CRI is derived from the GEOTEM responses at each measurement point taking into account of the decay of the signal. There are 6356 of 570122 points failing to calculate CRI due to unqualified decay data.

Main Findings from the map:

It is noted that (1) the orange curve represents the surficial boundary between Paskapoo and Scollard formations while the dark curve represents the surficial boundary between Scollard and Horseshoe Canyon formations; (2) logging statistics show that Paskapoo is the most resistive formation.

➢ The GEOTEM CRI map displays the same results as mentioned above. As well, those results are consistent with regional lithology/geology.

➢ Although there are local differences, we believe that

- ➢ The GEOTEM CRI map provides well defined edges of resistivity anomalies
- ➢ The GEOTEM CRI map provides resistivity variations of local details within the anomalies
- ➢ Such variations of local details could be correlated with local lithology and/or geology

➢ On the GEOTEM CRI map, all the layers/formations are featured as inhomogeneous in terms of resistivity. The presence of such inhomogeneity would suggest that the bedrock aquifers are distributed non-uniformly in the Region.

Geophysical Assumptions

➢ The GEOTEM CRI were calculated using Channel 7-12 data of GEOTEM dBz/dt because (1) these 6 are early off-time channels and (2) we believe that these channels mostly reflect resistive layers.

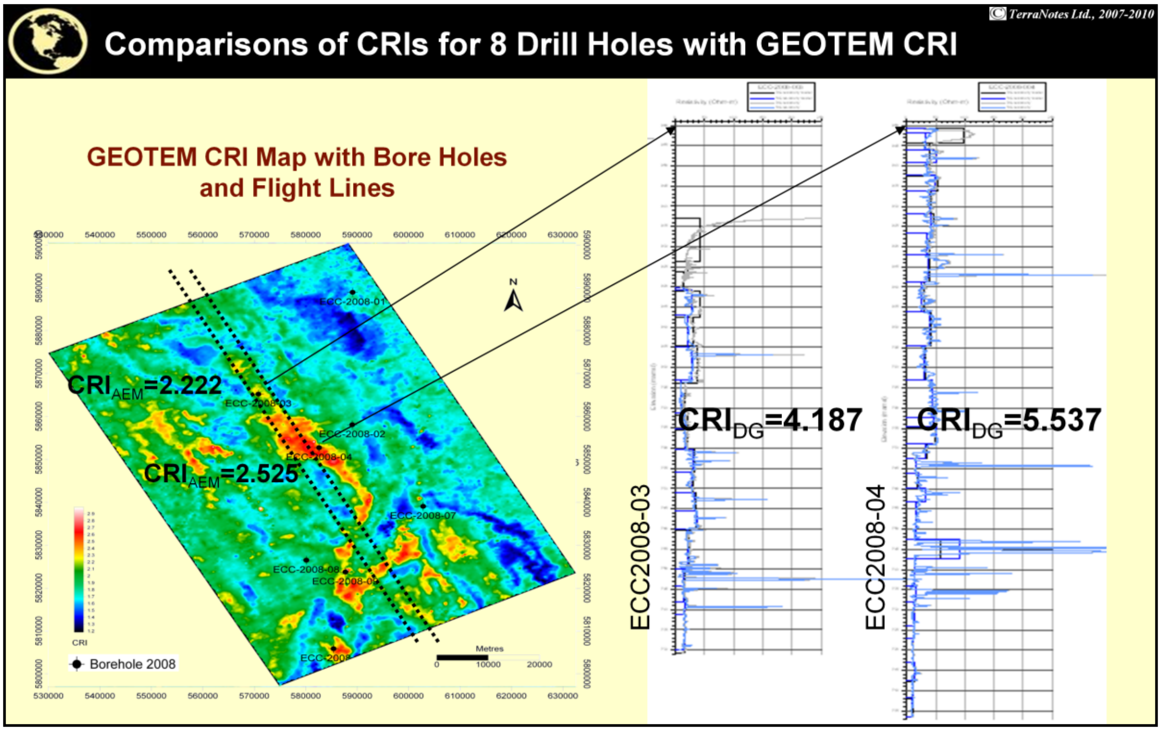

Figure 38. Comparison of borehole CRIs with GEOTEM CRI (no units for CRI).

Purpose of the calibration:

The purpose of the calibration is to analyze GEOTEM and/or other AEM data combined with down-hole loggings in the areas where there is no stratigraphic context.

Main Findings from the map:

- The CRI calculations show that the cumulative layers at ECC2008-04 are more resistive than those at ECC2008-03 (on right panel)
- The GEOTEM CRI map (on left panel) demonstrates that the overall resistivity of subsurface layers around ECC2008-04 is higher than that around ECC2008-03
- This suggests that the GEOTEM CRI is consistent with the borehole CRI
- The same procedure has been carried out for ECC2008-01 & ECC2008-02 , ECC2008-08 & ECC2008-09 and ECC2008-10. These results also suggest such a high level of consistency.

Delineating Zones of Interest for Aquifers Using Borehole–Calibrated GEOTEM Data

Result # 1

CRI helps to delineate zones of potential regional aquifers

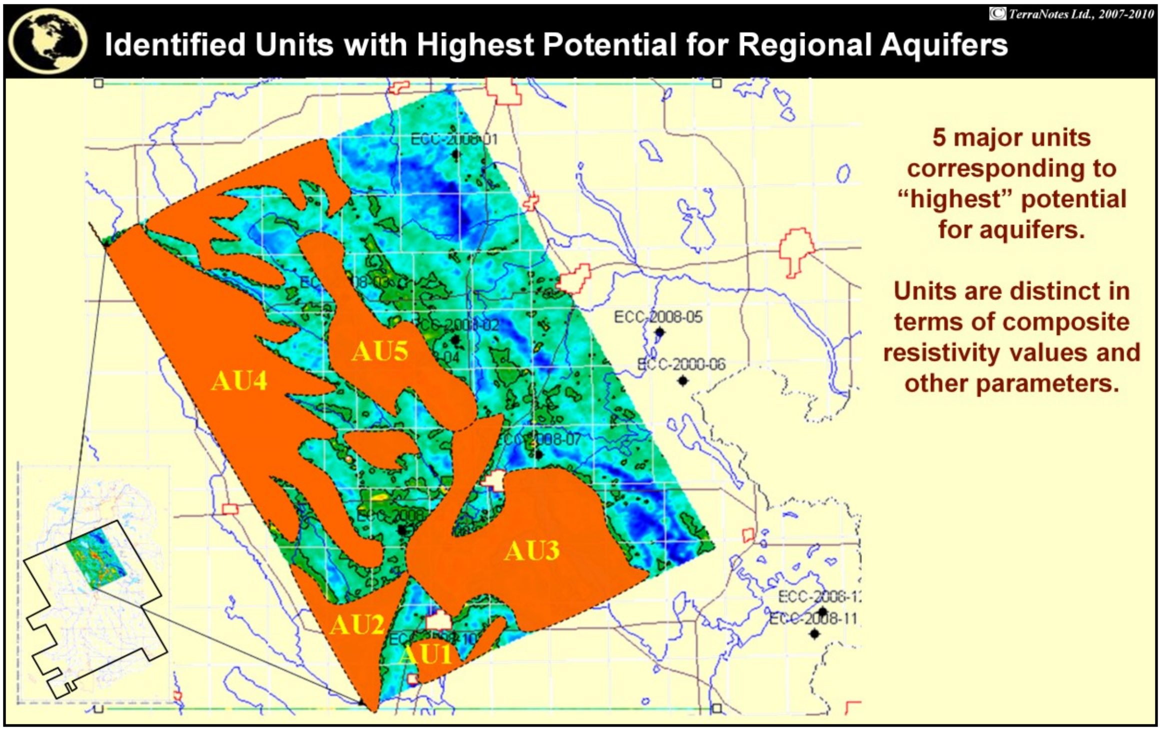

Figure 39. Identified units in the GEOTEM CRI map (no units for CRI).

Main Findings from the map:

- Major potential aquifer areas have been identified using the GEOTEM CRI map.
- Potential aquifers cover the whole western and southwestern portions of the Region.
- Potential aquifers regionally bounds with a low CRI (conductive) trend in the northeast.
- Five units for areas of interest can be divided regionally based on GEOTEM CRI features.
- The units are named as AU1, AU2, AU3, AU4 and AU5.
- Layers in all five units are interpreted as potential aquifers.

- AU1 is situated at the south corner of the Region, between Blackfalds and Lacombe.
- The ECC-2008-010 is located within the AU1.
- AU1 seems to extend from the south

- AU2 is triangularly-shaped and located at the south corner of the Region.
- It seems to extend from the southwest

- AU3's location and shape suggests that the aquifers stem from the known big channel and branch into 2, one extends continually in the northeast then turns broadly in the southeast, another goes towards northeast and connects to AU5.
- The branching point is close to ECC2008-009.
- Within AU3, some features of conductive trends suggest that there are channels cut through this identified resistive area.

- AU4's features show that the potential aquifer could extend from the northwest.
- AU4 is geophysically different from the other Units not only based on its location, but also on its shape. Within AU4, there are conductive trends branching out from the northwest to the southeast which are not present in the other Units. These conductive trends are interpreted burried channels.

- AU5 is located at the centre of the Region in the orientation of southeast-northwest.
- Two bore holes, ECC2008-003 and ECC2008-004, are located within this Unit.
- There is no clear point separating AU3 form AU5. However, AU5 could extend from the northwest to the southeast and join with one branch of AU3, or vice versa: the branch of AU3 extends toward the northwest and joins to AU5.

Delineating Zones of Interest for Aquifers Using Borehole–Calibrated GEOTEM Data

Result # 2

CRI helps differentiating the zones of potential regional aquifers

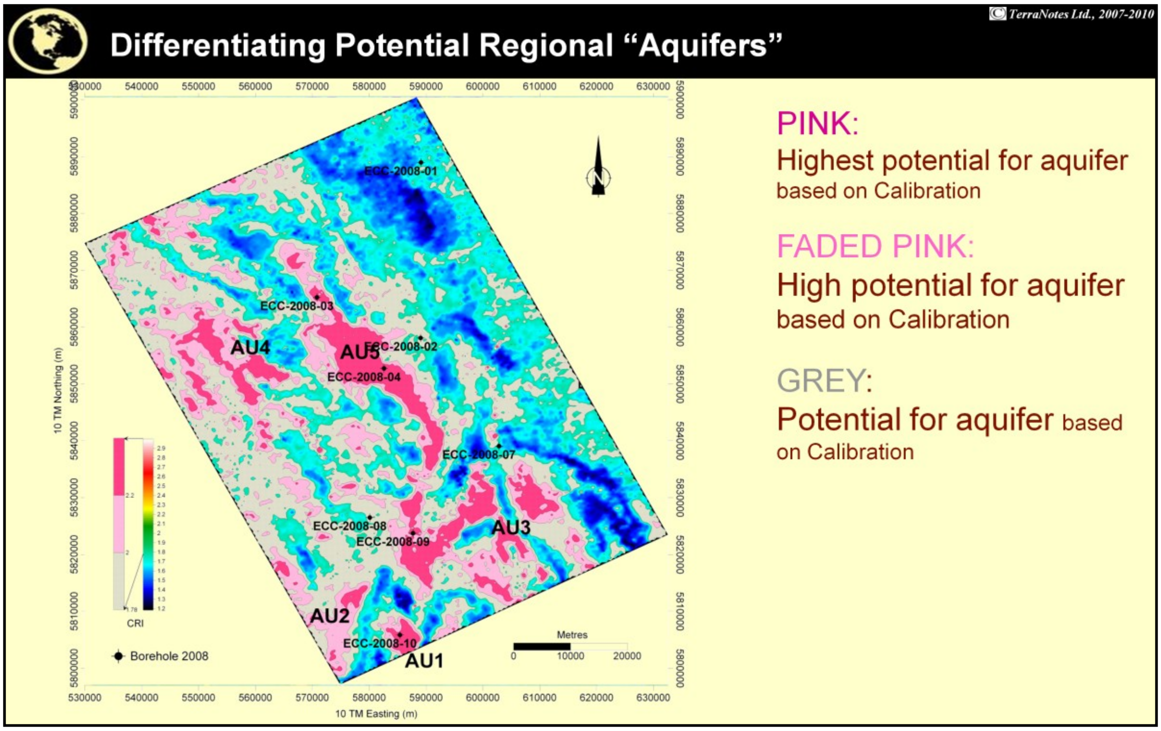

Figure 40. Differentiating potential regional aquifers (no units for CRI).

Main Findings from the map:

➢ This map shows the classification of areas with highly potential for aquifers in the five Units. Three classes are displayed with pink, faded pink and grey colours:

➢ Pink indicates the highest potential areas for aquifers

➢ Faded pink indicates the high areas for aquifers

➢ Grey indicates the potential areas for aquifers

Geophysical Assumptions and Comments

➢ Based on extensive comparison and correlations between GEOTEM CRI and sand layers identified in lithology columns provided by AGS, the threshold cut-offs of GEOTEM CRI for differentiating potential areas are as follows:

- Highest Potential area if GEOTEM CRI > 2.2 (pink)
- High Potential area if GEOTEM CRI > 2.0 and < 2.2 (faded pink)
- Potential area if GEOTEM CRI > 1.78 and < 2.0 (grey)

➢ The lower limit, 1.78, was determined based on the CRIs of ECC2008-01 and ECC2008-07. The upper limit, 2.2, was determined based on the CRIs of ECC2008-02, ECC2008-04 and ECC2008-10. The middle threshold, 2.0, was fixed in reference to the CRIs of ECC2008-03 and ECC2008-08. In Figure 40, it is assumed that the changes of GEOTEM CRI are linear.

➢ A number of methods could be used to further investigate the cut-offs and their relations among each other. This exercise could be used to scientifically formalize the process of precisely delineating areas of highest potential for aquifers.

Identified Units with Highest Potential for Regional Aquifers

Result # 3

Comparison of CRI and RDI

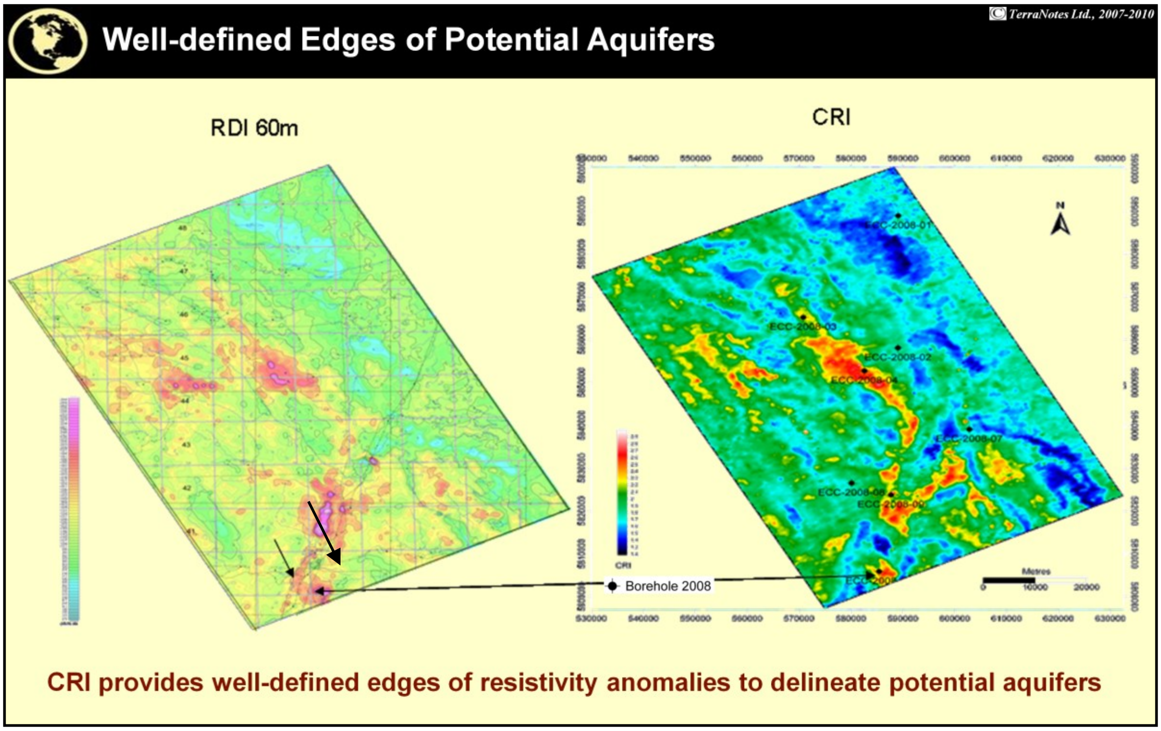

Figure 41. Comparison of GEOTEM CRI (no units for CRI) with Fugro's RDI results (Ω.m).

The maps compare RDI from FUGRO with our GEOTEM CRI. The line across the two maps point to two comparison areas.

Main Findings from the map:

As an example we use a resistive zone in which bore hole ECC2008-010 is located

- For this zone, both RDI and CRI show a high resistivity value.
- The edge of this zone is better defined on the CRI map and is more round on the RDI map
- The RDI map shows more average resistivity values inside the zone, while the CRI map provides more details of resistivity variations.
- On the RDI map, in the northwest of the zone, there is a linear resistive trend (pink-clored, pointed by short arrow), while on the CRI map there is a discontinuous conductive trend (cyan and blue-colored)

Relation Between GEOTEM CRI Results and Sand/Gravel Thickness

Result # 4

Sand & Gravel Thickness

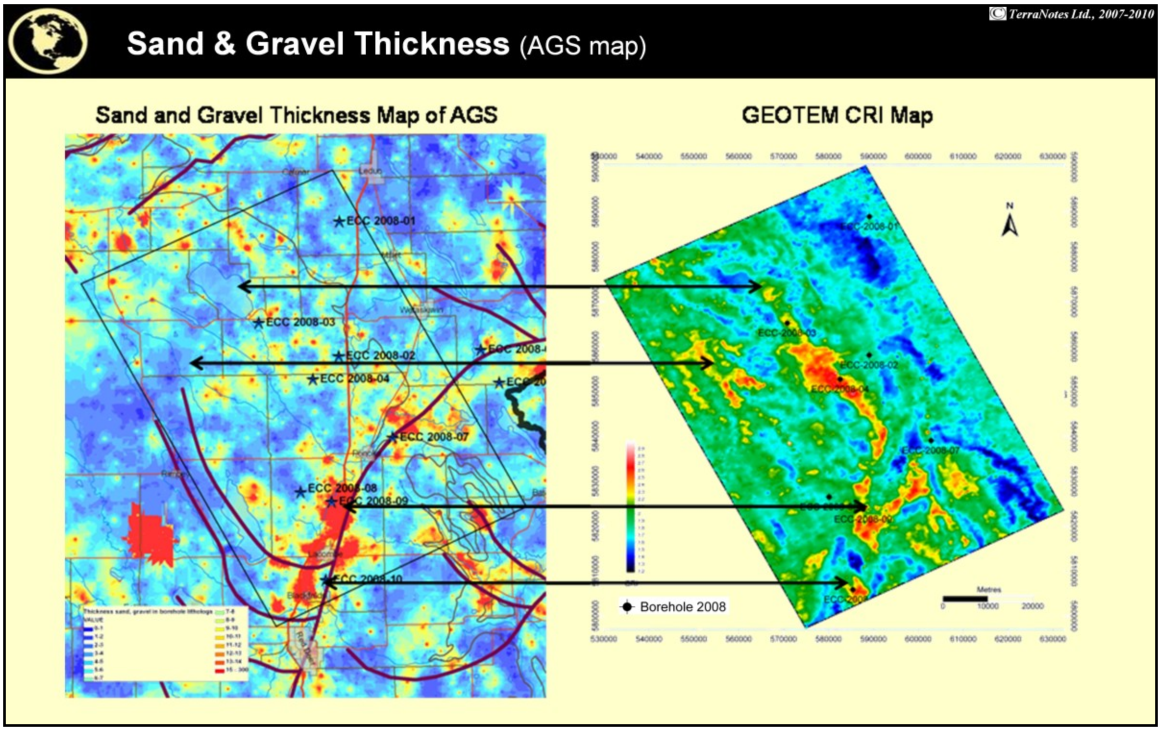

Figure 42. Regional Correlation between Sand & Gravel Thickness Map (m) provided by AGS (on the left) and the CRI map (no units for CRI on the right).

Main Findings from the map:

As an example we have compared at 4 points between the two maps.

➢ The zone of ECC2008-010: both maps show a resistive area. However, the CRI map provides well-defined edges. The major body of this resistive zone could be located the east of the bore hole.

➢ The zone of ECC2008-009: both maps show a resistive area. On the CRI map it is clear that the resistive trend extends toward the north-northeast and northeast, respectively.

➢ The zone in the western portion: There could be less information about sand & gravel thickness. In the CRI map, the resistive layers distribute in finger-like shape from the northwest to the southeast. It is regionally consistent with the orientations of ground creeks and rivers.

➢ The zone in the northwest from ECC2008-003: The map shows the thickness of sand and gravel is less than 10m; the CRI shows that the thickness of the resistive layers in this zone is comparable to that in ECC2008-003.

Geophysical Comments

➢ The CRI reflects not only the sand and gravel near the surface, but also the resistive layers beneath them within the exploration depth of GEOTEM 30Hz. Although there are differences between the CRI and Sand & Gravel Thickness – perhaps due to near surface sand and gravel or deeper sandstones - many features are still comparable.

Comparison of TDEM and its Amplifications with FDEM data

This section was prepared to illustrate that TDEM amplification methods of TerraNotes succeeds to get as high horizontal resolution as the FDEM data. Thus, TerraNotes' amplification methods may replace the high resolution FDEM data in other areas where FDEM is not available or very expensive to acquire.

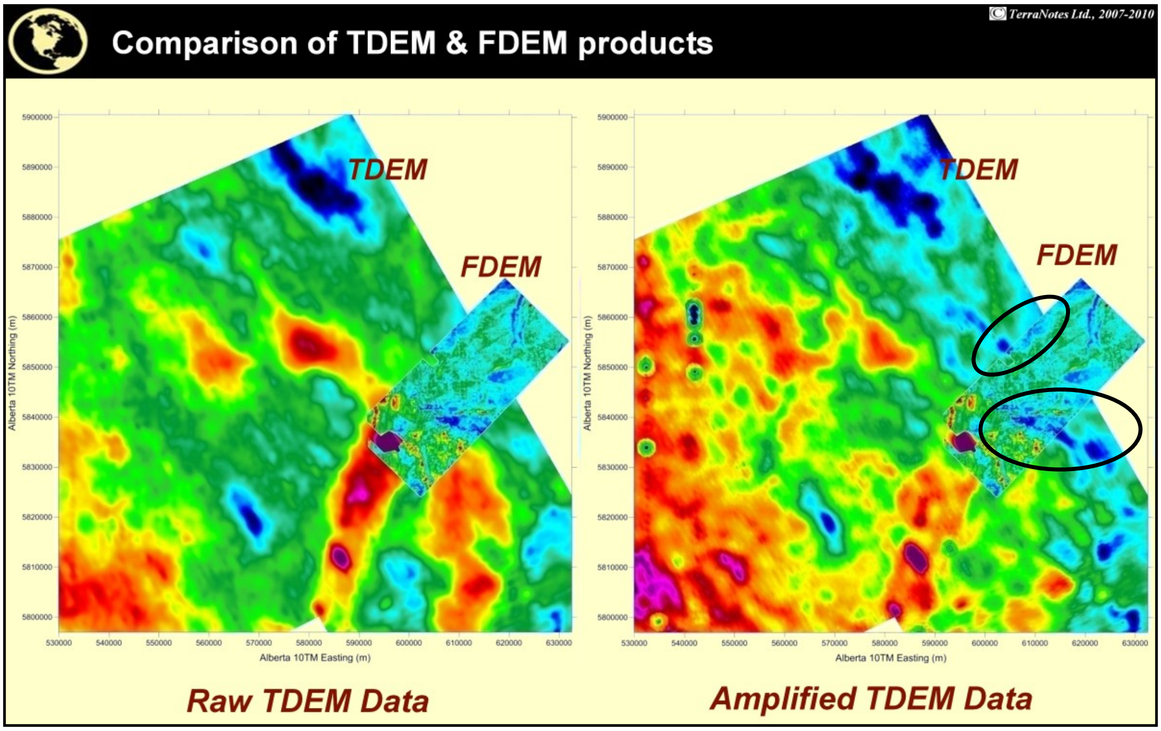

Figure 43. Comparison of raw TDEM data (pT/s) with Fugro's Inversion of the FDEM data (Ω.m).
Figure 44. Comparison of amplified TDEM data (S) with Fugro's Inversion of the FDEM data (Ω.m).

- This page compares the RESOLVE (FDEM) data with the time-domain EM (TDEM) data.
- The left panel compares the FDEM with raw TDEM data.
- The right panel compares the FDEM with amplified TDEM data.

Main Findings from these maps

- FDEM data gives much more details then the TDEM data, in the top 50 metres.
- Regional anomalies can be extracted from the TDEM data.
- Local anomalies can be extracted from the FDEM.
- However, note that the Amplified TDEM data can be used to obtain the local details about the subsurface geoelectrical structure.
- Black ellipses show the continuous features on both maps. This suggests that the Amplification can be used to obtain additional details about the geoelectrical structure in areas where FDEM has not been flown.

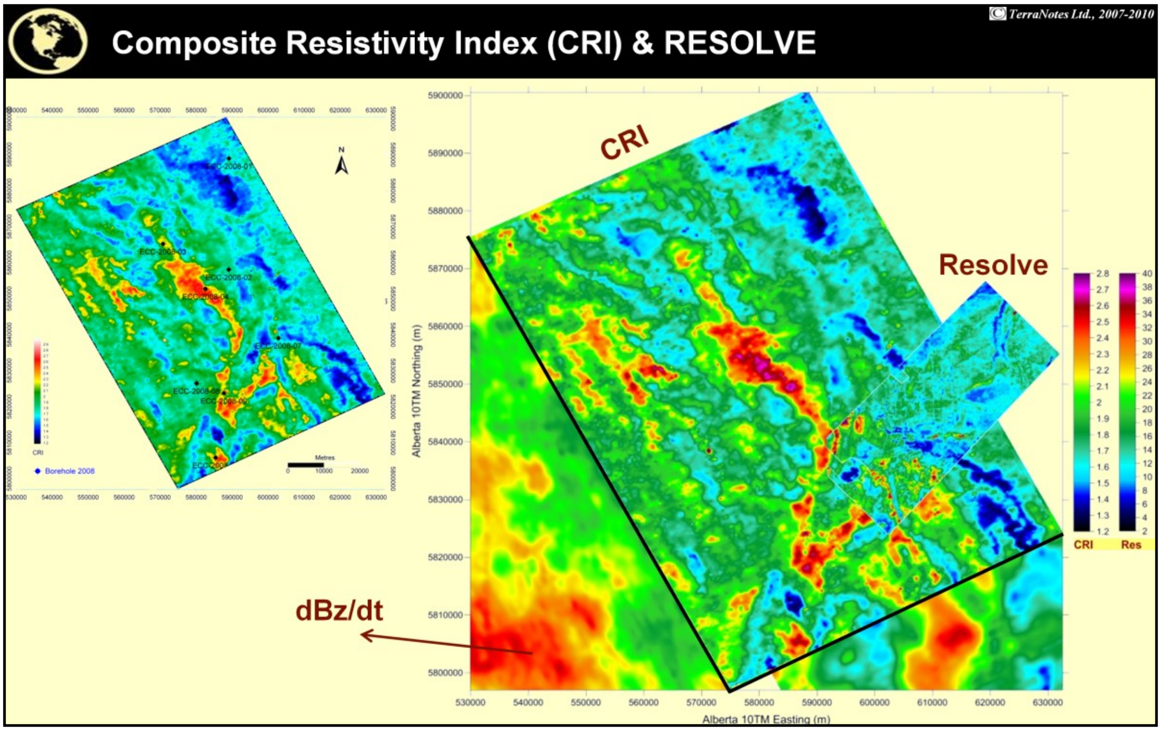

Figure 45. Composite Resistivity Index (CRI) calculation (no unit) results in comparison to the GEOTEM (pT/s) and RESOLVE data (Ω.m).

➢ CRI is a measure of the resistance of a rock matrix to the eddy currents. CRI is used to delineate the resistive subsurface features observed in the GEOTEM data.

Main Findings from these maps

➢ CRI map gives very detailed delineation of the resistive structures.
➢ It is possible to see the local anomalies within the large scale regional anomalies.
➢ Note that the CRI map shows details comparable to those from the RESOLVE map.
➢ This suggests that the CRI technique can be used to obtain resolutions of details similar to those obtained by FDEM surveys.

Comparison of Sand/Gravel Thickness Map with Electromagnetic Anomalies

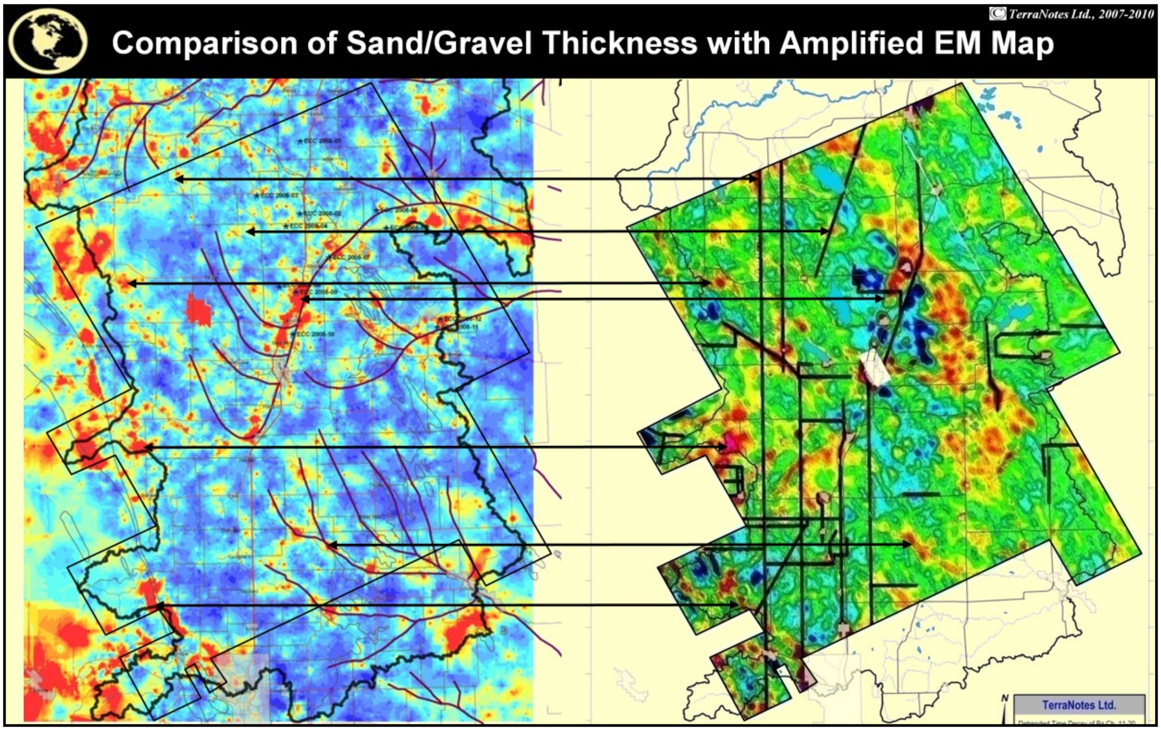

Figure 46. Sand/gravel thickness (m) derived from the boreholes in the ECC region (AGS map).
Figure 47. Amplified EM map (s) illustrating local resistive (hot colours) and local conductive (cold colours) zones.

Main Findings from these maps

➢ One can visually locate coincidental thicker sand/gravel zones and the resistive zones.
➢ Black arrows show some examples of the coincidental thick sand/gravel zones and resistive zones.
➢ It could be concluded that the EM amplification could locate the total thickness of 9-10 metre sand and gravel in the region.

Geophysical Assumptions and Comments

➢ Regional resistivity trend were removed from the map on the right, and only local anomalies are shown.
➢ The differences between each zone could be due to differences in 1) geologic unit thickness 2) grain sizes, 3) porosity, 4) stratigraphy, 5) topography and/or 6) water geochemistry.

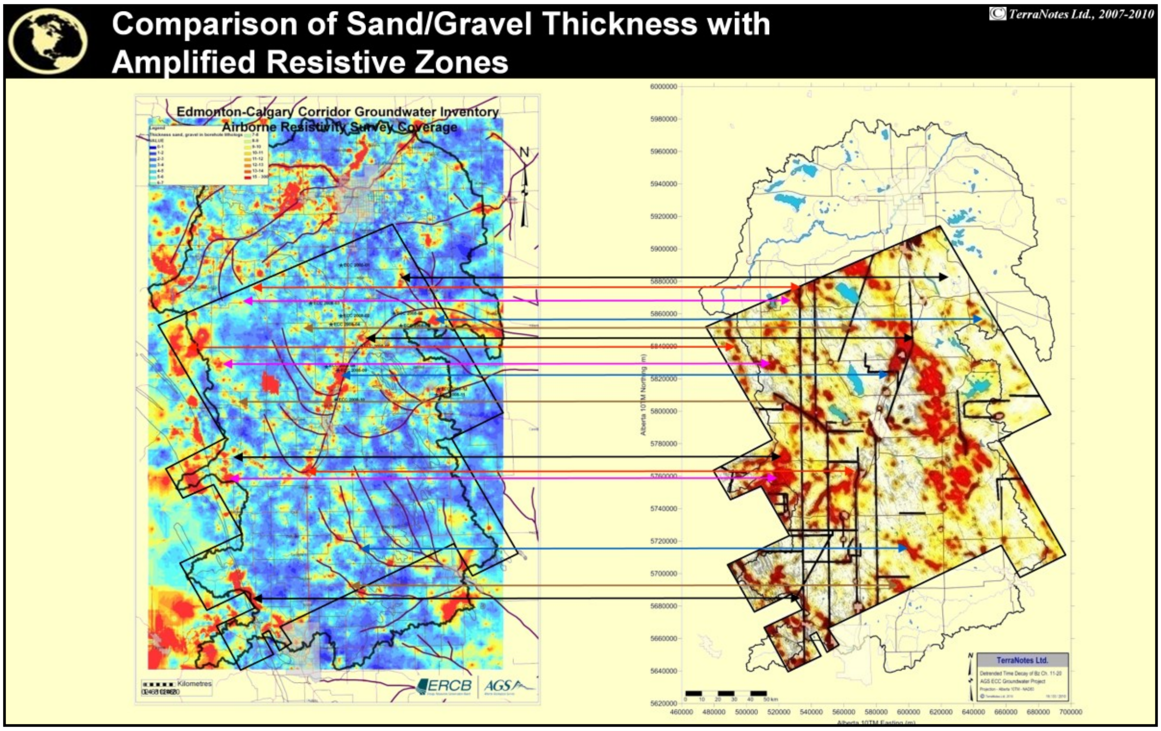

Figure 48. Sand/gravel thickness (m) derived from the boreholes in the ECC region (AGS map).
Figure 49. Amplified EM map (s) illustrating only local resistive zones with reddish colours.

Main Findings from these maps

- There is a coincidence between the thicker sand/gravel zones and the resistive zones.
- Coloured arrows show more examples of coincident thick sand/gravel and resistive zones.
- It could be concluded that the EM amplification could locate the total thickness of 9-10 metre sand and gravel in the region.

Geophysical Assumptions and Comments

- Regional resistivity trend were removed from the map on the right, and only local anomalies are shown.
- Only resistive anomalies are shown with colours in right panel.
- The differences between each zone could be due to differences in 1) geologic unit thickness 2) grain sizes, 3) porosity, 4) stratigraphy, 5) topography and/or 6) water geochemistry.

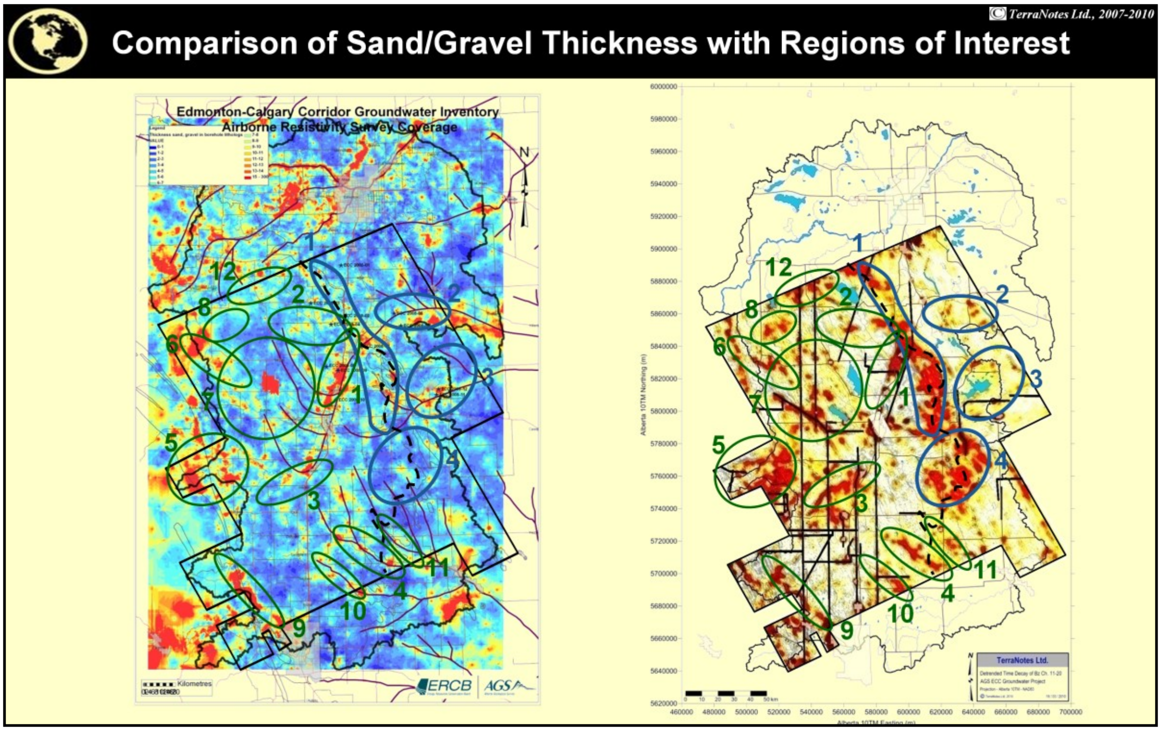

Figure 50. The regions of interest overlaid on sand/gravel thickness (m) derived from the boreholes in the ECC region.
Figure 51. The regions of interest overlaid on the amplified EM map (s) that illustrates only local resistive zones with reddish colours.

Main Findings from these maps

➢ There is a coincidence between the thicker sand/gravel zones and the resistive zones.
➢ Green ellipses show the twelve regions of interest selected within the Paskapoo formation.
➢ Blue ellipses and polygon show the four regions of interest selected within the Horseshoe Canyon / Scollard /Ardley/ Battle formations.
➢ It could be concluded that the EM amplification could locate the total thickness of 9-10 metre sand and gravel in the region.
➢ Most of the regions of interest show coincident anomalies, but there are some exceptions.
➢ Green 8 and Blue 4 looked resistive in the right panel, but there is no or very little coincident thick sand/gravel zone. These zones could be related to high topography zones.

Geophysical Assumptions and Comments

➢ Regional resistivity trend were removed from the map on the right, and only local anomalies are shown.
➢ Only resistive anomalies are shown with colours on right panel.
➢ The differences between each zone could be due to differences in 1) geologic unit thickness 2) grain sizes, 3) porosity, 4) stratigraphy, 5) topography and/or 6) water geochemistry.

Conclusions

✓ After performing data basing and processing routines, the raw GEOTEM data were submitted to a number of enhancement, filtering and amplification processes. The resulting relevant maps were interpreted. As a result, 12 regions of interest for potential aquifers in the Paskapoo formation were identified, as well as 4 regions of interest in the other formations. The regions of interest were delineated, mapped and interpreted. Some cultural effect and noise possibly due to pipelines, power lines, microwave towers, etc were visually identified.

✓ Simultaneously, the GEOTEM data was calibrated against eight drill holes and resulting resistivity maps were produced. As a result, 5 zones of interest for potential aquifers were identified and characterized.

✓ We conclude that resistivity contrasts obtained from logging data between Paskapoo and other formations (Scollard, Ardley, Battle and Horseshoe Canyon) is sufficient to image with AEM.

✓ Frequency domain RESOLVE data was mapped with respect to both frequency and depth, and intersecting NW-SE trending aquifer was imaged at near surface. The main NE-SW aquifer was more visible in the amplified maps beneath the intersecting NW-SE trending aquifer.

✓ Zones of interest from both GEOTEM amplification and calibration methods were compared to frequency domain maps. Although GEOTEM flight line spacing was 4 times larger than RESOLVE, the results show that amplification and calibration methods used to image GEOTEM provided similar level of details as those obtained from RESOLVE.

✓ Zones of interest for potential aquifers were compared to sand & gravel thickness maps. As a result, in many instances 9-10m thick sands & gravels were coincident with our regions of interest. This suggests that our amplification method could image zones of sand & gravel with ~ 10 metre thickness.

✓ Some of the aquifers were characterized and their topographical relationships were investigated through 3D imaging with the inclusion of surface topography.

Recommendations for Further Analyses

This limited project did not allow for a number of possible analyses and maps. We would recommend the following analyses to extract more information and interpretation from the raw and processed data:

❖ Discussions with geologists would be required to use the geophysical knowledge from this project to assess grain size thresholds for each selected regions. We recommend weekly meeting to discuss the relationship between the geophysical findings and the geologists input for each regions of interest.

❖ Porosity estimations can be made from the airborne and drill-hole resistivity data for selected regions of interest. A number of geophysical methods can be used and discussed to obtain 3D estimations of porosity.

❖ Surface area can be calculated for each selected regions of interest.

❖ 3D volumetric imaging, slices and isosurface should be created for other GEOTEM datasets and 3D interpretation should be extended to those areas.

❖ Volumes of each regions of interest should be calculated for each selected regions of interest.

❖ Topography should be included into the voxel models of the GEOTEM datasets, and the effect of topography should be examined for each resistive zones.

❖ Since calibration was done for one dataset, we recommend expanding the calibration between airborne electromagnetic data and the drill-holes for the other GEOTEM datasets as well.

❖ Newly acquired GEOTEM and TEMPEST datasets can be used to evaluate the extension of the anomalies that were located at the edges of the current data coverage.

❖ TerraNotes' Composite Longitudinal Conductance (CLC) technique can be used to differentiate the Horseshoe Canyon, Scollard, Ardley and Battle formations from each other.

General Assumptions

- The resistivity of a media can be increased or decreased due to the factors below:
  1. Sand / gravel thickness or Clay / mud thickness
  2. Grain sizes
  3. Porosity
  4. Stratigraphy
  5. Topography
  6. Water geochemistry / Salinity
  7. Cultural /man-made structure
- It is generally accepted that early time channels reflects more near surface information while late time channel reflects more deeper information in the time-domain EM data. However, variations may occur.
- It is generally accepted that high frequency channels reflect more near surface information while low frequency channels reflect more deeper information in the frequency-domain EM data. However, variations may occur.
- Amplification methods amplifies the weaker resistive and conductive anomalies and provide higher resolution details about the regional anomalies.
- Amplification processing may also amplify the cultural noise effects. However, this effect can be used to locate the noise sources.

Glossary

Amplification: A proprietary suite of mathematical approaches to increase the strength/frequency of the geophysical anomalies to emphasize the weaker anomalies, increase the contrast at the edges of the geophysical anomalies.

Regional Anomaly (or Feature): Geophysical anomalies that cover more than one third of the entire survey area, (for example stratigraphic unit boundaries).

Local Anomaly (or Feature): Geophysical anomaly that covers a small portion in the survey area (<10 %) and is thick enough (approximately 10 m) to be recorded as an anomaly.

Trend: A general direction of the geophysical anomaly that could be a plane or a surface that could be defined by a single mathematical function. This would be an effect coming from very deep and it would not be of interest to the purpose at hand (Sheriff, 2006).

Detrending: Removing a trend that is of no interest to the purpose at hand.

Half-space model: A mathematical model bounded only by one plane surface, i.e. the model is so large in other dimensions that only the surface boundary affects the results. Features within the model are usually assumed to be homogeneous and isotropic (Sheriff, 2006).

Thin-sheet model: An assumption of an earth model with extremely thin layer that does not have a thickness.

1^{st}, 2^{nd}, 3^{rd} - n^{th} order: An order of an EM amplification method. The first order estimate is an indicative of the material in the top 50 to 100 m, while higher-orders are indicative of deeper materials.

DISCLAIMER

This report has been prepared exclusively for Alberta Geological Survey. It is not intended for public information. The report reflects the professional opinion of TerraNotes Ltd. based on the data and information provided by Alberta Geological Survey. TerraNotes Ltd. will not assume or otherwise accept responsibility or liability for losses incurred by Alberta Geological Survey or other parties as a result of the circulation, publication, reproduction, use of or reliance on this report contrary to the provisions discussed in this paragraph.

As per Agreement between Alberta Geological Survey and TerraNotes Ltd. pertaining to this project, Alberta Geological Survey understands and agrees that it is quite possible that errors and omissions may occur in data input and/or programming to convert the data in the form desired, and Alberta Geological Survey further understands and agrees that the data may not meet user's standards as to accuracy or completeness; notwithstanding, Alberta Geological Survey agrees to take the data "as is", fully expecting that there may well be errors and omissions in the data obtained from TerraNotes Ltd.

TerraNotes Ltd. has checked with sources believed to be reliable in their efforts to provide information that is accurate, comprehensive, and timely at the date of publication. However, human error and changes may occur. Alberta Geological Survey further understands that TerraNotes Ltd. has produced this document in good faith with the information available at the date of production of this report and makes absolutely no warranty whatsoever, whether expressed or implied, as to the accuracy, thoroughness, value, quality, validity, suitability, condition, or fitness for a particular purpose of the data or any programming used to obtain the data, nor as to whether the data is error-free, up-to-date, complete or based upon accurate meaningful facts.

Appendix A

A-0 Borehole Logging Data Analysis

General Description:

All the results of Borehole Logging Data Analysis have been archived into the folder "*AGS_2008_Drillholes_and_Loggings*" in which there are three sub-folders as follows:

1) *Statistics_of_LoggingData*
2) *Stratification_of_LoggingCurves*
3) *RDI_Resistivity*

Logging Plots in Format of PNG

AGS_2008_Drillholes_and_Loggings >

- ECC2008-001_DG_SG_RDI.png
- ECC2008-002_DG_SG_RDI.png
- ECC2008-003_DG_SG_RDI.png
- ECC2008-004_DG_SG_RDI.png
- ECC2008-005_DG_SG_RDI.png
- ECC2008-006_DG_SG_RDI.png
- ECC2008-007_DG_SG_RDI.png
- ECC2008-008_DG_SG_RDI.png
- ECC2008-009_DG_SG_RDI.png
- ECC2008-010_DG_SG_RDI.png
- ECC2008-011_DG_SG_RDI.png
- ECC2008-012_DG_SG_RDI.png

A-1 Logging Data Statistics

Descriptions:

Each logging data of borehole was analyzed.
The analyses were carried on based on stratigraphy identified by AGS.
The stratigraphic formations are as follows:

a) Paskapoo
b) Scollard including Ardley
c) Battle
d) Horseshoe Canyon

The results have been archived in the folder "*Statistics_of_LoggingData*". The files of statistical results were titled with both Borehole ID and formation's name for user's convenience, for example:

Folder (Statistics_of_LoggingData) >

Sub-folder (Statistics_of_ECC2008-001) >

- 01_STAT_HorseShoeCanyon.DAT

represents that the statistical results of ECC2008-001 logging data for Horseshoe Canyon Formation is located at the sub-folder "*Statistics_of_ECC2008-001*" in the folder "*Statistics_of_LoggingData*"

List of folders and files:

Statistics_of_LoggingData >

Statistics_of_ECC2008-001 >

- 01_STAT_HorseShoeCanyon.DAT

Statistics_of_ECC2008-002 >

- 02_STAT_DisplacedBedrock.DAT
- 02_STAT_Scollard.DAT
- 02_STAT_Battle.DAT
- 02_STAT_HorseShoeCanyon.DAT

Statistics_of_ECC2008-003 >

- 03_STAT_Paskapoo.DAT
- 03_STAT_Scollard.DAT

Statistics_of_ECC2008-004 >

- 04_STAT_Paskapoo.DAT
- 04_STAT_Scollard.DAT

Statistics_of_ECC2008-005 >

- 05_STAT_HorseShoeCanyon.DAT

Statistics_of_ECC2008-006 >

- 06_STAT_HorseShoeCanyon.DAT

Statistics_of_ECC2008-007 >

- 07_STAT_Paskapoo.DAT
- 07_STAT_Scollard.DAT
- 07_STAT_Battle.DAT
- 07_STAT_HorseShoeCanyon.DAT

Statistics_of_ECC2008-008 >

- 08_STAT_Paskapoo.DAT
- 08_STAT_Scollard.DAT

Statistics_of_ECC2008-009 >

- 09_STAT_Paskapoo.DAT
- 09_STAT_Scollard.DAT

Statistics_of_ECC2008-010 >

- 10_STAT_Paskapoo.DAT
- 10_STAT_Scollard.DAT

Statistics_of_ECC2008-011 >

- 11_STAT_DisplacedBedrock.DAT
- 11_STAT_HorseShoeCanyon.DAT

Statistics_of_ECC2008-012 >
- 12_STAT_HorseShoeCanyon.DAT

(Two Brief Summaries in format of XLS)
- Brief_Statistics_of_12Borehole_DG_Resistivity.xls
- Brief_Statistics_of_12Borehole_GR.xls

A-2 Stratification of Logging Curves

Descriptions:

The logging curves of borehole were stratified for further use.
The stratification analyses were carried on especially for Deep Guard and Short Guard resistivity data.
In stratification the minimal thickness was specified as 2m. This threshold was set up through a set of experimenting using 0.2m, 0.5m, 1.0m and 2.0m respecitively with ECC2008-002 and ECC2008-004 logging data

The files with the character-string "_CRI" in file's name include the CRI value calculated using DG stratification results.

All the results have been archived in the folder "*Stratification_of_LoggingCurves*". Each of files was titled with both Borehole ID and Log ID for user's convenience, for example:

Folder (Stratification_of_LoggingCurves) >
Sub-folder (Strat_ECC2008-001) >
- 01_STRATI_DG.TAB

represents that that stratification of DG data in ECC2008-001 is located at the sub-folder "*Strat_ECC2008-001*" in the folder "*Stratification_of_LoggingCurves*"

List of folders and files:

Stratification_of_LoggingData >
Strat_ECC2008-001 >
- 01_STRATI_DG.TAB
- 01_STRATI_DG_CRI.TAB
- 01_STRATI_SG.TAB

Strat_ECC2008-002 >
- 02_STRATI_DG_Min02m.TAB
- 02_STRATI_DG_Min05m.TAB
- 02_STRATI_DG_Min1m.TAB
- 02_STRATI_DG_Min2m.TAB
- 02_STRATI_DG_Min2m_CRI.TAB
- 02_STRATI_SG_Min02m.TAB
- 02_STRATI_SG_Min05m.TAB
- 02_STRATI_SG_Min1m.TAB

- 02_STRATI_SG_Min2m.TAB
- 02_STRATI_GR_Min02m.TAB
- 02_STRATI_GR_Min05m.TAB
- 02_STRATI_GR_Min1m.TAB
- 02_STRATI_GR_Min2m.TAB
- 02_STRATI_PORDen_Min02m.TAB
- 02_STRATI_PORDen_Min05m.TAB
- 02_STRATI_PORDen_Min1m.TAB
- 02_STRATI_PORDen_Min2m.TAB
- 02_STRATI_DeltaT_Min02m.TAB
- 02_STRATI_DeltaT _Min05m.TAB
- 02_STRATI_DeltaT _Min1m.TAB
- 02_STRATI_DeltaT _Min2m.TAB

Strat_ECC2008-003 >

- 03_STRATI_DG.TAB
- 03_STRATI_DG_CRI.TAB
- 03_STRATI_SG.TAB

Strat_ECC2008-004 >

- 04_STRATI_DG_Min02m.TAB
- 04_STRATI_DG_Min05m.TAB
- 04_STRATI_DG_Min1m.TAB
- 04_STRATI_DG_Min2m.TAB
- 04_STRATI_DG_Min2m_CRI.TAB
- 04_STRATI_SG_Min02m.TAB
- 04_STRATI_SG_Min05m.TAB
- 04_STRATI_SG_Min1m.TAB
- 04_STRATI_SG_Min2m.TAB
- 04_STRATI_GR_Min02m.TAB
- 04_STRATI_GR_Min05m.TAB
- 04_STRATI_GR_Min1m.TAB
- 04_STRATI_GR_Min2m.TAB
- 04_STRATI_PORDen_Min02m.TAB
- 04_STRATI_PORDen_Min05m.TAB
- 04_STRATI_PORDen_Min1m.TAB
- 04_STRATI_PORDen_Min2m.TAB
- 04_STRATI_DeltaT_Min02m.TAB
- 04_STRATI_DeltaT _Min05m.TAB
- 04_STRATI_DeltaT _Min1m.TAB
- 04_STRATI_DeltaT _Min2m.TAB

Strat_ECC2008-005 >

- 05_STRATI_DG.TAB
- 05_STRATI_DG_CRI.TAB
- 05_STRATI_SG.TAB

Strat_ECC2008-006 >
- 06_STRATI_DG.TAB
- 06_STRATI_DG_CRI.TAB
- 06_STRATI_SG.TAB

Strat_ECC2008-007 >
- 07_STRATI_DG.TAB
- 07_STRATI_DG_CRI.TAB
- 07_STRATI_SG.TAB

Strat_ECC2008-008 >
- 08_STRATI_DG.TAB
- 08_STRATI_DG_CRI.TAB
- 08_STRATI_SG.TAB

Strat_ECC2008-009 >
- 09_STRATI_DG.TAB
- 09_STRATI_DG_CRI.TAB
- 09_STRATI_SG.TAB

Strat_ECC2008-010 >
- 10_STRATI_DG.TAB
- 10_STRATI_DG_CRI.TAB
- 10_STRATI_SG.TAB

Strat_ECC2008-011 >
- 11_STRATI_DG.TAB
- 11_STRATI_DG_CRI.TAB
- 11_STRATI_SG.TAB

Strat_ECC2008-012 >
- 12_STRATI_DG.TAB
- 12_STRATI_DG_CRI.TAB
- 12_STRATI_SG.TAB

A-3 FUGRO's RDI Resistivity Data Related to Boreholes and Logging Plots

Descriptions:

The RDI resistivity data in depths calculated by Fugro were selected at/close to each of boreholes.

All the selected RDI data have been archived in the folder "*RDI_Resistivity*". The files are titled with Borehole ID for user's convenience, for example:

Folder (*RDI_Resistivity*) >
- RDI_resistivity_vs_ECC2008-001.dat
- Coordinates_for_RDI_resistivity_vs_ECC2008-001.dat

The first .dat file is the RDI resistivity data in elevations versus Borehole ECC2008-001, and the second one provides the 10TM coordinates of location where RDI data were selected.

List of folders and files:

RDI_Resistivity >

- RDI_resistivity_vs_ECC2008-001.dat
- Coordinates_for_RDI_resistivity_vs_ECC2008-001.dat
- RDI_resistivity_vs_ECC2008-002.dat
- Coordinates_for_RDI_resistivity_vs_ECC2008-002.dat
- RDI_resistivity_vs_ECC2008-003.dat
- Coordinates_for_RDI_resistivity_vs_ECC2008-003.dat
- RDI_resistivity_vs_ECC2008-004.dat
- Coordinates_for_RDI_resistivity_vs_ECC2008-004.dat
- RDI_resistivity_vs_ECC2008-005.dat
- Coordinates_for_RDI_resistivity_vs_ECC2008-005.dat
- RDI_resistivity_vs_ECC2008-006.dat
- Coordinates_for_RDI_resistivity_vs_ECC2008-006.dat
- RDI_resistivity_vs_ECC2008-007.dat
- Coordinates_for_RDI_resistivity_vs_ECC2008-007.dat
- RDI_resistivity_vs_ECC2008-008.dat
- Coordinates_for_RDI_resistivity_vs_ECC2008-008.dat
- RDI_resistivity_vs_ECC2008-009.dat
- Coordinates_for_RDI_resistivity_vs_ECC2008-009.dat
- RDI_resistivity_vs_ECC2008-010.dat
- Coordinates_for_RDI_resistivity_vs_ECC2008-010.dat
- RDI_resistivity_vs_ECC2008-011.dat
- Coordinates_for_RDI_resistivity_vs_ECC2008-011.dat
- RDI_resistivity_vs_ECC2008-012.dat
- Coordinates_for_RDI_resistivity_vs_ECC2008-012.dat

Logging Plots in Format of PNG

RDI_Resistivity >

- ECC2008-001_DG_SG_RDI.png
- ECC2008-002_DG_SG_RDI.png
- ECC2008-003_DG_SG_RDI.png
- ECC2008-004_DG_SG_RDI.png
- ECC2008-005_DG_SG_RDI.png
- ECC2008-006_DG_SG_RDI.png
- ECC2008-007_DG_SG_RDI.png
- ECC2008-008_DG_SG_RDI.png
- ECC2008-009_DG_SG_RDI.png

- ECC2008-010_DG_SG_RDI.png
- ECC2008-011_DG_SG_RDI.png
- ECC2008-012_DG_SG_RDI.png

Appendix B

B-0 GEOTEM flight-line Data Analysis

General Description:

The results of GEOTEM flightline Data Analysis have been archived into the folder "*Selected_Flightlines_close_to_2008Drillholes*" in which five sub-folders were created for each of types of data:

1) *GEOTEM30_DTMData_Flightlines*
2) *GEOTEM30_MagneticData_Flightlines*
3) *GEOTEM30_dBzdt_profiles*
4) *GEOTEM30_BzF_profiles*
5) *GEOTEM30_CRI_profiles*

List of files in format of XLS

Selected_Flightlines_close_to_2008Drillholes >

- AGS_2008_Drillholes_and_GEOTEM_Flightlines.xls

B-1 DTM data of Selected Flightlines close to Boreholes

Descriptions:

The DTM data along the flightline which is closest to a borehole was selected from the original dataset "2007a"

The selected data has been archived in the folder "*GEOTEM30_DTMData_Flightlines*". The files were named with flightline ID for user's convenience.

List of files:

Selected_Flightlines_close_to_2008Drillholes >
GEOTEM30_DTMData_Flightlines >

- Flightline_10180_DTM.dat
- Flightline_10250_DTM.dat
- Flightline_10320_DTM.dat
- Flightline_10321_DTM.dat
- Flightline_10390_DTM.dat
- Flightline_10440_DTM.dat
- Flightline_10550_DTM.dat
- Flightline_10580_DTM.dat

- Flightline_10740_DTM.dat
- Flightline_20113_DTM.dat
- Flightline_20120_DTM.dat
- Flightline_20121_DTM.dat
- Flightline_30340_DTM.dat
- Flightline_30341_DTM.dat
- Flightline_30350_DTM.dat
- Flightline_30351_DTM.dat
- Flightline_30360_DTM.dat
- Flightline_30361_DTM.dat
- Flightline_30371_DTM.dat
- Flightline_30371_DTM.dat

B-2 Magnetic data of Selected Flightlines close to Boreholes

Descriptions:

The magnetic data along the flightline which is closest to a borehole was selected from the original dataset "2007a"

The selected data has been archived in the folder "*GEOTEM30_MagneticData _Flightlines*". The files were named with flightline ID for user's convenience.

List of files:

Selected_Flightlines_close_to_2008Drillholes >
GEOTEM30_MagneticData_Flightlines >

- Flightline_10180_Mag.dat
- Flightline_10250_Mag.dat
- Flightline_10320_Mag.dat
- Flightline_10321_Mag.dat
- Flightline_10390_Mag.dat
- Flightline_10440_Mag.dat
- Flightline_10550_Mag.dat
- Flightline_10580_Mag.dat
- Flightline_10740_Mag.dat
- Flightline_20113_Mag.dat
- Flightline_20120_Mag.dat
- Flightline_20121_Mag.dat
- Flightline_30340_Mag.dat
- Flightline_30341_Mag.dat
- Flightline_30350_Mag.dat
- Flightline_30351_Mag.dat

- Flightline_30360_Mag.dat
- Flightline_30361_Mag.dat
- Flightline_30371_Mag.dat
- Flightline_30371_Mag.dat

B-3 GEOTEM dBz/dt data of Selected Flightlines close to Boreholes

Descriptions:

The data of GEOTEM dBz/dt along the flightline which is closest to a borehole was selected from the original dataset “2007a”

The selected data has been archived into the folder “*GEOTEM30_dBzdt_Flightlines*”. All the files were named with flightline ID for user’s convenience.

List of files:

Selected_Flightlines_close_to_2008Drillholes >
GEOTEM30_dBzdt_Flightlines >

- Flightline_10180_dBzdt.dat
- Flightline_10250_dBzdt.dat
- Flightline_10320_dBzdt.dat
- Flightline_10321_dBzdt.dat
- Flightline_10390_dBzdt.dat
- Flightline_10440_dBzdt.dat
- Flightline_10550_dBzdt.dat
- Flightline_10580_dBzdt.dat
- Flightline_10740_dBzdt.dat
- Flightline_20113_dBzdt.dat
- Flightline_20120_dBzdt.dat
- Flightline_20121_dBzdt.dat
- Flightline_30340_dBzdt.dat
- Flightline_30341_dBzdt.dat
- Flightline_30350_dBzdt.dat
- Flightline_30351_dBzdt.dat
- Flightline_30360_dBzdt.dat
- Flightline_30361_dBzdt.dat
- Flightline_30371_dBzdt.dat
- Flightline_30371_dBzdt.dat

List of Profiles in format of PNG:
The Digital Terrain Model (DTM), GPS elevation of aircraft (GPSz), Residual Magnetic Intensity (RMI) and the First Vertical Derivative (1VD) are combined in each of dBzdt profiles.

Selected_Flightlines_close_to_2008Drillholes >
GEOTEM30_dBzdt_Flightlines >

- Flightline_10180_dBzdt.png
- Flightline_10250_dBzdt.png
- Flightline_10320_10321_dBzdt.png
- Flightline_10390_dBzdt.png
- Flightline_10440_dBzdt.png
- Flightline_10550_dBzdt.png
- Flightline_10580_dBzdt.png
- Flightline_10740_dBzdt.png
- Flightline_20113_dBzdt.png
- Flightline_20120_20121_dBzdt.png
- Flightline_30340_30341_dBzdt.png
- Flightline_30350_30351_dBzdt.png
- Flightline_30360_30361_dBzdt.png
- Flightline_30370_30371_dBzdt.png

B-4 GEOTEM BzF data of Selected Flightlines close to Boreholes

Descriptions:

The GEOTEM BzF data along the flightline which is closest to a borehole was selected from the original dataset “2007a”

The selected data has been archived into the folder “*GEOTEM30_BzF_Flightlines*”. The files were named with flightline ID for user’s convenience.

List of files:

Selected_Flightlines_close_to_2008Drillholes >
GEOTEM30_BzF_Flightlines >

- Flightline_10180_BzF.dat
- Flightline_10250_BzF.dat
- Flightline_10320_BzF.dat
- Flightline_10321_BzF.dat
- Flightline_10390_BzF.dat
- Flightline_10440_BzF.dat
- Flightline_10550_BzF.dat
- Flightline_10580_BzF.dat

- Flightline_10740_BzF.dat
- Flightline_20113_BzF.dat
- Flightline_20120_BzF.dat
- Flightline_20121_BzF.dat
- Flightline_30340_BzF.dat
- Flightline_30341_BzF.dat
- Flightline_30350_BzF.dat
- Flightline_30351_BzF.dat
- Flightline_30360_BzF.dat
- Flightline_30361_BzF.dat
- Flightline_30371_BzF.dat
- Flightline_30371_BzF.dat

List of Profiles in format of PNG:
The Digital Terrain Model (DTM), GPS elevation of aircraft (GPSz), Residual Magnetic Intensity (RMI) and the First Vertical Derivative (1VD) are combined in each of BzF profiles.

Selected_Flightlines_close_to_2008Drillholes >
GEOTEM30_BzF_Flightlines >

- Flightline_10180_BzF.png
- Flightline_10250_BzF.png
- Flightline_10320_10321_BzF.png
- Flightline_10390_BzF.png
- Flightline_10440_BzF.png
- Flightline_10550_BzF.png
- Flightline_10580_BzF.png
- Flightline_10740_BzF.png
- Flightline_20113_BzF.png
- Flightline_20120_20121_BzF.png
- Flightline_30340_30341_BzF.png
- Flightline_30350_30351_BzF.png
- Flightline_30360_30361_BzF.png
- Flightline_30370_30371_BzF.png

B-5 GEOTEM dBzdt-CRI data of Selected Flightlines close to Boreholes

Descriptions:

The Composite Resistivity Index (CRI) along flightline which is closest to a borehole was calculated using the channel-7-12 data of GEOTEM30Hz dB/dt.

The CRI values have been calibrated using CRI values of borehole. The CRI values of borehole please see files in the folder "*Stratification_of_LoggingCurves*".

The CRI results have been archived in the folder "*GEOTEM30_CRI_profiles*". The files were named with flightline ID for user's convenience.

List of files:

Selected_Flightlines_close_to_2008Drillholes >
GEOTEM30_dBzdt_Flightlines >

- Flightline_10180_dBzdt_CRI.dat
- Flightline_10250_dBzdt_CRI.dat
- Flightline_10320_dBzdt_CRI.dat
- Flightline_10321_dBzdt_CRI.dat
- Flightline_10390_dBzdt_CRI.dat
- Flightline_10440_dBzdt_CRI.dat
- Flightline_10550_dBzdt_CRI.dat
- Flightline_10580_dBzdt_CRI.dat
- Flightline_10740_dBzdt_CRI.dat

List of Profiles in format of PNG:

The Digital Terrain Model (DTM) was combined into each of CRI profiles.

Selected_Flightlines_close_to_2008Drillholes >
GEOTEM30_dBzdt_Flightlines >

- Flightline_10180_dBzdt_CRI.png
- Flightline_10250_dBzdt_CRI.png
- Flightline_10320_dBzdt_CRI.png
- Flightline_10321_dBzdt_CRI.png
- Flightline_10390_dBzdt_CRI.png
- Flightline_10440_dBzdt_CRI.png
- Flightline_10550_dBzdt_CRI.png
- Flightline_10580_dBzdt_CRI.png
- Flightline_10740_dBzdt_CRI.png

Appendix C

C-0 Calculation and Analysis of CRI

General Description:

The Composite Resistivity Index (CRI) was calculated using the Channel 7-12 data of GEOTEM 30Hz dBz/dt.

The CRI values have been calibrated using CRI values of borehole. For the CRI values of borehole please see files in the folder "Stratification_of_LoggingCurves".

The CRI and CLC data files have been archived into the folder "*CRI_Calculations_of_Region_2007a*".

List of files

CRI_Calculations_of_Region_2007a >

- 2007a-dBzdt_CRI_Ch07_12.DAT

List of maps/images in format of PNG

CRI_Calculations_of_Region_2007a >

- AGS_CRI_2007a.png

APPENDIX D

In addition to Appendices A, B and C, a total of 265 maps were created as part of the TerraNotes processing to obtain the final 64 pages that constitute this report.

Images Overlaid on top of Geographical Features

0. ECC geographical features
0. Google Earth
1. DTM
2. TMI
3. RMI
4. Vertical derivative
5. dBx/dt channel 6
6. Bx channel 8
7. dBz/dt channel 10
8. Bz channel 12
9. dBz/dt channel 16
10. Bz channel 20
11. 2nd order Amplification map (no Waveform removed)
12. 7th order Amplification map
13. 7th order Amplification map (no Waveform removed)
14. Apparent conductance from AEM Amplification from 1st and 2nd order
15. Apparent conductance from AEM Amplification from 2nd and 3rd order
16. Apparent Conductivity from X component
17. Apparent Conductivity from Z component
18. Apparent Conductance from X component of 1st order AEM Amplification
19. Apparent Conductance from Z component of 1st order AEM Amplification
20. Apparent Conductance from X component of 2nd order AEM Amplification
21. Apparent Conductance from Z component of 2nd order AEM Amplification
22. Apparent Conductance from X component of 3rd order AEM Amplification
23. AEM Amplification of dBz/dt from channel 8 to 20
24. AEM Amplification of Bz from channel 8 to 20
25. AEM Amplification of Bz from channel 7 to 14
26. AEM Amplification of Bz from channel 11 to 20
27. AEM Amplification of Bz from channel 8 to 20 (Local)
28. Composite Resistivity Index vs dBz/dt channel 16
29. Composite Resistivity Index vs 7th order AEM Amplification
30. Detrended AEM Amplification of Bz from channel 11 to 20 (1)
31. Detrended AEM Amplification of Bz from channel 11 to 20 (2)

AGS 30 Hz GEOTEM Images

FOLDER 1 - dBx/dt

1 image Ch 16

FOLDER 2 - dBz/dt

16 images Ch 3-5-6-7-8-9-10-11-12-13-14-15-16-17-18-19-20

FOLDER 3 - Bx

19 images Ch 3-5-6-7-8-9-10-11-12-13-14-15-16-17-18-19-20 + 3 discussion images

FOLDER 4 - Bz

17 images Ch 3-5-6-7-8-9-10-11-12-13-14-15-16-17-18-19-20 + 1 discussion image

FOLDER 5 -AEM Amplifications

13 images 0-9th order amplification images
2nd, 3rd and 4th also calculated without waveform removal

FOLDER 6 - Variations between AEM Amplifications

1 image

FOLDER 7 - Apparent Conductance from AEM Amplifications

8 images

FOLDER 8 - Conductivity/Conductance Models from AEM Amplification

7 images 4 from X-component data and 3 from Z component data
4 near-surface (including 2 X- component and 2 Z- component)
2 mid-depth (including 1 X- component and 1 Z- component)
1 mid-depth to deeper ((including X- component only)

FOLDER 9 - Other AEM Amplifications

6 images Mid-depth to deeper amplification of regional and local anomalies
1 comparison image

FOLDER 10 - Other Images

14 images Digital Terrain Model, (4 images)
Magnetics, (3 images)
Flight Paths, (1 image)
CRI, (1 image)
Trends, (1 image)
AEM map overlays on 3D topography, (4 image)

AGS 90 Hz GEOTEM Images

FOLDER 1 - dBx/dt

16 images Ch 3-5-6-7-8-9-10-11-12-13-14-15-16-17-18-19-20

FOLDER 2 - dBz/dt

16 images Ch 3-5-6-7-8-9-10-11-12-13-14-15-16-17-18-19-20

FOLDER 3 - Bx

16 images Ch 3-5-6-7-8-9-10-11-12-13-14-15-16-17-18-19-20

FOLDER 4 - Bz

16 images Ch 3-5-6-7-8-9-10-11-12-13-14-15-16-17-18-19-20

FOLDER 5 -AEM Amplifications

6 images 0-1-2-3-6-9th order amplification maps

FOLDER 6 - Variations between AEM Amplifications

9 image

FOLDER 7 - Apparent Conductance from AEM Amplifications

9 images

FOLDER 8 - Conductivity/Conductance Models from AEM Amplification

6 images 4 near-surface (including 3 X- component and 3 Z- component)
1 mid-depth (including 1 X- component and 1 Z- component)
1 mid-depth to deeper ((including X- component only)

FOLDER 9 - Other AEM Amplifications

1 image Comparison image of 8 different amplifications

FOLDER 10 - Other Images

7 images Satellite (1 image)
Digital Terrain Model (2 images)
Magnetics (4 images)

RESOLVE IMAGES (28 images)

1	Digital Elevation Model image
1	Residual Magnetic Intensity image
5	Differential Resistivity image
10	Differential Depth image (5 with same colour scheme, 5 with individual colour scheme)
5	Inversion results from different depth layers
1	Image comparing different depth layer of inversion results and their amplified resistivity values
1	Comparison image of CRI and Resolve
1	Comparison image of raw EM data (dBz/dt ch-10) and Resolve
1	Comparison image of amplified EM data and Resolve
3	3D resistivity images (scatter plots of resistivity distribution).

APPENDIX E

In addition to Appendices A, B, C, and D a total of 626 grid, data and shape files were created as part of the TerraNotes processing to obtain the final 65 pages that constitute this report.

1. GEOTEM 30 Hz

- **1.01 dBx/dt**
- **1.02 dBy/dt**
- **1.03 dBz/dt**
- **1.04 Bx**
- **1.05 By**
- **1.06 Bz**
- **1.07 Other Raw data**
- **1.08 First Phase Amplification**
  - **a. No Waveform Removal**
- **1.09 First Product of First Phase Amplification**
  - **a. No Waveform Removal**
- **1.10 Apparent Conductance First Phase Amplification**
  - **a. No Waveform Removal**
- **1.11 Apparent Conductivity from Half-space Model**
- **1.12 Apparent Conductance from Thin-sheet Model**
- **1.13 Apparent Conductivity from Thick-Layer Model**
- **1.14 Second Phase Amplification**
  - **a. dBx/dt**
  - **b. dBz/dt**
  - **c. Bx**
  - **d. Bz**

2. GEOTEM 90 Hz

- **2.01 dBx/dt**
- **2.02 dBy/dt**

2.03 dBz/dt

2.04 Bx

2.05 By

2.06 Bz

2.07 Other Raw data

2.08 First Phase Amplification

a. No Waveform Removal

2.09 First Product of First Phase Amplification

a. No Waveform Removal

2.10 Apparent Conductance First Phase Amplification

a. No Waveform Removal

2.11 Apparent Conductivity from Half-space Model

2.12 Apparent Conductance from Thin-sheet Model

2.13 Second Phase Amplification

a. dBx/dt

b. dBz/dt

c. Bx

d. Bz

3. RESOLVE

4. ASCII Data Files

4.1 . Reorganized GEOTEM RDI Datasets

4.2. Reorganized RESOLVE Inversion Datasets

5. Shape Files

5.1 Cultural Noise

5.2 Inferred Paskapoo Boundary from GEOTEM

5.3 Regions of Interest (ROI)